THE UNIVERSITY
of EDINBURGH

Design and implementation of transgenic tools to visualise cell cycle progression in mammalian development

Matthew Ford

THE UNIVERSITY *of* EDINBURGH

Doctor of Philosophy – The University of Edinburgh – 2017

Declaration

I declare that this thesis was composed by myself, that the work contained herein is my own except where explicitly stated otherwise in the text, and that this work has not been submitted for any other degree or processional qualification except as specified.

Parts of this work have been published in Mort et al., 2014.

30/01/2017

Matthew Ford Date

Abstract

Cell cycle progression is the series of steps a cell has to take in order to duplicate its DNA and produce two daughter cells. Correct spatial and temporal coordination of the cell cycle is key for the normal development of any organ or tissue and is stringently controlled during embryogenesis and homeostasis. Misregulation of cell cycle progression is causal in many developmental disorders and diseases such as microcephaly and cancer. Fucci (Fluorescent Ubiquitination based Cell Cycle Indicator) is a system that allows for the visualisation of cell cycle progression by the use of two differently coloured fluorescent probes whose abundance is regulated reciprocally during the cell cycle. The probes contain the E3 ligase recognition domains of Cdt1 and Geminin fused to the fluorophores mCherry (red fluorescence) and mVenus (yellow fluorescence) respectively. Cells are therefore labelled red during G1, yellow in the G1/S transition and green during late S/G2 and M phases of the cell cycle. In order to study development and tissue homoeostasis a Fucci expressing mouse line was developed however this has several key limitations: First, the two Fucci probes are expressed from separate loci complicating mouse colony maintenance. Second, the constructs were not inducible, making it impossible to follow cell cycle progression in specific cell lineages and third the mice were generated by random transgenesis which is prone to silencing and can exhibit variation in expression between different tissues.

Here I have characterised an improved version of the original Fucci system known as Fucci2a designed by Dr Richard Mort (University of Edinburgh) to overcome these limitations. The *Fucci2a* genetic construct contains both Fucci probes fused with the *Thosea asigna* virus self-cleaving peptide sequence T2A. This allows expression of both probes as a single bicistronic mRNA with subsequent cleavage by ribosomal 'skipping' during translation to yield separate proteins. A Fucci2a mouse (*R26Fucc2aR*) was generated by homologous recombination into the ROSA26 locus using the strong, ubiquitous CAG promoter to drive expression and incorporating a floxed-Neo stop cassette. This allows tissue specific activation by Cre recombinase when combined with a second Cre expressing mouse line.

Building on the bicistronic Fucci2a technology I have gone on to develop and characterise four new tricistronic reporter constructs which allow for the dual visualisation of cell cycle progression with apoptosis, cytokinesis and ciliogenesis. In each case an additional fluorescent probe was added to the original Fucci2a construct separated by the self-cleaving peptide P2A and the construct characterised in 3T3 stable cell lines. The combination of a dual cilia and cell cycle reporter construct proved fruitful and I have gone on to investigate the relationship between cell cycle progression and ciliogenesis in 3T3 cells and have generated and characterised the *R26Arl13b-Fucci2aR* mouse line.

I have also illustrated the utility of the *R26Fucci2aR* mouse for generating quantitative data in development research in two development situations; melanocyte development and lung branching morphogenesis. Melanocytes are specialised melanin producing cells responsible for the pigmentation of the hair, skin and eyes. Their precursors, melanoblasts, are derived from the neural crest where they migrate and proliferate before becoming localised to hair follicles and their study provides a good model for understanding the development of other neural crest derived lineages such as the peripheral nervous system. Using time-lapse imaging of *ex vivo* skin cultures in which melanoblasts are labelled with the Fucci probes I have characterised melanoblast migration and proliferation. In addition, I have shown that Kit signalling, which is necessary for melanoblast migration and survival, controls melanoblast proliferation in a density dependent manner and that melanoblast migration is more persistent in S/G2/M phases of the cell cycle.

Lung branching morphogenesis requires constant proliferation at the apical tip of a growing epithelial branch. Loss of epithelial symmetry through an unidentified mechanism (requiring BMP, FgF10, Shh and Wnt signalling) within a branch is required to initiate branching either latterly from the side of a elongating branch by domain branching or by bifurcation of the tip. In the final section of this thesis I performed a comparative analysis of the behaviour of the developing lung epithelium using proliferative status (Fucci2a expression) to categorise each cell. Using a combination of live imaging and immunohistochemistry I have identified a transition zone 100-150μm from the tip of the branching lung epithelium where epithelial cells

become stationary and drop out of the cell cycle corresponding with the onset of proximal bronchial progenitor marker Sox2. A comparative gene expression analysis of the proliferating and non-proliferating regions using Fucci2a to distinguish them has eluded to several interesting genes which could influence branching morphogenesis during lung development.

Lay Summary

The cell cycle is a series of events that take place within a cell leading to the replication of that cell. When this occurs in a population of cells it is known as proliferation. Controlling the rate of proliferation is key for the correct development, growth and maintenance of an organism. It is therefore important to understand how rates of proliferation change during the development of complex structures such as organs and tissues. However it would be impossible to see or measure the rates of proliferation within a specific tissue at a specific time in development within the mass of all the other developing structures. To overcome this problem I have improved a system developed by Sawano and colleagues known as Fucci (Fluorescent Ubiquitination-based Cell Cycle Indicator) to visualize cell cycle progression within a developing organism. Fucci in principle is made up of two different fluorescently tagged proteins whose abundance within a cell is carefully regulated with respect to the cell cycle. In this system cells actively dividing have high levels of a green fluorescently tagged protein whereas cells in an undividing state contain high levels of a red fluorescently tagged protein which therefore allows you to see and measure the rate of cell cycle in real time within a developing organism. The original Fucci system however had two major limitations. Firstly it was made up of two separate constructs and secondly it would label all cells within a developing organism making it very difficult to isolate a particular population of cells for analysis. To overcome these limitations Dr Richard Mort fused the two constructs together into one construct and made the construct inducible so that expression of the Fucci fluorescent proteins can be limited to a specific sub set of cells. I have gone on to characterise this mouse and develop four new reporter constructs in which I have combined the Fucci probes with four different fluorescent

reporters of apoptosis (programed cell death), cytokinesis (cell division) and cilia. The dual cilia cell cycle reporter construct proved fruitful and I have gone on to generate and characterise a reporter mouse line.

In addition to this in this thesis I have used the genetic tools mentioned above to investigate melanoblast migration during development and the process of lung branching morphogenesis in the developing lung to illustrate the utility of the tools I have characterised. Melanoblasts are specialised melanin producing cells responsible for the pigmentation of the hair and skin. During development melanoblasts originate from a migratory population of cells known as the neural crest in the dorsal region of the mouse. From here they migrate and proliferate ventrally to colonise the developing skin before localising to hair follicles. Using an *ex vivo* skin culture system I was able to characterise the migratory behaviour of melanoblasts during this process and show that melanobast migration is not directed as previous reports have suggested but random. In addition I have provided evidence which supports the hypothesis that the protein KIT promotes melanoblast proliferation during development in a density dependent manner.

During mammalian lung development the lung epithelium begins as a single epithelial tube which undergoes rounds of stereotyped branching to build the characteristic bronchial tree. This process is driven by proliferation in the epithelial tip in combination with cell shape changes and interactions with the surrounding lung mesenchyme. By expressing Fucci specifically in the lung epithelium I was able to undertake a comparative analysis of gene expression and cell behaviour of cells in the branching and non-branching regions based on the colour of the Fucci probes.

Publications

A tissue specific tricistronic mouse reporter of cell cycle progression and ciliogenesis. **Ford M.J.**, Keighren M.A., Budd P., Jackson I.J., Mill P and Mort R.L. (In preparation)

Fucci2a: A bicistronic cell cycle reporter that allows Cre mediated tissue specific expression in mice. Richard Lester Mort, **Matthew Jonathan Ford**, Asako Sakaue-Sawano, Nils Olof Lindstrom, Angela Casadio, Adam Thomas Douglas, Margaret Anne Keighren, Peter Hohenstein, Atsushi Miyawaki and Ian James Jackson, Cell cycle, 2014.bb

Acute Versus Chronic Loss of Mammalian Azi1/Cep131 Results in Distinct Ciliary Phenotypes. Emma A. Hall, Margaret Keighren, **Matthew J. Ford**, Tracey Davey, Andrew P. Jarman, Lee B. Smith, Ian J. Jackson and Pleasantine Mill1, Plos Genetics, 2013.

Abbreviations

%	Percent
^{o}C	Degrees Celsius
3D	Three dimensional
APC	Anaphase-promoting complex
ATP	Adenosine triphosphate
Brd-U	Bromodeoxyuridine
BSA	Bovine serum albumin
cDNA	Complementary deoxyribonucleic acid
CFP	Cyan flourescent protein
CO2	Carbon dioxide
CSF	Cerebrospinal fluid
DAPI	4',6-diamidino-2-phenylindole
DMSO	Dimethyl sulfoxide
DNA	Deoxyribonucleic acid
dNTP	Deoxyribonucleic nucleoside triphosphate

e	Embryonic day
ECM	Extra cellular matrix
EDTA	Ethylenediaminetetraacetic acid
EMT	Epithelial–mesenchymal transition
ESC	Embryonic stem cells
FACS	Fluorescence-activated cell sorting
FBS	Fetal bovine serum
FCS	Fetal calf serum
FITC	Fluorescein isothiocyanate
FMDV	Foot-and-mouth disease virus
FRET	Fluorescence resonance energy transfer
Fucci	Fluorescence ubiquitination-based cell cycle indicator
G0/1/2	Growth or Gap phase 0/1/2
GAP	GTPase-activating protein
GFP	Green fluorescent protein
H20	Water

HCL	Hydrochloric acid
HRP	Horseradish peroxidase
ICM	Inner cell mass
iPS cells	Induced pluripotent stem cells
IRES	Internal ribosome entry site
KO	Knock-out
LIF	Leukemia inhibitory factor
MCM	Minichromosome maintenance protein complex
MEFS	Mouse embryonic fibroblasts
MET	Mesenchymal–epithelial transition
mESC	Mouse embryonic stem cells
MgCl2	Magnesium chloride
Min	Minutes
M-phase	Mitosis phase
mRNA	Messenger ribonucleic acid
ms	Millisecond

MSA	Migration staging area
NaCl	Sodium chloride
NaOAc	Sodium acetate
Neo	Neomycin
Nls	nuclear localisation signal
OCT	Optimal cutting temperature compound
ORF	Open reading frame
pA	Polyadenylation tail
PBS	Phosphate-buffered saline
PCP	Planar cell polarity
PCR	Polymerase chain reaction
Pen/Strep	Penicillin Streptomycin
PFA	Paraformaldehyde
PMSF	Phenylmethylsulfonyl fluoride
qRT-PCR	Quantitative reverse transcription PCR
RNA	Ribonucleic acid
RPM	Revolutions per minute

RT	Reverse transcriptase
SCF	Skp, Cullin, F-box containing complex
SCP	Schwann cell precursors
S-Phase	Synthesis phase
t-RNA	Transfer RNA
UV	Ultraviolet
V	Volts
v/v	volume to volume
Wt	Wildtype
w/v	Weight to volume

List of Figures

List of tables

List of supplementary videos

Table of Contents

1 Chapter 1: Introduction

The cell cycle is the fundamental process by which multicellular organisms grow and reproduce. Rudolf Virchow's realisation in 1855 that all cells come from cells, "omnis cellula e cellula", has led an intense investigation by the scientific community into the mechanisms of cell cycle progression and control during development and disease (Nurse, 2000). The correct spatial and temporal control of cell cycle progression, coupled with appropriate cell growth and differentiation, is at the heart of all tissue morphogenesis. This is highlighted by the myriad of developmental and somatic disorders caused by cell cycle dysregulation such as cancer and cystic kidney disease, characterised by uncontrolled proliferation and primordial dwarfism caused by an overall reduction in proliferation during development (Bicknell et al., 2011; Jonassen et al., 2008; Vermeulen et al., 2003). The need to quantify proliferation and monitor cell cycle progression is therefore key for understanding how an organism and disease develops. As technology progresses, particularly in the fields of microscopy and cytometry, new techniques have become available for researchers to monitor the cell cycle with ever-greater precision. In this thesis I have characterised an improvement on one such technique known as the Fluorescent Ubiquitination-based Cell Cycle Indicator (Fucci). Fucci is a genetic based reporter which enables the visualisation of cell cycle progression by the use of two fluorescently tagged probes, the abundance of which are regulated in a cell cycle dependent manner resulting in cells being labelled red in G1, yellow during the G1/S transition and green during late S/G2/M phases of the cell cycle (Sakaue-Sawano et al., 2008).

Fucci2a is an improvement on the original Fucci system which allows the visualisation of cell cycle progression from a single bicistronic construct (Mort et al., 2014). The Fucci2a reporter mouse line has several advantages over current Fucci reporter lines due to its Cre-inducibility (allowing for tissue specific labelling) and expression from a single locus. I have gone on to design and characterise four novel tricistronic reporter constructs that allow the dual visualisation of cell cycle progression with apoptosis, cytokinesis and ciliogenesis. Finally, to illustrate the usefulness of the genetic tools I have applied them to two developmental systems.

First, I have used live imaging techniques to describe melanoblast migration during epidermal colonisation and investigated the role of the receptor tyrosine kinase KIT (Steel et al., 1992). Second, I have conducted a comparative analysis of the branching lung epithelium separated by proliferative state using a combination of RNA sequencing and imaging technique

1.1 The Cell Cycle

The cell cycle is the stereotyped sequence of events that cells undertake in order to replicate their DNA and subsequently divide into two daughter cells. In eukaryotes the cell cycle consists of four main phases: G1 (Gap 1) during which time the cell grows, S-phase when the DNA is replicated, a second G2-phase (Gap 2) which is followed by chromosome segregation and cytokinesis in mitosis (M-phase) (fig 1.2A). Collectively the first three phases are known as interphase. During G1 cells synthesise the proteins necessary for cell growth, cell function and DNA synthesis (Schafer, 1998). The length of G1 is varied between different cell types and is adapted to be particularly short in embryonic stem cells to allow for rapid proliferation and to restrict differentiation (Coronado et al., 2013; Savatier et al., 1994). Terminally differentiated cells or quiescent cells such as adult stem cells that are not cycling through the cell cycle are said to be in G0 (Coller et al., 2006; Oki et al., 2014; Venezia et al., 2004; Zetterberg & Larsson, 1985). During S phase the DNA is replicated once to produce two pairs of chromosomes. DNA is first "licensed" for replication in G1 by the binding of a specialised group of proteins known as the pre-replication complex (including ORC1-6, CDT1 and CDC6) to the origins of replication (Bell & Stillman, 1992; Hartwell, 1976; Méchali, 2010; Nishitani et al., 2000). Subsequently this permits the loading of MCM (minichromosome maintenance) helicases to from the pre-replication complex which unwinds the DNA at the start of S-phase (Ishimi, 1997; Labib et al., 2000; Méndez & Stillman, 2003). DNA synthesis is then initiated in unwound DNA forks at the prereplication complex by the binding of an RNA primer and the subsequent extension by DNA polymerases (Leman & Noguchi, 2013). Due to the requirement of DNA synthesis to occur in a 5' to 3' direction two distinct methods of DNA synthesis occur. On the leading stand DNA polymerase ε synthesises DNA in a continuous fashion in the same direction as the extending DNA fork. On the reverse stand DNA polymerase δ synthesis DNA in short strands or "Okazaki fragments"

100-200 base pairs long which are then fused by DNA-ligase 1 (Leman & Noguchi, 2013; Okazaki et al., 1968; Sugimoto et al., 1968). After DNA replication there is another short gap phase (G2) during which time the cell synthesises the proteins required for mitosis. Mitosis then initiates with the condensing of the chromosomes and binding to the mitotic spindle via the kinetochore. The chromosomes are then separated to the opposite poles of the cell via contraction of the mitotic spindle. In the final stages of mitosis, chromosomes are separated and the cell splits into two daughter cells via cytokinesis to form two daughter cells each containing a complete set of diploid chromosomes (fig1.1) (Alberts et al., 2002; Kanda et al., 1998).

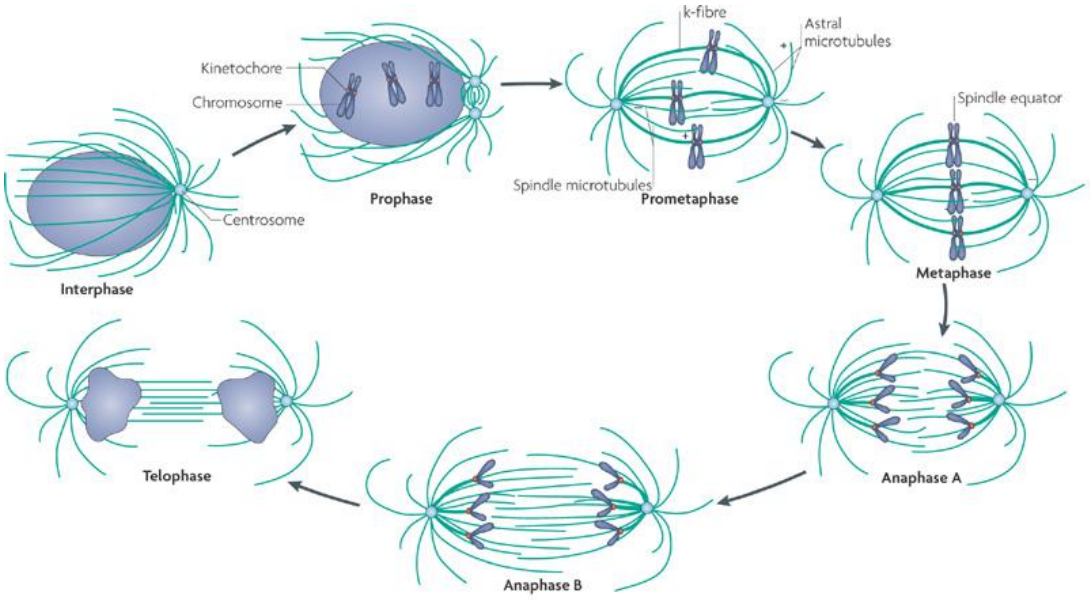

Fig 1.1: Stages of mitosis. Interphase contains G1, S and G2 phases of the cell cycle during which time the cell replicates its DNA and synthesises proteins in preparation for mitosis. During this stage of the cell cycle centrosomes are free to move around the cell and the chromatin is highly decondensed to allow for transcription of genes and DNA replication. Prophase is the first stage of mitosis and is characterised by the condensation of DNA into visibly distinct pairs of chromosomes connected by a kinetochore. By prometaphase the nuclear envelope has broken down and the centrosomes have moved to opposite poles of the cell. Kinetochore (K)-fibres (bundles of stabilised microtubules) connect the kinetochore to the centrosomes and start to orientate the chromosomes towards the equator of the cell defining metaphase and is supported by spindle and astral microtubules. The less dynamic microtubule minus ends reside near the centrioles while the more dynamic plus ends extend toward the equator and cell cortex. The two pairs of chromosomes are then separated into single pairs during anaphase A and B. Finally the nuclear envelop starts to reform during telophase as the DNA begins to decondense before cytokinesis divides the cell into two daughter cells. Figure adapted from Walczak et al 2010.

1.2 Intrinsic cell cycle control

Within an organism the cell cycle of individual cells is regulated by a combination of internal signalling pathways and external signals known as mitogens that promote cell cycle progression. Cyclins, first identified as cycling proteins in embryonic sea urchins (*Arbacia punctulata),* have been shown via their interaction with cyclin dependent kinases (cdks) to be the key signalling molecules that control the cell cycle (Evans et al.,1983; Schafer, 1998). Throughout the cell cycle Cdks are activated by cyclins to initiate cell cycle progression including, DNA replication in S-phase and mitosis in M-phase. In the classical model for cell cycle control, D-type cyclins with CDK4 and CDK6 regulate events in early G1 (Matsushime et al., 1994). Cyclin E accumulates in late G1 and activates CDK2 to initiate entry into S-phase (Ohtsubo et al., 1995). Cyclin A in separate complexes with CDK1 and CDK2 regulates the completion of S-phase while Cyclin B activating CDK1 is responsible for mitosis (fig 1.2B and C) (Hochegger et al., 2008; Lindqvist et al., 2009; Lindqvist et al., 2007; van den Heuval & Harlow, 1993; Zindy et al., 1992). However, based on recent data from CDK knock out studies in mice a new threshold model has been suggested in which cyclin A bound to either CDK1 or 2 is sufficient to control interphase and cyclin B bound to CDK1 is necessary for entry into mitosis. The model suggests simply that an increase in CDK activity without the need for substrate specificity is sufficient to dive the cell through the cell cycle with S and M phases being initiated at specific thresholds of CDK activity (fig 1.2D) (Hochegger et al., 2008). This hypothesis is strongly supported by the viability of mice to midgestation in the absence of all interphase CDKs (CDK2,3,4,6) (Santamaría et al., 2007). In response to extracellular signals or intracellular stimuli such as DNA damage, cell cycle progression is also regulated by a number of "checkpoints" at which time the cell is able to elongate a particular cell cycle phase or halt the cell cycle altogether until conditions have changed or, for example, the DNA damage has been resolved (Kastan & Bartek, 2004). The prominent checkpoint for DNA damage is at the G1/S transition and is mediated through the p53 signalling pathway. DNA damage in the form of double stranded breaks is sensed by the MRN complex, which

has been shown to recruit and activate tyrosine kinase ATM (Lee & Paull, 2005; Uziel et al., 2003). In addition ssDNA (single stranded DNA) exposed by double stranded breaks has been shown to recruit ATRIP and activate another tyrosine kinase ATR (L. Zou & Elledge, 2003). ATR has also been shown to monitor and repair fragile sites formed by stalling replications forks (Casper et al., 2002). Activated ATR and ATM phosphorylates a host of downstream effectors, including the transcription factor and tumour suppressor P53. P53 is also activated by the inhibition of ubiquitin ligase MDM2, which regulates P53 abundance (Maya et al., 2001). Activated P53 promotes the expression of P21, an inhibitor of CDK2, to prevent entry S-phase there by elongating G1 and allowing time for DNA repair. (Harris & Levine, 2005). Conversely Cyclin E-CDK2 has been shown to phosphorylate P27 resulting in its degradation thereby promoting cell cycle progression (Sheaff et al., 1997). A second checkpoint before the onset of mitosis is able to elongate the G2 phase of the cell cycle in response to DNA damage or incomplete DNA replication during S-phase primary regulated by inhibition of the mitosis promoting activity of cyclin B bound CDK1 (Kastan & Bartek, 2004). A final mitotic spindle checkpoint occurs during metaphase to ensure correct loading and alignment of all chromosomes onto the mitotic spindle (Lara-Gonzalez et al., 2012). In addition to the mentioned checkpoints, a restriction point exists in G1 which determines if a cell will re-enter the cell cycle. G1 can be split into two phases, post mitosis the cell enters a growth factor dependent phase of G1 at which point the cell will only enter the late growth factor independent phase if sufficient growth factor signalling is present. Once past this restriction point the cell will progress through the cell cycle independent of growth factor signalling (Pardee, 1974). Growth factors have been shown to simulate the accumulation of cyclins E and D during G1, which via activation of CDKs, phosphorylates retinoblastoma protein (Rbp) (Dou et al., 1993; Hinds et al., 1992; Won et al., 1992). Phosphorylation of Rbp relives transcription factor E2F to activate transcription of target genes involved in nucleotide metabolism and DNA synthesis (Nevins, 1998). In accordance with this, MEFS deficient in Rbp have been shown to progress

through to S-phase in the presence of cell cycle arrest compound methotrexate and showed elevated transcription of E2F target genes (Almasan et al., 1995).

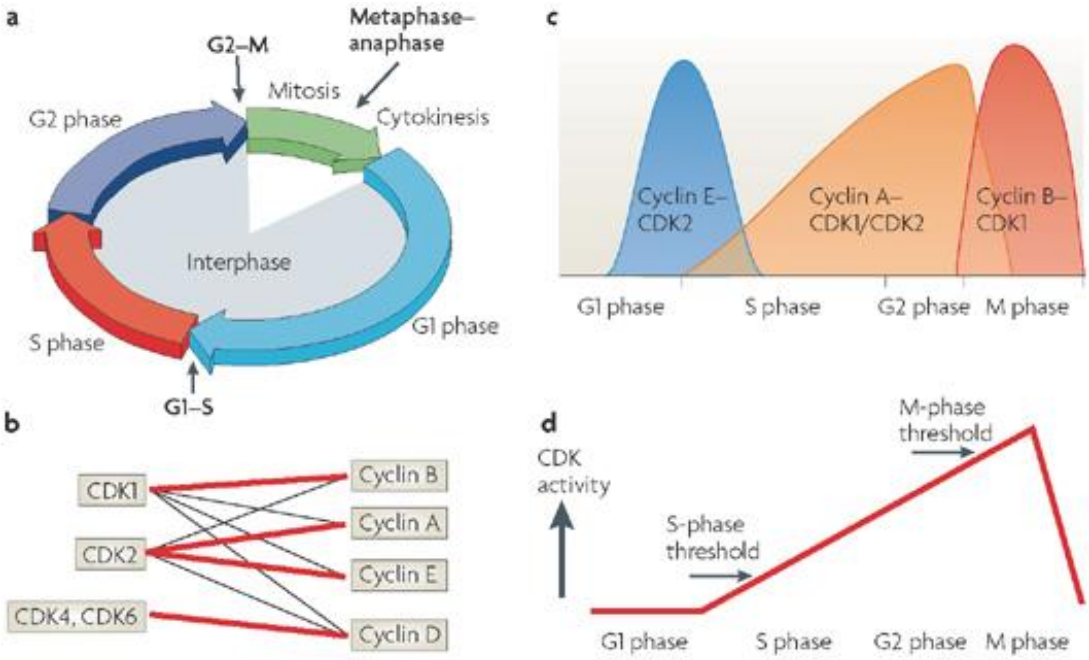

Fig 1.2: Models of cell cycle control by cyclins. (A) Activity cycling cells go through four cell cycle stages. G1 when proteins are synthesised in preparation of DNA replication and cell growth, S phase when DNA is replication, G2 when the cell prepares for mitosis and finally mitosis when the chromosome condense and are separated into two daughter cells. Entry into each of these phases is regulated by the activity of cyclin dependent kinases (CDKs) and their respective cyclins. **(B)** Binding partners of cylins and CDKs with red lines representing preferential binding partners. CDK4/6 exclusively bind to cyclin D. CDK1 and CDK2 interact with all cyclins (A,B,E and D) but preferentially bind to cyclin B and cylin A/E respectively. **(C)** In the classical model of cyclin/CDK dependent cell cycle control. High CDK4/6 and cyclin D activity regulates early G1 (not shown) before a switch to high CDK2 and Cyclin E activity triggers entry into S-phase. CDK2/3 and cyclin A regulate late S-phase and G2 while CDK1 and cyclin B are responsible for M-phase. **(D)** A new threshold based model has been inferred by the redundancies seen in CDK-knock studies questioning the need for cell cycle phase substrate specificities. Only Cylin B and CDK1 are essential for entry into M-phase while interphases specific CDKs and cyclins are not essential. Suggesting a threshold model in which S and subsequently M phase entry is triggered by non-specific CDK activity. Figure adapted from Hochegger et al 2008.

1.3 Extrinsic cell cycle control

Correct spatial and temporal control of cell cycle progression at a single cell level, and proliferation at the tissue level, is essential during development. Misregulation has been associated with defects in melanocyte, cortical and lung development among other developmental situations (De Schepper et al., 2008; Dehay & Kennedy, 2007; Motoyama et al., 1998; Shu et al., 2002). Control of the cell cycle within an organism is mediated via external signals that are transduced to modulate the intrinsic cell cycle control mechanisms outlined in the previous section. A good example of this can be seen during melanoblast development. Melanoblasts are the neural crest derived precursors of melanocytes, specialised melanin producing cells that produce the pigment in the hair, skin and eyes (Mort et al., 2015). During development a small number of melanoblasts are specified in the neural crest. These cells then delaminate through an epithelial to mesenchymal transition and migrate along a dorsal lateral pathway eventually becoming localised to hair follicles. From their tiny initial population melanoblast numbers must expand massively to colonise the entire developing epidermis and this is regulated in part by the extracellular signalling molecule, Kit ligand (also known as Stem Cell Factor or Steel Factor) located on the surface of cells within the dorsal lateral pathway and as a soluble ligand (B Wehrle-Haller & Weston, 1995). Kit ligand binds to the receptor tyrosine kinase Kit on the surface on melanoblasts promoting cell cycle progression via the Ras signalling pathway (Wehrle-Haller et al., 2001; Widmann et al., 1999). Genetic attenuation of Kit signalling by the use of knock out mouse lines has shown Kit signalling promotes proliferation in a dose dependent manner resulting in a hyperpigmentation phenotype when constitutively activated and hypopigmentation with an unpigmented belly spot in heterozygous Kit mutants (Diwakar et al., 2008; Mackenzie et al., 1997; Wehrle-Haller et al., 2001). Mutations in NF1, a negative regulator of Ras signalling down stream of kit in humans, has also been linked to a neurofibromatosis type 1 disorder called café-au-lait macules characterised by hyperpigmented spots as a result of melanoblast hyperproliferation (De Schepper et al., 2008). Cell cycle progression in all development situations mirrors this same

dependence on direct cell-cell interactions and soluble factors within a cell's microenvironment.

1.4 Techniques for quantifying proliferation

Traditional techniques for measuring proliferation predominantly relied on the use of S-phase markers such as 3H-Thymadine, Brdu and PCNA on fixed samples or indirectly using metabolically activated dyes such as tetrazolium salts and alamarBlue (Thermo Fisher) (Altman, 1963; Bubendorf et al., 1996; Gratzner et al., 1975;Gratzner, 1982; Kubben et al., 1994; O'Brian et al., 2000; Salic & Mitchison, 2008; Slater et al.,1963). The classical method for measuring proliferation, however, is the use of a haemocytometer to calculate growth curves and doubling times. The haemocytometer has the advantage that it is quick, cheap, and technically easy to use. However, there is a high degree of operator error and it requires reducing your sample to a single cell suspension for counting and, therefore, is only suitable for *in vitro* studies. Another method for determining the proliferative state of a tissue is calculation of the mitotic index or cell cycle phase indices such as Ki67, 3H-thymadine, Brd-u and PCNA, which has been used extensively in predicting cancer prognosis (Aaltomaa et al., 1992; Bubendorf et al., 1996; Gaglia et al., 1993; Katzenberger et al., 2006; Meyer et al., 2009; Silvestrini et al., 1990).

1.4.1 Calculating mitotic and cell cycle phase indices

The mitotic index gives a quantitative indication of the proliferative state of a tissue and can be simply calculated by the proportion of cells within mitosis in a field a view using the cellular morphology to identify cells within mitosis (Aaltomaa et al., 1992; Meyer et al., 2009).

Another common method for quantifying the proliferative state of a tissue is to monitor DNA synthesis by measuring the uptake of a thymidine analogue. Traditionally tritiated thymidine (HTdr) is added to an *ex vivo* organ culture or

injected intravenously (Altman, 1963). HTdr competes with endogenous thymidine and is incorporated into newly synthesised DNA during S-phase. Cells or tissues can then either be lysed and the levels of incorporated 3H-thymadine quantified with a scintillator or fixed and tissue sections imaged with an autoradiograph in order to count the number of cells that passed through S-phase during the Htdr 'pulse' (Silvestrini et al., 1990). The use of 3H-thymadine has essentially been replaced by bromodeoxyuridine (BrdU) and its analogues IdU, CdU and EdU which can be detected by antibody or chemically using the click-it reaction (Gratzner et al., 1975; Gratzner, 1982; Salic & Mitchison, 2008). The use of immunohistochemistry techniques greatly reduces the detection time compared to 3H-thymidine. However, it has been reported that incorporation of Brd-U during S-phase causes apoptosis and interferes with cell cycle progression and differentiation (Bannigan & Langman, 1979; Duque & Rakic, 2011). Similarly cell cycle defects due to interference with DNA replication have also been reported using 3H-thymadine (Hoy et al., 1990). EdU is an incremental improvement on the BrdU system that allows for even quicker detection time without the use of antibodies (Salic & Mitchison, 2008). EdU (5-ethynyl-2'-deoxyuridine) contains a terminal alkyne group that is detected by a fluorescent azide through a Cu(I)-catalysed [3 + 2] cycloaddition reaction ("click it chemistry")(Vsevolod et al., 2002). An additional advantage of EdU is that, due to the size of the reagents used in the reaction being $1/500^{th}$ of the size of regular antibodies, it makes penetration of large samples more efficient. A disadvantage for using thymidine isotopes is that the amount of time for the isotope to reach the tissue of interest after injection and the subsequent time the tissue is exposed to the isotope varies between each experiment and therefore requires optimisation.

Antibodies raised against PCNA (Proliferating Cell Nuclear Antigen), a DNA sliding clamp protein involved in DNA replication, is a widely used alternative S-phase marker that does not require pulsing with synthetic nucleotide analogous and has been shown to produce comparable results. (Kubben et al., 1994; Maga & Hubscher, 2003).

Calculation of the Ki67 index using antibodies raised against Ki67 is another widely used indictor of proliferation (Bubendorf et al., 1996; Katzenberger et al., 2006). Ki67 is a nuclear localised protein whose expression is required for cell cycle progression and is abundant in all stages of the cell cycle apart from G0 and therefore useful for determining the proportion of cells actively cycling within a tissue (Scholzen & Gerdes, 2000).

Using flow cytometry of fixed cells stained with a fluorescent DNA marker such as DAPI or propidium iodidie (PI) it is also possible to compare the DNA content profiles based on fluorescent intensity (Pozarowski & Darzynkiewicz, 2004). Changes in the proportions of cells in different cell cycle phases can then be used to infer changes in proliferation. An increase in the proportion of cells in G1 is indicative of a more slowly cycling population whereas an increase in the proportion of cells in S/G2/M is indicative of a faster cycling population.

The above methods rely on calculating an index or DNA content profile to compare between experimental groups. However, the approaches may be flawed as tissues with different mean cell cycle times may have the same index and DNA content profile for a given measure, especially if all cell cycle phases are changed proportionally to one another: for this reason an estimate of the cell cycle time may be required.

1.4.2 Calculating cell cycle times

Cell cycle times can be calculated using S-phase markers by dividing the length of a particular cell cycle phase by the proportion of cells within that phase. This can be calculated either by administering a continual pulse of a S-phase marker, followed by measuring the time taken for all cells to be labelled to give you the length of G2/M/G1 and then divide that by the proportion of cells in G2/M/G1, which is the proportion of unlabelled cells by a single pulse of the S-phase marker (Nowakoski ref 1989), or by a dual pulse and chase method in which two different S-phase markers are administered one after another, allowing you to measure the rate at

which cells are moving through S-phase (Bradford & Clarke, 2011; Martynoga et al., 2005). It is important to note that the use of these methods is based on the assumption that all cells within the population are cycling asynchronously. For example, Martynoga et al. used this method to calculate the cell cycle times of neuronal precursors during telencephalic neurogenesis (fig 1.3). Mice were given injections of IddU followed by an injection of BrdU after 1.5 hours and mice scarified 2 hours after the initial IddU injection. This allows for enough time for BrdU and IddU to circulate and accumulate in S-phase cells which takes around around 30 minutes after injection (Nowakowski et al.,1989). In a total of 42 cells, 23 cells were labelled with Brd-U, 9 cells solely with IddU and 10 cells unlabelled with either maker. This means that in 1.5 hours 9 cells have left S-phase. If there are 23 cells in S-phase at any one time then it would take 3.85 hours for all those cells to leave S-phase. This is calculated by dividing the length of time between injections and the proportion of cells that have left S-phase in that time. In this case 1.5 hours / (9 IddU cells / 23 Brd-U cells) = 3.85 hours. The cell cycle time for the population of neuronal precursors was then calculated based on the observation that the proportion of cells within a particular cell cycle phase is equal to the proportional length of that phase in relation to the cell cycle (Nowakowski et al., 1989). In this example, the calculated length of S-phase was divided by the proportion of cells in S-phase which was 3.85 hours / (23 S-phase cells / 42 total cells) = 7.1 hours (Martynoga et al., 2005). This is a useful method for calculating cell cycle times and can be done using fixed samples or quantified by flow cytometry (Bradford & Clarke, 2011). However, they are still limited to using fixed tissues and therefore only give you a snapshot of the proliferative state of a tissue and cannot give you details on the dynamic changes in cell cycle progression in space and time which, for example, have been shown to be key during neurogenesis in the subventricular zone. (Calegari & Huttner, 2003; Dehay & Kennedy, 2007). In addition, using these methods to calculate cell cycle times it is not possible to determine the change in length of individual cell cycle phases.

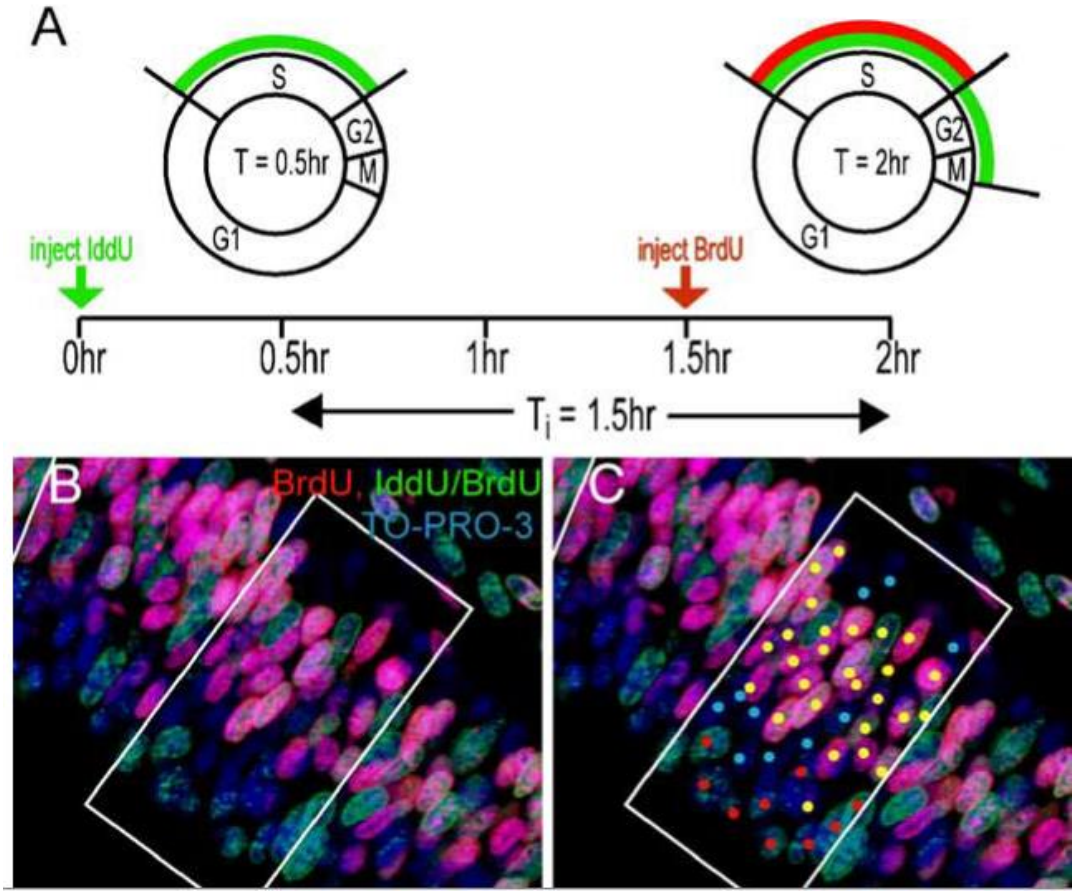

Fig 1.3: Calculation of cell cycle length by double labelling with BrdU and IddU. **(A-C)** Example experiment taken from Martynoga et al 2005. **(A)** IddU is injected into pregnant females followed by an injection of BrdU after a 1.5 hours lag period and embryos harvested 0.5 hours after the BrdU dose to allow time for BrdU to be incorporated. The length of S-phase is calculated by dividing the length of the lag phase by the proportion of cell which have left S-phase within that time or T_i / ($IddU^+$:$BrdU^-$ / $IddU^+$:$BrdU^+$). Cell cycle times can then be calculated with the assumption all cells are cycling asynchronously based on the observation that the proportion of cells within a particular cell cycle phase is proportional to the length of that phase (Nowakowski et al., 1989). In this example cell cycle times are then estimated by the following equation: Cell cycle time = length of S-phase / Proportion of cells in S-phase. **(B-C)** Immunofluoresence of the developing telencephalon stain with antibodies to IddU and BrdU. **(C)** Yellow dots indicate cells labelled with both IddU and BrdU, red dots IddU only and blue dots unlabelled cells. Figure adapted from Martynoga et al 2005.

1.4.3 Calculating cell densities by spectrophotometer

A popular indirect method for quantifying proliferation for *in vitro* studies uses tetrazolium salt MTT (3(-4,5-dimethylthiazol-2-yl)-2,5-diphenyl tetrazolium bromide). MTT can be added to culture media and will progressively be converted into a blue coloured product (formazan) by mitochondrial enzyme succinate-dehydrogenase (Slater et al, 1963). The enzymatic reaction takes place uniquely within living cells with the amount of formazan being produced being proportional to cell number (Mosmann, 1983). The assay has since been improved in the form of AlamarBlue or resazurin (O'Brian et al., 2000). AlamarBlue is blue in colour but is reduced by mitochondrial enzymes to resorufin which emits a red fluorescence and is less toxic than tetrazolium salts and soluble without the use of DMSO. These metabolic assays, however, suffer from inaccuracies due to their indirect measurement of proliferation that can be influenced by variation in metabolic behaviour during cell culturing and are limited to *in vitro* experiments (Quent et al., 2010). A more accurate method for calculating changes in cell number *in vitro* is the use of cyanine dyes such as PicoGreen and CyQuant to fluorescently label DNA (Blaheta et al., 1998; Jones et al., 2001). Although having the advantage of being able to track cell numbers live, these methods have the limitation of only being applicable for *in vitro* experiments.

1.4.4 Tracking cell divisions by live imaging

A useful *in vivo* method for tracking cell numbers live has arrived with the advent of the intracellular covalent coupling dye caroxyfluorescein diacetate succinimidyl ester (CFSE) (Lyons & Parish, 1994). Intracellular esterases convert non-fluorescent membrane permeable 5-(and-6)-carboxyfluorescein diacetate, succinimidyl ester (CFDASE) into highly fluorescent non-membrane permeable CFSE (Parish, 1999). The dye remains within the cell and is split evenly between daughter cells allowing tracking of cells for up to eight cell divisions by live imaging and FACS. This method has proved extremely useful for the study of lymphocyte migration and proliferation *in vitro* and *in vivo* in adoptive cell transfer studies (Lyons, 2000), but is

limited in its tractability to different systems *in vivo* due to its reliance on adoptive cell transfer methodologies.

1.5 The Fucci system

To fully appreciate the role of the cell cycle during development you require a method that allows you to visualise cell cycle progression in space and time *in vivo*. Fucci (Fluorescence Ubiquitin Cell Cycle Indicator) is a system that allows the visualisation of cell cycle progression by the use of two fluorescently tagged probes, whose abundance is regulated reciprocally during the cell cycle by ubiquitin mediated proteolysis (Sakaue-Sawano et al, 2008).

Throughout the cell cycle DNA replication is stringently controlled to ensure the genome is only replicated once per cell cycle. Cell cycle protein Cdt1 is important in licensing DNA for replication in G1 and is directly inhibited by DNA replication inhibitor Geminin during S/G2/M (Wohlschlegel et al., 2000). The abundance of Cdt1 and Geminin is regulated by E3 ligases SCF^{Skp2} and APC^{Cdh1} respectively (McGarry & Kirschner, 1998; Nishitani et al., 2000). SCF^{Skp2} and APC^{Cdh1} are direct substrates and inhibitors of each other and oscillate in abundance throughout the cell cycle with SCF^{Skp2} being active during S and G2 phases and APC^{Cdh1} in late M and G1 phases (Ang & Harper, 2004; Ramla Benmaamar, 2005; Vodermaier, 2004). This results in an accumulation of Cdt1 during G1 and Geminin during S/G2/M phases of the cell cycle (fig 1.4A). When designing the Fucci probes the Miyawaki lab fused the E3 ligase recognition domain of Cdt1 and Geminin to mKO (monomeric version of Kusabira Orange) and mAG (the monomeric version of Azami Green) respectively (Sakaue-Sawano et al., 2008) (fig 1.4B). The Fucci probes' oscillating abundance mirrors that of the endogenous Cdt1 and Geminin, resulting in the nucleus of cells being labelled red during G1, yellow in the G1/S transition, green in late S, G2 and M phases and are briefly unlabelled during cytokinesis (fig 1.4C). Cells in G0 are also labelled red and are indistinguishable from cells in G1. The Fucci mouse was created by random transgenesis of the two constructs to create separate mouse

lines. Expression is driven by the CAG promoter (Niwa et al., 1991). The mKO2-hCdt1(30/120) and mAG-hGem(1/100) mice are then crossed to generate a ubiquitous Fucci expressing mouse. It is important to note that it is possible to determine cell cycle stage with expressing a single Fucci probe, however, the use of two probes greatly aids in live cell tracking. The Fucci mouse, have several key limitations. First, the two Fucci probes are expressed from separate loci complicating mouse colony maintenance. Second, the constructs were not inducible, making it impossible to follow cell cycle progression in specific cell lineages. Third, the mice were generated by random transgenesis, which is prone to silencing and can exhibit variation in expression between different tissues(Sakaue-Sawano et al., 2008, 2013). In fact eight mAG-hGem(1/110) and 16 mKO2-hCdt1(30/120) transgenic mice lines were originally generated with the majority of work being done with the combination of mAG-hGem(1/110) #504 and mKO2-hCdt1(30/120) #596 lines due to their near ubiquitous expression (Sakaue-Sawano et al., 2008), although, with the notable exception of the hematopoietic linage which can be visualized with a combination of mAG-hGem(1/110) #474 and mKO2-hCdt1(30/120) #610 (Sakaue-Sawano et al., 2013). Since the publication of the first Fucci mouse in 2008 two updated versions have been published to overcome these limitations (Abe et al., 2013). In both cases the original fluorophores mAG and mKO2 have been replaced with mVenus (mVenus-hGem(1/110)) and mCherry (mCherry-hCdt1(30/120)) respectively to give better colour contrast and spectral separation from GFP (Sakaue-Sawano et al., 2011). *R26p-Fucci2* is a constitutive bidirectional reporter in which expression of the Fucci2 probes is driven using a fragment of the *ROSA26* promoter flanked by chicken hypersensitive site 4 (cHS4) insulator sequences (Potts et al., 2000). The mouse was generated by random transgenesis and is homozygous lethal resulting in lines being maintained heterozygous and 50% of experimental crosses not containing the transgene (Abe et al., 2013). *R26-mVenus-hGem(1/110)* and *R26-mCherry-hCdt1(30/120)* are separate Cre inducible alleles targeted to *ROSA26* with expression driven by the endogenous *ROSA26* promoter with low levels of expression being reported in the *R26-mCherry-hCdt1(30/120)* allele (Abe et al., 2013). In conclusion

no stably expressed, inducible single Fucci expressing construct exists to date, which is currently limiting the functionality of the Fucci system in mammalian research.

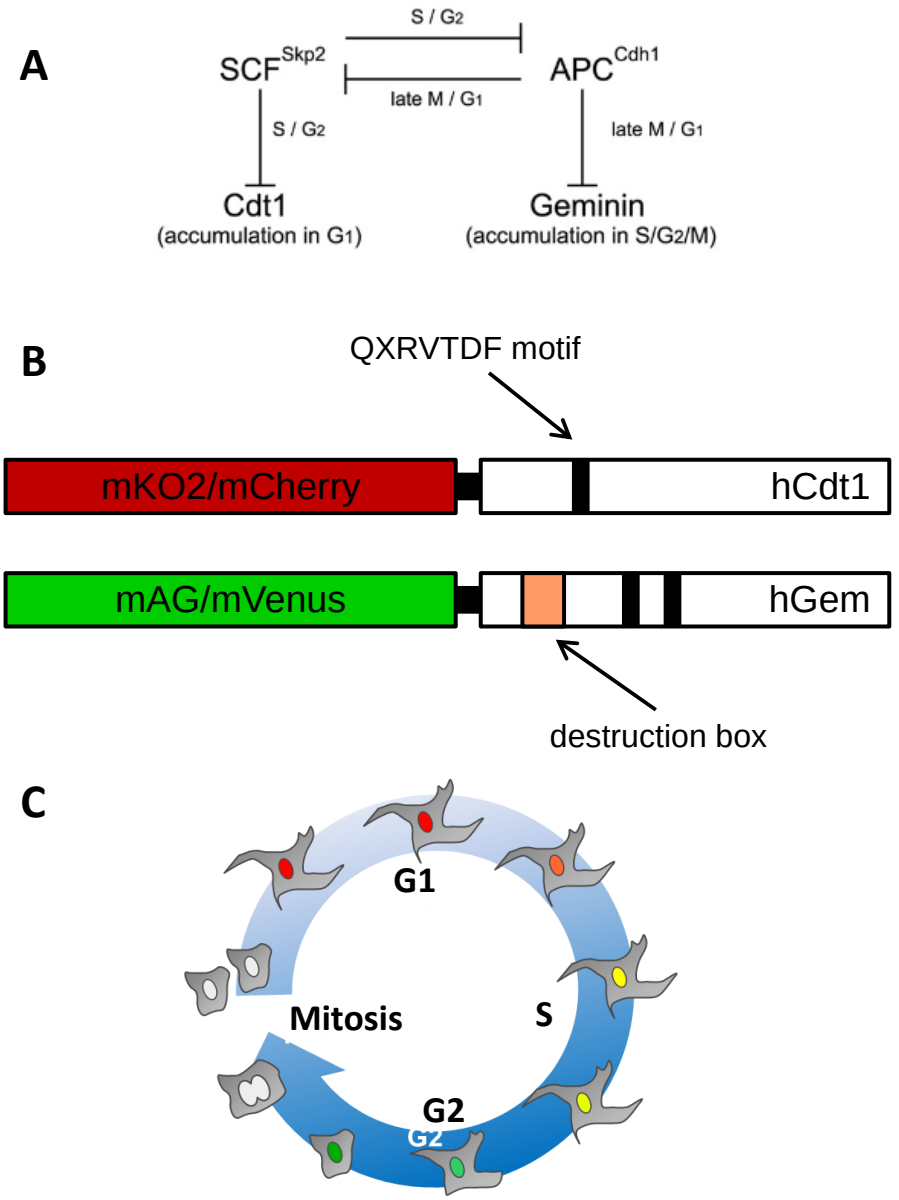

Fig 1.4: The Fucci system. (A) E3 ligases SCF^{Skp2} and APC^{Cdh1} are direct inhibitors of each other resulting in their cyclic activity in S/G2 and late M/G1 phases of the cell cycle respectively. Cdt1 is a direct target of SCF^{Skp2} and accumulates in G1 where it is involved in DNA licensing. Geminin is a direct target of APC^{Cdh1} and accumulates in S/G2/M where it inhibits DNA replication. **(B)** The Fucci probes contain the E3-ligase recognition domain of hCdt1 and hGminin fused to a red (mKO2/mCherry) and green (mAG/mVenus) fluorescent protein. These truncated fusion proteins are expressed continuously but their abundance is regulated by E3 ligases SCF^{Skp2} and APC^{Cdh1} so that they replicate endogenous Cdt1 and Geminin protein levels. **(C)** Fucci expressing cells are labelled red during G1, yellow during the G1/S transition, green during late S/G2/M phases and are briefly unlabelled during cell division. Fig 1.3A adapted from Sakaue-Sawano et al., 2008.

1.6 Aims

- The characterisation of the R26Fucci2aR mice line designed by Dr Richard Mort (Edinburgh University). The R26Fucci2aR moue line contains an inducible bicistronic version of the Fucci system, which overcomes the limitations with the previously published Fucci mouse models, and greatly improves the usability of the Fucci system.
- The development and characterisation of four novel tricistronic adaptations of the Fucci2a construct to visualise cell cycle progression simultaneously with apoptosis, cytokinesis and cilia. With the aim to generate tricistronic reporter mouse lines with clear applications for developmental and disease research.
- Illustrate the usefulness of the R26Fucci2aR mouse in two developmental systems:
    - Using an *ex vivo* skin culture system and time-lapsing imaging approach I will describe melanoblast migration during development and investigate the role of Kit signalling.
    - Using a combination of imaging and RNA sequencing techniques I will investigate the differences in gene expression and behaviour of cells in the branching and non-branching regions of the developing lung epithelium.

2 Chapter 2: Characterisation of *R26R-Fucci2a* mouse

2.1 Introduction

2.1.1 Designing a bicistronic construct

The two most common methods for achieving bicistronic gene expression are by the use of a viral internal ribosome entry site (IRES) or a 2A self-cleaving peptide. IRESs are non-coding RNA fragments which allow for cap independent initiation of translation (Hellen & Sarnow, 2001). Bicistronic gene expression is achieved by cloning a tandem cDNA sequence either side of the IRES sequence. Both genes are then translated into separate proteins by cap dependent translations at the first open reading frame (ORF) or cap independent initiation of translation at the IRES. However IRESs have two major flaws. First, IRESs are generally at least 500 nucleotides long, which can complicate cloning strategies, especially if multiple IRESs are used to generate mulicistronic constructs. Second, the dual translational initiation site rarely produces equimolar amounts of protein from each gene (Bochkov & Palmenberg, 2006; Borman et al., 1996; Mizuguchi et al., 2000). It is important to note that the original isolated IRES sequence has been commercially adapted over the years in different constructs resulting in different levels of translational efficiently (Bochkov & Palmenberg, 2006). The pCITE-1 (Novagen), due to a cloning error that was later rectified in the pCITE-2 plasmid, contains a mutation in a highly conserved bifurcation loop which is critical for the initiation of translation (Pestova et al., 1996). This change in conformation of the bifurcation loop has resulted in a variation of translation efficiencies of the two IRESs in different contexts due to the recruitment of different translation initiation proteins (Kaminski et al., 1994). In addition a third widely used IRES containing construct, pIRES (clonetech), contains an attenuated IRES sequence to reduce the cap independent translation to similar levels of cap dependent levels (Rees et al., 1996). This has been shown to result near equimolar production of proteins in a bicistronic construct. However this is at the cost of a significant reduction in the production of the cap

independently translated protein and therefore is not suitable if high levels of protein production are required (Bochkov & Palmenberg, 2006).

2A peptides were identified in the foot-and-mouth disease virus (FMDV) as a 19 amino acid sequence promoting cleavage of polyproteins and are an attractive alternative to IRESs (Ryan et al., 1991). Cleavage occurs between between the penultimate glycine residue and the final proline contained within the conserved C-terminal of the 2A peptide by a process of "ribosomal skipping" thereby allowing bicistronic expression from a single ORF (Donnelly et al., 2001). Almost 100% cleavage efficiency has been reported in bicistronic constructs expressed in human cell lines, zebrafish and mice (Kim et al., 2011). Although variation in cleavage efficiency was reported between the different 2A sequences, with *porcine teschovirus-1 2A* (P2A) being the most efficient in all scenarios.

The mouse *ROSA26* locus is located on chromosome 6 and was identified by gene trap experiments to contain promoter sequences capable of driving ubiquitous gene expression in all embryonic tissues (Friedrich & Soriano, 1991; Zambrowicz et al., 1997). Subsequent reporter knock-in mice to the *ROSA26* locus have confirmed *ROSA26* to be a permissive locus for the ubiquitous expression of transgenes with no reported adverse affects to the mouse (Soriano, 1999; Srinivas et al., 2001), making *Rosa2*6 the locus of choice for the safe harbouring of transgenes. In strategies that incorporate an exogenous promoter sequence into *ROSA26*, transcriptional interference from the endogenous *ROSA26* has been reported, therefore it has been suggested that transgenes should be inserted in the reverse orientation to ensure maximal expression (Strathdee et al., 2006).

Another commonly used permissive locus for the expression of transgenes is the *hypoxanthine phosphoribosyltransferase (HRPT)* locus (Bronson et al., 1996). Transgenes expressed from this locus have shown expression in a range of tissues including the heart, kidney and endothelial lineages with similar orientation effects reported (Cvetkovic et al., 2000; Guillot et al., 2000; Habets et al., 2003; Palais et al., 2009). However the *HRPT* locus is located on the X chromosome and is therefore susceptible to X-inactivation. It has been shown by targeted expression of GFP from

the *HRPT* locus that X-inactivation of GFP expression does occur, including when GFP is flanked by insulator sequences derived from the chicken β-globin locus (Ciavatta et al., 2006). Considering this *ROSA26* is a more desirable harbour for the ubiquitous expression of transgenes.

A comparative study of expression levels driven by different promoters from the *ROSA26* locus has shown CAG to produce the highest level of expression (Chen et al., 2011). The CAG promoter is a synthetic promoter which contains the cytomegalovirus early enhancer element: the promoter, first exon and first intron of the chick b-actin gene and the b-globin splice acceptor sequence (Miyazaki et al., 1989). In the comparative study by Chen and colleagues, the expression of bioluminescent reporter luciferase was driven by promoters CMVd1, CMV, β-actin, MC1, PGK, EF1α, Ubc, CAG or the endogenous *ROSA26* promoter in mESCs to ensure that expression is driven from a single locus. Using bioluminescence as a measure of expression, mESCs expressing luciferase under the CAG promoter were two times brighter than the next promoter Ubc and bioluminescence was reported to be almost ten times higher than the endogenous *ROSA26* promoter (Chen et al., 2011).

Inducible expression of a reporter is essential for visualising subsets of cells within the soup of a developing organism. The bacteriophage P1 recombinase Cre is a tyrosine recombinase enzyme, which is able to catalyse site specific recombination between two DNA recognition sites known as LoxP sites (Sternberg & Hamilton, 1981). The Cre-recombinase catalyses cleavage within a spacer region within the LoxP site between two 13 pair inverted repeats and initiates recombination between the two LoxP sites (Hoess & Abremski, 1985). For example, it has been shown in yeast that inserting the *LEU2* gene flanked by LoxP sites enables Cre-recombinase dependent excision of *LEU2* (Sauer, 1987). In the generation of transgenic mice the Cre-LoxP system has been utilised for tissue specific expression of a transgene by crossing a tissue specific Cre line, which express Cre-recombinase under the control of a lineage specific promoter with a line containing an inducible allele (Delmas et a., 2003; Engert et al., 2009; Lakso et al., 1992). The expression of Cre recombinase

in a specific subset of cells excises a floxed transcriptional stop cassette to active expression of the transgene specifically within those cells (Soriano, 1999; Srinivas et al., 2001). The LoxP system has also be utilised to lineage specifically disrupt gene function by flanking essential exons with LoxP sites (F. Lin et al., 2003; Plosa et al., 2014; Zhu et al., 2001a).

Temporal control over Cre-recombinase activity has also been development by fusing Cre-recombinase to the mutated ligand binding domain of the human oestrogen receptor (Cre-ERT) (Feil et al., 1996). This sequesters Cre-recombinase in the cytoplasm therefore preventing recombination at LoxP sites. Administration of tamoxifen or 4-0HT (a synthetic oestrogen ligand) results in the translocation of Cre-ERT to the nucleus and subsequent recombination at LoxP sites (Brocard et al., 1997; R Feil et al., 1996). An improved mutated version of cre-ERT containing the triple mutation G400V/M543A/L544A (Cre-ERT2) has been shown to have higher efficiency and sensitivity of tamoxifen induced recombination (Engert et al., 2013; Feil et al., 1997; Indra et al., 1999).

The ever increasing list of publically available tissue specific Cre lines and the advent of chemically inducible Cre lines gives researchers unprecedented precision of transgene expression and gene manipulation in time and space. However, although transgenic Cre mouse lines have been used with few reported side effects, it is important to note that prolonged exposure of high levels of Cre-recombinase in mammalian cells has been reported to result in chromosomal rearrangements, an increase in aneuploidy and impaired cell cycle progression (Loonstra et al., 2001). In addition high expression of Cre-recombinase under the control of the *Protamine 1 (Prm1)* promoter in postmeiotic spermatids resulted in 100% sterility due to chromosomal rearrangements (Schmidt et al., 2000). This suggests Cre-recombinase may have the potential to induce promiscuous LoxP independent recombination events and therefore the expression level and exposure time of Cre-recombinase should be considered.

In the first chapter of this thesis I will describe the characterisation of the cre-inducible bicistronic *R26Fucci2aR* reporter mouse. This mouse contains the Fucci2a

construct (discussed below) targeted to the *ROSA26* locus in the reverse orientation with expression driven by the CAG promoter and overcomes the limitations of the previously published Fucci mice. This work was published in 2014 (Mort et al., 2014). The initial construct design, characterisation in 3T3 cells and ES targeting, was undertaken by Dr Richard Mort (The University of Edinburgh) outlined below.

2.1.2 Work leading to project

2.1.2.1 Characterisation of Fucci2a in 3T3 cells

The bicistronic Fucci reporter construct coined "Fucci2a" was constructed by fusing Fucci2 probes (Abe et al., 2013) mVenus-hGem(1/110) with mCherry-hCdt1(30/120) separated by the self-cleaving peptide *Thosea asigna* virus 2A (T2A) (fig 2.1A). Because the majority of the amino acids from the T2A peptide are left on the C-terminus of the protein in the N-position (De Felipe, 2004), The construct was developed with the probes in both positions in order to test if the additional residue affected the cell cycle specificity or nuclear localisation of either probe (fig 2.1L). Both constructs were characterised in 3T3 stable cell lines generated using the Flp-In system (Invitrogen). The Flp-In system enables generation of a stable cell line expressing a single copy of your chosen transgene via site-specific Flp recombination mediated integration (fig 2.1B). Live imaging of both cell lines showed populations of cells labelled with mVenus-hGem(1/110) and mCherry-hCdt1(30/120) and a sub-population labelled with both probes. The mVenus-hGem(1/110) probe in the 5V3C-Fucci2a cell line (mVenus-hGem(1/110)-mCherry-hCdt1)30/120)) was shown to be partially mislocalised to the cytoplasm due to addition of a few amino acids to the C-terminus (fig 2.1C-K). This mislocalisation is likely due an interference with the nuclear localisation signal of two clusters of arginine and lysine residues located between amino acids 28-79 (Boos, Lee, Thompson, & Kroll, 2006; Okorokov et al., 2004). The 5C3V-Fucci2a construct, from now on referred to just as Fucci2a, was taken on for further characterisation by time-lapse imaging and FACS analysis. Time-lapse imaging showed normal cell behaviour and mitosis with cyclic

abundances of mCherry-hCdt1(30/120) and mVenus-hCdt1(1/110) which appeared to label G1 and S/G2/M phases of the cell cycle respectively (fig 2.2A and B sup video 1). The cell cycle specificity of the two probes was confirmed by FACS analysis using DAPI staining as a measure of DNA content. Red labelled cells were clearly in G1 and had a DNA content of 2n, whereas green labelled cells had a higher DNA content because they have replicated their DNA during S-phase and have a peak at 4n (fig 2.2C). To illustrate the ability to generate quantitative cell cycle data using the Fucci2a system, time-lapse imaging was performed on cultured 3T3 cells in 10% and 15% fetal calf serum (FCS). Individual cells were tracked and the changes in fluorescence of mCherry-hCdt1(30/120) and mVenus-hGem(1/110) measured and plotted against time to produce normalised fluorescence intensity plots from which the lengths of G1, G1/S, S/G2/M and total cell cycle length were calculated (fig 2.2B). 3T3 cells cultured in 15% serum showed a significant reduction in total cell cycle time from 25.62 ± 2.69 hours (n = 20 mitoses) to 20.23 ± 2.20 hours (n = 20 mitoses). This was primarily down to a shortening of G1 from 12.7 ± 2.57 hours to 8.90 ± 1.81 hours. A non-significant shortening of G1/S and S/G2/M was also seen (fig 2.2D).

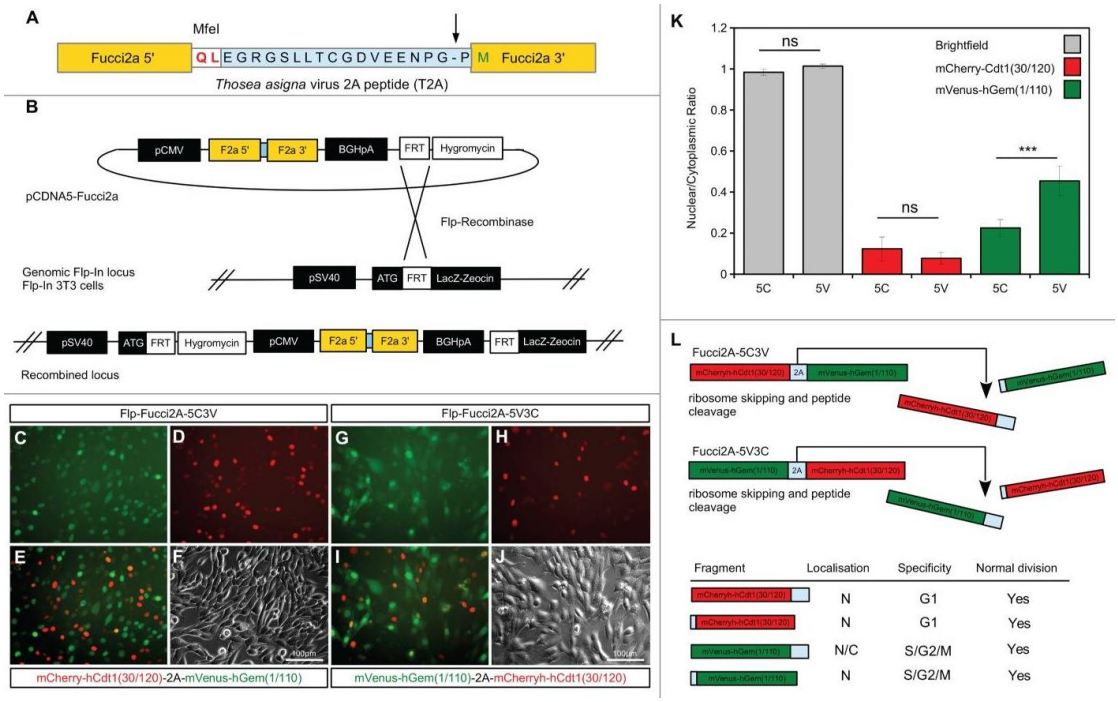

Fig 2.1: Design and validation of bicistronic Fucci2a expression constructs. (**A**) The Fucci2 probes mVenus-hGem(1/110) and mCherry-hCdt1(30/120) were fused using the *Thosea asigna* virus 2A peptide, the core T2A sequence is highlighted in blue and was inserted between the Fucci2 probes in both orientations. The T2A sequence comprises 18 amino acids, cleavage occurs between the final glycine and proline (arrow in A). In addition to these 17 amino acids 2 amino acids were added to create an MfeI restriction site for cloning; in total the 5′ Fucci probe has 19 amino acids added to its C-terminus while the 3′ Fucci probe incorporates one additional amino acid. (**B**) The resulting 2 versions of Fucci2a were termed Fucci2a-5C3V (**5**′ m**C**herry-hCdt1(30/120) **3**′ mVenus-hGem(1/110)) and Fucci2a-5V3C (**5**′ mVenus-hGem(1/110) **3**′ m**C**herry-hCdt1(30/120)) and were targeted to a single locus in NIH 3T3 cells using the Flp-In system to create 2 isogenic polyclonal Fucci2a cell lines. (**C–J**) Imaging of the resulting stable cell lines revealed that the addition of the 19 T2A amino acids resulted in mVenus-hGem(1/110) partially loosing its nuclear localization, mCherry-hCdt1(30/120) remained nuclear with the same addition (compare C to G and D to H). (**K**) Quantification of the nuclear to cytoplasmic ratio for both Fucci2 probes for the 2 Fucci2a cell lines revealed a statistically significant increase in the nuclear to cytoplasmic ratio of mVenus-hGem(1/110) in the Fucci2a-5V3C cell line (2-way ANOVA P = <0.0001, Tukey's HSD P < 0.0001). (**L**) Summary of the initial characterization showing that only mVenus-hGem(1/110) is sensitive to the additional 18 amino acids. Error bars in K = 95% Confidence interval. Figure taken from Mort et al., 2014.

2.1.2.2 Calculating population cell cycle times from the length of S/G2/M

In an asynchronous population of cycling cells, with the assumption that all cells in the population are cycling, it is possible to calculate a cell cycle time if you measure the length of a particular cell cycle phase and the proportion of cells within that phase using the following equation,:

Cell cycle time = length of cell cycle phase / proportion of cells within that phase

This method has been used extensively in single and double labelling of cells with thymidine analogues to estimate a cell cycle time for a population of cells (see 1.4.2 for detailed example) (Martynoga et al., 2005; Nowakowski et al., 1989; Quinn et al., 2007). In single labelling thymidine experiments thymidine is constantly administered and the time taken for all cells to be labelled measured to give the length of G2/M/G1, which is then divided by the proportion of unlabelled cells at the first time point (Nowakowski et al., 1989). For dual labelling experiments two injections of different thymidine analogs are injected. The time between the injections is divided by the proportion of cells which have left S-phase (labelled with the first thymidine analog but not the second) to calculate the length of S-phase. This is then divided by the proportion of cells within S-phase at any one time point. Using the Fucci system it is therefore be possible to calculate cell cycle times for a population of cells by measuring the length of S/G2/M and dividing that by the proportion of cells in S/G2/M or mVenus-hGem(1/110) positive cells:

Cell cycle time = length of S/G2/M / proportion of cells in S/G2/M

To test this theory the cell cycle times of cells cultured in 10% and 15% serum were calculated resulting in a cell cycle time of (mean ± CI) 25.10 ± 2.50 hours and 18 ±

1.48 hours respectively. A statistical difference between these two calculated rates was confirmed by student's t-test ($p < 0.001$) and was in close agreement to rates calculated by direct measurement of cell cycle length from time-lapse imaging (fig 2.2D).

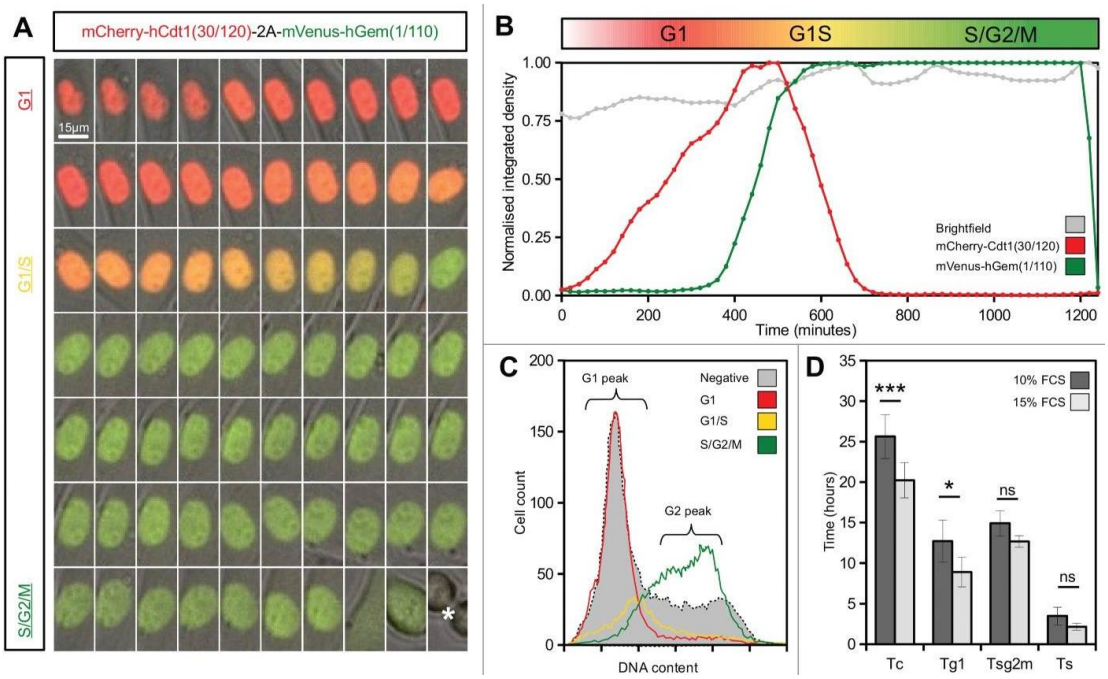

Fig 2.2: Live imaging of Fucci2a stable 3T3 cell line. (**A**) A montage of a time-lapse sequence showing nuclear expression of Fucci2a throughout the progressing cell cycle. mCherry accumulates during G1 and is lost during the G1/S transition as mVenus reaches its peak. Both probes are lost at mitosis (asterisk in final panel). (**B**) Plot of the relative intensities of the Fucci2a probes during a single cell cycle showing the mCherry and mVenus peaks. (**C**) Confirmation by FACS that the Fucci2a probes accurately predict cell cycle phase defined by DAPI staining for DNA content. Cells positive for mCherry peak in the G1/2n population, while mVenus positive cells peak in the 4n population immediately prior to mitosis. (**D**) Quantification of the length of cell cycle phases by live cell imaging and image analysis. Increasing the serum concentration from 10–15% resulted in a statistically significant shortening of the cell cycle (students t-test with Bonferroni correction $P < 0.001$) and a reduction in the length of G1 (students t-test with Bonferroni correction $P < 0.05$). Tc = cell cycle time; Tg1 = G1 length; Tsg2m = S/G2/M length; Ts = G1/S transition length. Error bars in D = 95% Confidence interval. Figure taken from Mort et al., 2014.

2.1.2.3 Targeting to *ROSA26* in mESCs

The Fucci2a mouse was generated by homologous recombination to the *ROSA26* locus in mouse embryonic stem cells (mESCs) (fig 2.3). A Neomycin stop cassette flanked by LoxP sites was inserted between Fucci2a and the CAG promoter to allow for tissue specific expression and the whole construct inserted in the reverse orientation to limit transcriptional interference from the endogenous *ROSA26* promoter. Targeting was undertaken by Joe Mee from the Scottish Centre for Regenerative Medicine Transgenic Service. Subsequent screening of targeted ES cells was performed by Dr Richard Mort by 5' and 3' long range PCR spanning the *ROSA26* homology arms (fig 2.3).

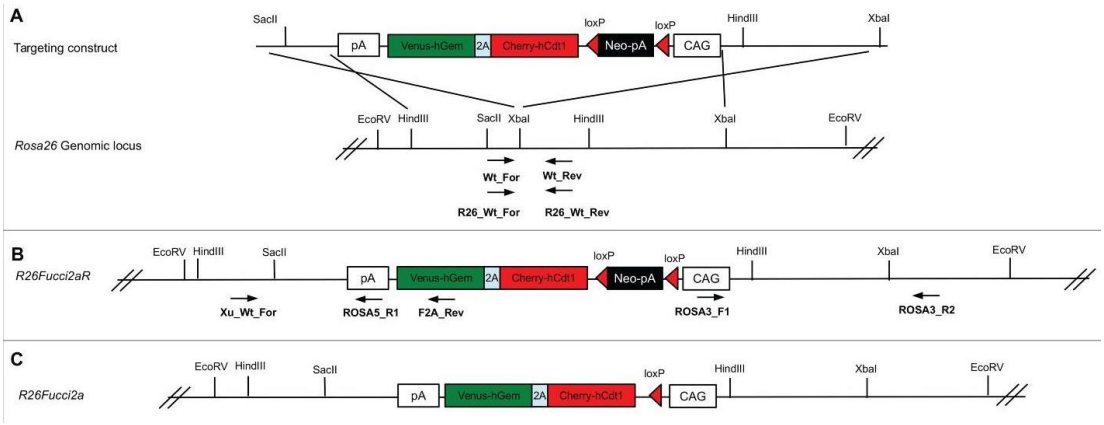

Fig 2.3: Generation of *R26Fucci2aR* ES cells. A single copy of the Fucci2a transgene under the control of the *CAG* promoter was inserted into the *Rosa26* locus by homologous recombination in mouse embryonic stem cells (mESCs). (**A**) Targeting construct used, a stop cassette containing a *loxP* flanked neomycin resistance gene and polyadenylation sequence was inserted between *CAG* and *Fucci2a*, this construct was inserted in the reverse orientation to the endogenous *Rosa26* promoter to avoid transcriptional interference. (**B**) The targeted *R26Fucci2aR* inducible allele, screening for correct homologous recombination was done using PCR across the 5′ and 3′ homology arms of the targeting construct. To test the *R26Fucci2aR* ES cell lines they were transfected with a Cre-recombinase expressing plasmid (pPGK-Cre), plated at low density and screened for G418 sensitive Fucci2a expressing clones (*R26Fucci2a*). (**C**) The targeted *R26Fucci2a* allele after Cre-mediated excision of the *floxed-Neo-pA* stop cassette. Figure adapted from Mort et al., 2014.

2.2 Results

2.2.1 Fucci2a expression in mESCs

Mouse ESCs have a short cell cycle compared to somatic cells which is characterised by a short G1 phase. A link has been proposed between the length of G1 and the onset of differentiation with a lengthening of G1 seen in differentiating mESCs and differentiation being induced by chemical lengthening of G1 (Jovic et al., 2013; Roccio et al., 2013). In both these studies the fucci system was used to directly follow cell cycle progression in cultured mESCs. Jovic et al used mESCs derived from a *R26-mCherry-hCdt1*/*R26-mVenus-hGem(1/110)* cross, while Roccio et al dual infected mESCs with the original FUCCI lentiviral vectors (Abe et al., 2013; Sakaue-Sawano et al., 2008). In both studies the Cdt1 probe did not label G1 which was put down to G1 being too short for the probe to accumulate (G1 = 2.2 hours (Roccio et al., 2013). Interestingly it has been reported that Cdt1 levels are higher in mitotic mESCs compared to differentiated cells (Ballabeni et al., 2011). This is thought to compensate for high CDK activity during S/G2/M phases of the cell cycle and enables efficient loading of MCM proteins onto chromatin for rapid initiation of DNA replication. This would therefore suggest that the Cdt1 probe is not faithfully tracking endogenous Cdt1 abundance in these systems. To investigate if this is the case in our system and if the shortness of G1 is the cause of the absence of the Cdt1 probe, *R26Fucci2aR* ES cells (made by targeted insertion into *ROSA26* see fig 2.3) were transfected with a Cre-recombinase expressing plasmid (pPGK-Cre), to excise the neo-stop cassette and induce expression of Fucci2a. Upon initial live imaging the majority of cells appeared to be labelled with mVenus-hGem(1/110) , with a few cells around the edge of colonies labelled with mCherry-hCdt1(30/120) (fig 2.4A). However FACS analysis showed the majority of cells (52±8.3%) were unlabelled with either probe having similar proportions to what has been previously reported (Roccio et al., 2013) (fig 2.4B). Cell cycle analysis of negative and mVenus-hGem(1/100) positive cells by FACS, using DAPI intensity as a measure of DNA content, confirmed mVenus-hGem(1/100) positive cells to be in S/G2/M phases of the cell cycle and negative cells to be in G1 (fig 2.4C). This suggests that the

mCherry-Cdt1(30/120) levels does not faithfully reflect endogenous Cdt1 protein level in mESC.

To confirm expression of Fucci2a from the *ROSA26* locus faithfully labeled G1 in differentiated cells, *R26Fucci2a* ES cells were differentiated by culturing with retinoic acid and LIF removed. After 4 days an increase in the proportion of mCherry-hCdt1(30/120) positive cells was seen and confirmed by FACS (fig 2.5A and B). Cell cycle analysis confirmed mCherry-hCdt1(30/120) positive cells are in G1 and therefore showing the loss of mCherry-hCdt(30/120) is an ES cell specific problem in accordance with previous reporters using other Fucci systems (fig 2.5C). A previous report has suggested an adaptation in mESC where there is an increase in the abundance and expression of Cdt1 to counteract the high levels of G2 cyclin dependent kinases (Ballabeni et al., 2011). Considering this, it is possible the length of G1 is too short for mCherry-hCdt(30/120) to accumulate before it is degraded upon entry into S-phase. However it is also possible that the abundance of mCherry-hCdt1(30/120) is being regulated differently to endogenous Cdt1 due to its truncation which has removed potentially stabilising interactions.

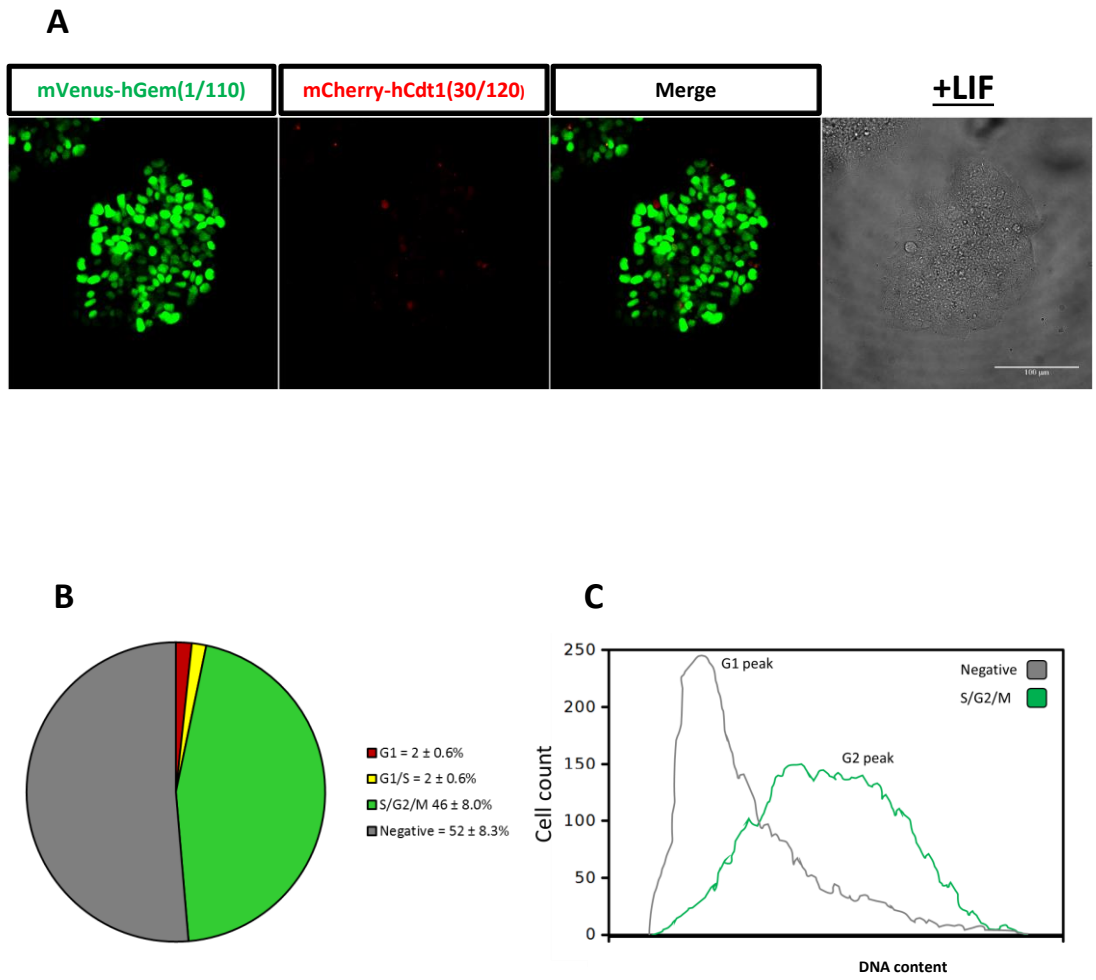

Fig 2.4: Expression of Fucci2a in mESCs. Characterisation of Fucci2a expression in mESCs was achieved by transfection of the *R26Fucci2aR* ES cell line with a Cre-recombinase expressing plasmid (pPGK-Cre). **(A)** Confocal imaging showing the majority of cells within an ES clone labelled with mVenus with a few mCherry positive cells around the edge of the clone. **(B)** FACS analysis shows the majority of cells unlabelled with either probe (n = 7 sorts). **(C)** Quantification of DNA content within the different labelled populations achieved by DAPI staining FACS sorted cells and quantification by FACS showing the majority of unlabelled cells in G1. Error in pie chart B = 95% Confidence interval.

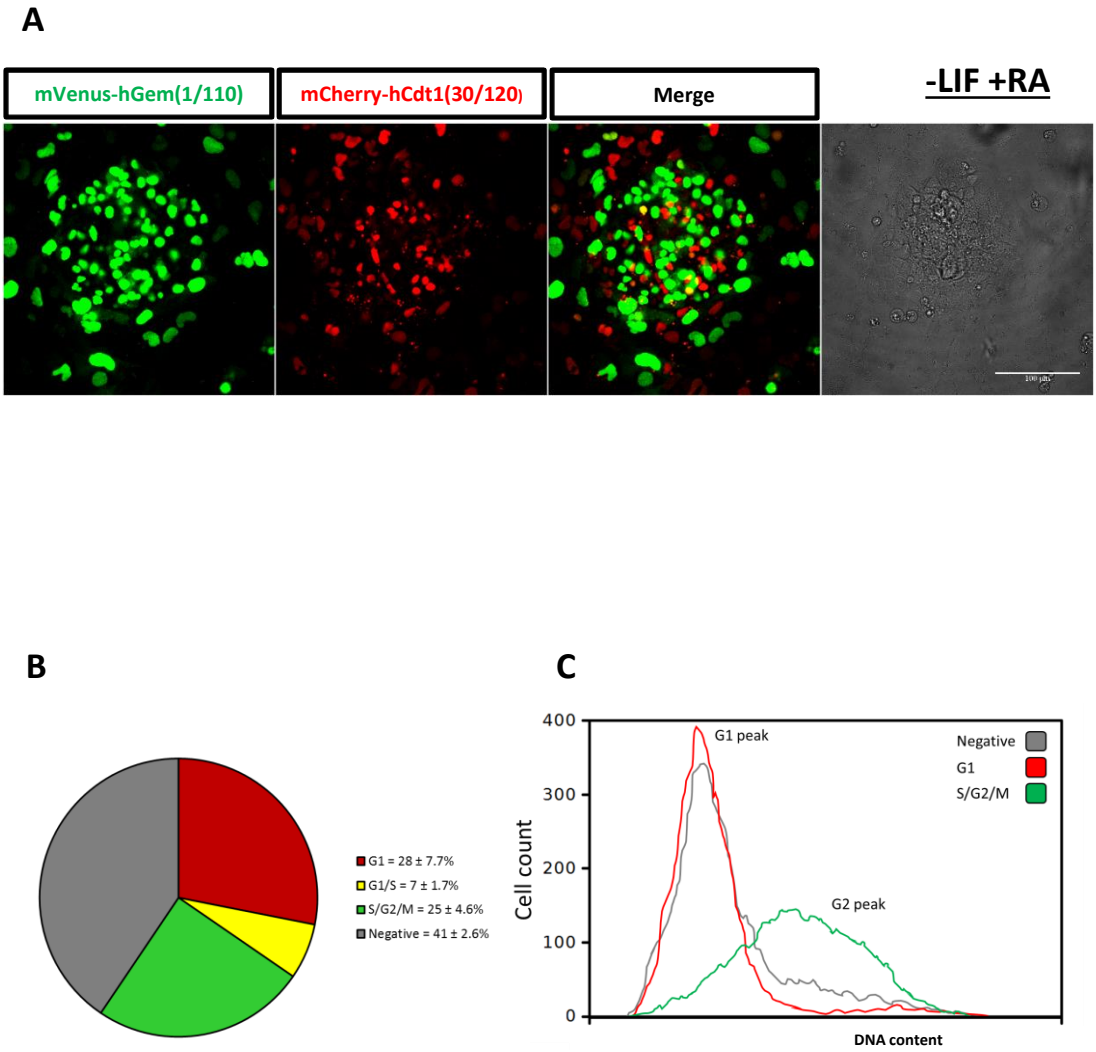

Fig 2.5: mCherry-hCdt1(30/120) returns in differentiated mESC (A) Differentiation of *R26Fucci2aR* ES cells by culturing without lif and in the presence of 1mM retinoic acid (RA) for four days results in an increase in the proportion of mCherry labelled cells. **(B)** This is confirmed by FACS (n = 4 sorts). **(C)** DNA content analysis by FACS confirms the mCherry population are in G1. Error in pie chart B = 95% Confidence interval.

To test if G1 is too short for mCherry-hCdt1(30/120) to accumulate the length of G1 was measured directly from time-lapse imaging. To allow tracking of ES cells through the entire cell cycle a stable *R26Fucci2a* ES cell line expressing H2B-Cerulean was generated by transfection of linearised pCerulean-H2B-6 followed by G418 selection (fig 2.6A). (sup video 2 for an example time-lapse). By manually tracking cells and measuring the changes in the fluorescence intensity of mVenus-hGem(1/100) the length of G1 could be determined by measuring the length of time between mitosis and the accumulation of mVenus-hGEM(1/110) from normalised fluorescence intensity plots (fig 2.6B). To aid with image analysis fluorescent cells were mixed with non-fluorescently labelled E14 mESCs so individual cells could be tracked. The mean cell cycle time for cycling mESC cultured under standard conditions (containing LIF) was 12.15± 2.94 hours, with G1 and S/G2/M accounting for 3.65±1.71 and 8.50±2.51 respectively (fig 2.6C and D). In Fucci2a 3T3 cells we have previously shown that it takes 2 hours for the mCherry-Cdt1(30/120) probe to accumulate after mitosis (fig 2.2B), which suggests that the reason we are not seeing mCherry-Cdt1(30/120) in mESC is not due to G1 being too short. Unfortunately, after multiple attempts with multiple different Cdt1 antibodies I was unable to detect endogenous Cdt1 in mESC lysate by western blot, therefore making it impossible to determine if mCherry-hCdt1(30-120) faithfully recapitulates endogenous Cdt1 levels in mESCs.

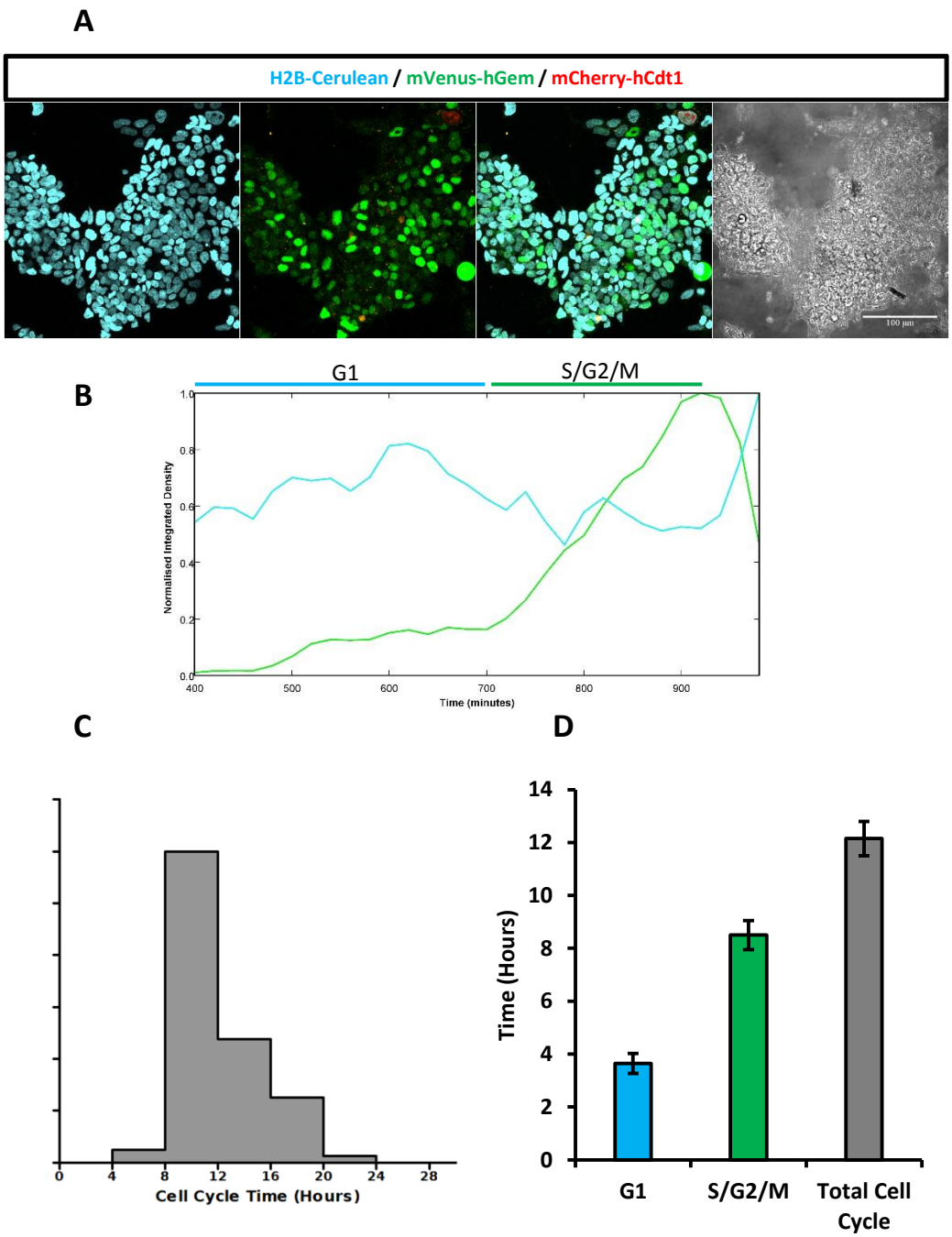

Fig 2.6: G1 in mESCs is long enough for mCherry-hCdt1(30/120) to accumulate. **(A)** Confocal image taken from Fucci2a mESCs stability expressing H2B-Cerulean after G148 selection. **(B)** Normalised fluorescent intensity plot of a single tracked mESC progressing through the cell cycle. **(C)** Histogram of mESC cell cycle times when cultured in serum. **(D)** Quantification of time spent in each stage of the cell cycle measured by manual tracking and normalised fluorescence intensity plots. (n = 100) Error bars in (C) = 95% Confidence interval.

2.2.2 Characterisation of *R26Fucci2aR* mouse

2.2.2.1 Regionalised expression of Fucci2a in *R26Fucci2aR*$^{+/Tg}$/*CAG::Cre*$^{+ve}$ embryos

Characterisation of the *R26Fucci2aR* mouse line was achieved by crossing with the ubiquitous *CAG::Cre* (Sakai & Miyazaki, 1997), followed by live imaging of a selection of different tissues (fig 2.7A-P). In the E11.5 limb bud there are distinct regions of mesenchyme in which cells are in G1 or G0, labelled in red (fig 2.7F), and were starting to condense into the presumptive digits. This is in stark contrast to the interdigitary mesenchyme (fig 2.7E), which at this point was still highly proliferative with the majority of cells being in S/G2/M stages of the cell cycle (fig 2.7E-H). The pattern of mCherry-hCdt(30/120) positive cells is similar to that reported for Sox9 expression at e12.5 (Akiyama et al., 2002). Sox9 expression was shown to be necessary for bone and cartilage development in the limb development. The overlapping patterns therefore show differentiation of the limb mesenchyme is coupled with a decrease in proliferation in the regions of the presumptive digits.

In the lung there appeared to be a gradient of highly proliferating cells within the actively branching regions labelled with mVenus-hGem(1/110), followed by a steadily higher proportion of cells in G1 in the more proximal non-branching regions. With almost all cells within the most proximal bronchial regions being in G1/G0 labelled with mCherry-hCdt1(30/120) (fig 2.7I-L). This is in coherence with *ex vivo* lung cultures where Brd-U positive cells reside in the actively branching regions (Nogawa et al., 1998).

In the kidney, the nephron progenitors contained within the cap mesenchyme were largely composed of cells in G1/G0 (fig 2.7N). In contrast cells within the ureteric bud as well as those adjacent to the bud were predominantly in S/G2/M (fig 2.7M). Inspection of *R26Fucci2aR* embryos (non-Cre excised) showed no fluorescence, therefore confirming the functionality of the floxed-Neo-pA stop cassette to prevent *Fucci2a* expression (data not shown).

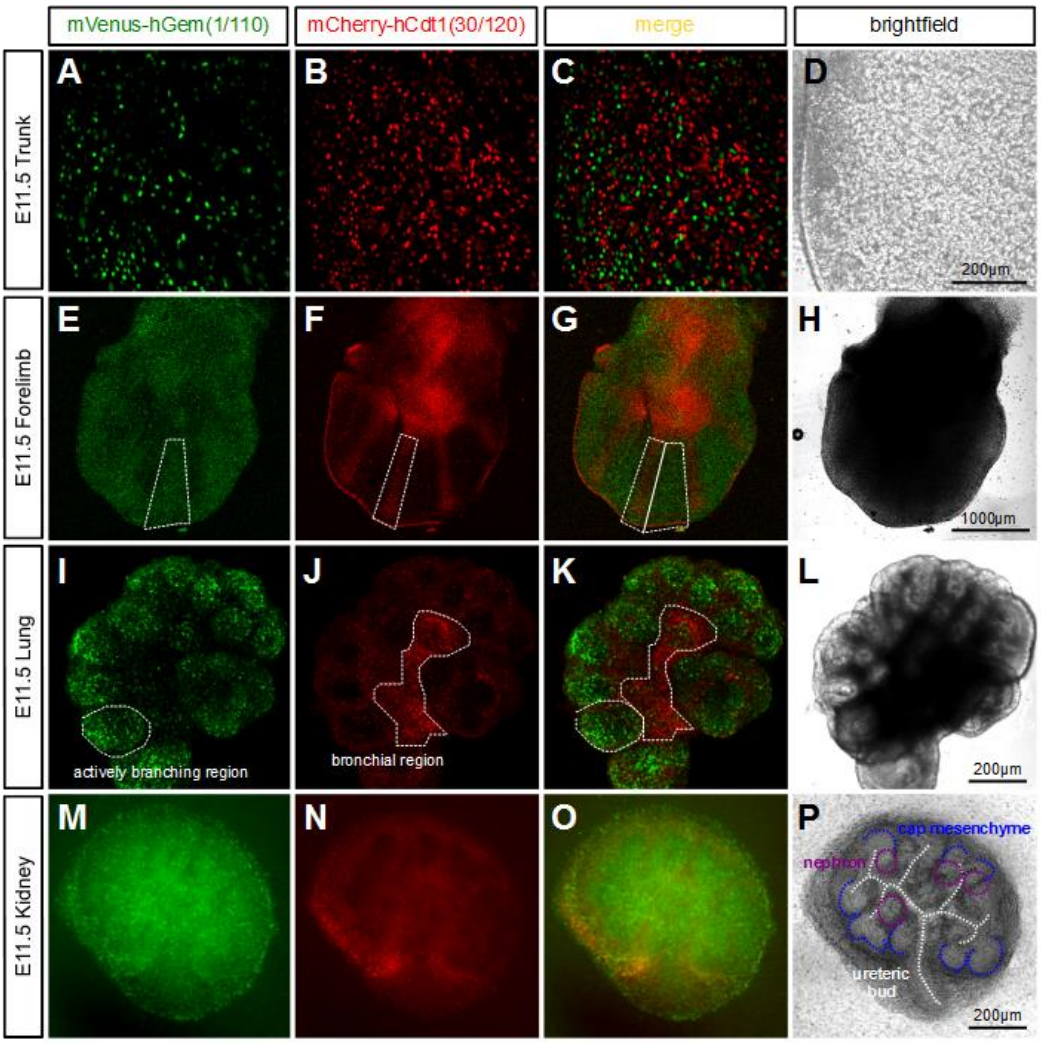

Fig 2.7: Analysis of live *R26Fucci2aR*$^{+/Tg}$*/CAG::Cre*$^{+/-}$ embryos. (A-D) Whole mount of e11.5 trunk. Specific nuclear localisation of mCherry-hCdt1(30/120) and mVenus-hGem(1/110) seen localised to different cells with a few double labelled cells. **(E-H)** Whole mount of an embryonic forelimb at e11.5. Distinct regions of mesenchymal cells in the regions of presumptive ditgits have slowed their cell cycle with the majority being labelled with mCherry-hCdt1(30/120). In contrast interdigitary mesenchyme is still highly proliferative. **(I-L)** Whole mount of an embryonic lung at e11.5. Actively branching regions are highly proliferative shown by the high proportion of mVenus-hGem(1/110) positive cells. In contrast the more proximal non-branching bronchial regions contain a high proportion of cells in G1/G0. **(M-P)** Whole mount of an embryonic kidney at e11.5. Cells within the cap mesenchyme are predominantly in G1/G0 labelled with mCherry-hCdt1(30/120) while the ureteric bud and presumptive nephrons are highly proliferative with the majorty of cells labelled with mVenus-hGem(1/110). Nils Lindstrom assisted with the imaging and interpretation of the kidney cultures. Figure adapted from Mort et al 2014.

2.2.2.2 Proliferation in the distal tip of the branching lung and kidney epithelium is restricted to elongating regions

Time-lapse imaging was performed on *R26Fucci2a*$^{+/Tg}$*/CAG::Cre*$^{+/Tg}$ embryonic lung and kidney cultures at e11.5 to investigate the role of cell cycle progression during branching morphogenesis. In the lung, successive rounds of epithelial branching was observed by both domain branching perpendicular from the elongating tip and bifurcation at the tip (fig 2.8B, E and H and sup video 3). In the actively elongating and branching regions the majority of cells were in S/G2/M stages of the cell cycle suggesting a high level of proliferation in these regions (fig 2.8C). There did not appear to be an increase in proliferation prior to bud formation or after suggesting proliferation is passive in the bud formation process. This is in concordance with the current belief that cell shape change and polarity are responsible for bud formation and orientated cell division drives subsequent elongation, as seen in other systems such as the drosophila trachea (Affolter & Caussinus, 2008; Nogawa et al., 1998). Although from these time-lapses it is impossible to tell if the plane of division is parallel to elongation. In the more proximal non-branching epithelium there is a high proportion of cells in G1/G0 suggesting a slowing down of the cell cycle in anticipation of differentiation into the ciliated, secretory and neuroendocrine cells lining the bronchial airways which occurs from e14.5. (Post et al., 2000; Rawlins et al., 2007; Tichelaar et al., 1999) (fig 2.8I). The surrounding lung mesenchyme contains a mixture of cells in all stages of the cell cycle but predominantly in G1/G0 suggesting that at this stage the mesenchyme is not highly proliferative. It has been shown that the mesenchyme grows in proportion to the epithelium and is important in guiding branching (Blanc et al., 2012). Considering mesenchymal development occurs around the distal regions of the epithelium (Shu et la., 2002), it is possible that the majority of mesenchyme proliferation occurs within this region, which is indistinguishable from the proliferating distal epithelium due to the ubiquitous expression of Fucci2a.

In the kidney nephrogeneses is observed (sup video 4). During kidney development in the mouse the mesoderm derived ureteric bud forms at e10.5 from the nephric tube

where it invades the metanephric mesenchyme and bifurcates at e11.5. The ureteric bud or duct then undergoes around 11 cycles of branching and elongating to generate the branched collecting duct system (Cebrian et al., 2004). As in the lung, there is a reciprocal signalling relationship between the ureteric bud and the surrounding mesenchyme to control branching morphogenesis. The ureteric bud also induces a sub set of the surrounding metanephric mesenchyme to differentiate into nephrons via a mesenchyme to epithelial transition (MET) followed by morphological folding of renal vesicles to S-shaped bodies and eventual fusion to the collecting duct (Davidson, 2008). In cultured e11.5 *R26Fucci2a*$^{+/-}$*/CAG::Cre*$^{+/-}$ kidneys the ureteric bud and renal vesicles are highly proliferative with the majority of cells in S/G2/M (fig 2.9B and C). The cap mesenchyme at this stage is less proliferative and contains a majority of cells in G1/G0. As the kidney continues to develop in culture renal vesicles continue to proliferate and mature into S-shaped bodies (figs 2.9E and F). At this stage presumptive podocytes in the visceral epithelium, which go on to form the specialised sieve-like structure of the bowman's capsule for blood filtration, start to drop out of the cell cycle. By 68.5 hours of culture as the nephrons continue to develop, mature glomerular structures can be easily identified constituted of podocytes in G1/G0 (fig 2.9H and I). Cells within the proximal non-branching regions of the ureteric bud have also dropped out of the cell cycle by this point.

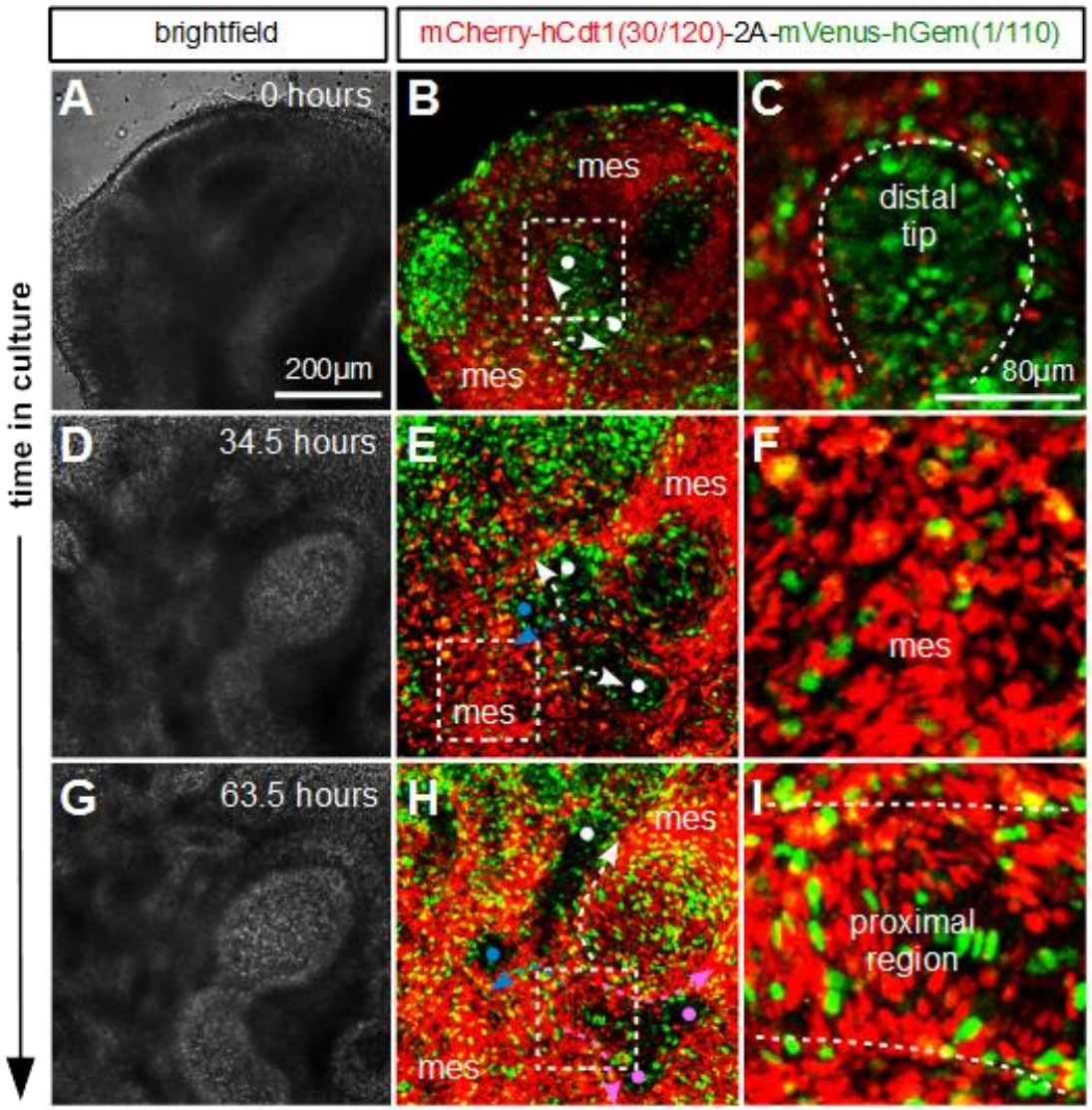

Fig 2.8: Live confocal imaging of cultured e11.5 *R26Fucci2aR$^{+/Tg}$/CAG::Cre$^{+/-}$* lungs. (**A and B)** The lung epithelium, identified by brightfield, can be seen to branch by bifurcation of the tip indicated by the two white arrows. **(C)** The majority of cells within the distal tip of the epithelium are labelled with mVenus-hGem(1/110) suggesting a high level of proliferation involved in epithelial elongation. **(D and E)** As the lung develops in culture the bifurcated epithelium can see to elongate (white arrows) and branch again by domain branching (blue arrow). **(F)** The surround mesenchyme is predominantly made up of cells in G1/G0, labelled with mCherry-hCdt1(30/120). **(G and H)** Further rounds of bifurcation can be seen as the lung continues to develop in culture (purple arrows) while existing branching continue to elongate (white and blue arrows). **(I)** Cells within the proximal epithelial regions have started to drop out of the cell cycle shown by the increase in mCherry-hCdt1(30/120) labelled cells. Abbreviations: mes = mesenchyme. Figure adapted from Mort et al 2014.

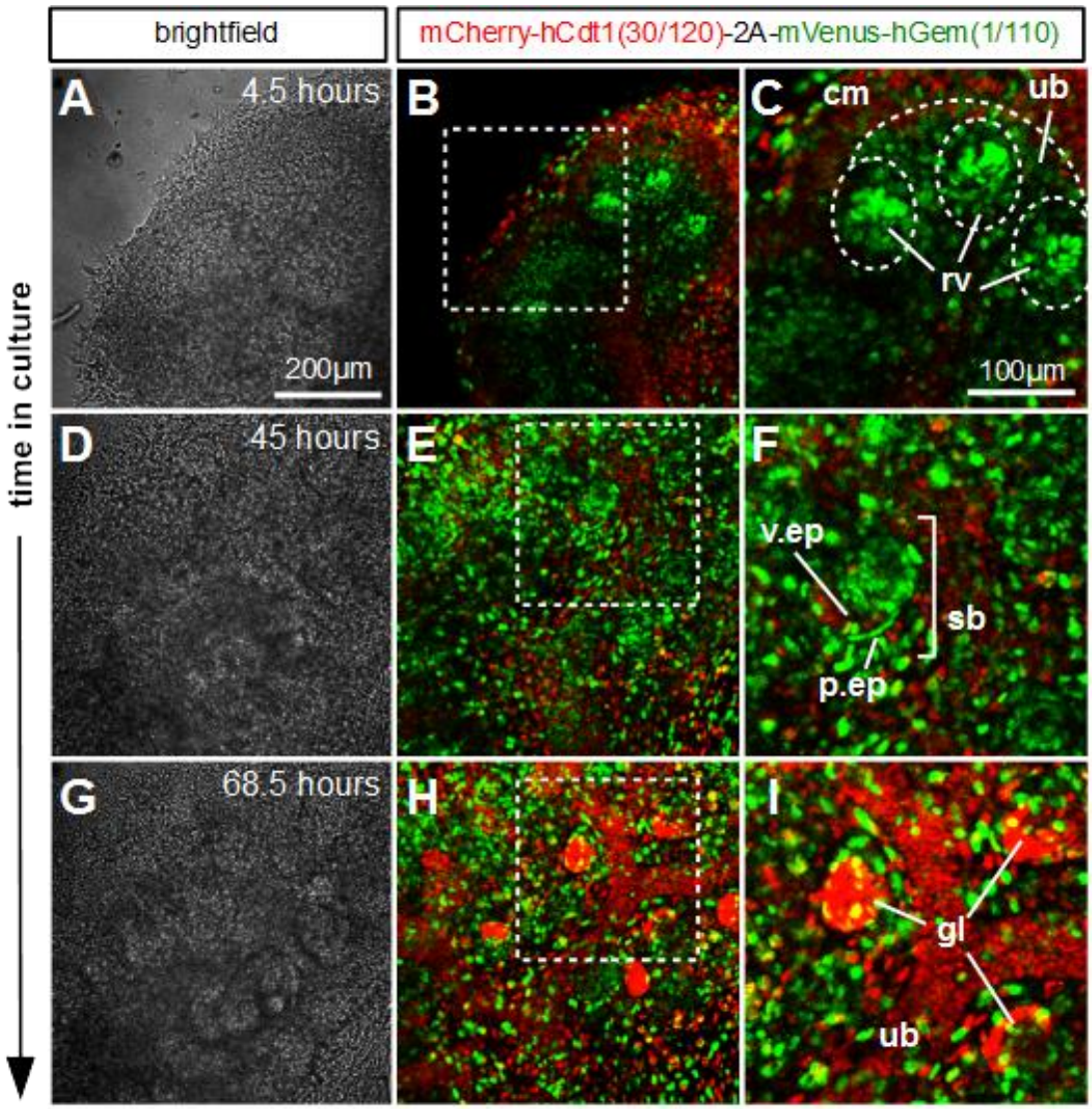

Fig 2.9: : Live confocal imaging of cultured e11.5 *R26Fucci2aR$^{+/Tg}$/CAG::Cre$^{+/Tg}$*kidneys. (A-C) Cells within the renal vesicles and ureteric bud are highly proliferative with the majority of cells labelled with mVenus-hGem(1/110). This is in contrast to the surrounding cap mesenchyme which contains a higher proportion of cells in G1/G0. **(D-F)** As the kidney continues to develop in culture the S-shape bodies derived from the renal vesicles continue to be highly proliferative however presumptive podocytes within the visceral epithelium have begun to drop out of the cell cycle. Indicated by the increase in mCherry-hCdt1(30/120) positive cells. **(G-H)** As the S-shaped bodies continue to develop into more mature glomeruli structures. Cells within these regions are almost exclusively in G1/G0 labelled with mCherry-hCdt1(30/120). Similarly cells within the proximal non-branching region of the ureteric bud are exclusively in G1/G0.Abbreviations: cm = cap mesenchyme, ub = ureteric bud; rv = renal vesicle; v.ep = visceral epithelium; p.ep = parietal epithelium; sb = S-shaped body; gl = glomeruli. Nils Lindstrom assisted with imaging and interpretation. Figure adapted from Mort et al 2014.

2.2.3 Tissue specific Fucci2a expression

To test the ability to induce Fucci2a expression within specific cell lineages, *R26Fucci2aR* mice were crossed with *Tyr::CreB* animals (Delmas et al, 2003) to label melanoblasts (not exclusively as *Tyr::CreB*is also expressed in the peripheral nerves and parts of the brain), a neural crest derived lineage that differentiates into adult melanocytes responsible for the production of pigment in the hair and skin (Mort et al., 2015). *Ex vivo* embryonic skin cultures at e14.5 from *R26Fucci2aR*$^{+/Tg/}$*Tyr::CreB*$^{+/Tg}$ embryos were set up as previously described (Mort et al, 2010) to allow live imaging of melanoblasts migrating through the epidermis before localising to hair follicles (fig 2.10A) (Bonaventure et al, 2013). Supplementary video 5 is an example of one of these time-lapses showing melanoblasts and peripheral nerves specifically labelled confirming the effectiveness of the Cre-loxP system. Melanoblasts can be distinguished from nerves by their migratory behaviour and are seen to be migrating and proliferating throughout the developing epidermis, as previously observed (Mort et al., 2010).

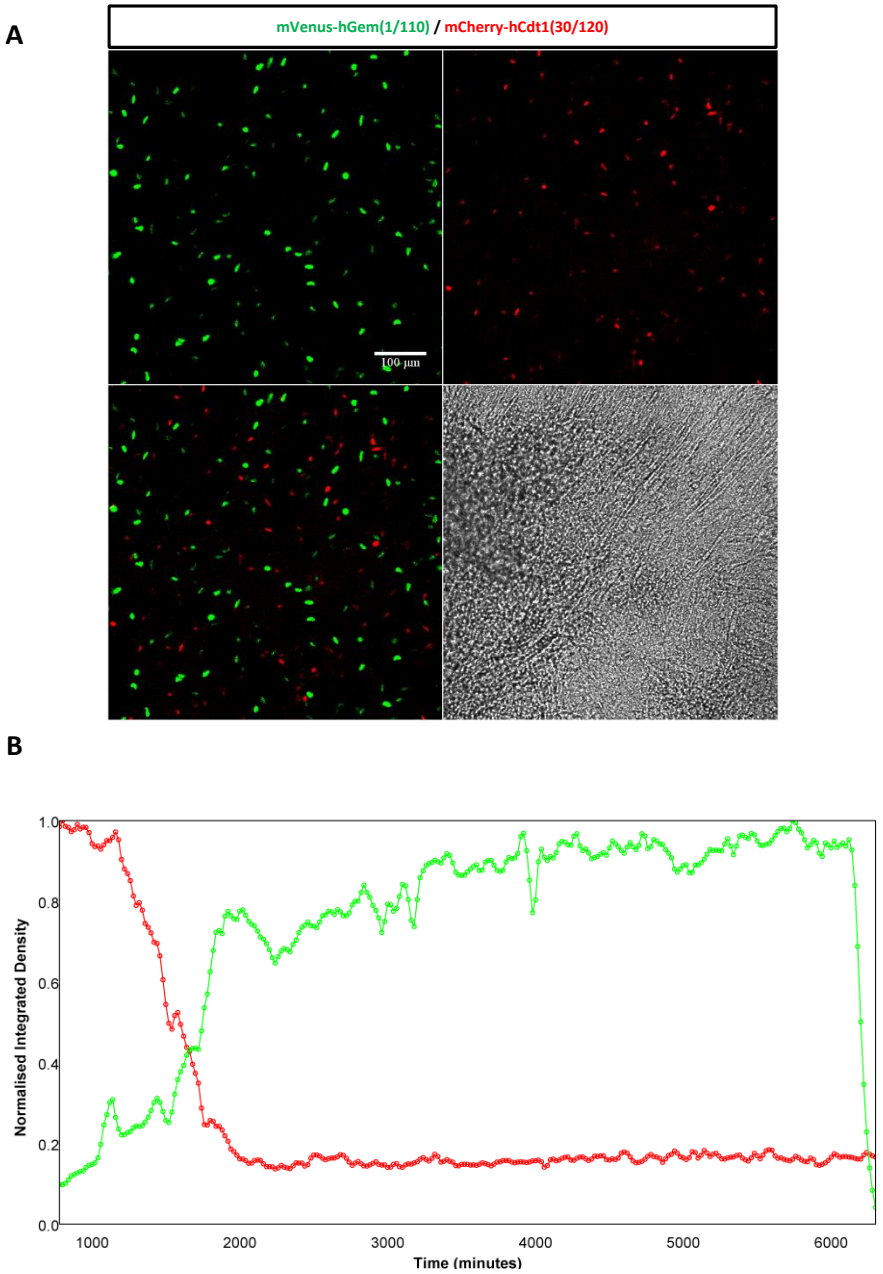

Fig 2.10: Lineage specific expression of Fucci2a: Lineage specific expression of Fucci2a was achieved by crossing *R26Fucci2aR*$^{Tg/Tg}$ with *Tyr::CreB*$^{Tg/Tg}$ animals and visualised by live confocal imaging of e14.5 *ex vivo* skin cultures. **(A)** Melanoblast and peripheral nerves are clearly specifically labelled with the Fucci2a reporter. Melanoblast and nerves are proliferating and can be distinguished from static nerves by their migratory behaviour (see sup video 5). **(B)** An example normalised fluorescent intensity of a single tracked melanoblast progression through S/G2/M phases of the cell cycle. The length of S/G2/M was measured from the point at which fluorescence of mVenus-hGem(1/110) reaches 0.2 normalised integrated density to the point at which mVenus-hGem(1/110) drops bellow 0.2 normalised integrated density.

2.2.3.1 Quantitative cell cycle analysis of migrating melanoblasts

Unfortunately, due to the loss of fluorescence of the Fucci probes immediately during cytokinesis, it is impossible to track melanoblast through mitosis and therefore directly measure cell cycle times. However, using the observation outlined in work leading to this project (see 2.1.2.2), adapted from Nowakowski et al., 1989, it is possible to calculate a cell cycle time for a population of cells from the length of an arbitrary cell cycle stage and the proportion of cells in that stage, with the assumption that all cells within that population are cycling asymmetrically. This equation has been shown in previous work leading to this project (see 2.1.2.2) to produce similar cell cycle times as those calculated from the mean of directly measured cell cycle lengths. To calculate cell cycle times for the migrating melanoblast from these time-lapses the mean length of S/G2/M (the green phase) was calculated from normalised fluorescence intensity plots of a tracked melanoblast (fig 2.10B). This was then divided by the proportion of green labelled cells at the start of the time-lapse. Based on 24 independent skin cultures the mean cell cycle time for migrating melanoblast at e14.5 was 17±3 hours. The use of this equation over direct measurement of cell cycle length greatly reduces the need for excessively long time-lapses as cell cycle times can be calculated from a single cell cycle phase.

2.3 Discussion

Traditional methods of monitoring the proliferative state of a tissue rely on the use of cell cycle phase specific markers such as thymidine analogues that label cells in S-phase (3H-thymidine, Brd-U) and PCNA. These methods rely on immunohistochemistry or radiography on fixed tissues (see 1.4 in introduction) and therefore only give a snapshot of the proliferative state of the tissue and cannot be combined with live imaging which is required to fully appreciate the dynamics of cell cycle progression in tissue development and disease. The Fucci system is a powerful tool that enables live visualisation of cell cycle progression by the use of two fluorescently tagged probes whose abundance is regulated to different stages of

the cell cycle (Sakaue-Sawano et al., 2008). The Fucci probes contain the E3-ligase recognition domain of Cdt1 and Geminin fused to a red and green fluorophore, resulting in cells being labelled red during G1, yellow during the G1/S transition, green during late S/G2/M phases and are briefly unlabelled in early G1 after cell division (Sakaue-Sawano et al., 2008). The use of the Fucci system *in vivo* however has been limited due to the expression of the two Fucci probes from different loci and the ubiquitous expression of the probes (see "The Fucci system" in the induction). As outlined in the introduction previous attempts were made to rectify these limitations, such as the constitutive *R26p-Fucci2* line in which both Fucci probes were expressed from a single bidirectional construct separated by insulator sequencing and the Cre-inducible *R26-mVenus-hGem(1/110)* and *R26-mCherry-hCdt1(30/120)* lines (Abe et al., 2013). However *R26p-Fucci2* suffered from homozygous lethality and *R26-mCherry-hCdt1(30/120)* from low expression. In addition neither system was able to produce inducible expression of both Fucci probes from a single locus. In this chapter I have described the characterisation of the *R26Fucci2aR* mouse designed to overcome these limitations by expression of both Fucci probes from a single inducible bicistronic construct targeted to the mouse *ROSA26* locus (Mort et al., 2014). The expression of both Fucci probes from a single locus by the use of the self-cleaving peptide T2A greatly simplifies mouse colony maintenance, while targeting to *ROSA26* and driving expression under the CAG promoter ensures strong ubiquitous expression in all tissues examined. In addition, considering the myriad of Cre and Cre-ERT lines available, having inducible expression dependent upon excision of a neomycin-stop cassette via the Cre-loxP system allows for precise temporal and spatial labelling of cells *in vivo*. The *R26Fucci2aR* mouse is therefore a vast improvement on the currently available *in vivo* Fucci systems and will greatly improve its utility in mammalian research.

2.3.1 2A peptides cleave asymmetrically which can influence the behaviour of the gene in the 5' position

The Fucci2a bicistronic construct was designed and characterised in 3T3 cells by Dr Richard Mort (University of Edinburgh). Due to the asymmetric cleavage of the self-cleaving peptide sequence the majority of amino acids are left on the C-terminus of the protein in the N-position (J. H. Kim et al., 2011). Dr Mort showed by expressing the construct with the Fucci probes in different positions that the addition of the residue amino acids to the C-terminus of mVenus-hGem(1/110) in the 5V3C-Fucci2a cell line results in its miss-localisation to the cytoplasm (fig 2.1). This is most likely due to interference with the nuclear localisation sequence located between amino acids 28-79 of the truncated hGeminin cDNA (Boos et al., 2006; Okorokov et al., 2004). This highlights the importance of considering the order of genes within bicistronic or multicistronic constructs using 2A peptides as the additional amino acids left after ribosomal skipping of the 2A peptide could interfere with the localisation, function or stability of the expressed protein. In addition the order of genes in bicistronic constructs and the sequence to the N-terminal of the 2A sequence has been shown to influence cleavage efficiently (Anderson et al., 2012; De Felipe et al 2010; Donnelly et al., 2001; Ibrahimi et al., 2009)

2.3.2 mCherry-hCdt1(30/120) does not faithfully recapitulate endogenous Cdt1 levels in mESCs

In the present work I describe the absence of mCherry-hCdt1(31/120) in Fucci2a mESCs during G1. Previous studies using lentiviral transection of the commercially licensed FUCCI constructs in mice have reported a similar phenomenon therefore confirming this problem is not restricted to the Fucci2a construct (Coronado et al., 2013; Roccio et al., 2013). In these studies a higher proportion of mKO-Cdt1(30/120) positive cells was reported (9.4% and 6% respectively). It has been hypothesised that the reason for the G1 to be unlabelled in mESCs is due to the very short G1 in mESCs, which does not give enough time for the Cdt1 probe to accumulate and the fluorophore to mature. This is supported by another report in

which a higher proportion of mKO-hCdt1(30/120) positive cells was seen in hESCs which have a longer G1 (Pauklin & Vallier, 2013). However, as described above the length of G1 in my cultured mESCs is ~3.65 hours and the estimated time for mCherry-hCdt1(30/120) to become visible after mitosis is around 2 hours in Fucci2a expressing 3T3 cells (fig 2.2B). This suggests that there should be enough time for the mCherry-hCdt1(30/120) to accumulate. If the length of G1 is the sole reason for the absence of mCherry-hCdt1(30/120) the reason for the exceptionally low proportion of mCherry-hCdt1(30/120) positive cells (2%) in Fucci2a expressing mESCs may be down to a lower level of expression compared to the lentiviral vectors used in the previous reports. The lower level of expression in the Fucci2a mESCs would mean more time is required for mCherry-hCdt(30/120) to accumulate to a threshold which can be detected. Therefore resulting smaller proportion of mCherry-hCdt(30/120) positive cells.

Paradoxically, endogenous Cdt1 protein levels have been shown to be higher in mitotically synchronised undifferentiated mESCs compared to differentiated stem cells (Ballabeni et al., 2011). This has been attributed to increased levels of known APC/C inhibitor Emi1 (Reimann et al., 2001), which results in an increased abundance of APC/C substrates including Cyclin A and B, cdc20 and Geminin known for promoting cell cycle progression (Ang & Harper, 2004). Geminin is a known negative regulator of Cdt1 (C. Lee et al., 2004; Wohlschlegel et al., 2000), in addition CDKs have been shown to phosphorylate Cdt1, promoting the recruit of ubiquitin ligase SCF^{Skp2} which targets Cdt1 for degradation (Liu et al., 2004; Sugimoto et al., 2004). The high levels of CDKs reported in embryonic stem cells is thought to allow rapid progression through G1 (Ballabeni et al., 2011; J. White et al., 2005). Contradictorily to this, Geminin and CDK activity was shown to stabilise Cdt1 abundance in mitotic cells (Ballabeni et al., 2011). The stabilising influence of Geminin on Cdt1 during M-phase has also been reported in differentiated cell lines (Ballabeni et al., 2004). Therefore suggesting Geminin and CDKs have contrasting influences on Cdt1 depending on cell cycle phase. The adaptive increased abundance of Cdt1 in mESCs induced by higher levels of CDK and Geminin may also be

required to enable licensing of DNA replication in an environment of high CDK activity. Considering the published stabilising influences of Geminin and CDKs on Cdt1 during M-phase (Ballabeni et al., 2004, 2011), it is also possible that another contributing factor for the low proportion of mCherry-hCdt1(30/120) labelled cells in mESCs may be due to the truncation of Cdt1 which has removed potentially stabilising interactions.

The observations by Ballabeni and colleagues of higher Cdt1 abundance is based on cells that have been synchronised in mitosis which may not reflect endogenous levels in cycling mESCs. Using *R26Fucci2a* mESCs it is possible to separate cells into G1 and S/G2/M stages of the cell cycle without the need of synchronisation therefore creating the perfect platform for examining endogenous Cdt1 levels during the cell cycle. Unfortunately, contrary to documentation none of the Cdt1 antibodies I tested were able to detect mouse Cdt1 (see antibody table 8.1). Likely due to them being raised against the human Cdt1 antigen and no cross species reactivity. Custom made Cdt1 antibodies have been produced and used to detect Cdt1 in mouse, which would therefore be require to complete this experiment.

2.3.3 R26Fucci2aR as a tool for the *in vivo* study of proliferation

In the characterisation of the *R26Fucci2aR* reporter mouse I have demonstrated the capabilities of using this genetic system to study cell cycle progression live. Time-lapse imaging of *ex vivo* cultured kidneys and lungs at e11.5 derived from *R26Fucci2aR*$^{+/Tg}$*/CAG::Cre*$^{+/Tg}$ embryos revealed distinct regions of proliferation at the epithelial tip of the branching ureteric duct and lung epithelium (fig 2.9 and 10). This is in agreement with previously published data which has identified a high proportion of Brd-U positive cells within these regions (Michael & Davies, 2004; Nogawa et al., 1998). Being able to visualise cell cycle progression live gives the clear advantage for being able to monitor how proliferation is changing in time with tissue morphogenesis. This is information that would otherwise be lost using traditional techniques and fixed tissues. However it is important to consider the potential artefacts induced by using *ex vivo* culture systems for live imaging. As the

extending culture times and photo toxicity may influence cell behaviour and cell cycle progression. Therefore where possible observations see in *ex vivo* culture should be confirmed by other methods such as using fixed time points.

2.3.4 Generating quantitative data using Fucci2a

Another important facet of the Fucci system is the ability to generate quantitative as well as qualitative data which I have demonstrated *in vivo*. From time-lapse imaging of e14.5 *ex vivo* skin cultures dissected form *R26Fucci2aR*$^{+/Tg}$*/Try::CreB*$^{+/Tg}$ embryos, I have calculated the cell cycle time for the population of migrating melanoblasts from the length of S/G2/M and the proportion of melanoblast in S/G2/M, with the assumption that all melanoblasts are cycling asynchronously (Mort et al., 2014). The ability to estimate cell cycle times from a single stage of the cell cycle rather than tracking cells over an entire cell cycle reduces the need for long time-lapses, which can be technically challenging. The cell cycle time calculated for melanoblasts at e14.5 is comparable to melanoblast doubling times previously reported (17 hour compared to 16 hours) (Luciani et al., 2011). In addition a recently published study by Mort and colleagues used an almost identical method of calculating melanoblast cell cycle times from *ex vivo* time lapse data with similar results (Mort et al., 2016). However in this study the length and number of cells in M-phase was used to determine cell cycle length. Due to the short length of M-phase and therefore the small number of cells in M-phase in the field of view at any one time this method of calculating cell cycle time will suffer from a larger degree of error than cell cycle times calculated using the fluorescence of the Fucci probes. Traditional methods for quantifying cell cycle times require the use of double labelling with two thymidine analogs such as BrdU and IddU (see calculating cell cycle times in introduction) (Bradford & Clarke, 2011; Martynoga et al., 2005; Nowakowski et al., 1989). These methods should produce similar cell cycle times to those calculated using the Fucci system outlined above. However the Fucci system has the added advantage in reporting the lengths of different cell cycle phase so that changes in particular cell cycle phases can be quantified. This has been illustrated in

time-lapse imaging of 3T3 cells under different serum concentration, showing a shorting of the G1 phase in response to increased serum concentration (see work leading to project) (Mort et al., 2014). In addition the Fucci system allows quantitative tracking data to be segregated by cell cycle stage (as illustrated in results 4.2.4).

3 Chapter 3: Characterisation of tricistronic reporter constructs

3.1 Introduction

An intriguing attribute of 2A self-cleaving peptides is the ability to build multicistronic constructs to translate multiple proteins from a single transcript by the use of multiple 2A sequences. The use of this technology has been particularly useful in gene therapy for the delivery of the rescue gene expression in combination with fluorescent and bioluminescent reporters (Osborn et al., 2005). Multicistronic 2A constructs have also be used successfully to reprogram iPS cells from mouse and human somatic cells by lentivirus transfection of a single construct containing Oct4, Sox2, Kif4 and cMyc separated by self-cleaving peptides P2A,T2A and E2A (Carey et al., 2009). In another technologically challenging report, T-cell development and function was restored in CD3-deficient mice via the transfection of a multicistronic lentiviral vector expressing four components of CD3 complex showing almost 100% cleavage efficiency across 2A sequences (Szymczak et al., 2004). These examples highlight the potential use of this technology for gene therapy in correcting multi gene dysfunction.

Considering the success and high cleavage rates reported in these multicistronic constructs, I developed four novel tricistronic reporter constructs incorporating Fucci2a and designed to complement information of the cell cycle status with a third biosensor. To do this I designed fluorescent probes marking either apoptosis, cytokinesis or ciliogenesis. These were inserted to the 5’ end of the Fucci2a construct

separated by the P2A self-cleaving peptide. Addition of the third fluorescent marker had to be inserted at the 5' end of the Fucci2a construct because as was shown previously in the characterisation of the Fucci2a construct by Dr Richard Mort, addition of the 2A residue peptide to the 3' end of the mVenus-hGem(1/110) results in some mislocalisation to the cytoplasm resulting in an increase in the cytoplasmic to nuclear ratio of mVenus (Fig 2.1K). In all cases the fluorophore used was Cerulean to ensure optimal spectral separation from mVenus and mCherry and due to its brightness (2.5 times brighter than ECFP) (Rizzo et al., 2004). Each construct was first characterised in a stable 3T3 cell line generated using the Flp-In system (Invitrogen) by a combination of time-lapse imaging and FACS analysis. Generation of stable cells lines using the Flp-In system inserted a single copy of the transgene into the genome and, therefore, expression is more comparable to a Knock-In transgene to *ROSA26* than transient transfections or cell lines generated by random integration, which may contain multiple insertions of the transgene. If the construct was deemed suitable for *in vivo* work, based on sufficient spectral separation and fluorescent intensity, an inducible transgenic mouse line was generated by homologous recombination to the *ROSA26* locus in the reverse orientation to the endogenous promoter. Given the recent advances in live imaging techniques these constructs should prove to be useful tools for monitoring cell cycle progression with other developmental events. Their development will also provide a proof of principle for the development of future multicistronic genetic reporters.

3.1.1 Apoptosis – *CA/CC3AI-Fucci2a*

The process of development in vertebrates is not a predetermined sequence of events in which each individual cell stereotypically forms the appropriate connections with the surrounding cells and extra cellular matrix (ECM) in time and space. In reality excess cells are produced and only those that form the correct connections or receive trophic signals persist. The rest undergo a controlled form of cell death known as apoptosis (reviewed in Fuchs & Steller, 2011; Meier et al., 2000).

Two striking examples of apoptosis in development can be seen during cortical and limb development. During cortical development a complex neural network is constructed by first producing a vast excess of neurons. Over time excess neurons are removed by apoptosis. Apoptosis is thought to be induced in part by competitive loss of trophic factors such as NGF (nerve growth factor) and the inability to make synaptic connections which are thought to provide trophic support (Oppenheim, 1991). The importance of clearing these excess neurons is highlighted by the enlarged and malformed cerebral phenotypes of mutant mice stains with disrupted apoptotic pathways (Hakem et al., 1998; Kuida et al., 1998; Hiroki Yoshida et al., 1998).

In digit formation the digits are formed from the hand plate by removal of the interdigitary cells by apoptosis. In chickens, within the interdigitary mesenchyme BMP signalling has been shown to induce apoptosis. This BMP signalling was shown to be absent in species of duck with webbed feet due to expression of BMP inhibitor *Germlin* (Merino et al., 1999; H. Zou & Niswander, 1996). Interestingly, co-expression of *Germlin* and *Fgf8* has also been proposed to prevent apoptosis in the interdigitary mesenchyme of bat forelimbs suggesting a cross species evolutionary conserved mechanism for digit formation, which has been adapted to allow for retention of interdigitary webbing (Weatherbee et al., 2006).

Outside of development processes, apoptosis can also be induced in response to DNA damage, viral infection, pathogen infection and is important for the removal of immune cells after inflammation (Barber, 2001; Haanen & Vermes, 1995; Roos & Kaina, 2016; Weinrauch & Zychlinsky, 1999). Being able to visualise proliferation simultaneously with apoptosis would clearly be a powerful tool for understanding how these contrasting processes are coordinated during development and in response to infection.

3.1.1.1 Apoptosis reporters

Molecularly apoptosis can be induced via an extrinsic caspase-9 dependent signalling pathway down stream of death receptor activation or by an intrinsic caspase-9/ apoptosome-dependent pathway. Both pathways converge in activating the "executioner caspases" 3, 6 and 7 which trigger apoptosis (reviewed in (McIlwain et al., 2016). The executioner caspases specifically cleave at a recognition sequence comprised of amino acids DEVD therefore making this an ideal candidate sequence for a caspase activatable reporter.

All currently available genetic reporters of apoptosis rely on activation by executioner caspase cleavage. One limitation common in all caspase dependent reporters to consider is they are unable to detect caspase independent apoptosis (reviewed in Broker et al., 2005). An apoptosis reporter to be incorporated into the Fucci2a construct would need to contain a single fluorescent marker to enable spectral separation from mVenus and mCherry and have a large enough signal to noise ratio to be to be able to detect individual apoptotic cells from background flourescence *in vivo*.

One fluorescently based apoptosis reporter in use is based on FRET (Fluorescence Resonance Energy Transfer) (Rehm et al., 2002; Tyas et al., 2000). FRET is a widely used imaging technique used to determine the proximity of proteins by live imaging (Sekar & Periasamy, 2003). This technique is based on the principle of exciting one fluorophore that has a similar emission spectrum to the excitation spectrum of a second fluorophore. If the two fluorophores are in close proximity the emission of the first fluorophore is able to excite the second, which can then be detected and quantified as a measure of distance between the two fluorophores. For example, Miyawaki and colleagues have developed a Ca^{2+} reported by fusing CFP and YFP to either end of the Ca^{2+} binding protein calmodulin (Miyawaki et al., 1997). Upon binding to free Ca^{2+} ions calmodulin changes its conformation, bringing the two fluorophores closer together. By exiting the YFP fluorophore and measuring the emissions of both YFP and CFP Miyawaki and colleagues were able to determine the changes in cellular localisation of Ca^{2+}, with an increase in CFP emissions being

indicative of increased Ca^{2+} binding (Miyawaki et al., 1997). FRET based apoptosis markers contain CFP and YFP linked together by the executioner caspase recognition sequence DEVD thereby the induction of apoptosis is reported by a decrease in the amount of FRET (Rehm et al., 2002; Tyas et al., 2000).

Another published fluorescent-based apoptosis reporter is based on cell compartment localisation of the fluorophore and has reported good signal to noise ratio when expressed in the drosophila and chick (Bardet et al., 2008). In this reporter Bardet and colleagues have constructed a fusion protein containing mRFP fused to the transmembrane domain of the mouse CD8 gene linked to eGFP fused to a nuclear localisation signal via the caspase recognition domain of DIAPI (Bardet et al., 2008). Under normal cellular conditions the fusion protein remains attached to the cell membrane. Upon the induction of apoptosis caspases Drice and Dcp1 release eGFP, which translocates to the nucleus. However, due to use of two fluorophores in the above mentioned reporters it would be difficult to combine them with the Fucci2a construct and retain sufficient spectral separation.

Considering this I have chosen to test the capabilities of two single fluorophore caspase activating reporters to analyse which would be better suited for *in vivo* visualisation of apoptosis. One potential candidate called CA-GFP combines GFP with a quenching peptide, connected by a DVED sequence (fig 3.1A) (Nicholls et al.,2011). The hydrophobic quenching peptide is derived from the transmembrane domain of influenza M2 that tetramerises GFP to prevent its maturation. Capase-3 dependent removal of the quenching peptide allows GFP to fold and mature and act as a marker of apoptosis (Nicholls et al., 2011). The second candidate comprises a truncated fluorophore in which the N' and C' terminals have been linked via a DVED sequence and new N' and C' terminals created at residues A154 and D155. After cleavage the two subunits have the potential to from a functional fluorescent protein by bimolecular fluorescence complementation (BiFC), whereby the two non-fluorescent fragments form a fully fluorescent protein when in close proximity (Shyu & Hu, 2008). To aid the complementation process a split *Npu* DnaE interin was added to the newly synthesised N' and C' terminals catalysing trans-ligation of its

artificial exteins with over 98% efficiency (fig 3.1B) (Iwai et al., 2006; Zettler et al., 2009; Zhang et al., 2013). Zhang et al generated several different version of their caspase activated fluorophore including one based on Cerulean (CC3AI). I designed a Cerulean version of CA-GFP (CA-Cerulean) that was synthesised by Geneart. Both CA-Cerulean and CC3AI were combined in a tricistronic construct with Fucci2a and tested in stable 3T3 cell lines to determine suitability for generation of a dual cell cycle-apoptosis reporter mouse.

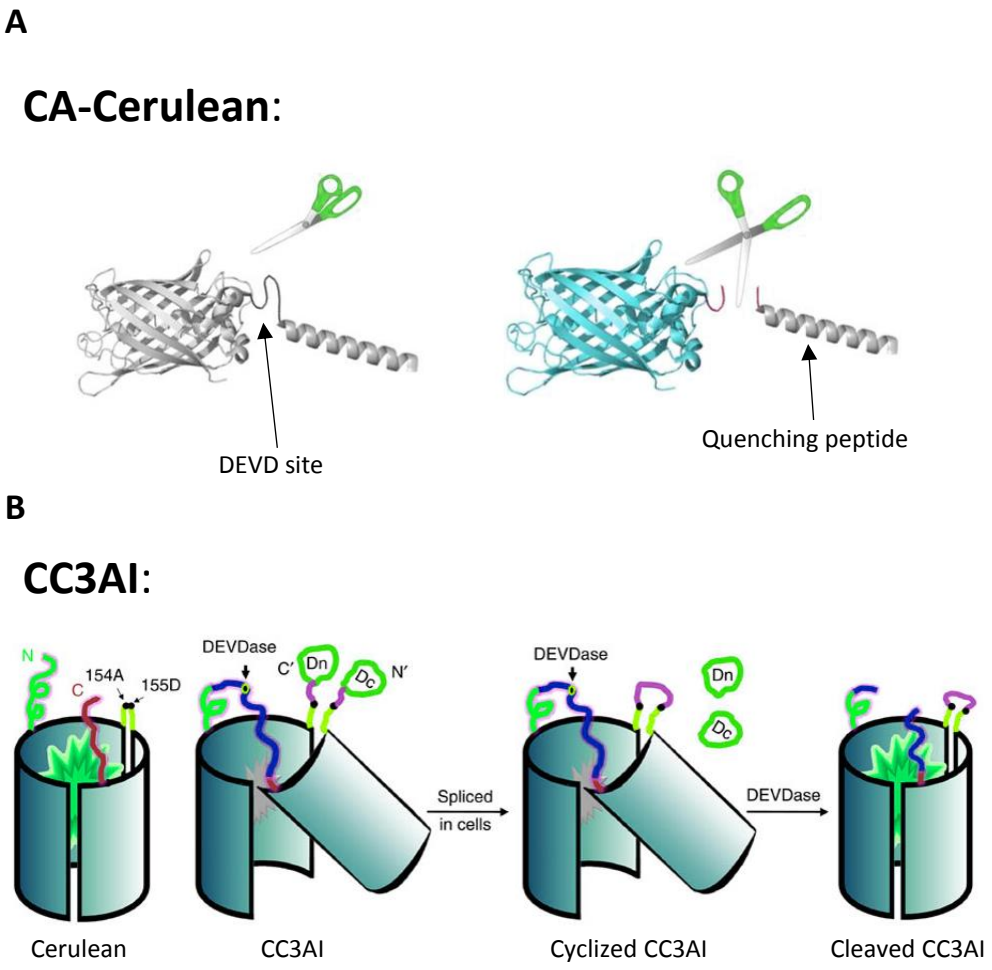

Fig 3.1:Apoptosis reporters. (A) CA-Cerulean is a cerulean derivative of CA-GFP originally publish by Nicholls et al., 2011. CA-Cerulean contains the cerulean fluorophore fused to a quenching peptide via the DEVD caspase recognition sequence which prevents cerulean maturation. Upon activation of apoptosis executioner caspases cleave away the quenching peptide allowing cerulean to form a functional β-barrel and act as a marker of apoptosis. **(B)** CC3AI is a truncated and split form of cerulean which has been fused together via a DEVD sequence. Upon induction of apoptosis executioner caspases cleave the synthetic bridge and allows cerulean to form a functional β-barrel by biomolecular fluorescence complementation (BiFC) which is aided by a split *Npu* DnaE intern that catalyses trans-ligation of the protein. Figure adapted from Nicholls et al., 2011 and Zhang et al., 2013.

3.1.2 Cytokinesis – *H2B-Fucci2a*

A major limitation of the Fucci system is the loss of fluorescent signal during mitosis. This makes tracking cells between late mitosis and early G1 impossible *in vivo.* A limitation that was highlighted in the inability to track melanoblast after mitosis in time-lapses of e14.5 *ex vivo* skin cultures (sup video 5). A way to overcome this limitation would be to introduce a cell marker that is present in all stages of the cell cycle including mitosis. Cytoplasmic and membrane bound markers, although having the benefit of giving details on the cells morphology, are not ideally suited for markers of cell tracking for two main reasons. First, it is difficult to locate the centre of the cell in manual and automatic tracking methods, which can result in increased error in tracking data. Second, if all cells within a tissue or epithelium are labelled it is impossible to distinguish and track an individual cell. A subcellular localised marker is therefore preferred. Nuclear makers are most commonly used in research because the nucleus is generally found in the centre of the cell and the accumulation of fluorophores in the nucleus concentrates the signal. Fluorophores fused to nuclear localisation signals (nls) such as those deerived from *Simian vacuolating* virus 40 (SV40) have been used to generate transgenic reporter mice (Stoller et al., 2009). However, such reporters suffer from a dilution of their nuclear signal at mitosis during the breaking of the nuclear envelope. By far the most commonly used nuclear markers are fluorescently tagged histones that have been widely used in cells, fruit flies, zebrafish and mice (Concha & Adams, 1998; Das et al., 2003; Gong et al., 2004; Hadjantonakis & Papaioannou, 2004; Kanda et al., 1998; Savoian & Rieder, 2002). Histones are a structural component of the nucleosome, the basic unit for DNA packaging of chromosomes that undergo post translational modification to regulate access to the DNA (reviewed in Campos & Reinberg, 2009). Previous work has shown overexpression of H2B-GFP has no adverse effect on cell function in cells or mice (Hadjantonakis & Papaioannou, 2004; Kanda et al., 1998). Fluorescently tagged H2B also gives the advantage of being able to visualise chromosomes during mitosis without the loss of signal and also allows distinction between interphase and anaphase based on chromosome morphology

(Kanda et al., 1998). In addition the fluorescence of chromatin bound GFP is not lost during fixation (Kanda et al., 1998).

To overcome the limitation of losing the fluorescence of the Fucci probes during mitosis that hinders tracking analysis, I have combined H2B-Cerulean with the original Fucci2a construct separated by another self-cleaving peptide (P2A) to make a tricistronic reporter construct which should improve the utility of the Fucci system. I have characterised this construct in a stable 3T3 cell line and generated the *R26H2B-Fucci2aR* mouse line by homologous recombination to the mouse *ROSA26* locus.

3.1.3 Cilia – *Arl13b-Fucci2a*

Cilia are microtubule-based protrusions found on almost every mammalian cell and exist in two forms; Motile cilia are found on specialised cells such as the multicilated cells lining the trachea and cerebral ventricles. They have a 9+2 axomine configuration with dynein arms on the outer microtubules to drive cilia motility (reviewed in Ibañez-Tallon et al.,2003). The importance and diverse function of motile cilia in development and homeostasis is highlighted by the variety of symptoms presented in patients with Primary Ciliary Dyskinesia (PCD) or Kartagener syndrome (Afzelius, B, 1976; Greenstone et al., 1984; Whitelaw et al., 1981), including infertility in males, bronchitis, hydrocephalus, sinusitis and situs inversus. Primary cilia are found on the majority of cell types, have a 9+0 axomine configuration and have been shown to be an important signalling centre for hedgehog and Wnt signalling (Corbit et al., 2008; Cortellino et al., 2009; Houde et al., 2006; Huangfu et al., 2003; Simons et al., 2005; Tran et al., 2016). For example, recessive null mutations in intraflagellar transport proteins (IFT) 88 and 172, shown to be necessary for the formation of primary cilia, have reproduced similar phenotypes seen in Shh mutants (Chiang et al., 1996; Huangfu et al., 2003). In particular Huangfu and colleagues showed a decrease in the expression of Shh target gene Patch in ventral neural tube cells known to be specified by Shh released from the notochord (Jessell, 2000). There is a regulatory relationship between primary cilia

assembly and disassembly in relation to the cell cycle. This is in part due to the centrosome being a component of the basal body found at the base of the cilia, which are also necessary for the formation of the mitotic spindle during mitosis. This results in cilia being disassembled prior to mitosis and assembled at some point during G1, therefore limiting the responsiveness of cells to extracellular ciliary dependent signals in a cell cycle dependent manner. (fig 3.2) (Seeley & Nachury, 2010). Because of this close association between the cilia and the centrosome it has been speculated that the cilium is able to put a "break" on the cell cycle by sequestering the centrioles in the basal body. This train of thought is supported by the observations of the loss of primary cilia in some cases of cancer and cystic kidney disease (Hassounah et al., 2013; Jonassen et al., 2008; Lin et al., 2003; Menzl et al., 2014; Yuan et al., 2010). Whether the loss of primary cilia is the cause of increased proliferation in these models or if the loss of primary cilia is as a result of increased proliferation is still an open question. Conversely, cilia dependent signalling such as Hh and Wnt signalling has also been shown to be necessary for the development of some tumours and in some forms of cystic kidney disease (Han et al., 2009; Ma et al., 2013; Wong et al., 2009). Han and Wong have showed that tumour growth as a result of constitutively active Smoothened in medulloblastoma and basal-cell carcinoma require primary cilia. But not in constitutively activated Gli tumours (Wong et al., 2009). Ma et al have reported an decrease in kidney cyst severity and proliferation in the absence of primary cilia but by an unknown mechanism (Ma et al., 2013). These studies show a context specific role of cilia in regulating cell cycle progression depending on the molecular context. A dual cilia and cell cycle live reporter would clearly be a useful tool considering the biological importance of motile cilia and the intriguing relationship between primary cilia and cell cycle progression.

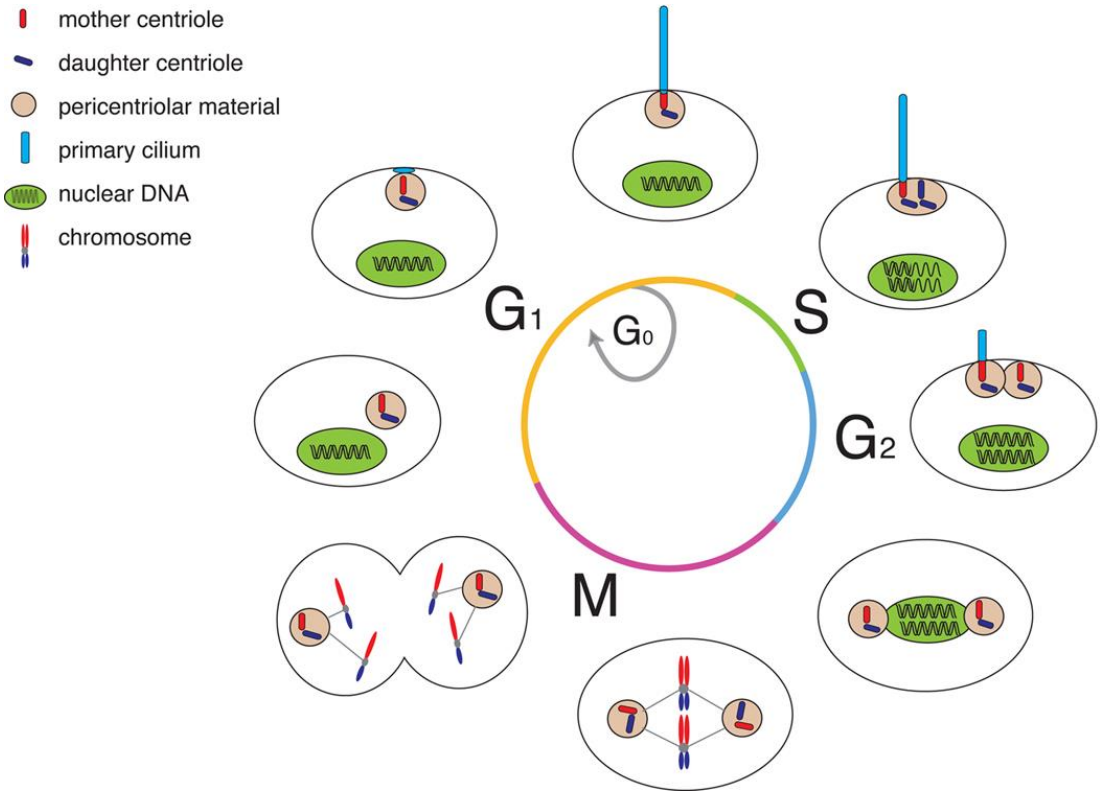

Fig 3.2. Cilia and the cell cycle. In most cells the primary cilia forms at some point during G1 by centrosomal docking to the membrane and subsequent building of the ciliary axoneme by IFTs and accessory proteins. The primary cilia then acts as an antenna for extracellular ciliary dependent signals such as Shh and Wnt. In most cell types the primary cilium is disassembled just prior to chromosome segregation. Figure adapted from Santos et al., 2008.

3.1.3.1 Cilia reporters

Currently there are three published cilia reporter mouse lines (Bangs et al., 2015; Delling et al., 2013; O ’Connor et al., 2013). Sstr3 is a G protein-coupled receptor localised to the cilia and although no other problems were reported, overexpression of other GPCRs like Sstr3 have been shown to affect the distribution of ciliary proteins and cilia morphology (Guadiana et al., 2013). O’Connor et al generated an inducible Sstr3-GFP reporter mouse by targeted recombination to the *ROSA26* locus. Impaired motility of sperm in Sstr3-GFP animals suggests overexpression may impair cilia function or motility in other tissues (O'Connor et al., 2013).

Arl13b is a small GTPase specifically localised to the cilia and has been shown to be essential for cilia integrity and for preventing Smoothened accumulation into the cilia in the absence of Shh signalling (Caspary et al., 2007; Larkins et al., 2011). Bangs et al and Delling et al alternatively generated by random transgenes, a constitutive reporter mouse line expressing Arl13b-mCherry and Arl13b-EGFP respectively. Using this line bangs et al have shown cilia first appear in the epiblast at e6.0 but are absent from all extraembryonic cell lineages (Bangs et al., 2015). Overexpression of Arl13b results in cilia lengthening *in vitro* and in the Arl13b-GFP mouse (37% longer in homozygous animals) (Bangs et al., 2015; Larkins et al., 2011). However no adverse affects or defects in Hh signalling were reported, suggesting increasing cilia length has no effect on cilia function in the mouse.

Considering the observations above, I have constructed a tricistronic cilia and cell cycle reporter construct containing full length Arl13b-Cerulean fused to Fucci2a separated by the self-cleaving peptide P2A. I have characterised this construct in a stable 3T3 cell line showing successful reporting of cell cycle progression and cilia assembly and disassembly. In addition I have used this cell line to determine the timing of ciliogenesis in relation to cell cycle progression and by time-lapsing imaging showed 3T3 cells orientate their cilia towards the leading edge during migration. Finally I have generated and characterised an inducible Arl13b-Fucci2a mouse line by homologous recombination in mESC to the *ROSA26* locus, which should prove a useful tool in the study of cell cycle, ciliary dynamics *in vivo*.

3.2 Results

3.2.1 Apoptosis: CA/CC3AI-Fucci2a

3.2.1.1 CA-Fucci2a / CC3AI-Fucci2a construct design and generation of 3T3 stable cell lines

Apoptosis (programmed cell death) and proliferation are two contrasting developmental process which are spatially and temporally controlled to ensure the normal development of tissues and organs. I set out to develop a strategy that would allow one to visualise these two processes simultaneously using the Fucci probes to report on cell cycle status. CA-Cerulean and CC3AI are both caspase activatable fluorescent reporters of apoptosis which uniquely mark apoptosis via a single fluorescent signal spectrally separated from the Fucci2a fluorophores (Nicholls et al., 2011; Zhang et al., 2013). I have designed CA-Fucci2a and CC3A-Fucci2a to contain these two apoptotic reporters fused to the cell cycle progression reporter Fucci2a separated by the self-cleaving peptide P2A (*porcine teschovirus*-1 2A). CA-Cerulean and CC3AI were synthesised by Geneart and sub-cloned in front of the original Fucci2a constructs in pcDNA-FRT-Fucci2a for Flp-In targeting. Synthesised CA-Cerulean contained a Kozak sequence (GCCACC), Cerulean (Rizzo et al.,2004), DEVD caspase-7 like recognition sequence and quenching peptide (Nicholls et al, 2011), followed by the self-cleaving peptide P2A (J. H. Kim et al., 2011). The entire construct was flanked by restriction sites MluI and BssHII to allow for one step restriction cloning into pcDNA5-FRT-Fucci2a via an MluI restriction site between the CAG promoter and the 5' of mCherry-hCdt1(30/120) (fig 3.3A). CC3AI, sequence taken from (J. Zhang et al., 2013), was synthesised with the addition of a Kosak sequence (GCCACC) at the 5' and P2A at the 3'. The whole construct was again flanked by restriction sites MluI and BssHII to allow for one step restriction cloning into pcDNA5-FRT-Fucci2a to generate CC3AI-Fucci2a (fig 3.3B). Stable

3T3 cell lines were generated for each construct using the Flp-In system (fig 2.1B) (Invitrogen).

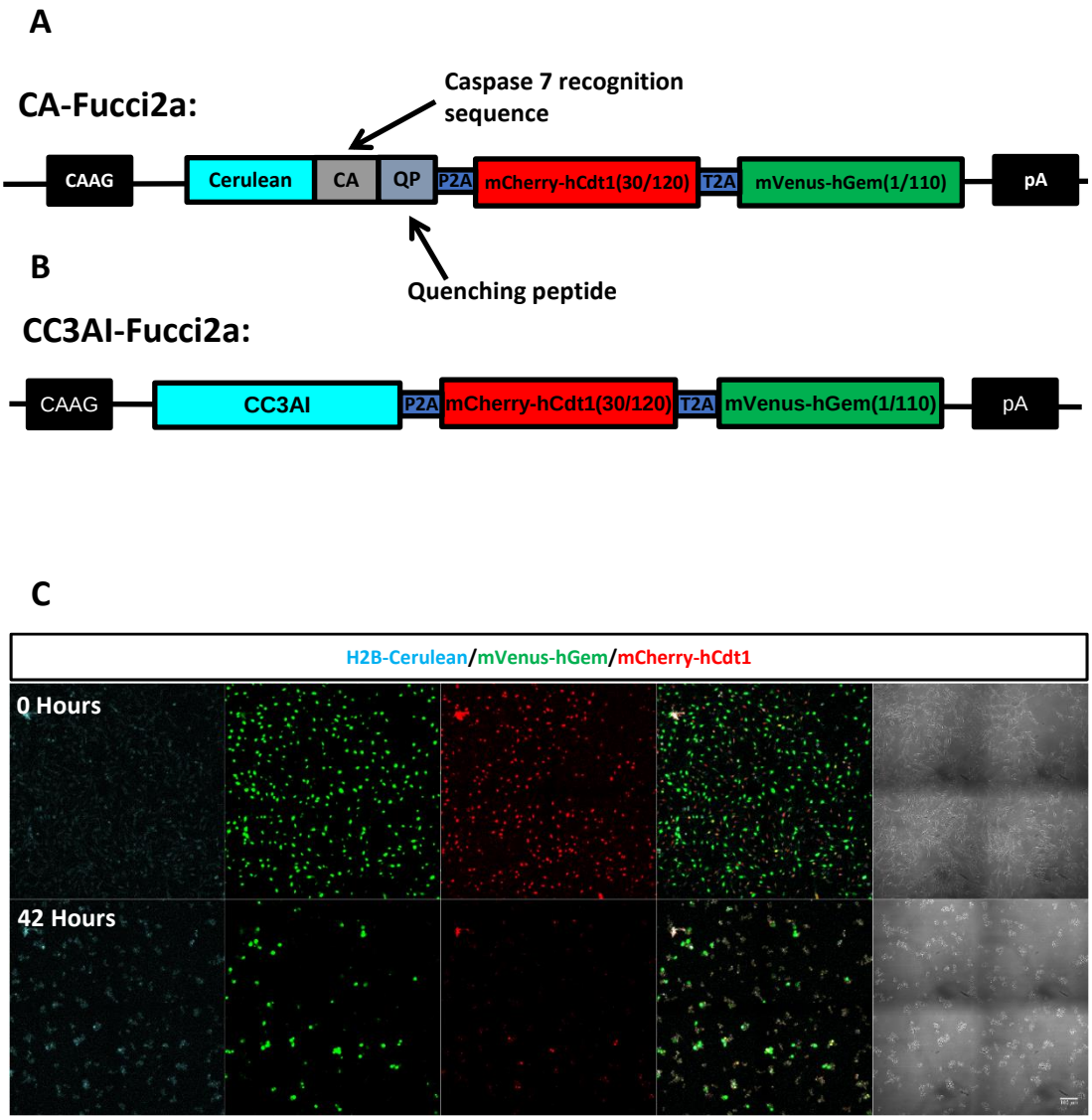

Fig 3.3: Generation of CA/CC3AI-Fucci2a 3T3 cell lines. (A) Schematic of CA-Fucci2a construct. CA-cerulean contains the Cerulean fluorophore fused to a quenching peptide separated by a capase-7 like recognition sequence. CA-Cerulean was synthesised by geneart and fused to Fucci2a separated by the self-cleaving peptide P2A. **(B)** Schematic of CC3AI-Fucci2a construct. CC3AI-cerulean contains the sequence for a caspase inducible modified Cerulean fluorophore which has been fused to Fucci2a separated by the self-cleaving peptide P2A. **(C)** Stills taken from a time-lapse of CA-Fucci2a 3T3 cells cultured in 1µm stauosporine showing an increase in cerulean fluorescence in cells undergoing apoptosis.

3.2.1.2 Characterisation of CA-Fucci2a / CC3AI-Fucci2a constructs

Initial imaging of the CA-Fucci2a 3T3 cell line showed correct localisation and cell cycle phase specificity of the Fucci probes and a low level of Cerulean fluorescence which increased after addition of 1µm staurosporine (fig 3.3C and sup video 6). Staurosporine inhibits kinases' activity by preferential binding to the ATP binding site and is a commonly used inducer of apoptosis (Chae et al., 2000; Feng & Kaplowitz, 2002; Nicholls et al., 2011; Thuret, 2003). In human melanoma and mouse lymphatic (L1210) cell lines, staurosporine has been shown to induce apoptosis by an early caspase dependent pathway and a late caspase independent mechanism (Belmokhtar et al., 2001; Zhang at al., 2003). Belmokhtar et al reported a variation in the time taken for staurosporine to induce apoptosis between different L1210 sublines. In my 3T3 cultures apoptosis was induced instantly from the start of the time-lapse. Concerned staurosporine treatment was too harsh in my 3T3 cultures and therefore not a good physiological model to test the effectiveness of CA-Fucci2a and CC3AI-Fucci2a, TNFα, another commonly used apoptosis inducer, was tested. TNFα (tumor necrosis factor alpha) is a cytokine produced by macrophages and is involved in regulating immune cells during inflammation (Wajant et al., 2003). TNFα induces apoptosis via activation of caspase-8 or can promote survival by the activation of transcription factor NF-kB (Micheau & Tschopp, 2003; Rath & Aggarwal, 1999; Wang et al., 2008). The effectiveness of both apoptotic reporter constructs was tested by addition of 50ng/ml TNFα in order to induce apoptosis followed by time-lapse imaging. Time-lapse imaging of CA-Fucci2a and CC3AI-Fucci2a 3T3 cell lines cultured in 50ng/ml TNFα showed an increase in Cerulean fluorescence in a subset of cells undergoing apoptosis (fig 3.4A-B and Sup videos 7 and 8). Cells were confirmed to be apoptotic by their detachment from the bottom of the dish and rounded morphology in brightfield images (Häcker, 2000).

Quantification of Cerulean fluorescence in 100 cells at the beginning to the end of the time lapse showed that even though CC3AI had a lower starting level of cerulean fluorescence (likely due to incomplete quenching of cerulean by the quenching peptide in CA-cerulean), an increase in cerulean fluorescence of 6816±682 mean

fluorescence integrated density and 9947±629 was seen for CC3AI-Fucci2a and CA-Fucci2a respectively (fig 3.4C). The CA-Cerulean construct produced the largest fold change with a 2.8 fold increase compared to a 2.3 fold increase for CC3AI (fig 3.4C). The same fold change was also seen when 5 individual cells were tracked throughout the time-lapse (fig 3.5A and B). A 3 fold change was reported by Nicholls et al for the original CA-GFP, therefore confirming similar behaviour of the reporter in my system using the cerulean fluorophore (Nicholls et al., 2011). The fold change of the CC3AI reporter is not reported by Zhang et al, however, the cerulean derivative of this apoptotic reporter is known to be dimmer than the original venus based version (VC3AI) characterised in the report (conversation with authors). This is likely due to Venus being a brighter fluorophore than cerulean (Shaner et al., 2005).

Although this small change in fluorescence is sufficient to mark apoptotic cells *in vitro* it was predicted that it would not be sufficient *in vivo* when there is a higher level of background fluorescence. The decision was therefore taken not to pursue the CA-Fucci2a or CC3AI-Fucci2a constructs *in vivo*.

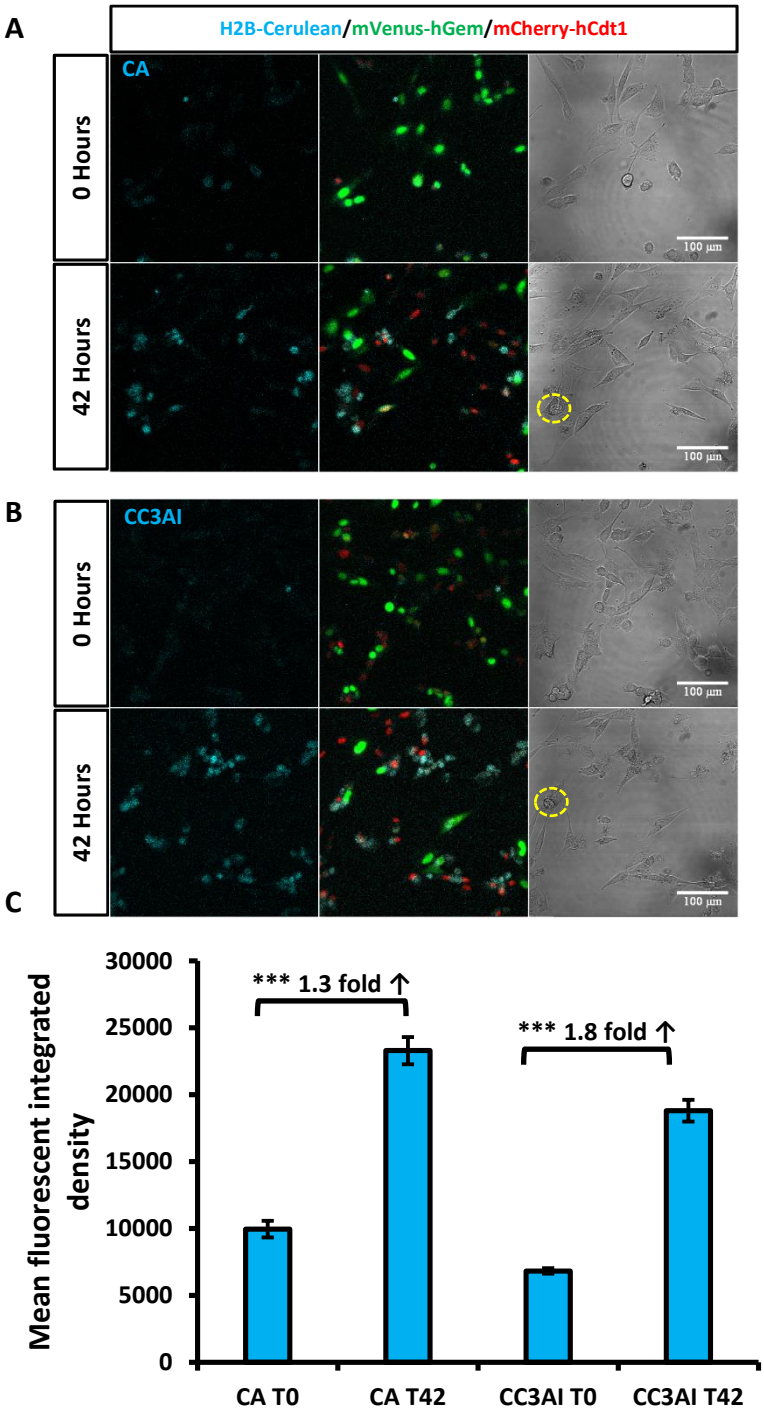

Fig 3.4: Characterisation of CA/CC3AI-Fucci2a reporter constructs. (A-B) Confocal images of CA-Cerulean-Fucci2a and CC3AI-Fucci2a 3T3 Flp-In cells taken before and after 42 hours culture in the presence of 50ng/ml TNFα. An increase in cerulean fluorescence was seen in cells undergoing apoptosis. Apoptosis was confirmed by morphological changes highlighted in bright field images. **(E)** Comparison of increased cerulean fluorescence between CA-Cerulean-Fucci2a and CC3AI-Cerulean-Fucci2a 3T3 cell lines after 42 hours culture in 50ng/ml TNFα (n = 100 cells). Error bars in C = 95% confidence interval. Statistically difference in C by student t test, *** = $p < 0.001$.

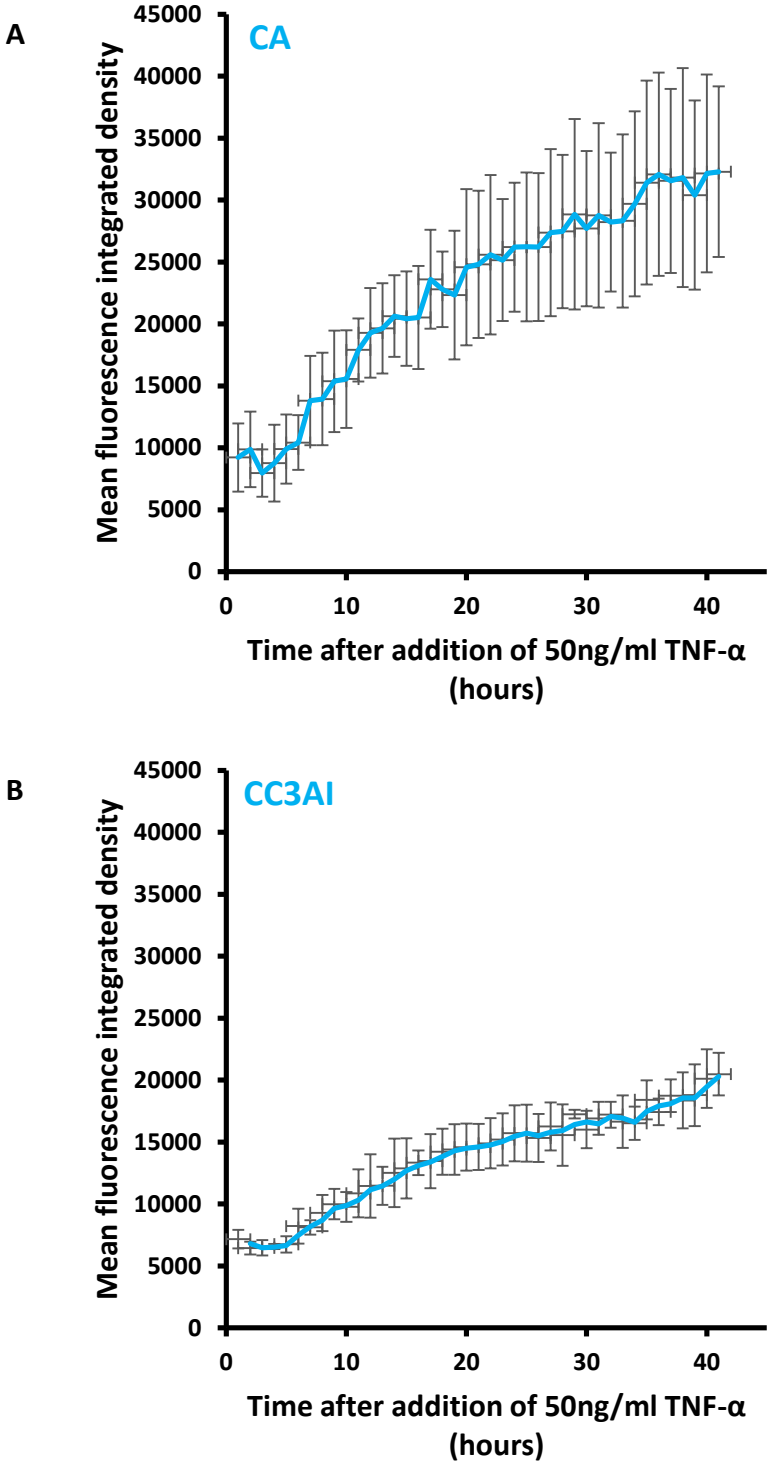

Fig 3.5: Quantification of fluorescence change induced by apoptosis in CA/CC3A-Fucci2a 3T3 cell lines. **(A and B)** Mean fluorescence change of 5 tracked cells undergoing apoptosis in CA/CC3AI-Fucci2a 3T3 cells. Error bars = 95% confidence interval.

3.2.2 Cytokinesis: H2B-Fucci2a

3.2.2.1 H2B-Fucci2a construct design and characterisation in stable 3T3 cell line

A major limitation of the Fucci system for tracking cells is the loss of fluorescence of both Fucci probes during cell division. This makes it impossible to track cells *in vivo* between cell divisions. To overcome this limitation the nuclear maker H2B-Cerulean was incorporated into the Fucci2a construct separated by another self-cleaving peptide (P2A) to allow tracking of cells through multiple cell divisions.

The H2B-Fucci2a construct was generated by PCR cloning H2B-Cerulean into pCAG-Fucci2a via an MluI restriction site between the CAG promoter and the 5' of mCherry-hCdt1(30/120) (Fig 3.6A). A Kozak sequence and the self-cleaving peptide P2A were added to the 5' and 3' ends of H2B-Cerulean by the forward and reverse primers respectively (cloning performed by Adam Douglas (University of Edinburgh). The entire CAG-H2B-Fucci2a construct was then restriction cloned into the Flp-In targeting vector pcDNA5-FRT to generate pcDNA5-FRT-H2B-Fucci2a. In brief, pCAG-H2B-Fucci2a and pcDNA5-FRT were digested with SalI and MluI respectively. These sites were then blunted before undergoing a second digest with KpnI and subsequent ligation. The stable H2B-Fucci2a cell line was generated using the Flp-In system from Invitrogen (fig 2.1B).

Characterisation of the H2B-Fucci2a 3T3 cell line was achieved by a combination of FACS analysis and live cell imaging to validate the behaviour of the H2B-Fucci2a construct and illustrate its usefulness in quantitative cell cycle analysis. Time-lapse imaging showed correct abundance of the Fucci probes in relation to the cell cycle and normal cell division. All nuclei were labelled throughout the cell cycle by H2B-Cerulean including immediately after cell division in the absence of the Fucci probes (fig 3.6B and sup video 9). The cell cycle phase specificity of the Fucci probes was confirmed by FACS analysis of DAPI stained cells (fig 3.6D). Cells were FACS sorted into mCherry-hCdt1(30/120) and mVenus-hGem(1/110) populations, fixed in 70% ethanol, DAPI stained and DNA content quantified by FACS based on DAPI

fluorescence intensity. mCherry-hCdt1(30/120) positive cells were clearly in G1 and have a peak at 2n whereas mVenus-hGem(1/110) positive cells had a higher DNA content due to DNA replication during S-phase and have a peak at 4n (fig 3.6D). Analysis of the FACS sorted cells further confirmed all cells are labelled with H2B-Cerulean (97±0.65%) (fig 3.6C).

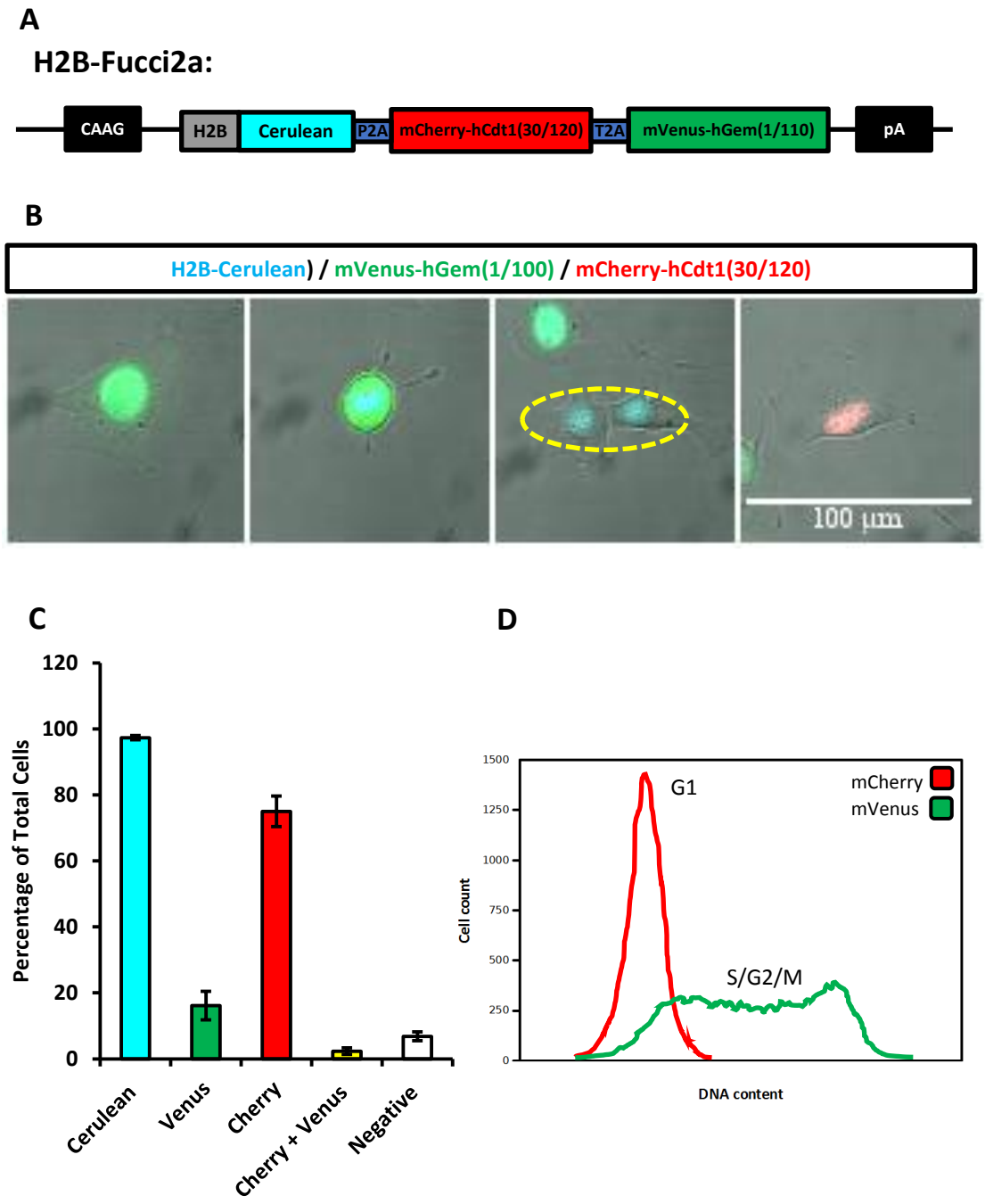

Fig 3.6: Characterisation of H2B-Fucci2a construct in 3T3 cells. (A) Schematic of H2B-Fucci2 construct. **(B)** Confocal images of a tracked H2B-Fucci2a 3T3 cell going through mitosis, highlighting the maintenance of cerulean fluorescence immediately after mitosis in the absence of Fucci2a. **(C)** FACS analysis from 5 independent FACS sorts of H2B-Fucci2a 3T3 cells. **(D)** FACS DNA content analysis of FACS sorted H2B-Fucci2a 3T3 cells using DAPI intensity to quantity DNA content. mCherry positive cells show a DNA content of 2n confirming G1 specificity where as mVenus positive cells are in S/G2/M showing a higher DNA content and a peak at 4n. error bars in (C) = 0.05 confidence.

3.2.2.2 Serum promotes cell cycle progression in 3T3 cells

To illustrate the utility of H2B-Fucci2a as a tool for generating quantitative cell cycle data, H2B-Fucci2a 3T3 cells were cultured in 10% and 20% fetal calf serum (FCS) and time-lapse fluorescent imaging performed. Cells were semi-automatically tracked using imageJ on the strong H2B-cerulean signal and the changes in fluorescence intensity of the two Fucci2a probes measured. The lengths of G1, the S/G1 transition, S/G2/M and total cell cycle time were calculated from normalised fluorescence intensity plots, based on the length of the green, yellow (green + red) and red phases respectively (fig 3.7A). The results are summarised in fig 3.7B. 3T3 cells cultured in 20% FCS showed a significantly shortened cell cycle of 18.06±1.26 hours compared to 22.72±2.10 hours for 3T3 cells cultured in 10% FCS. This is predominantly due to a statistically significant shortened G1 of 5.58±0.69 hours compared to 9.15±2.06 hours in cells cultured in 10% FCS. Although the same trend could also be seen in the other cell cycle stages, there was no statistically significant difference. Interestingly there was a highly significant correlation in cell cycle length between two paired daughter cells over a wide range of cell cycle times (fig 3.7C), but no relationship seen between randomly paired cells from the same data set (fig 3.7D). The similarity in cell cycle times between daughter pairs suggests that on top of the extrinsic factors, such as the availability of growth factors shown above, there are intrinsic determinants which influence cell cycle progression. Considering I am using a polyclonal cell line and the known heterogeneity of gene expression between clonal lines (Oh et al., 2003), it is likely the concordance seen between daughter pairs and not seen in randomly paired cells and is reflecting differential gene expression between cells originating from different clones.

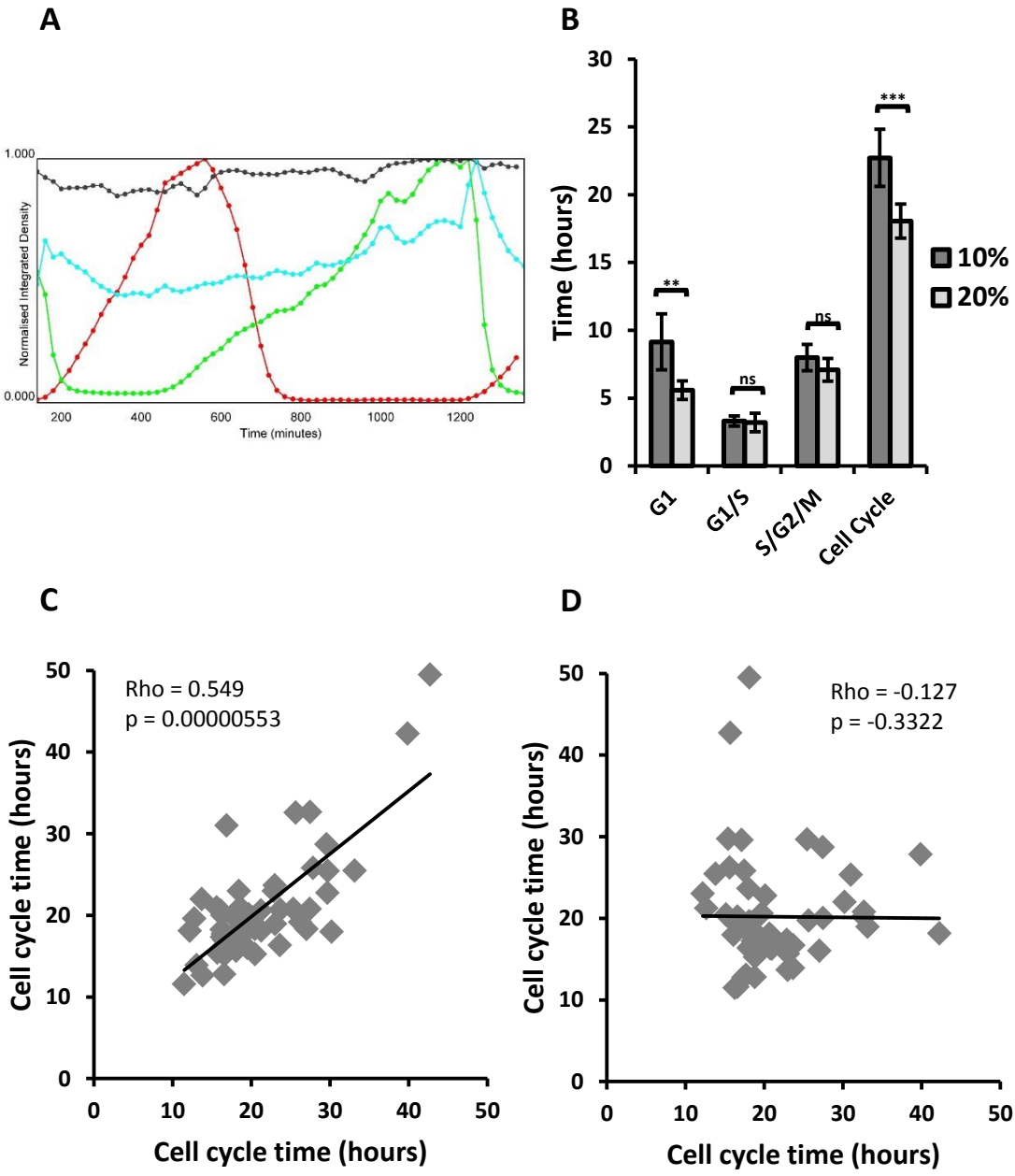

Fig 3.7: Quantitative cell cycle analysis using H2B-Fucci2a 3T3 cells. (A) Normalised fluorescence intensity plot of a tracked H2B-Fucci2a cell showing continual cerulean fluorescence throughout the whole cell cycle. **(B)** Comparison of cell cycle length between H2B-Fucci2a cells cultured in 10% and 20% serum separated by cell cycle stage. There is a significant shortening of the cell cycle in cells cultured in 20% serum, which is primary down to a shortening of G1 (n = 20). **(C and D)** Comparison of cell cycle times between two daughter cells and two randomly paired cells (n = 60 pairs). Relationship between daughter cells statistically confirmed by Spearman's Rank. Difference in length of cell cycle stages in (F) confirmed statistically by one way ANOVA $P < 0.0001$, Tukey's HSD ** = p<0.01, *** = p<0.001. error bars = 95% confidence interval.

3.2.2.3 *R26H2B-Fucci2aR* mESC and mouse have weak fluorescence signal

A conditional H2B-Fucci2a construct was generated by cloning H2B-Cerulean-P2A to the 5' end of Fucci2a in pROSA-CAG-floxNeo-Fucci2a. The inducible *R26H2B-Fucci2aR* mESC line was then generated by homologous recombination targeted to the *ROSA26* locus. Targeted mESCs were screened by 3' and 5' PCR to confirm insertion of the transgene into the *ROSA26* locus. Three clones in which the correct insertion of the transgene had been identified were expanded and karyotyped before three transgenic mouse lines were subsequently generated by mESC blastocyst injection (fig 3.8A-C). One of the transgenic lines from now on referred to as *R26H2B-Fucci2aR* (clone ♯31) was taken to further characterise, outlined bellow. In addition the entire transgene was sequenced from DNA isolated from cultured *R26H2B-Fucci2aR* (clone ♯31) mESCs and showed no mutations.

Expression of the tricistronic reporter construct was examined in mESC by transfection with a Cre-recombinase expressing plasmid (pGK-Cre). Fluorescent clones were picked, expanded and successful excision of the neomycin stop cassette confirmed by neomycin (G418) sensitivity. Live imaging showed the majority of *R26H2B-Fucci2a* mESCs were positive for mVenus-hGem(1/110) as seen previously in *R26Fucci2a* mESCs (fig 3.8D). However little to no H2B-Cerulean signal could be seen. One hypothesis would be that the P2A self-cleaving peptide may not be working efficiently, resulting in the production of a fusion H2B-Cerulean-P2A-mCherry-hCdt1(30/120) protein which would be degraded during G1. To test this, mESC were differentiated by culturing in the presence of retinoic acid (RA) with leukaemia inhibitory factor (LIF) removed for four days and live imaging repeated (fig 3.8E). As seen in *R26Fucci2a* mESC, upon differentiation the proportion of mCherry-hCdt1(30/120) cells increased. However this had no effect on H2B-Cerulean, which was still barely detectable by confocal microscopy. Live imaging of a whole mount limb bud at e12.5 in a *R26H2B-Fucci2a*$^{+/-}$*/CAG::Cre*$^{+/-}$ embryo showed very weak Fucci2a fluorescence and again almost undetectable H2B-

Cerulean fluorescence (fig 3.9A). Similar results were also seen in MEFS derived from e12.5 *R26H2B-Fucci2a*$^{+/-}$*/CAG::Cre*$^{+/-}$ embryos (fig 3.9B).

As the fluorescence intensity of all three fluorescent probes is reduced, these observations suggest either there is inefficient cleavage of the self-cleaving peptides, resulting in the production of a single protein with is degraded in all stages of the cell cycle. Or considering the success of using multiple 2A self-cleaving peptides in previous reports with almost 100% cleavage efficiency, this is unlikely (Carey et al., 2009; Szymczak et al., 2004). Another possibility is a *ROSA26* locus specific reduction in transcription of the entire transcript. Or the addition of the extra fluorescent marker has compromised mRNA stability.

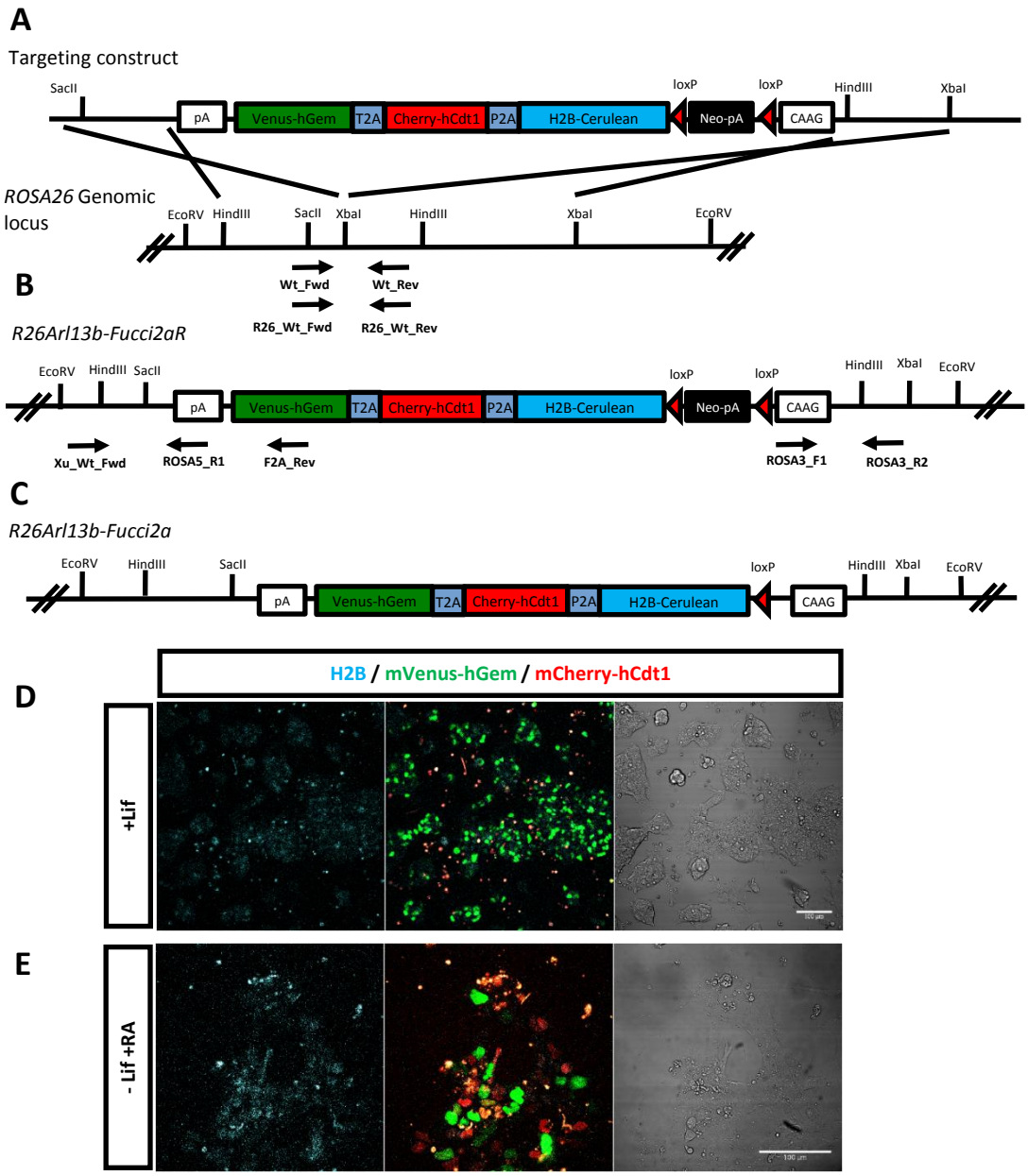

Fig 3.8: Generation of *R26H2B-Fucci2aR* mouse. (A) *H2B-Fucci2a* targeting construct. A stop cassette containing a *loxP* flanked neomycin resistance gene and polyadenylation sequence was inserted between *CAG* and *H2B-Fucci2a* . **(B)** The targeted R26H2B-Fucci2aR inducible allele, screening for correct homologous recombination was done using PCR across the 5′ and 3′ homology arms of the targeting construct. **(C)** The targeted R26H2B-Fucci2a allele after Cre-mediated excision of the floxed-Neo-pA stop cassette. **(D)** H2B-fucci2a mESC were cre-activated by transfection with a cre-expressing plasmid (pGK-Cre) and initial imaging showed the majorly of cells labelled with mVenus however H2B-cerulean was barely visible. **(E)** Differentiation of the H2B-Fucci2a mESC by culturing without Lif and in the presence of 1mM RA increased the proportion of mCherry labelled cells but had no affect on the brightness of the H2B-cerulean.

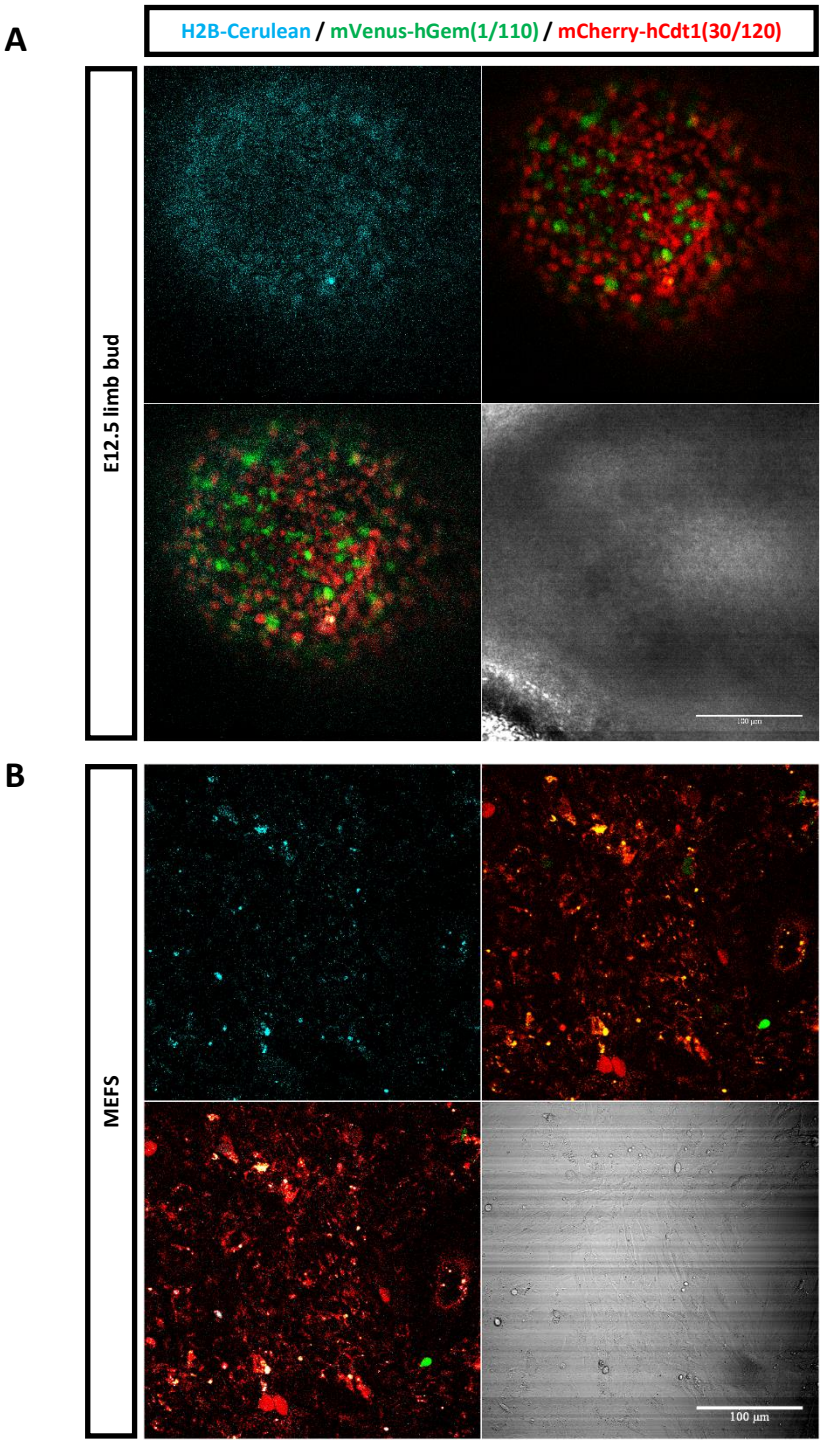

Fig 3.9: Characterisation of *R26H2B-Fucci2a*$^{+/Tg}$*::CAG-Cre*$^{+/Tg}$ mice (A) Whole mount of an e12.5 limb bud imaged between two coverslips showing very low nuclear H2B-cerulean fluorescence co-localising with the Fucci2a probes. **(B)** MEFS derived from e12.5 embryos showing dim fluorescence from the two Fucci2a probes and no detectible H2B-cerulean signal.

3.2.3 Cilia: Arl13b-Fucci2a

3.2.3.1 Arl13b-Fucci2a construct design and generation of 3T3 cell line

Primary cilia are small microtubule based structures found on the majority of cell types where they act as a signalling centre for extracellular signals such as Shh and Wnt (Corbit et al., 2008; Cortellino et al., 2009; Houde et al., 2006; Huangfu et al., 2003; Satir et al., 2010; Simons et al., 2005; Tran et al., 2016). Primary cilia are assembled during G1 and disassembled prior to cell division. This is because centrioles, which are necessary for the formation of the mitotic spindle during cytokinesis, are also found as part of a structural component at the base of the cilia known as the basal body (Seeley & Nachury, 2010). The loss of primary cilia has been associated with the onset of some cancers, while, conversely, ciliary dependent signalling is necessary for the formation of other cancers (Y. Han et al., 2009; Hassounah et al., 2013; Menzl et al., 2014; Wong et al., 2009; Yuan et al., 2010).

With the aim to study this relationship live, the Arl13b-Fucci2a construct was designed to allow dual visualisation of cell cycle progression with ciliogenesis. Adam Douglas (Edinburgh University) assembled the Arl13b-Fucci2a construct by replacing H2B from pCAG-H2B-Fucci2a via restriction sites NheI and AgeI with full length Arl13b (fig 3.10A). The entire CAG-Ar13b-P2A-Fucci2a construct was restriction cloned into pcDNA5-FRT (Invitrogen) to generate pcDNA5-FRT-Arl13b-Fucci2a, which was then used to generate the Arl13b-Fucci2a 3T3 stable cell using the Flp-In system (Invitrogen). Live imaging of Arl13b-Fucci2a cells showed normal cell behaviour with correct fluorescence of the Fucci probes in relation to the cell cycle and appearance of primary cilia labelled in cerulean as 3T3 cells entered confluency (fig 3.10B and sup video 10). Cell cycle specificity of the Fucci probes was further confirmed by cell cycle FACS analysis of FACS sorted cells counter stained with DAPI to measure DNA content (fig 3.11A). The presence of primary cilia could not be detected by FACS based on the cerulean signal, mostly likely due to reabsorption or shedding of the primary cilia during trypsinisation.

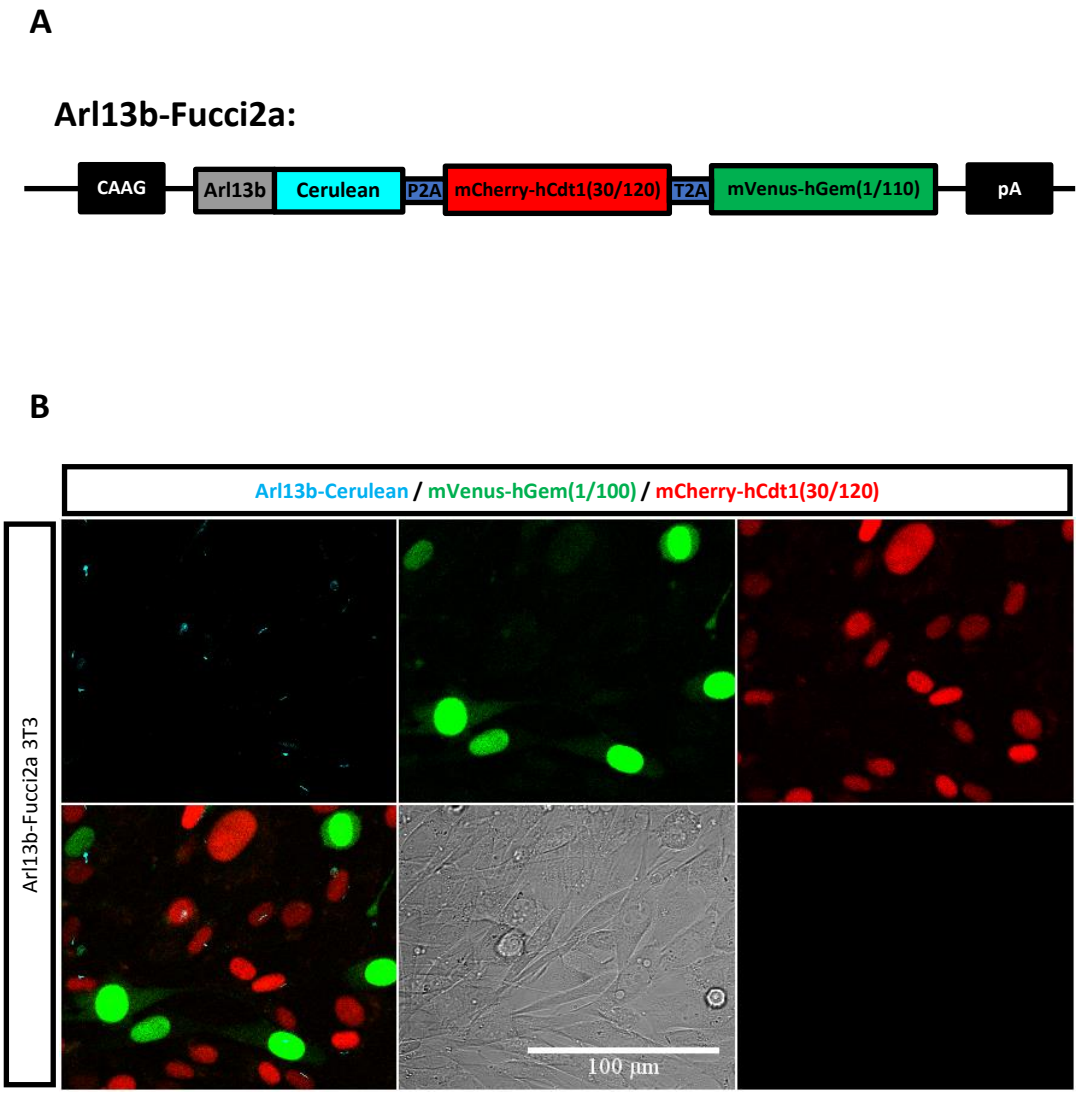

Fig 3.10: Generation of Arl13b-Fucci2a 3T3 stable cell line: (A) Schematic of Arl13b-Fucci2a construct. Arl3b-Fucci2a contains the full length mouse Arl13b sequence fused to Cerulean which has been combined with Fucci2a via the self-cleaving peptide P2A with expression driven by the CAG promoter. **(B)** Stills taken from a time-lapse of arl13b-Fucci2a 3T3 cells showing ciliated cells in all stages of the cell cycle.

3.2.3.2 Ciliary assembly time is reduced if mother cell is ciliated and concordant between daughter cells

To illustrate the ability to generate quantitative data from Arl13b-Fucci2a expressing cells, I analysed the influences on the timing of ciliary assembly using time-lapse imaging of cultured Arl13b-Fucci2a 3T3 cells. The timing of ciliary assembly after mitosis showed a large degree of variability with a mean of 500.83±128.25 minutes (fig 3.11B). Disassembly on the other hand occurred just prior to cytokinesis, simultaneously with the breaking of the nuclear envelope with the mean time for a cell to disassemble a cilia before mitosis being 74.95±25.38 minutes (fig 3.11B, sup video 11). A strong relationship was seen in the timing of cilia assembly between paired daughter cells, but not randomly paired cells from the same data set (fig 3.11C and D). To determine if cell cycle length of the previous or current cell cycle has any influence on the timing of ciliary assembly the ciliary assembly time was compared to the length of the current of G1 and previous S/G2/M (fig 3.12A-B). In both cases no statistically significant relationship was seen. This suggests that cell cycle length is not the determining factor for the timing of ciliary assembly in 3T3 cells under these conditions. Interestingly the speed of ciliary assembly is reduced if the mother cell was ciliated in its previous G1 (fig 3.12C), suggesting some biochemical properties must be inherited from the mother cell priming fast cilia assembly. Previous reports have shown the cell which inherits the older "mother centriole" will ciliate first and also retain a proportion of the primary cilium membrane (Anderson & Stearns, 2009; Paridaen et al., 2013). It is therefore possible that centriole modifications occurring in the mother cell enable faster cilia assembly. Although the timing of ciliary assembly between daughter cells was seen to be similar (fig 3.11C), there was a significant difference in the timing of the first daughter cell to ciliate to the second (fig 3.12 D and E). This is in accordance with the hypothesis that the daughter cell which inherits the mother centriole will assemble its cilia first (Anderson & Stearns, 2009; Paridaen, et al, 2013). Although, without being able to track which cell is receiving the mother centriole it is impossible to confirm that the first cell to ciliate received the mother centriole. In addition at the resolution of

imaging and without a centriole marker it was not possible to determine if a remnant of the cilia membrane labelled with Arl13b-cerulean was retained by the one of the daughter cells.

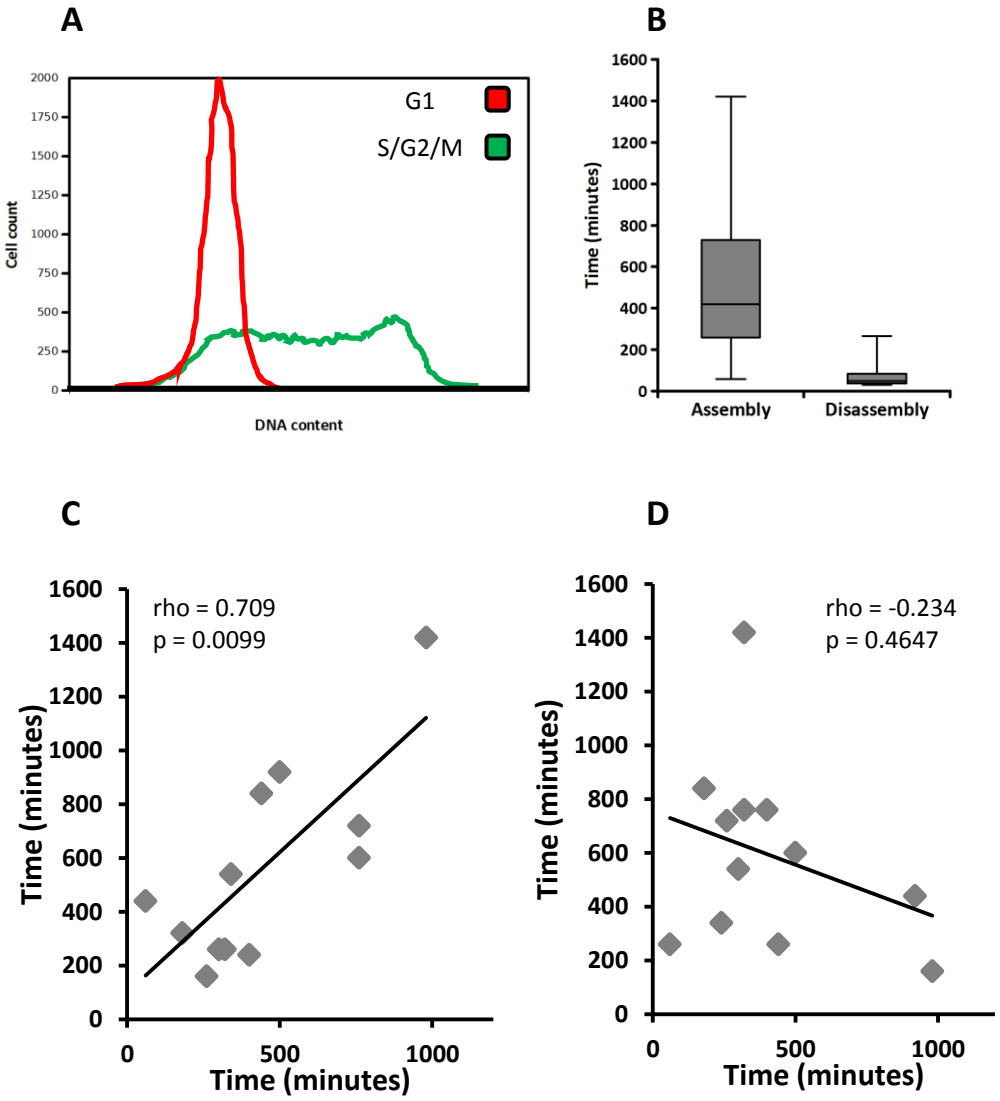

Fig 3.11: Characterisation of Arl13b-Fucci2a construct in 3T3 Flp-In cells. (A) FACS cell cycle analysis using DAPI intensity as a measure of DNA content. mCherry positive cells are in G1 where as mVenus positive cells have a higher DNA content due to DNA replication during S-phase. **(B)** Box plot showing the range of ciliary assembly and disassembly times. Assembly is measured from the point of cell division to the first appearance of a ciliary structure and disassembly from the complete loss of a cilia to cell division (n = 24 for assembly and 20 for disassembly). **(C and D)** Comparison of ciliary assembly times between daughter cells and randomly paired cells (n = 12 pairs). Relationship between daughter cells statistically confirmed by Spearman's Rank.

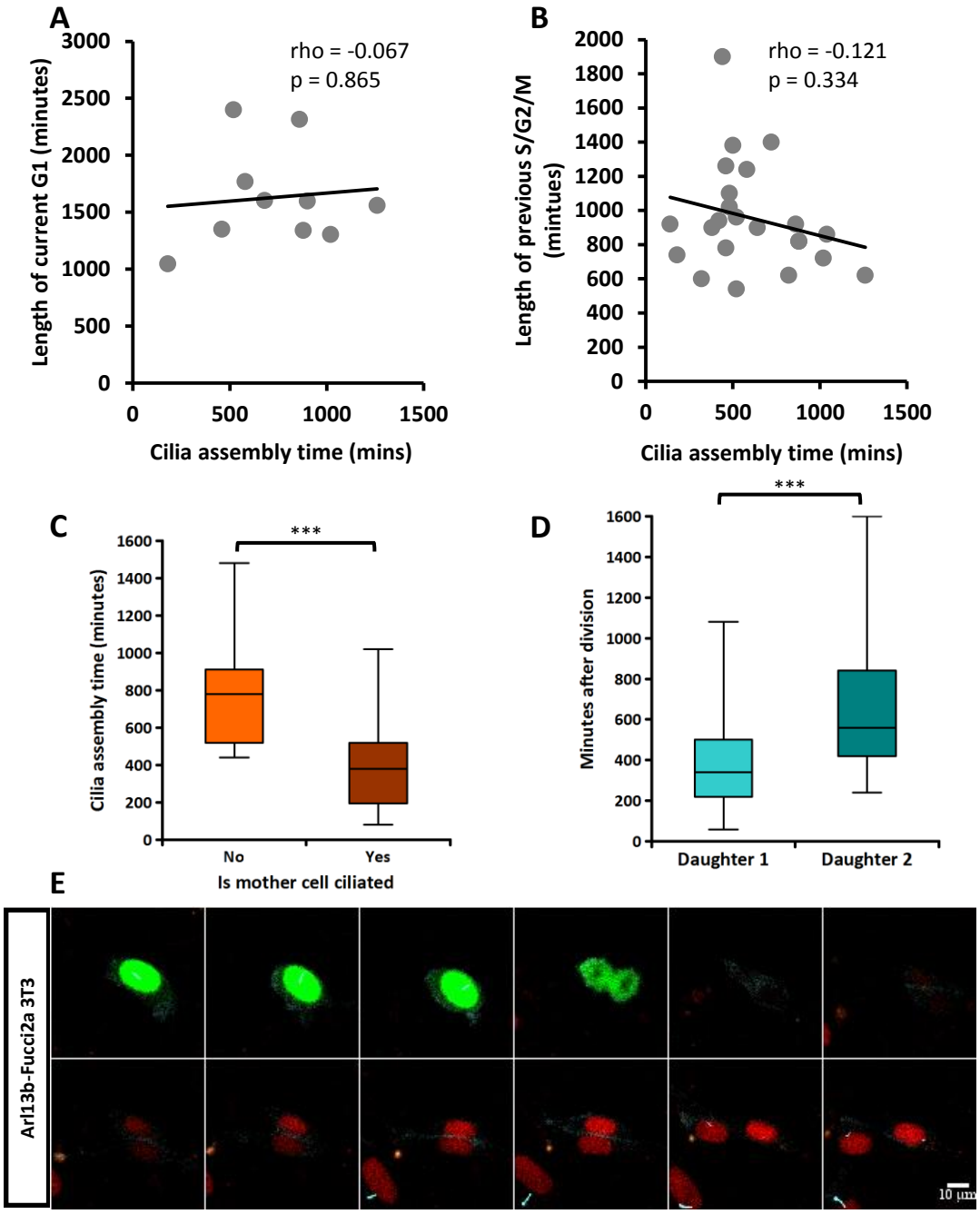

Fig 3.12: Dynamics of cilia assembly. (A) Scatter plot showing no significant relationship between the length of the current G1 and ciliary assembly time (n=10). **(B)** Scatter plot showing no significant relationship between the length of the previous cell cycle and ciliary assembly time (n=23). **(C)** Box plot showing cells significantly assemble their cilia faster when the mother cell is ciliated. **(D)** Box plot showing a significant difference in the timing of ciliary assembly between daughter cells suggesting the cell which inherits the mother centriole ciliates first. **(E)** Stills taken every hour showing cilia reabsorption just prior to cytokinesis and assembly 7 and 8 hours after cell division. Nonsignificant relationship in A and B shown by Spearman's rank correlation. Significant difference in C and D shown by student's t-test (*** = P<0.001)

3.2.3.3 3T3 cells orientate their cilia towards the leading edge in wound healing assay

To test the observation that cells orientate their primary cilia towards the leading edge during migration (Schneider et al., 2010), Arl13b-Fucci2a 3T3 cells were imaged migrating in a modified wound healing assay. Cells were seeded at high density inside a silicon well stuck to the bottom of a glass bottomed dish by surface tension. Once cells had ciliated the silicon well was removed and cells were imaged migrating from the leading edge into the surrounding open space (fig 3.13A and sup video 12). To examine the correlation between cilia angle and the angle of migration, the orientation of the primary cilia in relation to the centre of the cell's nucleus was calculated in ImageJ five and ten hours after removal of the silicon barrier and then corrected to the angle of migration (fig 3.13B). In a control experiment Arl13b-Fucci2a 3T3 cells were seeded evenly onto a plate with no directional movement. As expected there was an equal spread of cilia angles in 360^{o} (fig 3.13C). However after 5 hours in the migration assay cells were seen to be beginning to orientate their cilia towards the leading edge (fig 3.13D). This affect became statistically significant by two sample Kolmogorov-Smirnov test ($P = 0.013$) after 10 hours (fig 3.13E). This result is in accordance with observations seen by Schneider et al, 2010 using immunofluorescence techniques in a traditional wound-healing assay. In addition it also shows that in 3T3 cells migration occurs before cilia reorientation.

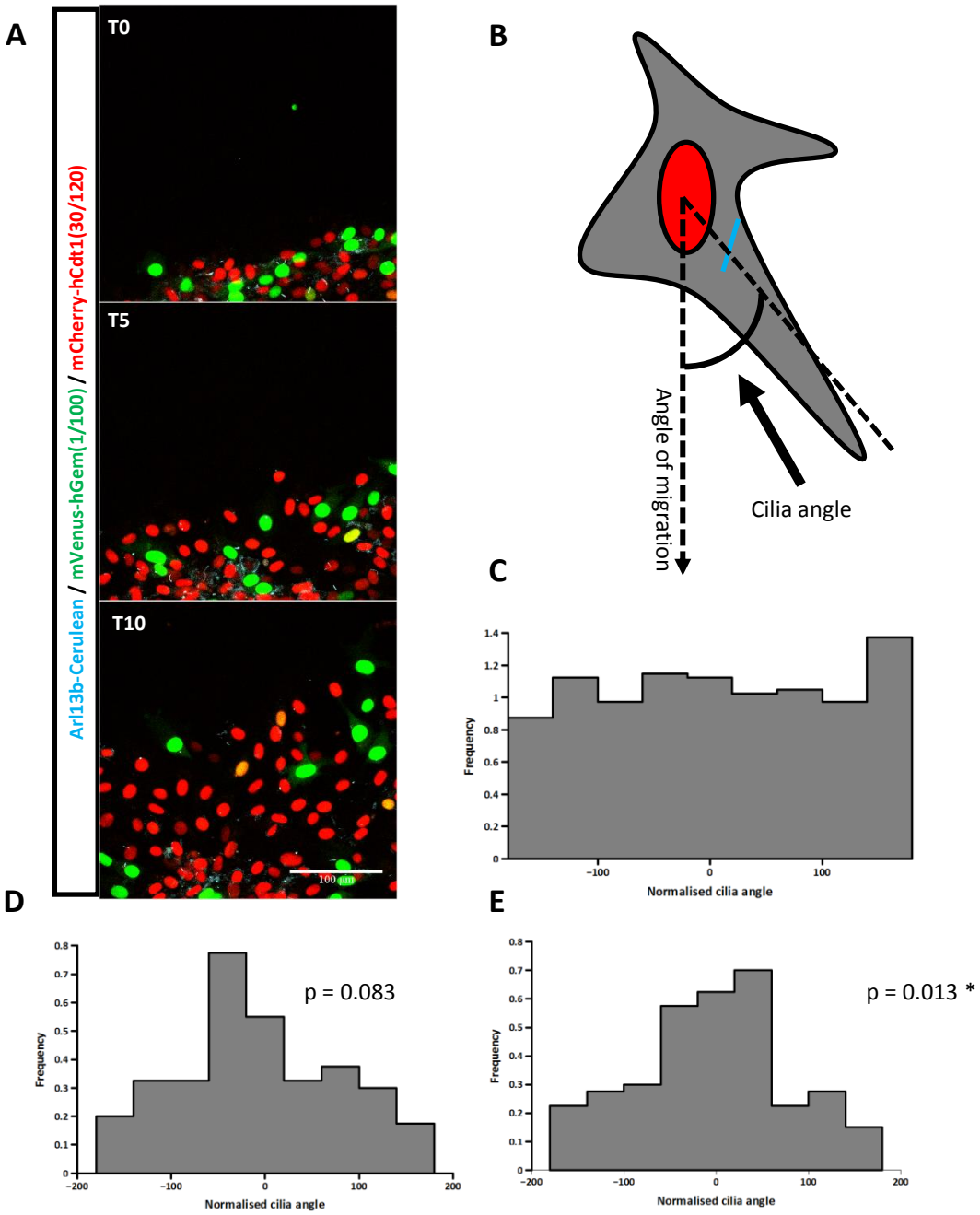

Fig 3.13: 3T3 cells orientate their primary cilia towards the leading edge in wound healing assay. (A) Stills of Arl13b-Fucci2a 3T3 cells migrating from the leading edge after removal of a silicon barrier. **(B)** Illustration of cilia angle calculation. The angle between the centre of the nucleus to the centre of the cilia is measured using imageJ. This angle is then corrected to the angle to migration to determine the position of the cilia in relation to the movement of the cell. **(C)** Histogram of ciliary angles corrected to the angle of migration under control conditions when there is no directional movement (n=387 cells) **(D and E)** Histogram of ciliary angles 5 and 10 hours after removal of the silicon barrier showing a rearrangement of cilia towards the leading edge which is significant by the Kolmogorov-Smirnov test (two sample) after 10 hours (n=133(5hours) n=135(10hours).

3.2.3.4 MEFS are ciliated but primary cilia are detected in mESC

R26Ar13b-Fucci2aR mice were generated by homologous recombination into the *ROSA26* locus in mESC (fig 3.14A-C). Three clones were identified by 3' and 5' PCR to have the transgene inserted into the *ROSA26* locus in the correct orientation. Each line was expanded and karyotyped before three transgenic mice lines were generated by blastocyst injection. The transgenic line generated from mESC clone ♯4 now referred to as *R26Arl13b-Fucci2aR* was taken on for further characterisation outlined in this section.

Expression of the *R26Arl13b-Fucci2a* transgene was assessed in mESC by transfection with a Cre expressing plasmid (pGK-Cre) to excise the neomycin stop cassette followed by live imaging (fig 3.15A). Under serum ES cell culture conditions (10% serum + LIF) both mCherry-hCdt1(30-120) and mVenus-hGem(1/110) positive cells were detected within ES clones. However in disagreement with previous reports no primary cilia were detected (Bangs et al, 2015; Hunkapiller et al, 2011). This discrepancy may be explained by the different culture methods used. Bangs et al used serum free 2i + LIF media. The presence of cilia on mESCs cultured in 2i but not mESCs is surprising considering 2i cultured mESCs are reported to be in a more pluripotent ground state (Marks et al., 2012; Ying et al., 2008). This represents an intriguing difference between these two culture conditions which should be investigated in more detail. Hunkapiller et al grew mESC in serum media + LIF but in suspension to form embryoid bodies. Embryoid bodies are more differentiated than ES cells and contain cells from the three embryonic germ layers (mesoderm, ectoderm and endoderm) (Desbaillets et al., 2000; Itskovitz-Eldor et al., 2000). Cilia have been identified as early as e6.0 in the epiblast and subsequently in all germ layers but not in extra embryonic lineages (Bangs et al., 2015). Considering mESCs are thought to be comparable to the ICM (inner cell mass) this would explain why cilia are not present in my cultures but are in embryoid bodies that represent a more differentiated lineage. However it is also important to consider that the reporter I have used does not label cilia in ES cells or is too dim for cilia to be detected. Considering this the conformation of the absence of cilia could

be confirmed by immunhistochemical techniques using primary antibodies raised against arl13b or acetylated tubulin. Live imaging of a primary ciliated cell line (mouse embryonic fibroblast), derived from *R26Atl13b-Fucci2a*$^{+/Tg}$*/CAG::Cre*$^{+/Tg}$ embryos, confirmed the ability of the *R26Arl13b-Fucci2a* reporter to label cilia with cell cycle progression (fig 3.15B).

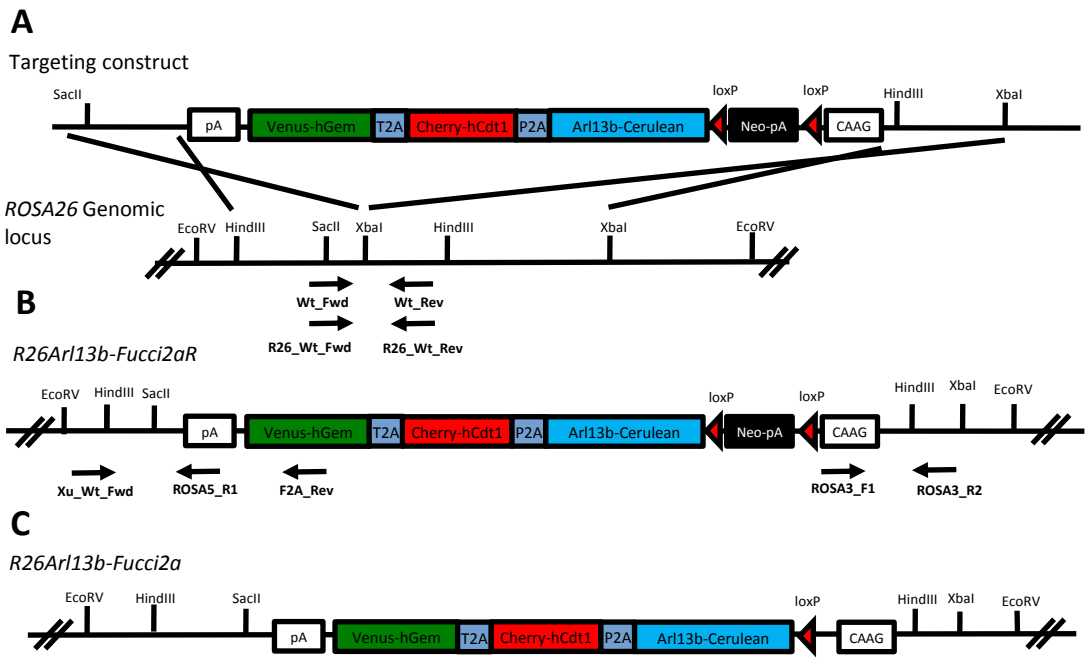

Fig 3.14: Generation of *R26Arl13b-Fucci2aR* mouse. (A) Arl13b-Fucci2a targeting construct, a stop cassette containing a loxP flanked neomycin resistance gene and polyadenylation sequence was inserted between *CAG* and *Arl13b-Fucci2a* . **(B)** The targeted *R26Arl13b-Fucci2aR* inducible allele, screening for correct homologous recombination was done using PCR across the 5′ and 3′ homology arms of the targeting construct. **(C)** The targeted *R26Arl13b-Fucci2a* allele after Cre-mediated excision of the floxed-*Neo-pA* stop cassette. *R26Arl13b-Fucci2aR* mouse was generated by targeted recombination of the *rosa26* locus in mESC and positive clones screened by 3' and 5' pcr. The entire construct was inserted in the reverse orientation to limit transcriptional interference from the endogenous *Rosa26* promoter and made inducible by a neo-stop cassette flanked by loxP sites after the CAAG promoter.

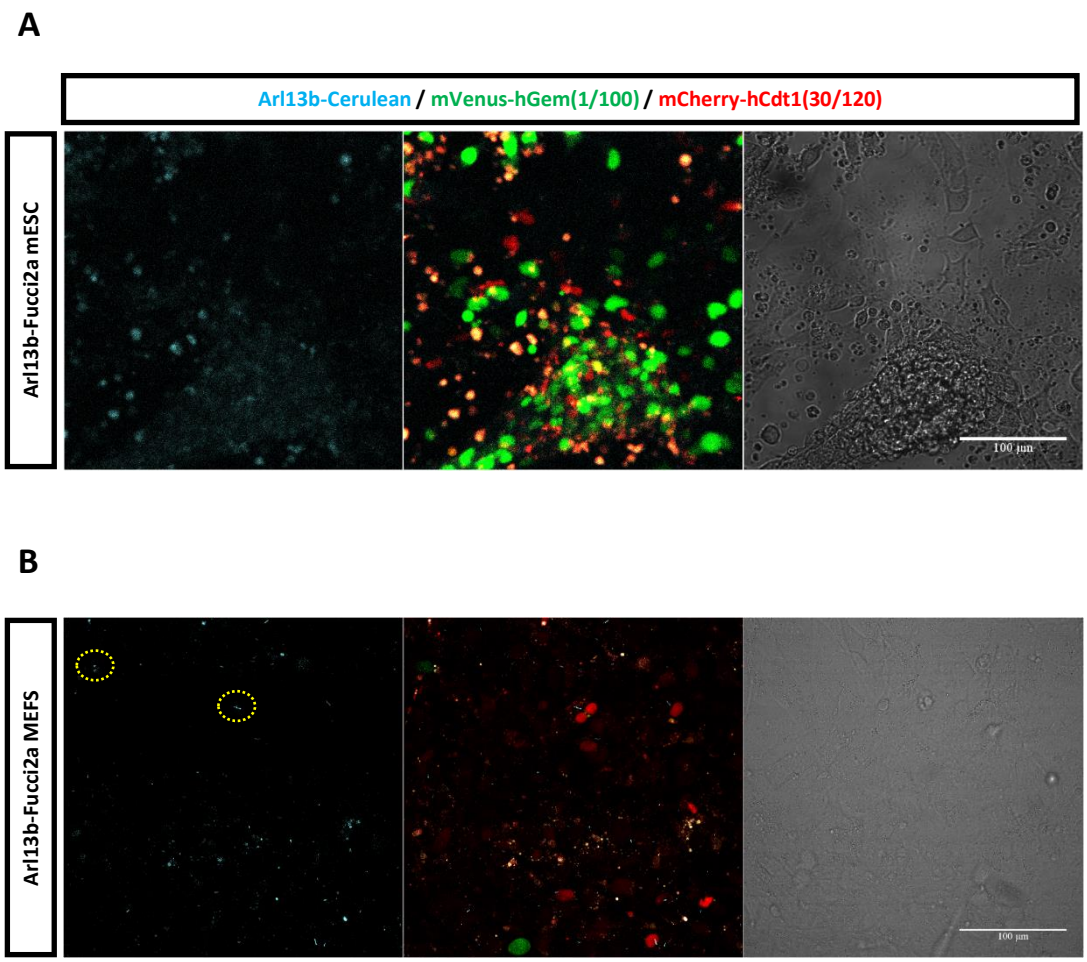

Fig 3.15: Arl13b-fucci2a expression in mESC and MEFS (A) Arl13b-Fucci2a expression was induced in mESCs by transfection with pPGK-Cre-bpA and selected by fluorescence. Fluorescence of the fucci2a probes is clearly visible although no obvious cilia could be identified. **(B)** Confocal images of *R26Arl13b-Fucci2a* MEFS derived from an R26*Arl13b-Fucci2a*$^{+/Tg}$/*CAG-Cre*$^{+/Tg}$ embryo. Fucci signal is easily detectible and cilia can be seen clearly labelled in cells in all stages of the cell cycle.

3.2.3.5 Expression of *R26Arl13b-Fucci2a in vivo* labels primary cilia and cell cycle stage

To characterise the *R26Arl13b-Fucci2aR* mouse it was crossed with the ubiquitous *CAG::Cre* and a selection of different embryonic tissues examined. Live imaging of a whole mount e8.5 embryo in the cranial region revealed the majority of cells to be ciliated, regardless of cell cycle stage (fig 3.16A) This is in agreement with a previous report using a constitutive Arl13b-mCherry transgenic mouse which reported the presence of primary cilia within all but extraembryonic lineages from e6.0 (Bangs et al., 2015). Very few cells within the head were mCherry-hCdt1(30/20) positive suggesting a high rate of proliferation at this stage in development. Cells surrounding the ventricles were orientated perpendicular to the lumen and were highly proliferative, as shown by the high proportion of cells labelled with mVenus-hGem(1/110) (fig 3.16A). The luminal cavity contained a high density of cilia projecting from the surrounding cells (fig 3.16B, see sup video 13 for Z-series). Considering motile cilia within the ventricles form postnatally in the mouse (Spassky et al, 2005), it is likely these are primary cilia. At this stage in development prior to neurogenesis, which commences around e11, the epithelium surrounding the ventricles is constructed of a single layer of neural stem cells organised into a pseudostratified neuroepthelium (Götz & Huttner, 2005). Little is known about the role of primary cilia during this stage of development. However, during neurogenesis it has been shown that the primary cilia is not fully disassembled during mitosis. This results in an asymmetric inheritance of rudimental ciliary structures associated with the mother centriole enabling the cell that inherits the mother centriole to ciliate first and retain its position in the multipotent niche, while the cell which does not receive the mother centriole is destined for differentiation (Paridaen et al., 2013;Wang et al., 2009). It has also been shown that the cerebrospinal fluid (CSF) provides proliferative and survival support to neural progenitors by Igf2 signalling with binding enriched along primary cilia (Lehtinen et al., 2011). At this stage in development, prior to neurogenesis and the onset on differentiation, the anchoring of cells to the ventricular lumen via a ciliated

membrane may therefore be required to detect signals in the CSF necessary to maintain their multipotent potential and promote proliferation.

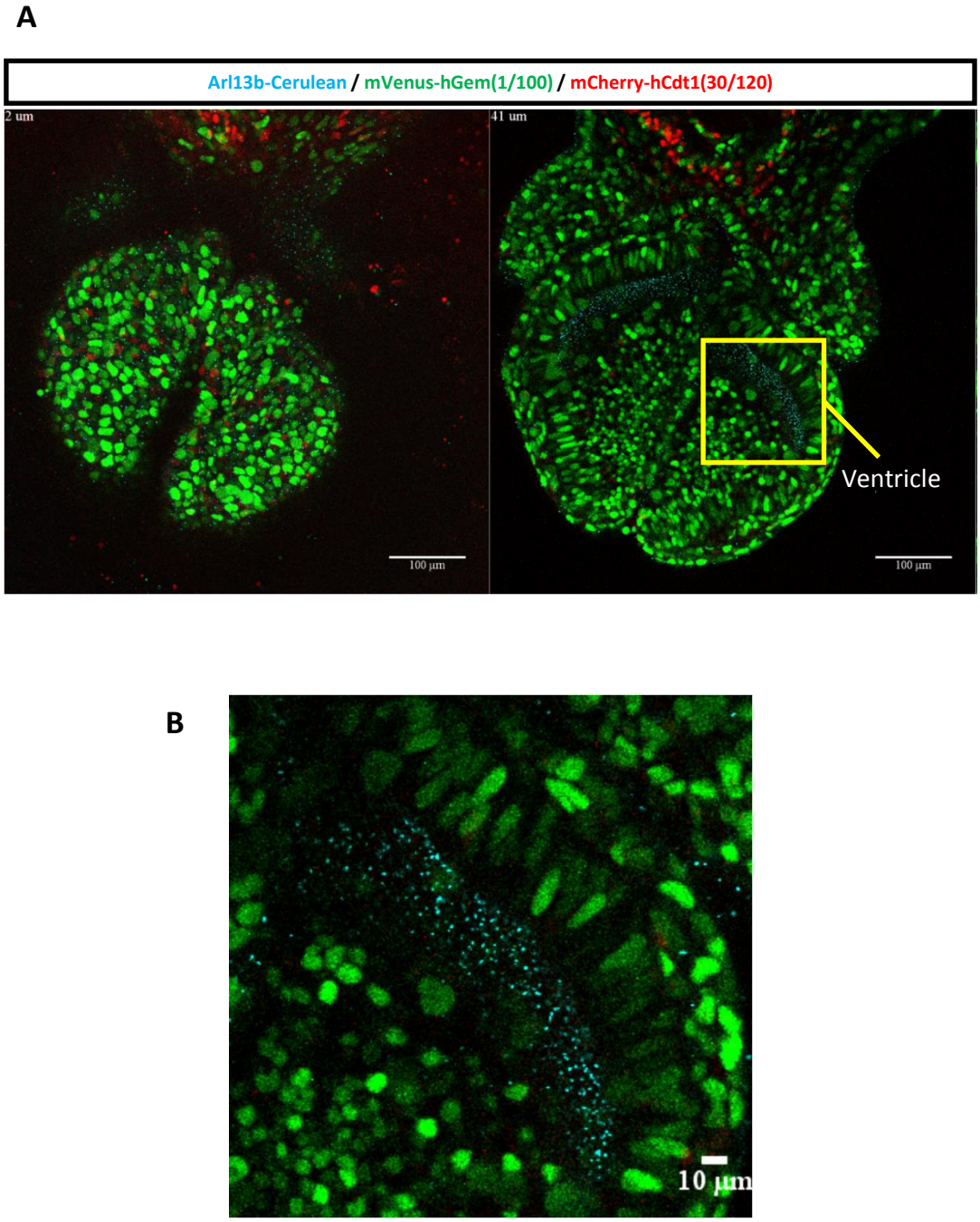

Fig 3.16: Analysis of live *R26Arl13b-Fucci2a*$^{+/Tg}$*/CAG::Cre*$^{+/Tg}$ embryos: (A) Live confocal imaging of an e8.5 head. Cilia are present on the majorly of cells regardless of cell cycle stage. **(B)** Magnification of boxed region in A highlighting a high concentration of primary cilia orientated into the lumen of the ventricles.

3.2.3.6 Transient node cells have are in G1/G0 of the cell cycle and have anterior orientated primary cilia

In the mouse at e7.5 a transient structure known as the node forms at the anterior tip of the embryo and is responsible for determining left-right asymmetry in the developing embryo (Babu & Roy, 2013). It has been shown that specialised motile primary cilia on these cells are necessary for producing a right to left nodal flow which induces nodal signalling specifically on the left side (Hirokawa, 2000; Nonaka et al., 1998; Nonaka et al., 2002). Two models have been suggesting for the transformation of this right to left nodal flow and the induction of left siding nodal signalling. Classically it was thought an as yet unidentified morphogen is moved to the left side and subsequently induces nodal signalling, however, recent evidence has shown only two rotating cilia are sufficient to break left-right symmetry (Shinohara et al., 2012). This brings into question how such a low fluid flow can create a morphogen gradient. A "two cilia" model has been suggested in which non-motile mechanosensory cilia located on surrounding perinodal crown cells are able to sense nodal flow via the Ca^{2+} channel Pkd2 (Yoshiba et al., 2012).

Whole mount live imaging of e7.5 *R26Arl13b-Fucc2a*$^{+/Tg}$*/CAG::Cre*$^{+/Tg}$ embryos clearly identified the node as a cluster of cells in stages G1 or G0 of the cell cycle labelled with mCherry-hCdt1(30/120) at the anterior tip of the embryo (fig 3.17A). Nodal cilia are orientated into a 10µm deep concave compartment on the edge of the embryo. By turning the embryo and imaging from the anterior perspective approximately 180 nodal cilia could be identified, consistent with previously reported numbers (200-300) (Shinohara et al., 2012) (fig 3.17B and see sup video 14 for Z-series). Under the culture conditions used it was not possible to capture time-lapse images of cilia movement. The *R26Fucci2aR* reporter line provides an opportunity to visualise cilia movement live and could be used to identify the two motile and sensing cilia populations proposed by the "two cilia" model in an appropriate culture system.

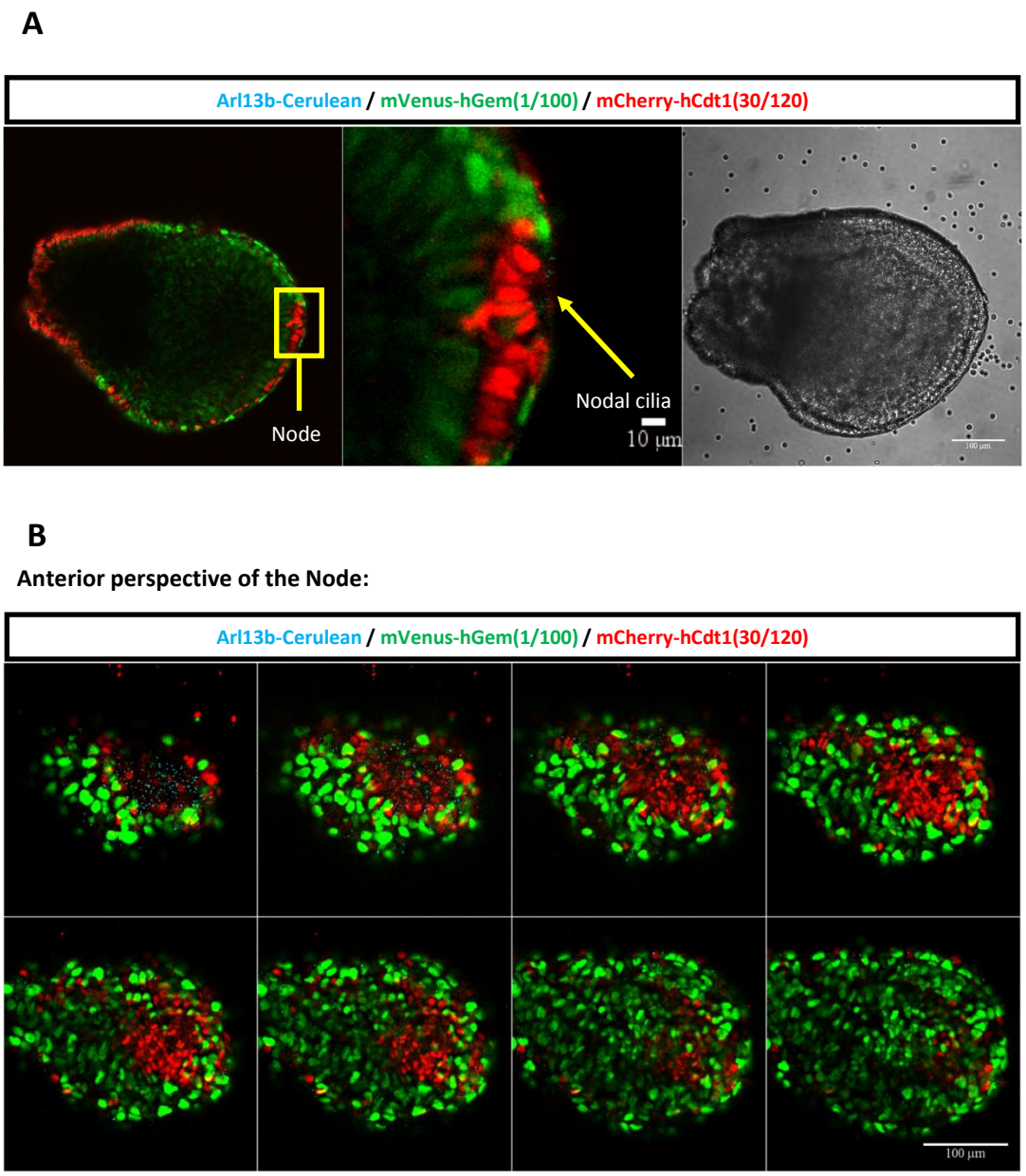

Fig 3.17: Arl13b-Fucci2a expression at the node in *R26Arl13b-Fucci2a$^{+/Tg}$/CAG::Cre$^{+/Tg}$* embryos: (A) Coronal confocal section through an e7.5 live embryo. Cells in the node have dropped out of the cell cycle and are clearly distinguishable at the anterior tip of the embryo labelled with mCherry-hCdt1(30/120). Nodal cilia can be seen labelled with Ar13b-Cerulean protruding into a concave compartment. **(B)** Transverse confocal sectioning through the node in 3µm sections (same embryo as imaged in (A)).

3.2.3.7 *R26Arl13b-Fucci2a* labels motile cilia

Arl13b-GFP has been previously shown to label motile cilia as well as primary cilia (Delling et al., 2013). To validate Arl13b-Fucci2a as a tool to visualise motile cilia I derived multiciliated primary ependymal cultures from e18.5 *R26Arl13b-Fucc2a*$^{+/Tg}$*/CAG::Cre*$^{+/Tg}$ embryos (Fig 3.18A). Briefly, the ventricular zone from e18.5 embryos was dissected and dissociated into a single cell suspension before being seeded onto a glass-bottomed plate (see 6.5.2 in methods). A mixture of cells in G1 and S/G2/M could be seen as the ependymal cells proliferated in culture with primary cilia clearly labelled on the majority of cells. Once the cultures had grown to confluency, allowing the formation of tight junctions, the ependymal cultures were serum starved. The proportion of cells in S/G2/M progressively dropped as ependymal cultures were grown to confluency with all cells being in G1/G0 labelled with mCherry-hCdt1(30/120) during differentiation. Seven days after serum starvation differentiated ependymal cells started to disassemble their primary cilium and assembled multiple motile cilia (fig 3.18B). High speed confocal imaging confirmed the motility of these cilia which moved in an unsynchronised unidirectional whip like motion (sup video 15).

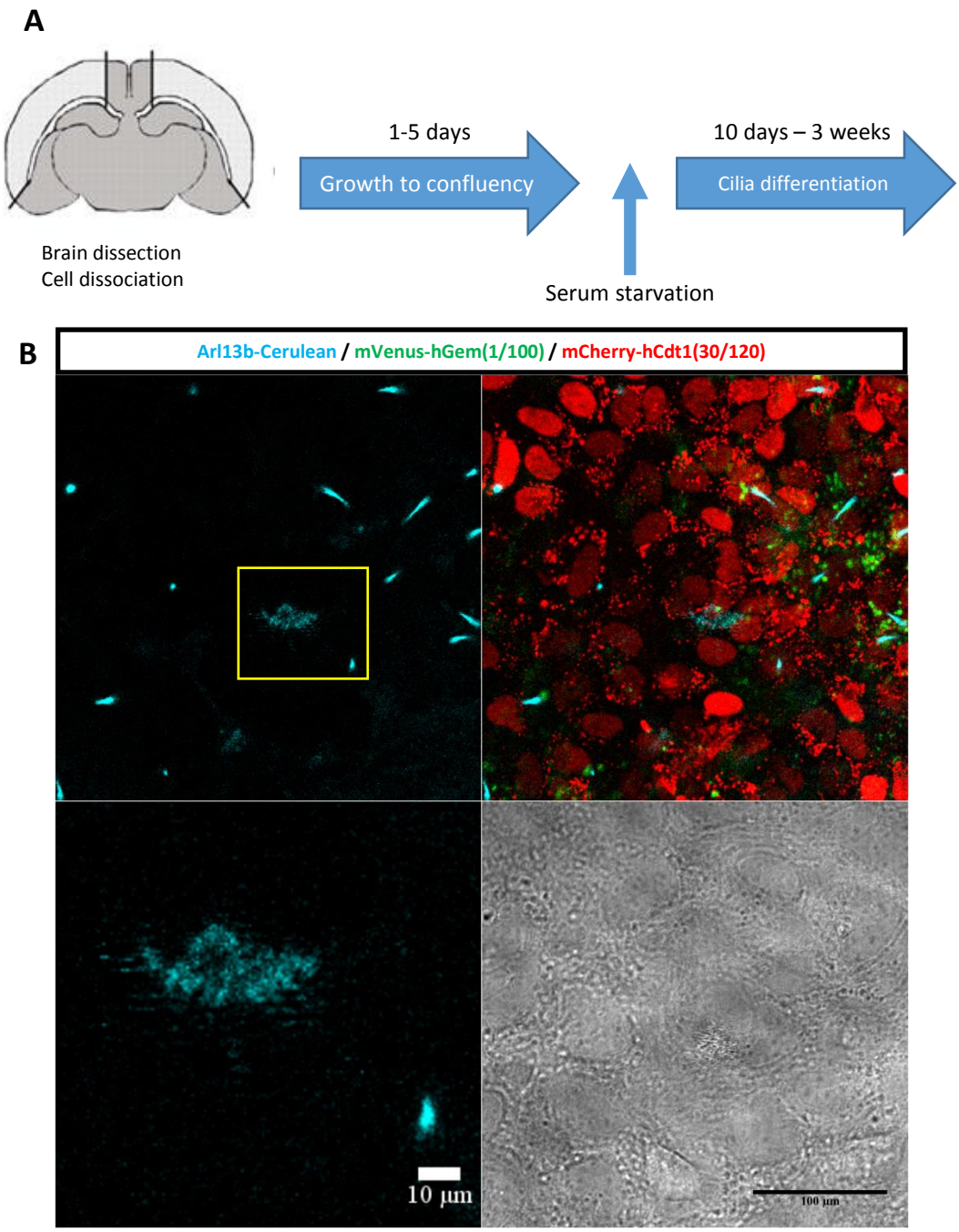

Fig 3.18: *R26Arl13b-Fucci2aR* labels motile cilia in primary ependymal cultures: (A) Schematic adapted from Zein et al, 2009. Primary ependymal cultures are prepared by dissecting the subventricular zone from the forebrain of e18.5 *R26Arl13b-Fucci2aR*$^{+/Tg}$*/CAG:Cre*$^{+/Tg}$ embryos. Cells are dissociated into a single cell suspension, plated and grown to confluency to enable tight junctions to form. Cells are then serum starved to induce ciliogenesis. **(B)** Live imaging of differentiated primary ependymal cultures 7 days after serum starvation. Ependymal cells have stopped cycling shown by all nuclei being labelled with mCherry-hCdt1(30/120). More differentiated ependymal cells have formed multiple motile cilia labelled with Ar13b-Cerulean. See sup video 15.

3.2.3.8 Tissue specific expression of *R26Arl13b-Fucci2a*

To confirm the functionality of the Cre-LoxP system to induce tissue specific expression of Arl13b-Fucci2a, *R26Arl13b-Fucci2aR* mice were crossed with endoderm specific *Sox17-2A-iCre* to induce Arl13b-Fucci2a expression in all endoderm derived tissues including the developing lung epithelium (fig 3.19A). e11.5 lungs were dissected from *R26Arl13b-Fucci2a*$^{+/Tg}$/*Sox17-2A-iCre*$^{+/Tg}$ embryos and embedded in matrigel on a lummox membrane as described in Methods. Live imaging showed restricted expression of *Arl13b-Fucci2a* to the lung epithelium and a sub-population of migratory cells (fig 3.19B). A high level of proliferation was seen in branching regions, indicated by the high proportion of cells labelled with mVenus-hGem(30/120). This was in contrast to the more proximal lung epithelium where cells have started to drop out of the cell cycle and are predominately labelled with mCherry-hCdt1(1/100) (fig 3.19B). These are results which have been seen previously with cultured lungs from *R26Arl13b-Fucci2a*$^{+/Tg}$/*CAG::Cre*$^{+/Tg}$ embryos (fig 2.8) (Mort et al., 2014). Interestingly, cilia were present along the entire length of the lung epithelium within actively branching regions and the more proximal lung epithelium. Increased magnification of the lung epithelium revealed cilia are orientated pointing into the lumen of the lung epithelium (fig 3.19C). Previous reports have identified primary cilia on the luminal surface of lung epithelial cells prior to the appearance of motile cilia (Jain et al., 2010). However very little is known about the role of primary cilia in the development of the lung epithelium. Considering the proposed chemosensory role for primary cilia in the lumen of ventricles (Lehtinen et al., 2011), it would be interesting to investigate if primary cilia have a similar function during lung branching morphogenesis. Another potentially intriguing role for primary cilia in lung branching morphogenesis is the association between primary cilia and the plannar cell polarity (PCP) pathway. PCP is the process by which a group of cells collectively polarise asymmetrically within a plane and is known to be essential for correct epithelial branching during lung development, in addition to gastrulation, neural tube closure and hair follicle alignment (Devenport, 2014; Yates et al., 2010). Recently it has been shown that

IFT88 (an intraflagellar transport protein essential for primary cilia assembly) is required for establishing epithelial PCP for convergent extension during mouse cochlear development (Jones et al., 2008), suggesting a potential link between primary cilia and PCP. The *R26Arl13b-Fucci2aR* mouse line would be a useful tool for investigating by live imaging the potential role for primary cilia in the PCP pathway and its influence on branching morphogenesis.

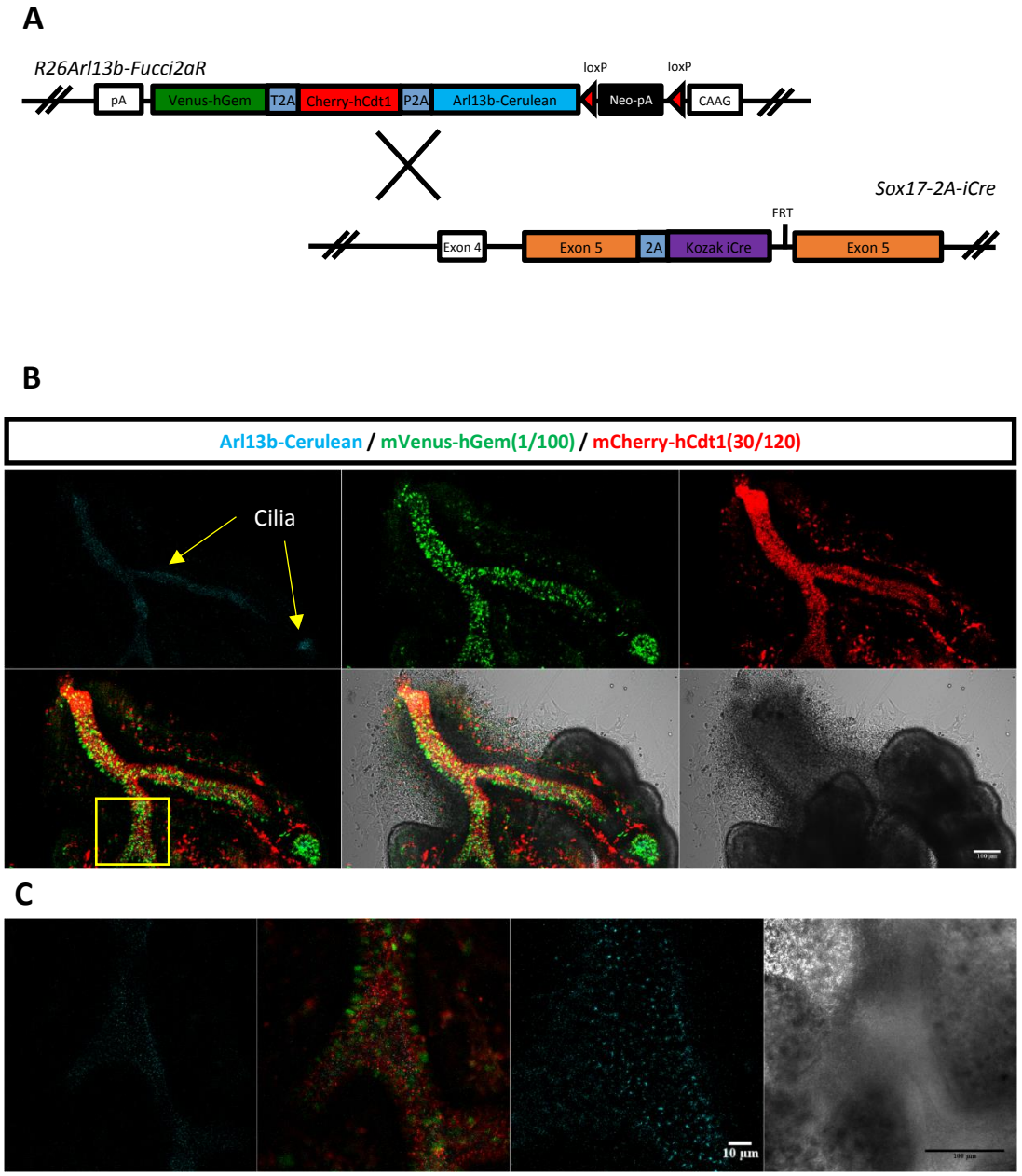

Fig 3.19: Primary cilia are orientated into the lung of the lung epithelium during branching morphogenesis (A) Tissue specific expression of *R26Arl13b-Fucci2aR* was achieved with crossing with *Sox17-2A-iCre* to specifically label the epithelium of all endoderm derived organs. **(B)** *Ex vivo* lung culture from an e11.5 *R26Arl13b-Fucci2aR*$^{+/Tg}$*/Sox17-2A-iCre*$^{+/Tg}$ embryo. Expression of *R26Arl13b-Fucci2a* is restricted to the lung epithelium and a sub population of migrating mesenchymal cells. Cilia are present along the entire length of the lung epithelium. **(C)** An enlargement of the boxed area in (B) confirming cilia localisation of the Cerulean signal. Cilia are protruding from the apical surface of lung epithelial cells into the lumen.

3.2.4 Investigation into the causes of reduced fluorescence in tricistronic reporter mice

3.2.4.1 Reduced mRNA transcript levels in tricistronic MEFS

There is a significant reduction in the fluorescence of the tricistronic reporter mice *R26H2B-Fucci2aR* compared to the original bicistronic *R26Fucci2aR* mouse. This is quite surprising considering there was no obvious difference in fluorescence intensity between H2B-Fucci2a and Fucci2a 3T3 stable cell lines. Also, when generating the H2B-Fucci2a construct by cloning in H2B-Cerulean-P2A to the 5' end of Fucci2a, a Kozak sequence was also added to increase the level of expression. To investigate whether this reduction in fluorescence is due to a reduction in the level of transcription or translation caused by having multiple 2A self-cleaving peptides, MEF lines were generated from e12.5 *R26Fucci2a*$^{+/-}$*/CAG::Cre*$^{+/-}$ *and R26H2B-Fucci2a*$^{+/-}$*/CAG::Cre*$^{+/-}$ embryos. MEFs were also isolated from e12.5 *R26Arl13b-Fucci2a*$^{+/-}$*/CAG::Cre*$^{+/-}$ embryos to see if the reduction in fluorescence was specific to the H2B-Fucci2a construct or was a more general problem with tricistronic constructs. A comparison of live fluorescence intensity showed a significant 4.7 fold decrease in mVenus-hGem(1/110) and a significant 9 fold decrease in mCherry-hCdt1 in Arl13b-Fucci2a MEFs compared to Fucci2a MEFS (fig 3.20A). It was not possible to measure the fold decrease in fluorescence of the H2B-Fucci2a MEFS due to the fact that when imaging was optimised to just under pixel saturation for the Fucci2a MEFS no signal was detectible in the H2B-Fucci2a MEFS, making it impossible to accurately segment nuclei. qRT-PCR targeted to mCherry revealed mRNA transcript levels of the Arl13b-Fucci2a and H2B-Fucci2a constructs were 36±11% and 5±2% of Fucci2a mRNA transcript levels respectively (fig 3.20B). Suggesting the loss of fluorescent signal is not a problem with translation or protein stability but is caused either by a reduced level of transcription or decreased RNA stability.

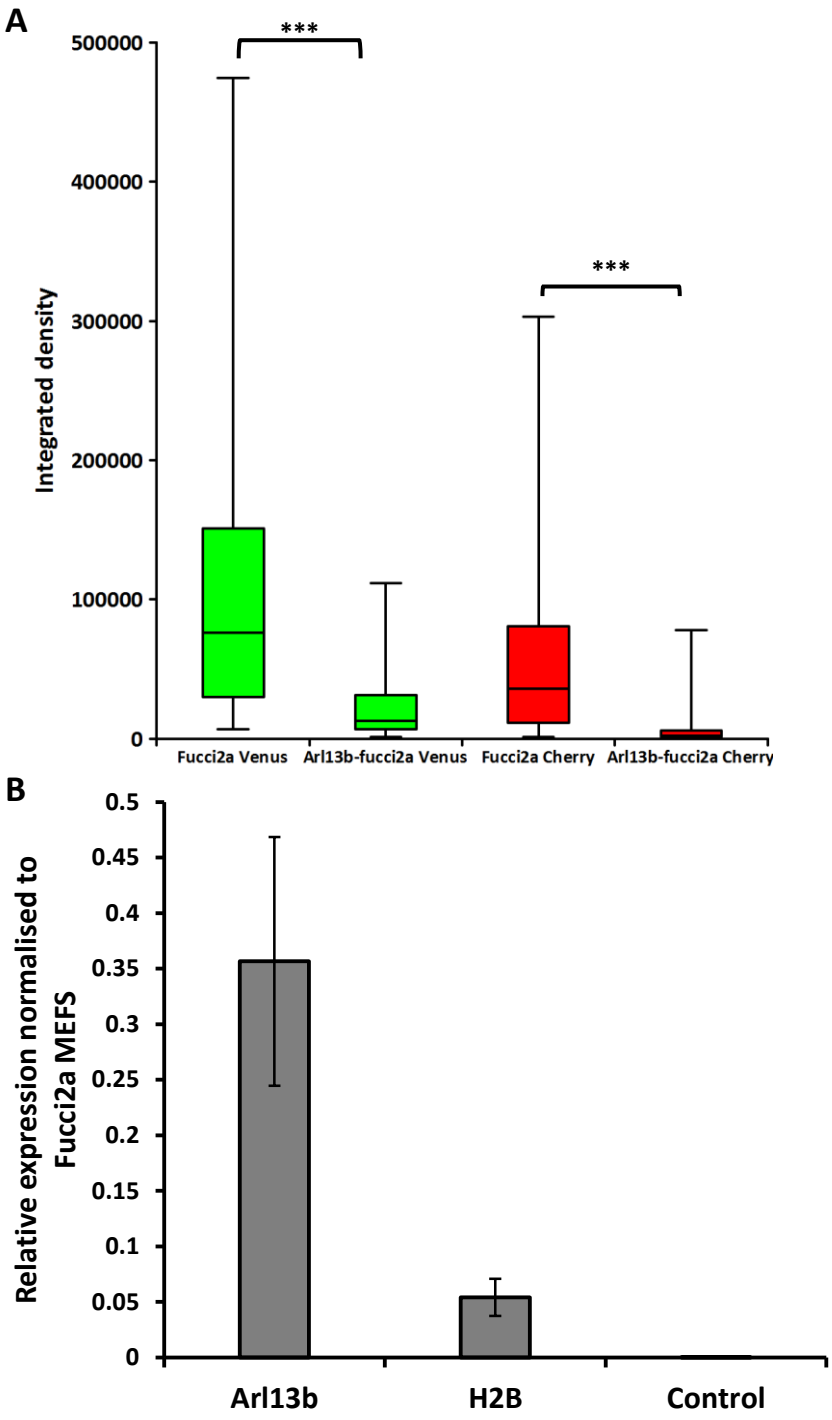

Fig 3.20: Reduction in fluorescence intensity of tricistronic reporter constructs is due to a decrease in mRNA levels. (A) Box plot showing a significant reduction in fluorescence intensity from MEFS derived from *R26Fucci2a*$^{+/Tg}$*/CAG::Cre*$^{+/Tg}$ embryos compared to *R26Arl13bFucci2a*$^{+/Tg}$*/CAG::Cre*$^{+/Tg}$ embryos (n = 100 cells). **(B)** Qrt-PCR results comparing mRNA transcript levels in MEF lines derived from Arl13b-Fucci2a and H2B-Fucci2a mice normalised to Fucci2a MEFS. Error bars in B = 0.05 confidence. Significant differences in A statically confirmed by One way ANOVA $P < 0.0001$, Tukey's HSD *** $P < 0.001$

3.2.4.2 Comparison of fluorescence between 3T3 lines

To investigate if the drop in mRNA transcript levels in the tricistronic constructs is specific to expression from *ROSA26*, the fluorescence intensity was compared in 3T3 cells. A significant 1 fold decrease in mVenus-hGem(1/110) intensity was seen between Fucci2a 3T3 cells and the two tricistronic constructs. But no significant change in mCherry-hCdt1(30/120) or between the Arl13b-Fucci2a and H2B-Fucci2a cells as seen in the MEFs (fig 3.21). This data suggests that the reduction in mRNA transcripts seen in the tricistronic MEF lines is locus specific to *ROSA26* or is specific to expression of the constructs *in vivo*. Although, the chance of multiple integrations of the tricistronic constructs in the 3T3 cells may be masking the reduced levels of mRNA seen in the MEFS where a single integration has been confirmed.

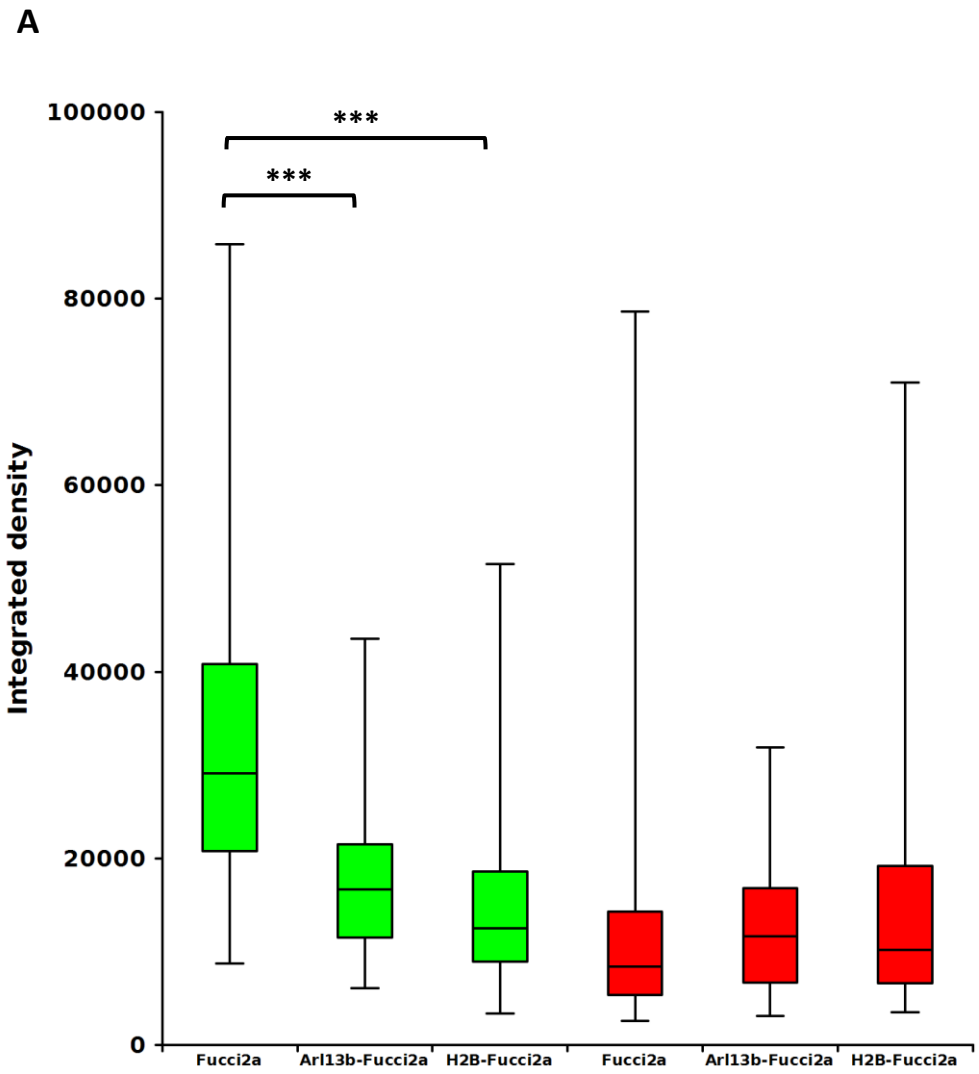

Fig 3.21: mVenus-hGem(30/120) fluorescence but not mCherry-hCdt(30/120) is reduced in tricistronic constructs (A) Box plot comparing the fluorescence intensity of Fucci2a, Arl13b-Fucci2a and H2B-Fucci2a 3T3 cell lines. A significant reduction in fluorescence was seen for mVenus-hGem(1/110) but not in mCherry-hCdt1(30/120). Significant differences in A statistically confirmed by One way ANOVA $P < 0.0001$, Tukey's HSD *** $P < 0.001$

3.2.4.3 Codon optimisation of H2B-Cerulean does not increase fluorescent signal in 3T3 cells

For protein synthesis there are 61 different codons coding for 20 amino acids. In light of this redundancy of the genetic code it has been shown that different species have a preference for particular codons, thought to be caused by a species specific differential abundance of tRNAs (Gustafsson et al., 2004; Ikemura, 1981). Codon optimisation of transgenes for expression in the host organism has been shown to significantly increase transcription levels of transgenes (Cormack et al., 1995; Sastalla et al., 2009; Yang et al., 1996; Zhang et al., 1996). As a proof of principle to improve the *R26H2B-Fucci2a*R mouse, the H2B-Cerulean coding sequence was codon optimised for mouse expression. H2B-Cerulean was codon optimised using the online software tool at IDTDNA.com and synthesised by Geneart. The codon optimised H2B-Cerulean-P2A was cloned into pcDNA5-FRT-Fucci2a via a single MluI site at the 5' end of mCherry-hCdt1(30/120) and a stable cell line generated using the Flp-In system (Invitrogen). A comparison of H2B-Cerulean fluorescence showed a significant 0.26 fold decrease in Cerulean florescence from 171191±13124 in noncodon optimised H2B-Fucci2a cells to 135358±7716 in codon optimised H2B-Fucci2a cells (fig 3.22A and B). A possible cause of this may be that codon optimisation had no effect on the expression of H2B-Fucci2a and the slight decrease in fluorescence is due to heterogeneity between the polyclonal cell lines. Potentially the higher fluorescence seen in the original cell line may be down to multiple integrations of H2B-Fucci2a although flp recombinase site specific integration should ensure only a single copy is integrated.

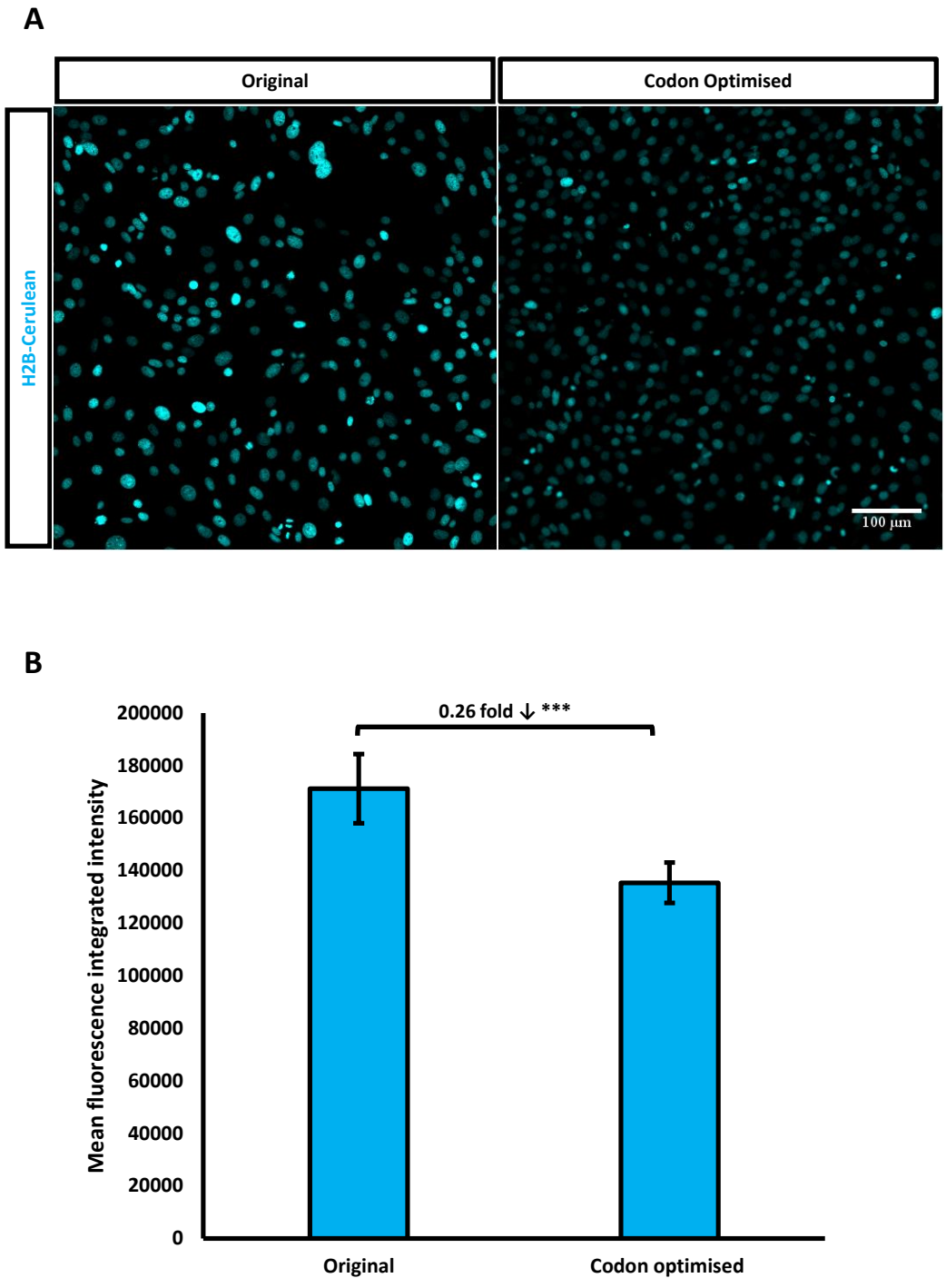

Fig 3.22: Codon optimisation of H2B-Cerulean. (A) Live image of H2B-cerulean fluorescence comparing original H2B-Fucci2a and codon optimised H2B-Fucci2a 3T3 cell lines. **(B)** Quantification of difference in H2B-cerulean fluorescence intensity (n = 100 cells). Error bars in B = 95% confidence and significant tested by Students T-test, *** = $P < 0.001$

3.3 Discussion

Self -leaving (2A) peptides allow one to generate multicistronic genetic constructs for the simultaneous expression of multiple genes from a single open reading frame (Carey et al., 2009; Osborn et al., 2005; Szymczak et al., 2004). The near 100% cleavage rate of self-cleaving peptides ensure almost equimolar production of proteins from multicistronic constructs and their small size give them a distinct advantage over traditional methods of multicistronic expression using IRESs (Bochkov & Palmenberg, 2006; J. H. Kim et al., 2011). In this chapter I describe the development and characterisation of four tricistronic reporter constructs that enable the dual visualisation of cell cycle progression (by utilizing Fucci2a (Mort et al., 2014)) alongside reporters of apoptosis, cytokinesis and ciliogenesis. In each case I have used the fluorescent protein Cerulean as a reporter because of its improved brightness and stability over CFP (Rizzo et al., 2004) and its optimal spectral separation from mCherry and mVenus, the reporters utilised in the Fucci2a construct (Mort et al., 2014). Each reporter was cloned at the 5' end of the Fucci2a construct separated by the self-cleaving peptide P2A. They were then characterised in stable 3T3 cells for their potential usefulness in generating transgenic animals by using the Flp-In system (ThermoFisher) to generate a single integration of the construct driven by the CAG promoter (Miyazaki et al., 1989), in order to mimic the conditions of a single copy transgenic insertion in mouse. Addition of the new reporter had to be a the 5' end of Fucci2a because the addition of the larger 5' fragment of the 2A peptide to the 3' end of mVenus-hGem(1/110) results in its mislocalisation to the cytoplasm (Mort et al., 2014).

3.3.1 Caspase activatable apoptotic reporters show limited sensitivity *in vitro*

I have tested the utility of two caspase dependent apoptotic reporters CA-Cerulean and CC3AI when combined in a tricistronic construct with Fucci2a in 3T3 cells (Nicholls et al., 2011; Zhang et al., 2013). Both reporters enabled visualisation of cell cycle progression and showed a significant increase in Cerulean fluorescence after

addition of apoptotic inducer TNFα, therefore confirming successful self-cleavage at both 2A sequences. A fold change of 2.8 was seen using the CA-Fucci2a cell line and 2.3 in CC3AI-Fucci2a cells. The similarities in fold change suggests that the efficiency of caspase cleavage at the DEVED sequence, which both constructs are dependent on, is the limiting factor. It was decided that such a small fold change in fluorescence although sufficient for *in vitro* would be difficult to visualise *in vivo* where autofluorescence levels of fluorescence are much higher and cells can be more tightly packed.

A potential method for improving the sensitivity of the apoptotic reporter in this construct would be to swap cerulean with tdTomato or Venus which are significantly brighter and therefore would give a brighter fluorescent signal (Shaner et al., 2005). This would require changing the fluorophore of one of the Fucci probes to maintain spectral separation and subsequent characterisation of the new Fucci probe. A mCyan-hGem(1/110) probe has been characterised and used in combination with mCherry-hCdt(30/120) and mVenus-p27K$^-$ (a quiescent G0 marker) would be a potential candidate (Oki et al., 2014). However, if the background level of fluorescence of these reporters (the level of fluorescence in cells before they undergo apoptosis) also increases proportionally with the brightness of the fluorophore, then the signal to noise ratio will not be improved, resulting in the same small fold change seen in the tested CA-Fucci2a and CC3AI-Fucci2a constructs. If the fluorophores were changed, it would therefore be important to quantify the signal to noise ratio *in vitro* to ensure there is a significant increase in fluorescence for *in vivo* applications.

3.3.2 H2B-Fucci2a enables tracking of cells through multiple cell divisions

The loss of fluorescence of both Fucci probes during cell division makes it impossible to track cells through multiple mitosis *in vivo* (see sup video 5 for example) and complicates *in vitro* tracking. Previous work by Abe and colleagues showed how, by crossing the Fucci2 single probe Cre-inducible lines, *R26R-mVenus-hGem(1/110)* and *R26R-mCherry-hCdt1(30/120)* with *R26H2B-mCherry* and

R26H2B-EGFP reporter mice lines respectively, they were able to track cells through multiple mitoses and measure the changes in fluorescence of the two reporters simultaneously in embryos during the formation of blastocysts (Abe et al., 2011, 2013). However because they are separate reporters targeted to *ROSA26* the reporters have to be maintained separately and crossed for each experiment, which complicates mouse maintenance. By inserting the nuclear marker H2B-Cerulean to the 5' end of the Fucci2a construct I have been able to label the nuclei of cells through all stages of the cell cycle and monitor cell cycle progression from a single ORF. I have characterised the H2B-Fucci2a construct in 3T3 cells and illustrated the ability to track cells through multiple cell cycles and calculate cell cycle times. I have shown that the addition of H2B-cerulean clearly improves the utility of the Fucci system *in vitro* and simplifies image analysis tracking techniques which have previously relied on the brightfield signal after mitosis (Roccio et al., 2013). Unfortunately the low levels of expression seen in the *R26H2B-Fucci2aR* mouse line mean that these improvements cannot be translated *in vivo*, without further improvements to the strategy as discussed in section 3.3.5.

3.3.3 Arl13b-Fucci2a is a powerful tool for visualising cilia and cell cycle dynamics *in vitro* and *in vivo*

Motile cilia are essential for a host of biological functions highlighted by the range of symptoms presented in patients with primary ciliary dyskinesia (PCD) from bronchitis to hydrocephalus (Afzelius 1976; Greenstone et al.,1984; Whitelaw et al., 1981). Primary cilia have been shown to be important signalling centres for hedgehog and Wnt signalling among other pathways. (Corbit et al., 2008; Cortellino et al., 2009; Houde et al., 2006; Huangfu et al., 2003; Simons et al., 2005; Tran et al., 2016). There is a physical and possibly regularity relationship between primary cilia assembly and cell cycle progression because disassembly of primary cilia is required to release the centrioles which are subsequently required for spindle assembly and completion of mitosis (Seeley & Nachury, 2010).

With the aim to study this relationship using live imaging techniques, I developed and characterised the Arl13b-Fucci2a construct to enable dual visualisation of cilia with cell cycle progression. I have shown in 3T3 cells that expression of Ar13b-Fucc2a labels cilia and reports on cell cycle phase. Using this cell line I have illustrated how this construct can be used to generate quantitative data on cilia dynamics during migration and timing of ciliogenesis in relation to the cell cycle. Previous reporters have shown the preference of cells to orientate their primary cilia towards the leading edge during migration and in response to a chemoattractant cues, inferring that primary cilia may be acting as an environmental antenna sensing the extracellular environment during migration (Lu et al., 2008; McGowan & McCoy, 2013; Schneider et al., 2010). In these studies the orientation of cilia in migrating cells was determined at specific time points by immunofluorescence staining and it was not determined if cilia reorientation was required for migration or if reorientation occurred during migration. By using the live Arl13b-Fucci2a reporter I was able to witness the migration of cells before cilia reorientation, therefore showing directed migration occurs before the orientation of cilia to the leading edge in 3T3 cells.

The timing of cilia assembly and disassembly has been shown to vary between different cell lines. Synchronisation of 3T3 cells and RPE1 (retinal pigment epithelial) cells in G1 by serum starvation has shown cells to be ciliated during G1/G0. Subsequent stimulation of cell cycle progression by the addition of serum has been shown to result in cilia disassembly followed by reassembly in late G1 and, finally, disassembly before S-phase (Spalluto et al., 2013; Tucker et al., 1979), whereas cilia disassembly in Ptk1 (rat kangaroo kidney epithelial) cells has been shown to occur during the early stages of mitosis (Rieder et al., 1979). In contrast to previous reporters, I have shown by time-lapse imaging that 3T3 cells assemble their cilia at some point during G1 and cilia disassembly occurs just prior to mitosis, often simultaneously with the breaking of the nuclear envelope. The discrepancy between my data and the previously published work on 3T3s is likely due to artefacts induced by the synchronisation step which can be avoided by using the live cell cycle and

cilia marker Arl13b-Fucci2a (Tucker et al., 1979). Considering centriole duplication has been shown to occur during late G1 or S-phase (Hinchcliffe & Sluder, 2001), my data suggests, along with previously published work showing cilia disassembly in late M-phase, (Paridaen et al., 2013; Rieder et al., 1979) that in some cell types cilia disassembly is not required for centriole duplication in S-phase, therefore suggesting centriole duplication can occur while the mother centriole is acting as the basal body at the base of the cilia. In addition cilia assembly occurs faster after mitosis in daughter cells originating from ciliated mothers and one daughter cell will always ciliate before another. This data supports previous reporters that the cell that inherits the mother centriole is primed to ciliate first (Anderson & Stearns, 2009). This phenomenon has been shown to be physiological relevant in embryonic neocortical stem cells (Paridaen et al., 2013), where the inheritance of the mother centriole, identified by the association with remnants of the cilia membrane, enabled one daughter to reassemble its primary cilia faster and asymmetrically retain its position in the stem cell niche.

The *R26Arl13b-Fucci2aR* mouse was generated by homologous recombination to the *ROSA26* locus. The mice were characterised by live imaging of embryos generated by crosses between *R26Arl13b-Fucci2aR* mice and ubiquitous *CAG::Cre* and tissue specific *Sox17-2a-iCre* (Engert et al., 2009; Sakai & Miyazaki, 1997). Strong labelling of cilia with Arl13b-cerulean and cell cycle progression was seen in all tissues examined and in MEFS, although the signal was significantly dimmer than the original *R26Fucci2aR* mouse line (Mort et al., 2014). This reporter mouse line uniquely allows inducible visualisation of cell movement and cell cycle progression with both primary and motile cilia. Previous cilia reporter mouse lines are either non-inducible, making it impossible to visualise cilia in specific cell lineages (Bangs et al., 2015; Delling et al., 2013), or overexpress a fusion protein containing G-protein couple receptor *Sstr3* with reported adverse effects on cilia function (Guadiana et al., 2013; O ’Connor et al., 2013). Overexpressing of Arl13b has been reported to increase cilia length in transgenic mice and cell lines but with no reported effects on cilia function (Bangs et al., 2015; Larkins et al.,2011). It would be important to

quantify the influence on cilia length in the *R26Arl13b-Fucci2aR* for future characterisation in both actively cycling and quiescent cells. A limitation of previously published cilia reporter lines is that it is impossible to identify live which cilia corresponds to which cell without fixation or crossing with another reporter line (Bangs et al., 2015; Delling et al., 2013; O 'Connor et al., 2013). The *R26Arl13b-Fucci2aR* reporter line overcomes this limitation by using the Fucci probes to label the nuclei of corresponding cells, therefore giving context to the visualisation of cilia dynamics in live imaging experiments. Furthermore, as the construct is inducible, the problem can also be addressed in densely packed tissues by administrations of low tamoxifen doses to generate tissue mosaics (Driessens et al., 2012). Considering the known relationship between primary cilia, cell cycle progression and its proposed influence on cancer development (Hassounah et al., 2013; Jonassen et al., 2008; Lin et al., 2003; Menzl et al., 2014; Yuan et al., 2010), the *R26Arl13b-Fucci2aR* line will be an attractive reporter line for studying this relationship live.

3.3.4 Tricistronic constructs have reduced mRNA abundance *in vivo when compared to bicistronic constructs*

I have reported a significant reduction in the fluorescence intensity of both tricistronic reporter constructs *H2B-Fucci2a* and *Arl13b-Fucci2a* when expressed from the *ROSA26* locus in mice and MEFS. It has been shown that expression of GFP as part of a 2A bicistronic construct *in vivo* results in a reduction of fluorescent signal when compared to expression from a monocistronic construct (Chinnasamy et al., 2006; Hasegawa et al., 2007). In a separate study GFP expression was shown to be reduced in tricistronic and quadcistronic constructs compared to bicistronic constructs (Gao et al., 2012). In addition, Gao et al reported a higher level of GFP expression when three T2A 2A sequences were used compared to a combination of E2A, T2A and F2A. Therefore, this suggests that reduced expression could be an innate property of multicistronic constructs. However in all these studies the abundance or fluorescence of GFP was used as a read out of expression, which does not take into account the known context dependent variability in cleavage efficiently

of the self-cleaving peptides (J. H. Kim et al., 2011). Low cleavage efficiently could result in the formation of fusion proteins that may influence GFP fluorescence and abundance independent of expression. Cleavage efficiently has been shown to vary between different 2A self-cleaving peptides with P2A showing the highest efficiency *in vivo* (J. H. Kim et al., 2011). In addition, the sequence to the N-terminal of the 2A sequence and the order of genes in bicistronic constructs has been shown to influence efficiently in cell lines (Anderson et al., 2012; De Felipe et al., 2010; Donnelly et al., 2001; Ibrahimi et al., 2009).

It is hard to determine the cleavage efficiency in the Fucci2a construct as non-cleavage of T2A would result in a fusion protein which is degraded in all stages of the cell cycle. However, considering the *H2B-Fucci2a* and *Arl13b-Fucci2a* constructs are comparable in brightness to the *Fucci2a* construct when expressed in 3T3 cells driven by the CAG promoter and that significantly lower levels of mRNA are observed in MEFS generated from their respective mouse lines, cleavage efficiency is not likely to be the cause of this reduced fluorescence. It is more likely to be due either to reduced mRNA stability or reduced levels of transcription. To my knowledge there have been no studies that have investigated the influence of self-cleaving peptides on transcription or mRNA stability. It could be possible that the inclusion of multiple 2A self-cleaving peptides destabilises the mRNA, resulting in its degradation, or that the large regions of homology between the fluorescent proteins in the constructs generates detrimental secondary mRNA structure, such as the formation of mRNA hairpins that are known to be important sites for the regulation of mRNAs (Svoboda & Di Cara, 2006; Zanier et al., 2002). A simple experiment to determine the stability of RNA transcripts would be to calculate mRNA half-lifes by measure the abundance of RNA transcription at set time points by qrt-PCR after addition a transcription inhibitor such as actinomycin D (Harova et al., 2009).

Reduced levels of transcription has been reported at the *ROSA26* locus in transgenes inserted in the forward orientation, presumably due to transcriptional interference from the *ROSA26*promoter (Strathdee et al., 2006). Another possible explanation is

that the reduced mRNA levels are caused by sequence specific transcriptional interference specific at the *ROSA26* locus, which is not present at the 3T3 Flp-In locus, therefore explaining why the effect is not reproduced in the 3T3s. This theory could be tested by generating and comparing 3T3 cell lines in which each construct has been targeted to *ROSA26* using the same method for generating the mice lines in mESCs.

Fluorescence and mRNA level are both significantly lower in *R26H2B-Fucci2aR*$^{+/Tg}$*/CAG::Cre*$^{+/Tg}$ MEFS compared to *R26Arl13b-Fucci2aR*$^{+/Tg}$*/CAG::Cre*$^{+/Tg}$ MEFS. As both constructs contain the same 2A peptides the cause of this variation is sequence specific to H2B. Histone mRNA abundance is stringently controlled in a cell cycle dependent manner by a combination of transcriptional and mRNA regulation to ensure translation of core histones (H2A, H2B, H3 and H4) occurs during S-phase (Marzluff et al., 2008). The four core histones (H2A, H2B, H3 and H4) are the only known non-polyadenylated mRNAs in eukaryotes. It has been shown that a specialised stem-loop at the 3' end of core histone mRNA transcripts and the binding of SLBP (stem loop binding protein) is essential for regulating core histone transcript levels outside of S-phase (Harris et al., 1991; Luscher et al., 1985; Wang et al., 1996). The H2B-Fucci2a transcript contains only the protein-coding region of H2B and, therefore, the regulatory 3' stem loop is absent. However, considering the evolutionary importance of regulating core histone transcript levels throughout the cell cycle, it is possible the protein-coding region of H2B is prematurely targeting the entire H2B-Fucci2a mRNA transcript for degradation.

3.3.5 Rescuing the *R26H2B-Fucci2aR* mouse

Combining Fucci2a with a nuclear marker that labels cells during mitosis is a significant improvement on the original Fucci system enabling tracking of cells after cell division. More work would need to be done to elude the mechanism causing the reduced levels of mRNA seen in the *R26H2B-Fucci2aR* mouse, which is outside the time scale of this thesis. One potential method to introduce H2B-Cerulean into the

Fucci2a construct would be to insert CAG-H2B-Cerulean flanked by HS4 insulator sequences after the Fucci2a construct (Potts et al., 2000). The expression of H2B-Cerulean would not be conditional but segmentation of specific lineages could be achieved using fluorescence of the Fucci probes.

4 Chapter 4: A description of melanoblast behaviour using *R26Fucci2aR* during migration and investigation into the role of Kit signalling

4.1 Introduction

Melanocytes are specialised melanin producing cells responsible for the pigmentation of the hair, skin, eyes, feathers and scales of vertebrates (Lin & Fisher, 2007). Among other roles melanin is important for photoprotection against harmful UV radiation and for thermoregulation. Pigmentation has proven useful in genetic research as a read out of genetic contribution in the formation of chimeras (Mintz, 1967). In addition research into melanocyte development has been classically studied due to the easily identifiable pigmentation phenotypes. During development melanoblasts (melanocyte precursors) are derived from the multipotent neural crest that undergoes epithelial to mesenchyme transition (EMT), migrate and proliferate throughout the embryo where they respond to external cues before localising to specific sites in the body and set up stem cell populations (fig 4.1) (Mort et al., 2015; Theveneau & Mayor, 2012). These developmental processes are mirrored in other systems and disease states, which in combination with the easily tractable phenotypes make melanocytes an excellent model system to study.

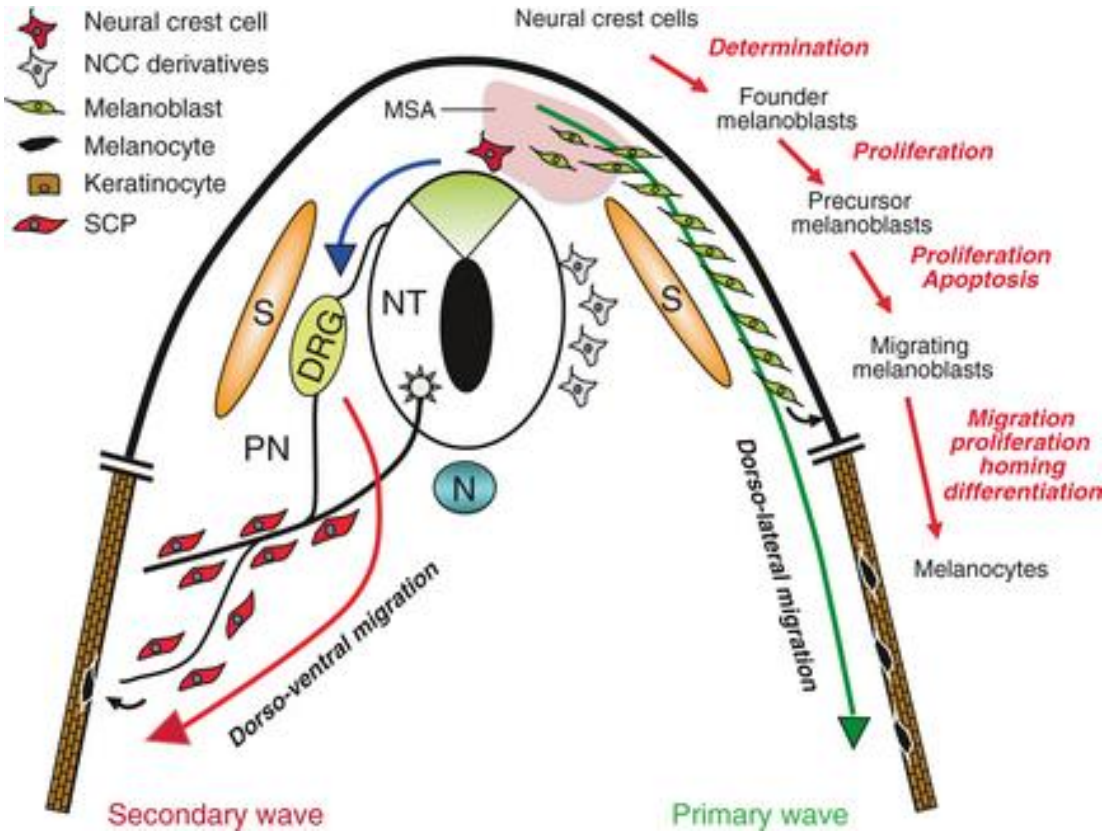

Fig 4.1: Melanoblast specification and migration pathways in the mouse. Melanoblasts (melanocyte precursors) are specified from the trunk region of the neural crest at e9. Specified melanoblasts proliferate in the migration staging area (MSA) before migrating along the dorso-lateral migration pathway between the somites and ectoderm at e10.5. From e12.5 to e15.5 melanoblast continue to proliferate, infiltrate the epidermis and eventually become localised to hair follicles. Interfollicular melanoblast disappear possibly due to a loss of Kit signaling. A second wave of melanoblast derived from Schwann cell precursors (SCPs) also contributes to colonisation of the epidermis via a dorso-ventral migration pathway. DRG = Dorsal Root Ganglion, NT = Neural Tube, NCC = Neural Crest Cells, S = Somites. Figure adapted from Bonaventure et al 2013.

4.1.1 Melanoblast development

The neural crest is a transient migratory multipotent population of cells that delaminate from the dorsal-most aspect of the neural tube by EMT. Lineages derived from the neural crest include the neurons and glia of the peripheral nervous system, melanocytes, the cartilage and bone of craniofacial structures, endocrine, cardiac pacemaker cells, smooth muscle and tendons (Reviewed in Theveneau & Mayor, 2012). Melanoblasts are specified in the trunk region of the neural crest at e9 by the expression of melanoblast transcription factor *Mitf* and down regulation of transcription factors *Foxd3* and *Sox2* (Kos et al., 2001; Nitzan et al., 2013; Wakamatsu et al., 2004). These founder melanoblasts congregate in a triangular region known as the migration staging area (MSA) between the ectoderm, neural tube and somites where they proliferate and start to express the melanocyte specific markers *Dct* and *Pmel* (Erickson et al., 1992; Mackenzie et al., 1997; Wehrle-Haller et al., 2001). At e10.5 the melanoblasts in the mouse trunk continue to proliferate and begin to migrate from the MSA along a dorsal lateral pathway between the developing somites and ectoderm ultimately becoming localised to hair follicles around e15.5 (Hirobe, 1984; Mackenzie et al., 1997; B Wehrle-Haller & Weston, 1995). At e12.5 on the dorsolateral pathway, melanoblasts start to cross from the dermis to the epidermis where they continue to migrate and proliferate. Melanoblast continue to proliferate in both dermal and epidermal compartments but melanoblast within the dermal compartment migrate into the epidermis so that the population of melanoblast within the dermal compartment remains constant (Luciani et al., 2011). Based on this observation and previous reports of melanoblasts' entry into the epidermis from e12, it is believed that melanoblast migration across the basal lamina occurs in one direction, suggesting a preference for melanoblasts to be in the epidermis (Takahiro Kunisada et al., 1996; Luciani et al., 2011; Mayer, 1973). It has been proposed that asymmetric division or orientated cell division may preferentially send one daughter cell into the epidermis leaving one in the dermis (Larue et al., 2013; Luciani et al., 2011). Additionally, membrane bound Kit ligand found on the surface of cells along the dorsal lateral pathway including keratinocytes in the

epidermis has been shown to promote melanoblast survival, proliferation and formation of tight junctions to surrounding epithelial cells in 3D cultures (Tabone-Eglinger et al., 2012). Melanoblast are also seen to change their adhesive properties to match their surroundings *in vivo* from E-cadherin^{-}/P-cadherin^{-} in the dermis to E-cadherin^{high}/P-cadherin^{low} in the epidermis (Nishimura et al., 1999). Taken together this could suggest a model in which melanoblasts randomly cross into the epidermis at which point they are maintained by a combination of physical adhesive and survival signals from the surrounding keratinocytes which prevents them returning to the dermis.

Recently a second origin of melanoblasts has been identified from schwann cell precursors (SCP) in the mouse and chick (Adameyko et al., 2009). These cells have been shown to originate due to insufficient neural specification by Hmx1 gene expression and migrate along a ventral migratory pathway where they contribute to colonisation of the epidermis (fig 4.1). However the use of Plp-Cre-ERT2 as a SCP lineage tracer, which is instrumental to Adameyko et al's findings in the mouse, has come into question. PLP has been shown by microarray to be expressed in melanoblasts at e15.5 (Colombo et al., 2012). The use of Plp-Cre-ERT2 in another study has shown melanoblast and neurons labelled at e11.5, e12.5 and e14.5 (Hari et al., 2012). In addition to this the Jaegle et al study did not report lineage tracing of melanoblast using a Desert hedge specific Cre (Dhh-Cre) which is proposed to label SCP (Jaegle et al., 2003). Adameyko et al also claim all adult melanocytes are derived from SCP by lineage tracing *Plp* expressing cells from E11.5. However this contradicts classical transplantation studies in which grafted tissue from the dermis at e11 and dermis/epidermis at e12 contained functional melanoblast populations able to produce pigment in the coelomic cavity of a developing chick embryo (Mayer, 1973; M. Rawles, 1940; M. Rawles, 1947). So, whilst the existence of a melanocyte population derived from SCP is not disputed, the contribution of this population to the colonisation of the epidermis still needs to be investigated using alternative Cre lines.

Once melanoblast have colonised the epidermis, invasion of the hair follicles starts around e15.5 and is characterised by a change in adhesion molecules from E-cadherin^{high}/P-cadherin^{low} in dermal populations to E-cadherin^{-}/P-cadherin$^{med-high}$ in the follicle populations (Nishimura et al., 1999). In the mouse, the skin is not pigmented and the majority of interfollicular melanoblasts disappear, although some populations have been identified to persist including the tail, ear and eye (Aoki et al., 2009; Glover et al., 2015; Hirobe, 1984). Kit ligand has been shown to disappear from the intrafollicular epidermis around this time (Yoshida et al., 2001; Yoshida et al., 1996). In addition ectopic expression of Kit ligand under the control of the human keratin 14 promoter in epidermal keratinocytes resulted in hyperpigmentation of the skin and maintenance of the intrafollicular melanocyte population (Kunisada et al., 1998), therefore suggesting the loss of melanoblasts from the intrafollicular epidermis may be due to a loss of Kit ligand. Fully developed melanocytes in the hair follicle produce melanin, which is then transported to neighbouring keratinocytes via melanosomes (Mort et al., 2015).

4.1.1.1 Specification of melanoblast from the neural crest

Melanoblast migration from the neural crest to eventual colonisation of hair follicles relies on extrinsic melanoblast promoting factors to guide and support migration and the intrinsic expression of melanoblast specific genes to direct differentiation. The melanocytes' specific isoform of MITF (microphthalmia-associated transcription factor) has been identified as the master regulator transcription factor for determination of the melanocyte fate. Loss of MITF in mice and zebrafish results in a complete loss of melanocytes, while ectopic expression of *mitfa* in zebrafish is sufficient to induce the production of melanophores (Lister et al., 1999; Steingrímsson et al., 2004). In humans mutations in MITF have been shown to cause Waardenburg syndrome type 2 characterised by pigmentation abnormalities and hearing loss (Tassabehji et al., 1994). In addition, ectopic expression of *Mitf* is sufficient to induce expression of melanocyte markers in 3T3 mouse fibroblasts and

differentiation of ES cells into melanocyte like cells (Béjar et al., 2003; Tachibana et al., 1996). MITF is one of the first markers of the melanocyte lineage and is induced by the activity of PAX3 and SOX10 in concert with the inhibition of *Foxd3* and *Sox2* expression. The activation of *Mift* via this mechanism is a critical junction in neural crest cell specification towards the melanocyte lineage and away from the neural and glial lineages. Transcription factors *Pax3* and *Sox10* bind to the MITF promoter and synergistically promote *Mitf* expression (Bondurand et al., 2000; Potterf, Furumura et al., 2000; Watanabe et al., 2002). Mouse models of Waardenburg syndrome harbouring mutations in either *Pax3* or *Sox10* results in a lack of melanocytes and disruption of the neural crest derived enteric nervous system (Tachibana et al., 2003). Conversely *Sox2* expression is anticorrelated with melanoblasts in the neural crest during chick and mouse development and has been shown to repress MITF expression by binding to the MITF promoter *in vitro*. In agreement with this, the conditional deletion of *Sox2* in the mouse neural crest enlarges the melanoblast lineage and, conversely, ectopic Sox2 expression administered by electroporation reduced the number of $MITF^{+}$ cells in the chick (Adameyko et al., 2012). Similarly Knock down of *Foxd3* in cultured neural crest cells and *Foxd3* null mice exhibit an expansion of the melanoblast population (Kos et al., 2001; Nitzan et al., 2013). FOXD3 has been shown *in vivo* to inhibit *Mitf* expression by directly interacting with PAX3 and preventing its binding to the *Mitf* promoter (Thomas & Erickson, 2009). However FOXD3 has also been shown in the zebrafish to directly repress *mift* expression by binding directly to the *mitf* promoter via an essential DNA binding domain (Curran et al., 2010; Curran et al., 2009). This discrepancy may be highlighting a difference of mechanism between species or *in vitro* verses *in viv*o.

4.1.1.2 Molecular influences on melanoblast migration

Once specified melanoblasts migrate along the dorsal ventral pathway and infiltrate the epidermis from the dermis at e12. Migration along this pathway is dependent on two extrinsic proteins, endothelin-3 and Kit ligand (Kitl) (also known as steal factor,

stem cell factor (SCF) and mast cell growth factor (MGF)) and their respective receptors endothelin receptor-Beta (EDNRB) and the receptor tyrosine kinase Kit. Signalling via EDNRB is not required for melanoblast specification but is necessary during early dermal melanoblast migration between e10.5 and e12.5 as melanoblast leave the MSA but is no longer required when melanoblast start infiltrating the epidermis (Lee et al., 2003; Shin et al., 1999).

Once migration onto the dorsolateral pathway has been initiated melanocyte migration, survival and proliferation is depended on Kit signalling (Yoshida et al.,1996). Homozygous null mutations in the Kit receptor results in a complete loss of melanoblasts at e12.5, while heterozygous mutants have a reduced number of melanoblast resulting in a hypopigmentation phenotype with an unpigmented belly spot (Mackenzie et al., 1997). Conversely, ectopic expression of Kit ligand in keratinocytes has shown to promote melanocytes' survival and differentiation in regions not usually populated by melanocytes (Kunisada et al., 1998a; Kunisada et al.,1998b). The KIT receptor is a receptor tyrosine kinase found on the surface of melanoblasts shorty after their emergence from the neural crest around e10 (Steel et al., 1992). Mutations located within the *Kit* receptor gene in humans has been linked to piebaldism in humans (Jackson, 1997), a rare autosomal dominant disorder characterised by a congenital white forelock and unpigmented patches of skin. The KIT ligand exists in two forms, synthesised from two alternatively spliced mRNAs that have different influences on migrating melanoblasts. Soluble Kit ligand has been shown to have a chemokinetic but not chemoattractive affect on migrating melanoblast but is insufficient to sustain melanoblast migration in the dermis after leaving the MSA without membrane bound KIT ligand (Jordan & Jackson, 2000; B Wehrle-Haller & Weston, 1995). Membrane bound ligand is found on the surface cells along the dorsolateral pathway and is required for adhesion to the intraepithial niche and promoting melanoblast survival (Tabone-Eglinger et al., 2012). Down stream of the Kit receptor migration, survival and proliferation have been shown to signal through independent mechanisms. Mice carrying a homozygous mutation in neurofibromin 1 (*Nf1*), a GAP that negatively regulates Ras activity down stream of

Kit, enabled melanoblast survival and proliferation in the absence of Kit ligand (B Wehrle-Haller et al., 2001). However melanoblasts do not migrate from the MSA in these mutants, suggesting survival is dependent on RAS activity down stream of Kit but migration is not. Melanoblast migration is modulated by RAC1 activity, which regulates actin cytoskeletal assembly.

RAC1 mutants have impaired migration due to an inability to form long pseudopod projections. This restricts the speed of melanoblast migration but does not affect the route of migration (A. Li et al., 2011). In addition RAC1 mutants exhibit reduced numbers of melanoblast after e13.5 suggesting reduced levels of melanocyte proliferation or increased apoptosis. No difference was reported in the proportion of Ki67 or cleaved caspase 3 (CC3) positive melanoblasts. However the proportion of BrdU and PH3 (mitosis marker) positive melanoblast was significantly decreased in RAC1 mutants. Using flow cytometry and PI staining to determine DNA content, Li and colleagues show a significant increase in the proportion of cells in G1 therefore suggesting the loss of RAC1 is impeding entry into S phase. In addition cytokinesis *in vivo* was reported to take three times as long as in wild type melanoblast, suggesting RAC1 is also important but not essential for cell separation. This affect however was not replicated in cultured primary melanoblasts suggesting this defect is dependent on adhesion to a 3D environment (A. Li et al., 2011).

4.1.1.3 Kit signalling in melanoblast migration

Kit signalling is clearly essential for melanoblast migration and survival during development as shown by the pigmentation defects in mice containing mutation at the loci harbouring the Kit receptor and Kit ligand genes respectively (Jackson, 1997). However how migration, proliferation and survival is finely controlled by Kit signalling and the mechanisms behind the formation of unpigmented belly spots in Kit mutants is still not fully understood. This is in part due to the use of classical immunohistochemical methods on fixed tissue to visualise melanocytes which does not allow live monitoring of melanoblast behaviour. Using a recently developed *ex*

vivo skin culture system which allows for live confocal imaging I have investigate the behaviour and cell cycle characteristics of migrating melanoblast in the epidermis at e14.5 (Mort et al., 2016; Mort et al., 2010; Mort et al., 2014). R26*Fucci2a*$^{+/-}$ */Try:Cre*$^{+/-}$ embryos were used to enable live tracking of cell cycle progression within the melanoblast lineage (Delmas et al., 2003; Mort et al., 2014). In order to further dissect the influence of Kit signalling in melanoblast migration and proliferation I have conducted an identical analysis on *ex vivo* skin cultures from mice containing a loss of function mutation in the Kit receptor and a floxed exon in the Ras GAP Nf1 downstream of the Kit receptor which results constitutively activates Ras dependent Kit signalling (Mackenzie et al., 1997; Zhu et al., 2001). In addition I have shown melanoblast are more persistent in their movement during S/G2/M phases of the cell cycle by separating migration analysis by cell cycle phase using the Fucci system.

4.2 Results

4.2.1 Migrating melanoblasts show density dependent proliferation reliant on KIT signalling

In order to investigate the influence of Kit signalling on proliferation of melanoblast during colonisation of the developing epidermis, I have carried out time-lapse confocal imaging of *ex vivo* e14.5 skin cultures from *R26Fucci2aR*$^{+/Tg}$*/Try::CreB*$^{+/Tg}$ embryos using a previously published culture technique (Mort et al., 2010). Melanoblast were identified from labelled peripheral neurons by their migratory behaviour and I have adapted an analysis to estimate cell cycle times using the proportions of cells in S/G2/M (green phase) and the length of S/G2/M (Mort et al., 2016; Nowakowski et al., 1989). This is a novel method for generating quantitative data from time-lapse imaging Fucci expressing cells and has been validated in 3T3 cells (see 2.1.2.2 for description). This method has the assumption that all cells within the population are cycling asynchronously. Confirmation that all melanoblasts are cycling, and therefore validation of this method for calculating melanoblast cell

cycle times, was obtained by staining for Ki67, a well characterised marker for actively cycling cells (Scholzen & Gerdes, 2000). 96% of FACS sorted melanoblast from *Pmel17-CMN*$^{+/-}$ embryos were Ki67 positive indicating all melanoblasts are cycling (*Pmel17-CMN* (unpublished) is a highly specific melanoblast reporter, see fig 4.7). KIT signalling has been shown to be necessary for melanoblast survival and migration but its influence on melanoblast behaviour at the cellular level is still unknown (Mackenzie et al.,1997; Yoshida et al., 1996) To determine the role of KIT signalling during melanoblast migration two mutant mice lines were used to disrupt KIT signalling in a dose dependent manner. NF1 (Neurofilament 1) is a RAS-GAP that negativity regulates RAS signalling. Mutants in which NF1 function has been ablated are hyperpigmented due to an overactivation of the RAS pathway downstream of the kit receptor, which is thought to promote melanoblast proliferation and survival (Wehrle-Haller, et al 2001). In this study I used a conditional NF1 mutant containing floxed essential exons 31 and 32 to render NF1 non-functional and allow tissue specific loss of NF1 function to limited off target affects (Zhu et al., 2001a). Homozygous Kit$^{w\text{-}v}$ mutants containing a loss of function point mutation conversely, are unpigmented while heterozygous mutants are hypopigmented with an unpigmented belly spot. This is due to a loss or partial loss of KIT signalling which is necessary for melanoblast survival and migration (Mackenzie et al, 1997). Live imaging of *ex-vivo* embryonic e14.5 skin cultures from wild type (*R26Fucci2aR*$^{+/Tg}$*/Tyr::CreB*$^{+/Tg}$), Kit$^{w\text{-}v}$ heterozygous mutants (*R26Fucci2aR*$^{+/Tg}$*/Tyr::CreB*$^{+/Tg}$*/Kit*$^{+/w\text{-}v}$), NF1 heterozygous mutants (*R26Fucci2aR*$^{+/Tg}$*/Tyr::CreB*$^{+/Tg}$*/NF1*$^{+/-}$) and NF1 homozygous mutants (*R26Fucci2aR*$^{+/Tg}$*/Tyr::CreB*$^{+/Tg}$*/NF1*$^{-/-}$) was performed.

Cell densities were calculated at the start of each time lapse and proliferation rates quantified (fig 4.2A-C). Proliferation rates were calculated by tracking individual melanoblast during S/G2/M phases of the cell cycle and measuring the changes in the fluorescence of the Fucci probes. The length of the green phase was then measured from a normalised fluorescence intensity plot (fig 4.2D) and divided by the proportion of green labelled cells at the start of the time-lapse. There was a

significant decrease in the number of melanoblast in *Kit*$^{W\text{-}v}$ heterozygous mutants from 326 ± 77 cells/mm^2 to 91 ± 40 cell/mm^2 (fig 4.2B). However no significant increase was seen in melanoblast densities in *Nf1* heterozygous mutants, 303 ± 89 cells/mm^2. An increase in melanoblast density was seen in *Nf1* homozygous mutants, 545 cells/mm^2, but only two examples were seen so the trend could not be statistically confirmed (fig 4.2B). Surprisingly a comparison of cell cycle times showed no significant difference between the different genotypes (fig 4.2C). Therefore suggesting that increased proliferation in the *NF1* mutants and reduced proliferation in the *Kit*^{wv} mutants may have occurred prior to e14.5.

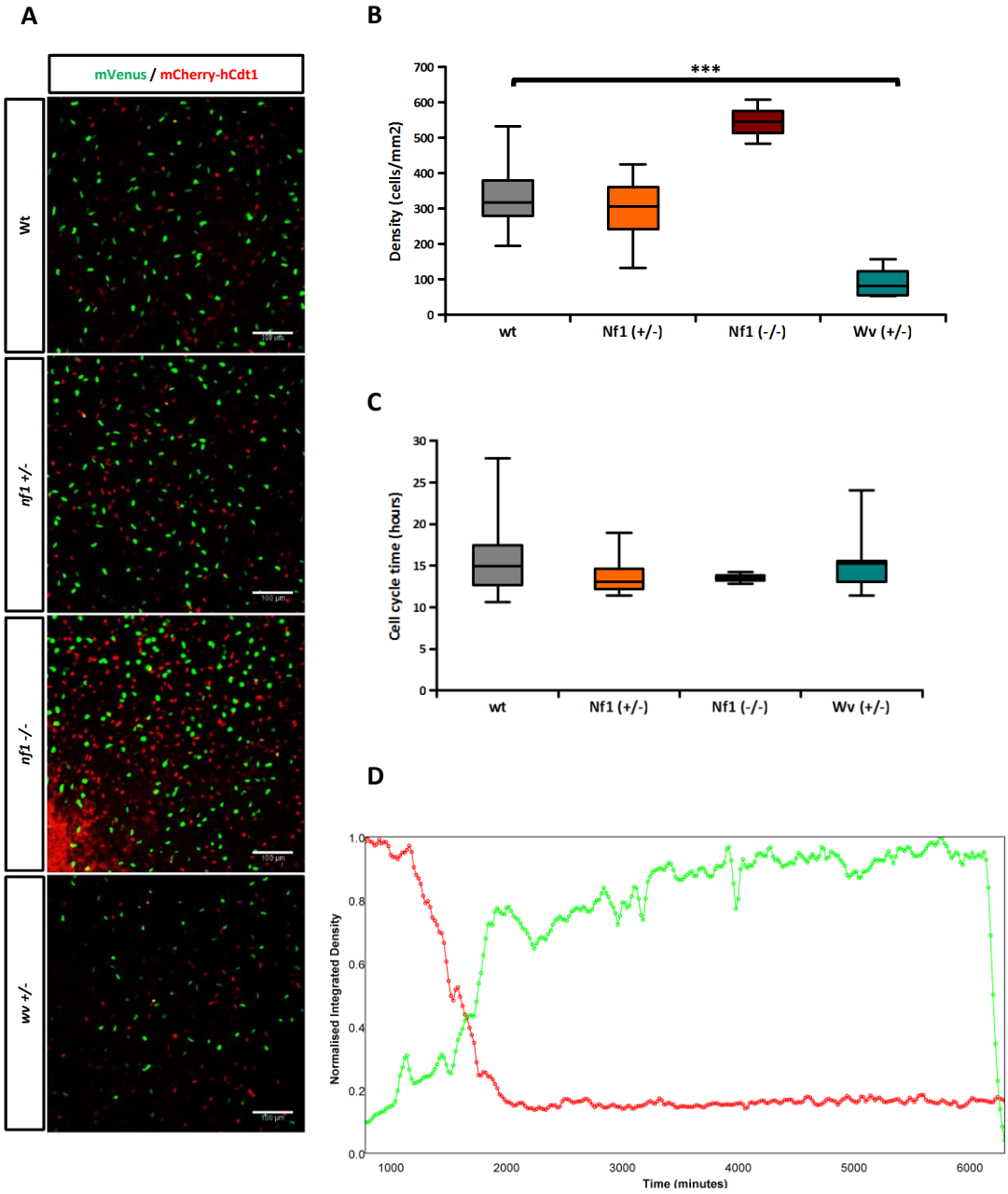

Fig 4.2: Comparison of melanoblast densities and cell cycle times in e14.5 embryonic skin cultures. (A) Z projection of confocal images taken at the start of *ex vivo* skin cultures. **(B)** Comparison of melanoblast cell densities between different genotypes. Showing a significant reduction in cells density in $Wv^{+/-}$. $NF1^{-/-}$ have a higher cell density compared to wild types but not enough examples to show significant change. **(C)** Box plot comparison of cell cycle times show no significant difference between genotypes. **(D)** Normalised fluorescence intensity plot tracking a melanoblast progressing through S/G2/M phases of the cell cycle. (n = *24 wt, 12* $nf1^{+/-}$, *2* $nf1^{-/-}$ *,8* $wv^{+/-}$*)* *** = T-test *p*-value = 4.728×10^{-12}

A recent study by Mort et al, 2016 reported a relationship between melanoblast density and cell cycle times in which cell cycle times increased with increased cell density. Mort et al used an identical method to calculate cell cycle times and densities but used the morphological length and proportion of cells in mitosis to calculate cell cycle times. To see if this relationship can also be seen in data quantified using the Fucci system, wild type cell cycle times were plotted against cell density (fig 4.3A). A weak non-significant relationship was seen. However when my data was combined with data presented in Mort et al, 2016 the correlation of the previously published data is increased from 0.574 (P=0.01) to Rho 0.617 (P=1.034x10^{-5}) (fig 4.3B). The lack of relationship in my data is down to the small range in melanoblast densities which is most likely caused by Mort et al, 2016 sampling over more diverse regions of skin which could have a higher melanoblast density. When mutant data is plotted with the combined wild type data *Kit*$^{W\text{-}v}$ mutants have a longer cell cycle than predicted by their density and *Nf1* mutants have a shorter cell cycle (fig 4.3C). This relationship was also seen by Mort et al, 2016 and suggests that KIT signalling promotes proliferation but in a density dependent manner. Interestingly, there in no relationship between cell cycle time and density in the *Nf1* mutants. RAS dependent signalling downstream of the KIT receptor is consecutively active in *Nf1* mutants. Considering this, it suggests that proliferation is density dependent through the RAS signalling pathway downstream of the KIT receptor and that *Nf1* mutants have overcome this dependence on KIT signalling and therefore their proliferation is no longer density dependent. *Kit*$^{w/v}$ mutants have reduced KIT signalling and therefore have a slower cell cycle time than predicted by their density but are still dependent on KIT signalling. In theory then density dependence proliferation should still exist in the *Kit*^{Wv} mutants, however, due to the small range of densities it is impossible to conclude if the density affect is still present.

During melanoblast development, melanoblast originating from the neural crest migrate along the dorsal lateral pathway between the developing somites and ectoderm where they emerge on the dorsal side of the embryo and migrate ventrally.

(Mackenzie et al., 1997; B Wehrle-Haller & Weston, 1995). This creates a wave of migrating melanoblast with a gradient of cell densities, the highest density of menlanoblast in more dorsal regions and a less dense melanoblast population at the edge of the wave. In order to see if density dependent proliferation is also occurring along the dorsal ventral axis, whole e14.5 *R26Fucci2aR*$^{+/Tg}$*/Try::CreB*$^{+/Tg}$ embryos were paraffin sectioned along the transverse plane in the trunk region and probed with anti-GFP and anti-Pmel (a highly specific melanocyte marker) to detect the proportion of cells in S/G2/M (fig 4.3D). The percentage of cells in S/G2/M (GFP positive) was then calculated in dorsal (1), middle (2) and ventral (3) regions (fig 4.3E). A small increase in the proportion of melanoblast in S/G2/M was seen in the most dorsal regions. This may be due to the fact that melanoblasts are emerging slightly ventrally to the midline and migrate both ventrally and dorsally. This would result in the highest melanoblast densities being within region 2. Region 3 may also be too large to detect a change in the proportion of melanoblasts in S/G2/M at the wave's edge. If time allowed, this experiment would need to be repeated comparing smaller regions.

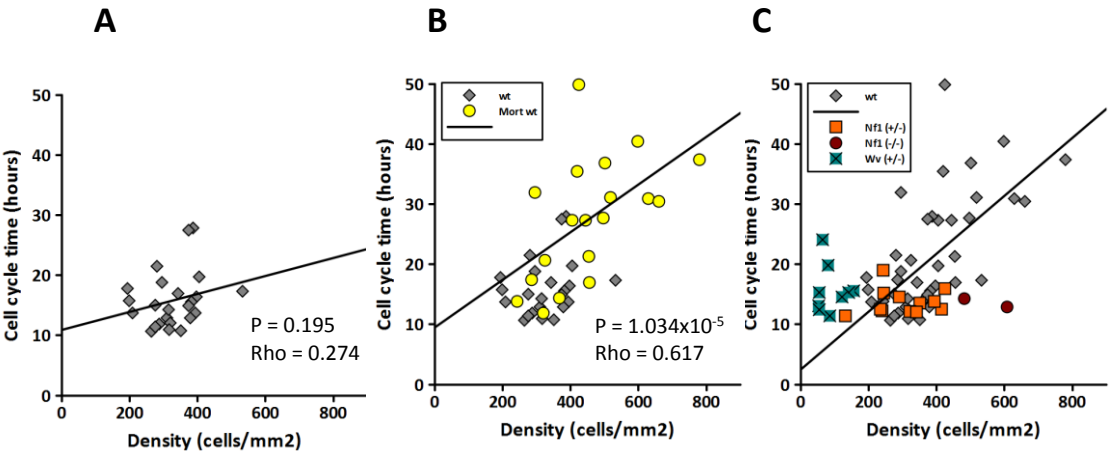

D

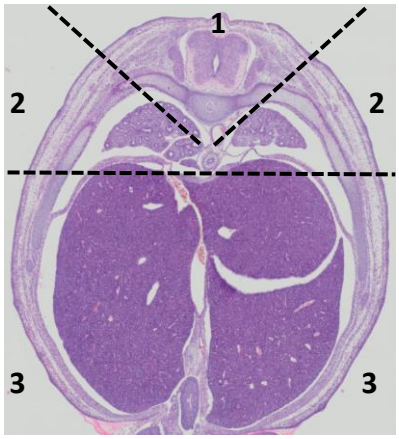

E

D/V position	Percentage of cells in S/G2/M
1	49
2	46
3	46

Fig 4.3: Cell cycle times in migrating melanoblast are density dependent. (A) A scatter plot of cell cycle times compared to cell densities from e14.5 *R26Fucci2aR$^{+/Tg}$/Try::CreB$^{+/Tg}$ ex vivo* skin cultures showing no significant relationship. **(B)** A scatter plot combining data in A with previously published data by Mort et al, 2016. (linear regression is derived from combined data) **(C)** A Scatter plot with data from B combined as wt data plotted with mutant data. *wv$^{+/-}$* melanoblast have a longer cell cycle time in relation to cell density where as *nf1$^{+/-}$* and *nf1$^{-/-}$* have a faster cell cycle time in relation to their cell density in comparison to wild type melanoblast (linear regression is derived from wt data). **(D)** A sample paraffin section through the trunk of an e14.5 embryo (http://www.emouseatlas.org).The proportion of cells in S/G2/M were counted in each of the regions highlighted. **(E)** Quantification of the proportion of melanoblasts in S/G2/M a different positions along the dorsal ventral axis (n = 119(1), 169(2), 111(3) melanoblast. Non-significant and significant relationships in A and B were calculated using Spearman's Rank Correlation. (n = *24 wt, 12 nf1$^{+/-}$, 2 nf1$^{-/-}$,8 wv$^{+/-}$)*

4.2.2 Melanoblast migration is undirected

KIT signalling via the soluble KIT ligand has been implicated in melanoblast migration. The addition of soluble KIT ligand has been shown to have a chemokinetic effect on migrating melanoblast (Jordan & Jackson, 2000). This effect appears to be independent of the RAS signalling pathway as mutants in *Nf1* were able to proliferate and survive in the absence of KIT ligand but unable to migrate from the MSA (Wehrle-Haller et al., 2001). To date the migratory behaviour of melanoblast has not been well characterised and the exact influence of KIT signalling during migration is unknown. Using live imaging techniques I have conducted a migration analysis of melanoblast at e14.5 and have showed melanoblast are migrating randomly throughout the epidermis and at the same velocity regardless of the level of KIT signalling (fig 4.4A and C). To determine if melanoblasts are migrating randomly, tracks were zeroed and plotted on a displacement plot for each time lapse (fig 4.4A). Visual inspection of each plot confirmed an equal spread of melanoblast tracks in all directions, confirming no uniform directed movement. The mean squared displacement (MSD) (the mean distance travelled by all tracks from zero at each time point squared) of the melanoblast population in each time lapse was then calculated. When (MSD) was plotted against time a linear relationship was observed for all time lapses, indicating melanoblasts are moving in a diffusive manor. The diffusion coefficient (D) was calculated from the gradient of the linear line of best fit (fig 4.4B) for each time lapse. The diffusion coefficient quantifies the spread of a population and no significant difference was seen between genotypes (fig 4.4D). Interestingly, $Kit^{w\text{-}v}$ showed a significant increase in persistence compared to wild types from 0.303±0.01 to 0.345±0.05. The lower levels of persistence in the *Nf1* mutants and wild type may be due to an increased chance of melanocytes bumping into one another due to higher cell densities and therefore changing direction more frequently. Considering no increase in velocity was seen in the *Nf1* mutants these results indicate RAS-dependent KIT signalling has no direct role on melanoblast migration at this stage of development suggesting the chemokinetic affect observed by Jordan and Jackson is signalling via a different pathway downstream of KIT

(Jordan & Jackson, 2000). Considering velocity is not reduced in the *Kit*$^{w/v}$mutants this might suggest the chemokinetic effect of KIT signalling operates by a threshold mechanism and *Kit*$^{w/v}$ are receiving sufficient KIT signalling to migrate phenotypically identically to wild types.

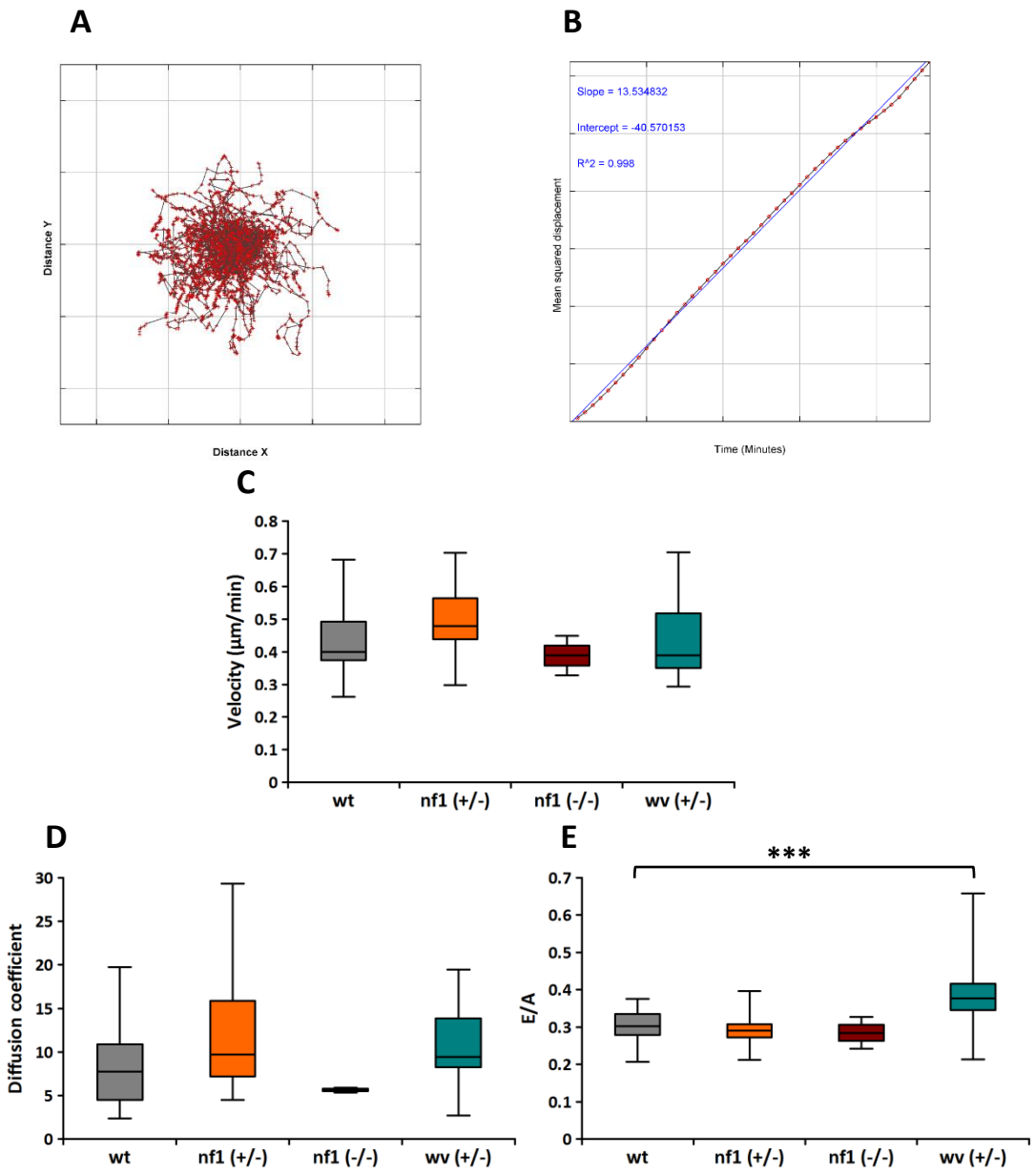

Fig 4.4: Melanoblast migration analysis from e14.5 *ex vivo* embryonic skin cultures. (A) A displacement plot of zeroed melanoblast tracks showing a homogenous spread and therefore no populational directed movement. **(B)** Plot of mean squared displacements of tracks at each time point. A straight line indicates a population is diffusing the slope of which is used to derive the diffusion coefficient (D). **(C)** A box plot comparing velocity between different genotypes. **(D)** A box plot comparing diffusion coefficents between different genotypes derived from mean squared displacement plots (B). **(E)** A box plot comparing persistence (euclidian / accumulated distance) between different genotypes. No significant difference between genotypes in C and D shown by one way ANOVA $P > 0.01$. Significantly more persistent movement of $wv^{+/-}$ melanoblasts in E confirmed by ANOVA $P<0.01$ and TukeyHSD $P<0.001$. (n = *24 wt, 12* $nf1^{+/-}$, *2* $nf1^{-/-}$ *,8* $wv^{+/-}$*)*

4.2.3 From e14.5 to e15.5 melanoblast continue to slow their cell cycle in a density dependent manner and have reduced velocity

To determine how melanoblast behaviour is changing over time an identical analysis was performed at e15.5. A small non-significant increase in cell density was observed from 327.88±30.6 cells/mm^2 to 389.66±54.3 cells/mm^2 (fig 4.5A). And a significant increase in cell cycle time was also seen from 15.75±1.9 hours at e14.5 to 22.93±3.6 hours at e15.5 (fig 4.5B). This is in accordance with the density dependent model of proliferation and strengthens the relationship when combined with the e14.5 data, although the relationship is still not statically significant (fig 4.5C). Interestingly, there is a significant reduction in the velocity of melanoblast from e14.5 to e15.5 from 0.429±0.03 μm/min to 0.337±0.03μm/min but no significant difference in persistence or diffusion coefficient (fig 4.5D-F). The reduction in velocity and proliferation seen at e15.5 coincides with the time melanoblast start to localise to hair follicles (Hirobe, 1984). A potential mechanism for this may be the depletion of KIT ligand in the epidermis over time resulting in melanoblast receiving less proliferative and chemokinetic signals. Two previous reports have shown a loss or reduction in melanoblast number when KIT ligand has been ectopically expressed in the developing somites and lateral mesenchyme, suggesting competition for KIT ligand as a possible mechanism (Duttlinger et al., 1993; Bernhard Wehrle-Haller et al., 1996).

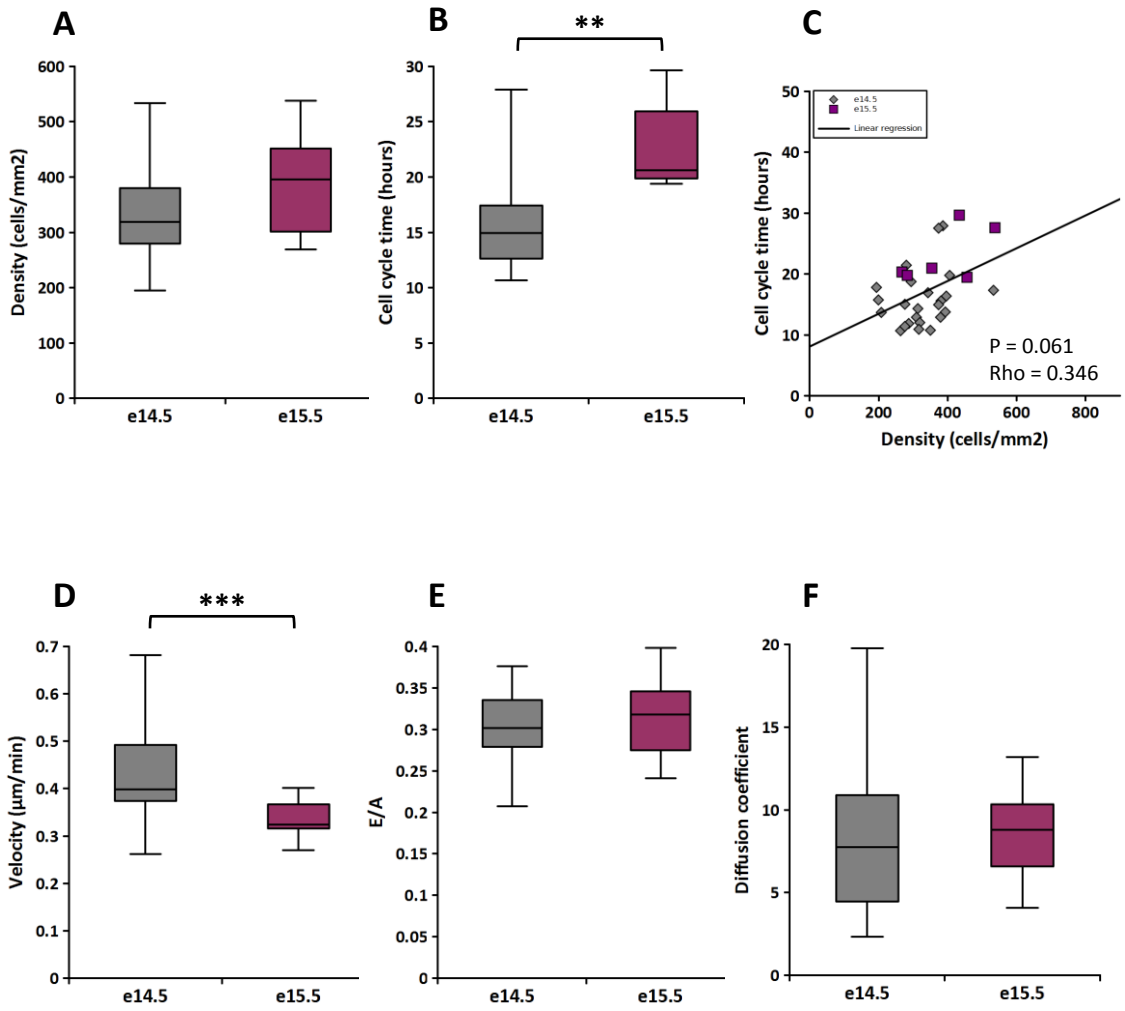

Fig 4.5: Melanoblast slow their migration and cell cycle prior to localisation to hair follicles. **(A)** From e14.5 to e15.5 melanoblast density increases but not significantly. **(B)** The cell cycle time of melanoblasts during this period significantly increases. **(C)** A scatter plot showing melanoblasts at e15.5 are following the same density dependent cell cycle trend as seen in e14.5 (linear regression derived from all data points). **(D)** A box plot showing a significant decrease in velocity between e14.5 and e15.5. **(E and D)** But there is no significant change in migratory behaviour shown by similar persistence (euclidian/accumulated distance) and diffusion coefficient between e14.5 and e15.5. Significant difference in B and C shown by Students' T-Test, ** = $P<0.01$, *** = $P<0.001$ n = 24 (e14.5) and 6 (e15.5) skin cultures .

4.2.4 Melanoblast movement is more directed during S/G2/M phases of the cell cycle

A unique advantage of the Fucci system is the ability to separate analyses by cell cycle stage based on the abundance of mCherry-hCdt1(30/120) in G1 and mVenus-hGem(1/110) in S/G2/M. Utilising this the migrational behaviour of wild type migrating melanoblast at e14.5 in G1 and S/G2/M phases of the cell cycle was compared (fig 4.6). There was no significant change in velocity as melanoblast progressed through the cell cycle, 0.424±0.04μm/min in S/G2/M to 0.433±0.04μm/min in G1 (fig 4.6A). There was however a small highly significant increase in persistence from G1 (0.275±0.01) to S/G2/M (0.331±0.01), which was also reflected in an increase in diffusion coefficient from 6.404±1.37 in G1 to 10.456±1.86 in S/G2/M (fig 4.6B and C). To further confirm the increased exploratory behaviour of melanoblast during S/G2/M the distribution of Hurst exponents of melanoblast tracks between and G1 and S/G2/M was compared (fig 4.6D). The Hurst exponent in this context is a measure of similar movements over a time series. A high *H* value is an indication of a high instant of repeated movements with an *H* value of 0.5 being random movement. Melanoblast tracks in S/G2/M have a distribution of higher *H* values, therefore indicating their movement is more persistent than in G1.

There was concern, however, that the differences seen in persistence, diffusion coefficient and Hurst exponent distribution could be down to an imaging analysis artefact for three possible reasons. First, the *TCB::CreB* also labels non-migratory nerves originating from the neural crest which are present in the skin. The majority of nerves are in G1 and are not migratory, therefore, if tracked, could bias the G1 tracking data to be less persistent. Second, G1 tracks are generally longer, which could increase the chance of the track becoming less persistent. Third, G1 tracks are biased towards the end of the time lapse and as melanoblast are seen to drop out of the cell cycle under present *ex-vivo* culture conditions it is possible that their behaviour could be influenced by the extended lazar exposure. To address all these potential caveats, *R26Fucci2aR* mice were crossed with *Pmel17-CMN,* tamoxifen

administered at e12.5 and e13.5 followed time-lapse imaging of *ex vivo* e14.5 skin cultures. *Pmel-CMN* (unpublished) is a highly melanoblast specific Cre line which will address the problem of accidental tracking of neurons (fig 4.7A and B). Upon analysis the number and length of tracks was kept the same for both S/G2/M and G1 tracks. Also, only tracks in the first 8.3 hours were analysed to remove any potential biases in the data. Once again there was no significant change in velocity from S/G2/M (0.459±0.04μm/min) to G1 (0.501±0.05μm/min) (fig 4.7C). The higher level of persistence still in melanoblasts from 0.564±0.05 in S/G2/M to 0.475±0.06 in G1 provides evidence that the increased persistence seen in fig 4.6 is not an imaging artefact (fig 4.7D). It is surprising that melanoblasts are more directed in their movement during S/G2/M as it is generally thought cells are more responsive to extra stimuli during G1 when the primary cilium is assembled (Seeley & Nachury, 2010). However, considering I have shown melanoblasts are migrating randomly at this stage in development it can be assumed they are not responding to a directional chemoattractant. It is possible that the increased persistence is due to cytoskeletal rearrangements taking place in the preparation of cell division, which is restricting the ability of the cell to change direction.

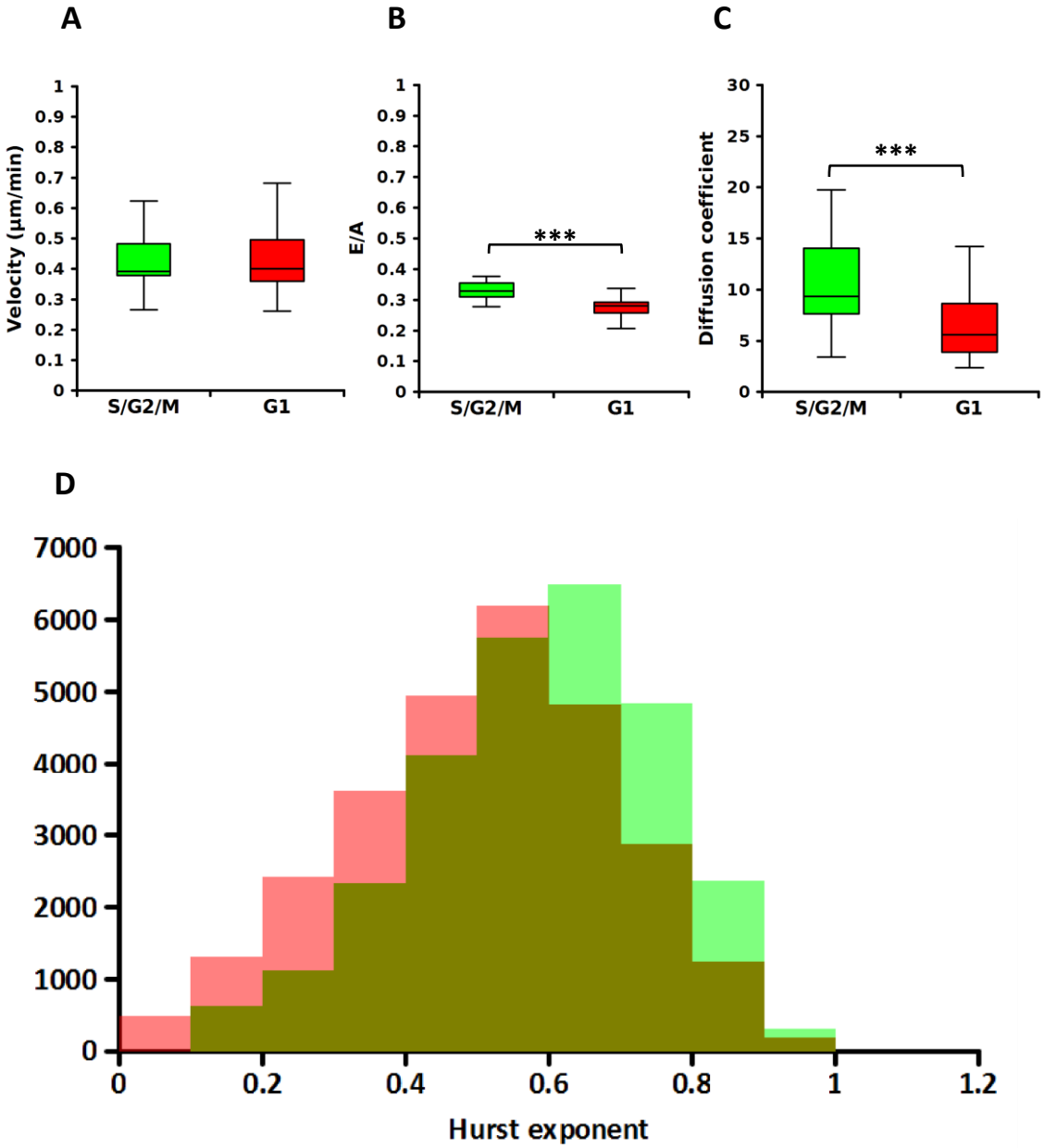

Fig 4.6: Melanoblast movement is more directed in S/G2/M (A-C) Box plots comparing velocity, persistence (euclidian / accumulated distance) and diffusion coefficient in wild type melanoblast from e14.5 *R26Fucci2a*$^{+/tg}$/*TCB::Cre*$^{+/Tg}$ embryos in S/G2/M and G1 (n=23 skin cultures). Melanoblasts show no change in velocity throughout the cell cycle but are significantly more persistent and have a higher diffusion coefficient in S/G2/M. **(D)** A histogram overlaying the distribution of hurst exponents for melanoblast in G1 (Red) and S/G2/M (Green). Melanoblast in S/G2/M have a distribution of higher hurst exponents confirming a more directional behaviour. Significant difference in B and C shown by Students' T-Test, *** = P<0.001.

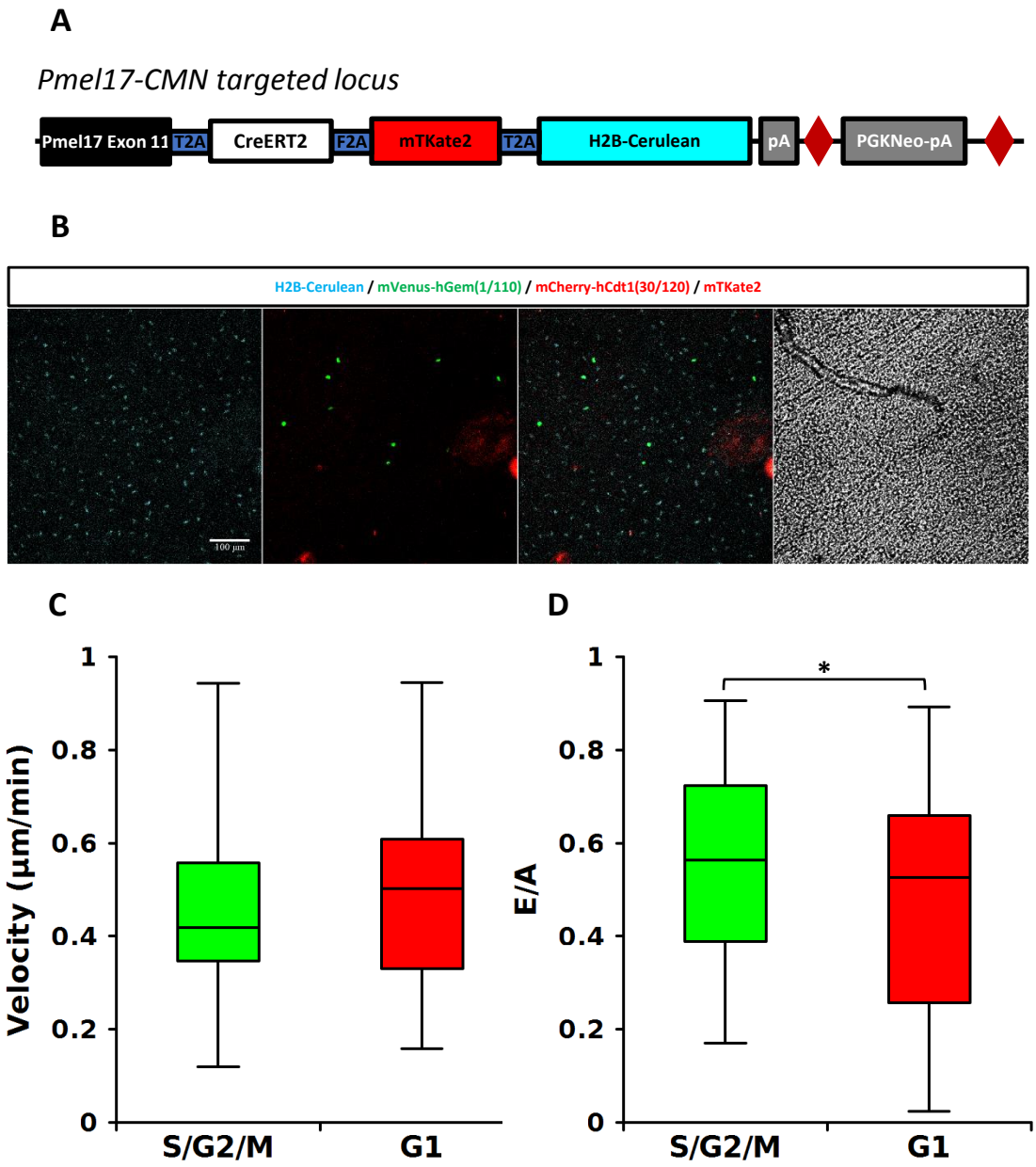

Fig 4.7: Conformation of increased persistence in during S/G2/M using a highly specific melanoblast CreERT. (**A)** Schematic of the *Pmel17-CMN* targeted locus. The Pmel17-CMN (unpublished) construct has been targeted to the 3' end of exon 11 (last exon). Resulting in highly melanoblast specific expression of CreERT, mTKate2 and H2B-Cerulean. **(B)** Confocal images taken of an e14.5 *R26Fucci2a*$^{+/Tg}$*/Pmel17-CMN*$^{+/Tg}$ *ex vivo* skin culture after administration of two doses of tamoxifen at e12.5 and e13.5. No membrane bound mKate signal could be detected. **(C and D)** Box plot comparing velocity and persistence in wild type melanoblast from E14.5 *R26Fucci2a*$^{+/tg}$*/Pmel17-CMN*$^{+/Tg}$ embryos in S/G2/M and G1 (n=6 skin cultures). Tracks were trimmed to 2.5 hours in length, analysed from the first 8.3 hours of the time-lapse and the same number of tracks for each cell cycle stage. Significant difference in B, C and F shown by Students' T-Test, * = *P<0.05.*

4.3 Discussion

In this chapter I have demonstrated the ability to generate quantitative data using the *R26Fucci2aR* inducible cell cycle reporter mouse. The techniques I have developed would not be possible with the original Fucci or *R26pFucci2* lines because they are constitutive reporters (1.5 in introduction) (Abe et al., 2013; Sakaue-Sawano et al., 2008). Or in the case of *R26-mVenus-hGem(1/110)* and *R26-mCherry-hCdt1(30/120)* lines are inducible but are separate alleles which would complicate already complex mouse crosses (Abe et al., 2013). The bicistronic design of the Fucci2a construct greatly increases the versatility of the *R26Fucci2aR* mouse when compared to the range other available alleles (Abe et al., 2013; Sakaue-Sawano et al., 2008). Because both Fucci probes are expressed from a single genomic locus in a bicistronic construct, the *R26Fucci2aR* model allows lineage specific expression using the Cre-loxP system and greatly simplifies otherwise complex genetic crosses.

Melanoblast development and migration studied using *ex vivo* skin culture (Mort et al., 2010) represents a tractable model system for the understanding of all neural crest derived lineages; such as the colonisation of the brachial arches by the cranial neural crest and the colonisation of the developing gut by enteric ganglia progenitors during development (Kulesa et al., 2011). Defects in the migration of these neural crests derived populations by disruption of the Bardet-Bied Syndrome (BBS) associated genes BBS4,6 and 8 results in morphological cranial-facial defects and a failure to innervate the gut resulting in impaired gut motility, hallmarks of BBS and Hirschsprungs disease (Tobin et al., 2008).

Melanoblast migration has been extensively studied and two key signalling pathways necessary for different stages of melanoblast migration have been identified. Signalling via the endothelin receptor-B (EDNRB) is essential for melanoblast migration from e10.5-e12.5 when melanoblast initially leave the migration staging area (MSA) and migrate in the developing epidermis, but is not required for subsequent melanoblast migration in the epidermis (Lee et al., 2003; Shin et al., 1999). KIT ligand exists as a soluble ligand and in a membrane bound form exposed on cells along the dorsolateral pathway. The interaction between KIT ligand and the

KIT receptor on the surface of melanoblasts is essential for melanoblast migration from the MSA along the dorsolateral pathway and survival (Mackenzie et al., 1997; B Wehrle-Haller et al., 2001). The two different forms of KIT ligand appear to have different effects on melanoblast behaviour with the soluble KIT ligand shown to be important in migration and the membrane bound form for melanoblast survival (Jordan & Jackson, 2000; Tabone-Eglinger et al., 2012; Wehrle-Haller & Weston, 1995). Migration and proliferation are also induced by independent signalling pathways downstream of the KIT receptor with RAS dependent signalling promoting proliferation and RAC1 migration and cell cycle progression (Li et al., 2011; Wehrle-Haller et al., 2001). The migratory behaviour of melanoblasts, the influence of KIT signalling and the mechanism by which impairing KIT signalling results in unpigmented belly spots is still poorly understood. Taking advantage of an *ex vivo* skin culture technique (Mort et al., 2016, 2014, 2010) that allows for live confocal imaging of melanoblasts, I have been able to directly characterise melanoblast behaviour and the influence of KIT signalling in terms of proliferation and migration using the *R26Fucci2a* reporter mouse crossed to a neural crest specific Cre (*Try::CreB*) (Delmas et al., 2003; Mort et al., 2014). In addition I have illustrated the ability to segregate analysis by cell cycle stage using the Fucci system to identify more persistence migration of melanoblasts during S/G2/M.

4.3.1 Melanoblast proliferation is density dependent

Using a novel method for calculating cell cycle times from time-lapse data of Fucci expressing cells (Richard Lester Mort et al., 2014), I calculated the cell cycle time of melanoblasts at e14.5 to be 17±3 hours. This is comparable to doubling times calculated by manually counting *Dct:lacZ* labelled melanoblasts during between developmental stages (16 hours) and performing linear regression (Luciani et al., 2011). Mort et al used a similar approach to calculate cell cycle times by measuring the length of melanoblast M-phase and the number of cells in M-phase in *ex vivo* skin culture (Mort et al., 2016). The study reported that melanoblast cell cycle times is density dependent with cell cycle times increasing with increased cell density. My

dataset contained less variation in cell density than this study and consequently I did not observe a similar relationship between density and cell cycle time when my data was considered in isolation. I suggest this is likely because I sampled consistently in the most dorsal regions of the epidermis to generate my data while Mort et al sampled semi-randomly over a greater range of dorsoventral positions (Mort et al., 2016). Melanoblasts emerge slightly ventrally to the midline and migrate in a dorsoventral direction filling the most dorsal space towards the end of the colonisation process. Therefore sampling more ventrally will result in higher cell densities (Mackenzie et al., 1997; B Wehrle-Haller & Weston, 1995). Another possible explanation is that the staging of embryos in my experiments was more consistent than Mort et al therefore resulting in more consistent cell densities. However, when combined with the data of Mort et al, my data is consistent with the relationship described (fig 4.3B) and the significance of the relationship is increased, therefore supporting the density dependent model proposed. In agreement with this, when cell cycle data from e15.5 embryos (where the melanoblast density is higher) was included, the density dependent relationship in my data was strengthened although still not statistically significant. Quantification of the proportion of cells in S/G2/M along the dorsal ventral axis did not show a dorsal ventral dependence on proliferation hypothesised due to melanoblast emerging from the dorsal region and migrating ventrally. This could be a technical issue in not having discreet enough regions to compare, considering the highly homogenous distribution of melanoblast in all but the most ventral regions observed in e14.5 *Dct::LacZ* mice (Luciani et al., 2011). The current work and the work described in Mort et al (2016) is based on the assumption that all melanoblasts are actively cycling. I have demonstrated here that indeed 98% of melanoblasts are Ki67 positive when isolated by FACS.

A potential mechanism for this density dependent affect could be the gradual sequestering of KIT ligand with increasing melanoblast cell density. Considering KIT signalling has been shown to promote proliferation through the RAS signalling pathway (Wehrle-Haller et al., 2001). If the source of KIT ligand is finite and receptor-ligand binding is followed by receptor ligand degradation. Then increasing

numbers of melanoblasts will over time deplete the stocks of KIT ligand, resulting in a reduction of KIT signalling in the migrating melanoblast population. Internalisation of receptor tyrosine kinases upon ligand-binding followed by ubiquitination and subsequent degradation in lysosomes is well documented (reviwed in Goh & Sorkin, 2013). The binding of Kit ligand has been shown to cause internalisation of the KIT ligand-receptor complex in cultured mast cells (Yee et al., 1994). Internalisation was shown to be partially dependent on the functional kinase activity of the KIT receptor and was followed by polyubiquintation of the ligand-receptor complex. It is possible therefore that KIT ligand receptor binding in melanoblast also results in internalisation of the ligand-receptor complex and degradation. This mechanism will therefore ensure the appropriate numbers of melanoblast are produced as it is dependent on the numbers of KIT ligand cell along the dorsal lateral pathway. This mechanism is supported by observations that ectopic expression of the KIT receptor in the developing somites and lateral mesenchyme results in a loss or reduction in melanoblasts as a result of aberrant KIT ligand sequestration (Duttlinger et al., 1993; Wehrle-Haller et al., 1996). In addition, the expression of KIT ligand has been shown to decrease from e13.5 to e15.5 and is absent from the interfollicular space in adult mice which has been implicated in the disappearance of melanoblast outside of hair follicles in mice (Yoshida et al., 2001;Yoshida et al., 1996). The reduction in proliferation and velocity seen at e15.5 in my data, at a time when KIT ligand expression is diminishing in the epidermis, is also in agreement with this model.

4.3.2 Melanoblasts colonise the developing epidermis by undirected migration

Based on the striped pigmentation patterns seen in classical chimera experiments it has been classically thought that melanoblast migrate and proliferate in a longitudinal manner along the dorsal to ventral axis (Mintz, 1967). However a recent study using a sporadically activated *Dct-LacZ* reporter to follow individual melanoblast clones showed significant mixing of clones, therefore questioning the hypothesis of directed longitudinal migration (Wilkie et al., 2002). Due to the difficulties in imaging

melanoblasts behaviour live, the migratory characteristics of melanoblasts are only recently beginning to be investigated (Li et al., 2011; Mort et al., 2016, 2010). Using *ex vivo* skin cultures of e14.5 *R26Fucci2aR*$^{+/Tg}$*/Try::CreB*$^{+/Tg}$ embryos I have shown that melanoblasts are migrating in a undirected manner throughout the developing epithelium, therefore disproving the theory of ventrally directed movement. Recently published work by Mort et al has used an identical method using YFP labelled melanoblasts to parameterise a mathematical model of melanoblast migration (Mort et al., 2016). The model combines experimentally derived cell cycle times, migratory behaviour and epithelial expansion to explain melanoblast colonisation of the developing skin with simulations that recapitulate clonal expansion seen by Wilkie et al (Wilkie et al., 2002). My data is in agreement with this model in suggesting undirected migration in combination with domain expansion and proliferation is sufficient to colonise the epidermis and produce the striped pigmentation phenotypes classically described by Mintz (Mintz, 1967).

4.3.3 KIT signalling via the RAS signalling pathway promotes proliferation in a dose dependent manner

Multiple mutations in the KIT receptor ligand have been associated with a loss of pigmentation and melanocytes (reviewed in Jackson, 1997). KIT signalling via the RAS signalling pathway has been shown to increase melanoblast number during development (Wehrle-Haller et al., 2001). While, conversely a reduction it KIT signalling reduces melanocyte number and results in an unpigmented belly spot (Mackenzie et al., 1997). The exact influence KIT signalling has on melanoblast proliferation is still poorly understood. To investigate this I calculated cell cycle times for melanoblasts at e14.5 in mice containing a loss of function mutation in the *Kit* receptor or a loss of function floxed exon in *Nf*1 which constitutive activates the RAS signalling pathway downstream of the KIT receptor (Mackenzie et al., 1997; Zhu et al., 2001a). Surprisingly, no difference in cell cycle time was observed. However, when plotted against density it is apparent *Kit*^{Wv} mutants have a longer cell cycle time and *Nf1* mutants a shorter cell cycle time than predicted by density

dependent proliferation in wild type cultures. Interestingly *Nf1* mutants show no relationship between cell cycle time and cell density. This suggests that constitutive RAS activity has removed the melanoblasts' dependence on KIT ligand and is unaffected by the depletion of KIT ligand at higher cell densities. Due to the small range in densities of the Kit^{Wv} mutants it is hard to tell if the density affect is still prevalent in this population. If KIT ligand depletion is the mechanism driving the density dependent proliferation, then the Kit^{Wv} mutants would not be immune to the density affect as they are still dependent on exogenous sources of KIT ligand.

4.3.4 A threshold model for KIT signalling in migration

KIT signalling has been shown to promote melanoblast migration in a chemokinetic manner. Addition of soluble KIT ligand to *ex vivo* skin cultures increases the speed at which melanoblast infiltrate the epidermis and localise to hair follicles (Jordan & Jackson, 2000). The migratory influence of KIT signalling appears to signal through a RAS independent pathway as mutations in *Nf1* can rescue melanoblast survival and proliferation but melanoblast fail to leave the MSA (Wehrle-Haller et al., 2001). My results support this observation as no increase in velocity was observed in the *Nf1* mutant skin cultures. However I saw no decrease in velocity in the Kit^{Wv} mutants, which would be expected if melanoblast within these cultures are receiving less KIT signalling. If velocity was also density dependent with velocity decreasing with increased cell density, then it could be said that Kit^{Wv} mutants are migrating slower for their given cell densities due to a reduction in KIT signalling. However I did not see any relationship between velocity and density in my data (data not shown). Although it is possible the small range in densities is masking this effect in my data. Another possible mechanism could be that the relationship between KIT signalling and velocity is not linear as for proliferation. A threshold hold system could exist and the amount of KIT signalling received by the Kit^{Wv} mutants is sufficient to drive normal migration, while KIT signalling has dropped below the threshold at e15.5 explaining the drop in velocity at this time point. It is also possible that the decrease in velocity is due to melanoblasts localising to the developing hair follicles at this

time (Hirobe, 1984). In the threshold model the chemokinetic affect reported by the addition of KIT ligand could be due to KIT signalling being driven above physiologically normal levels and the upper threshold thereby inducing increased mobility (Jordan & Jackson, 2000). I report no significant difference in the diffusion of melanoblast between the different genotypes in my data and saw no density dependent affect (data not shown). This is in contrast to data published using the same mutant mice strains and culture system (Mort et al., 2016). Mort et al report a density dependent relationship with diffusion irrespective of genotype. This suggest that less dense populations have innately more diffusive properties independent of KIT signalling, which is likely down to cells being more persistent and changing direction less to avoid neighbour cells. The increased persistence seen in my Kit^{Wv} mutants would support this hypothesis. However, without sufficient range of cell densities in my data it is not possible to confirm Mort et al's observations.

Taken together this data suggests KIT signalling enables migration at this stage in development but that the affect is not linear, suggesting that proliferation is in fact the key determinant in the hyperpigmentation phenotype seen in the *Nf1* mutants and the unpigmented belly spot in the Kit^{Wv} mutants. This hypothesis is supported by simulations of Mort et al's model, which is more sensitive to belly spot formation by changes in proliferation than migration (Mort et al., 2016).

4.3.5 Segregating tracking analysis by cell cycle stage using Fucci identifies melanoblast to be more persistent in S/G2/M

The Fucci system uniquely enables live tracking data to be separated by cell cycle stage and therefore any behavioural changes during cell cycle progression to be examined without the need for synchronisation. Classical methods for monitoring cell cycle phase specific behaviours rely on the use of toxins such as Thymidine (S-phase) and Nocodazole (M-phase) or growth factor starvation to synchronise cells within a specific cell cycle phase (Aktas et al., 1997; Ballabeni et al., 2011; N. Kim & Song, 2013; Benmaamar, 2005; Shirakawa et al., 2014). The synchronisation step

of these methods is not always efficient (Fujii-Yamamoto et al., 2005). Also the potential artefacts induced by the toxins used or as a results of holding cells in a particular cell cycle phase must be taken into consideration when drawing conclusions from these kinds of experiments.

A comparison of wild type melanoblasts in G1 and S/G2/M showed melanoblasts to be more persistent in S/G2/M. Interestingly, in other systems changes in cell migratory behaviour during the cell cycle has also been reported. Using the FUCCI system Shirakawa and colleagues have shown cultured primary mouse calvarial osteoblasts (PCOBs) migrate faster in S/G2/M than in G1, thought to be caused by PCOBs synthesising bone matrix during G1/G0 which may limit their migratory velocity (Shirakawa et al., 2014). Another report conversely showed a decrease in motility and dispersal during S/G2/M in cultured L929 (mouse), BT4Cn (rat) and HeLa (human) cell lines (Walmod et al., 2004). Constitutively active RAC1 in these cultures increased the velocity and dispersal of L929 cells in G2 to near G1 levels. The contrasting observations from these reports suggest that cell cycle phase specific changes in migratory behaviour is context dependent. Migration in melanoblasts is partially dependent on RAC1, which is essential for the formation and stability of long pseudopods via rearrangement of the actin cytoskeleton (A. Li et al., 2011). It would to interesting to see if RAC1 levels fluctuate throughout the cell cycle as a potential mechanism for the increased persistence observed during S/G2/M. This could be tested by FACS sorting melanoblast from dissected embryonic skin (as described in methods …) into mCherry-hCdt1(30/120) and mVenus-hGem(1/110) populations followed by quantification of RAC1 abundance by western blot.

In addition, considering I have shown melanoblasts to be more persistent during S/G2/M it can be inferred that more rapidly cycling melanoblast will be more persistent due to S/G2/M phases taking up a higher proportion of their cell cycle time than G1. This is with the assumption that the length of S/G2/M remains constant between fast and slow cycling melanoblast and the changes in the lengthening of the cell cycle is primary caused by a lengthening of G1. It would be interesting to test if increased persistence in melanoblasts at the front of the wave of migrating

melanoblast, which based on the density dependent model or proliferation will have a shorter cell cycle time, contributes to colonisation of the ventral trunk region of the developing skin. This could be tested in the in silico model of melanoblast colonisation of the embryonic mouse trunk constructed by Mort and colleagues (Mort et al., 2016). The model has been parameterised by experimental cell cycle, migration and domain expansion data to successfully simulate melanoblast colonisation of the trunk. In addition increasing cell cycle times of melanoblast in the model result in the formation of unpopulated ventral regions reminiscent of the unpigmented belly spots seen in $Kit^{W\text{-}v}$ mutants as a results of reduced proliferation (Mackenzie et al., 1997; Mort et al., 2016). Based on experimental observations the movement of melanoblasts in the model is random and undirected so at each time point each melanoblast has an equal probability to move in any direction. This therefore does not take into account persistent movement (repeated movements in the same direction), which could potentially influence the exploratory behaviour of migration melanoblast. Persistence could be added into the model by giving each cell a "memory" of its previous movement, which can then be used to bias the random decision of the next movement. Increase persistence can then be added as an increased level of bias to a movement in same direction as the previous movement. Using this it would be interesting to see if increased persistence in the faster cycling melanoblast during the early stages of migration and at the edge of the migrating wave aid in the colonisation of the ventral trunk.

5 Chapter 5: Comparative analysis of the developing lung epithelium separated by proliferative state

5.1 Introduction

The mammalian lung functions to provide a surface for gas exchange to occur between the external environment and circulatory system. Development of the bronchial tree is carefully orchestrated by signalling and physical interactions between the endoderm derived lung epithelium and surrounding mesenchyme and has evolved to maximise the surface area at which gas exchange can occur within specialised sacs of thin squamous epithelium closely associated with capillaries called alveoli.

5.1.1 Specification of the presumptive lung

In mice the presumptive lung is first specified at e9-9.5 as a region of Nkx2-1 expression located in the ventral wall of the foregut. This specification is dependent on Wnt signalling shown by lung and tracheal agenesis and complete loss of specification in targeted β-catenin and Wnt2/2b double knock-outs (Goss et al., 2009; Harris-Johnson et al., 2009). Conversely, ectopic expression of stabilised β-catenin throughout the foregut resulted in expansion of Nkx2-1 expression into regions of the foregut usually associated with stomach formation. From e9.5 to e10.5 the primary lung buds form and elongate posteriorly simultaneously with the separation of the trachea and oesophagus. A complex signalling network involving BMP, FGF, RA and Shh signalling regulates the initial bud outgrowth. BMP4 has been shown to be necessary for epithelial and mesenchymal proliferation during initial bud outgrowth but not specification (Li et al., 2008). Addition of an RA antagonist to cultured embryos prevents lung bud initiation via loss of FGF10 expression in the mesenchyme around the presumptive primary lung buds, suggesting RA is acting up stream of FGF10 (Desai et al., 2004). Genetic knock-out studies of FGF10 and its receptor FGFR2 also results in a loss of initial bud outgrowth with similarities to the *branchless* (FgF homolog) phenotype in drosophila (De Moerlooze et al., 2000; Min et al., 1998; Sekine et al., 1999; Sutherland et al.,1996). A double knock out study of Shh signal transducers Gli1 and Gli2 showed an overlapping dependency of Shh signalling via both transcription factors in initiation of pulmonary development (Motoyama et al., 1998).

5.1.1.1 Lung branching morphogenesis

From e10.5 to e16.5 (pseudoglandular stage) The lung epithelium undergoes a series of stereotyped branching into the surrounding mesenchyme to form the characteristic bronchial tree (Fig 5.1) (Metzger et al., 2008). Branching can occur by one of three mechanisms: domain branching, when new branches form perpendicular to the elongating branch; planar bifurcation, when the tip of a branch splits into two separate branches, and orthogonal bifurcation, when a tip of a branch splits into two separate branches followed by a rotation of 90^{o} in the plane of bifurcation before the next bifurcation. Rare trifurcations have also been observed (Blanc et al., 2012). Each branching mode has a different function during lung development. Domain branching is more prominently used at the beginning of branching morphogenesis to set up a "skeleton". Subsequently planar bifurcation is used to drive branching to the edge of the surround mesenchyme while orthogonal bifurcation is used to fill in the gaps (Metzger et al., 2008). The stereotyped branching mechanism has recently been brought into question, however, with the discovery of greater variation in the temporal and spatial branching pattern proposed by Metzger. The cause of this variation has been directly correlated to changes in the shape of the surrounding mesenchyme suggesting a model in which the lung epithelium is branching into where the available space is within the mesenchyme rather than being predetermined (Blanc et al., 2012). This would make the process of branching more adaptable and robust to biological variation, therefore preventing collisions that are not seen during development. A recent report showing the differentiation of smooth muscle cells in the cleft regions of bifurcating branches highlights again the importance of considering the physical interactions between the lung epithelium and surrounding mesenchyme during branching (Kim et al., 2015).

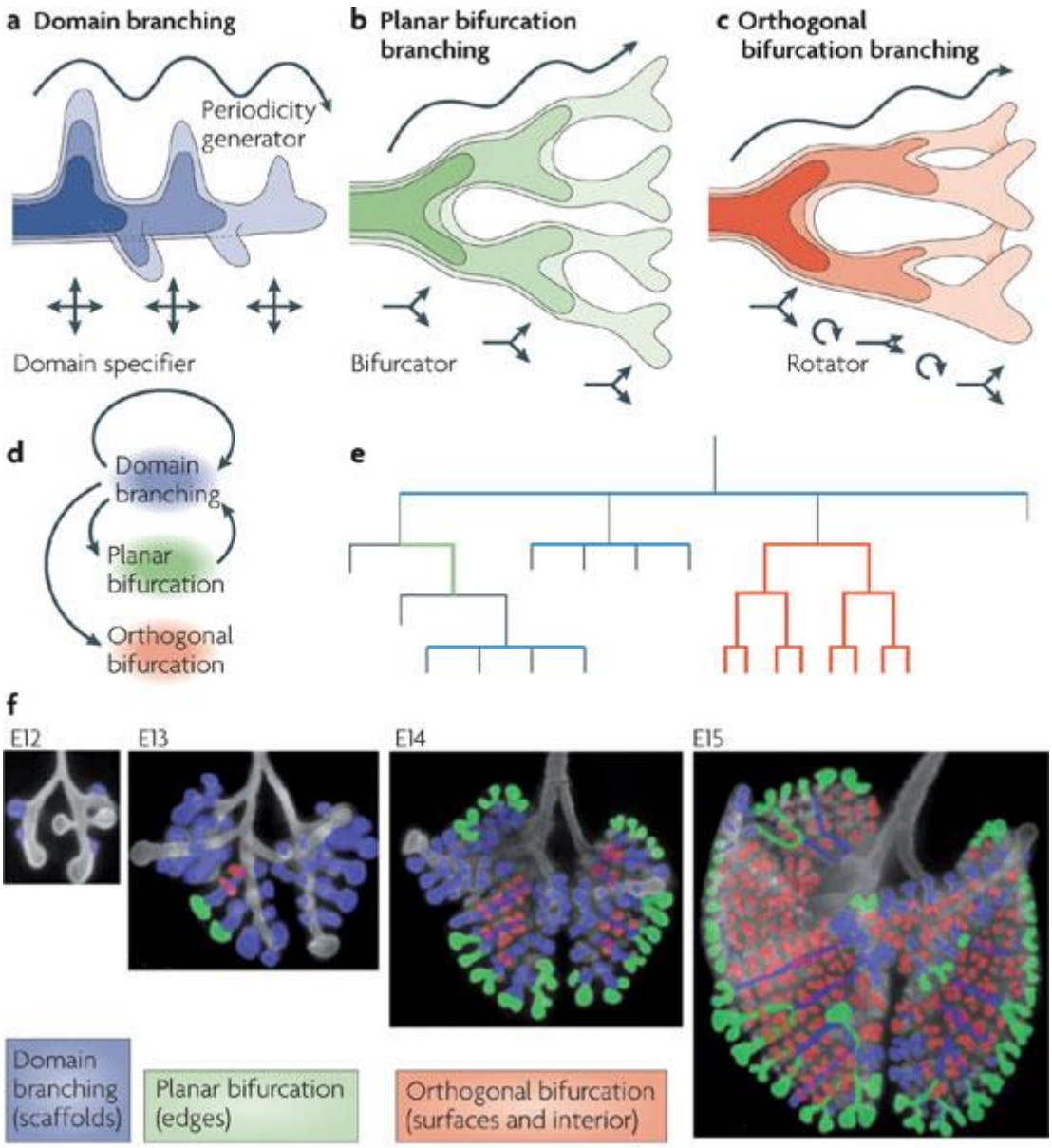

Fig 5.1. Branch mode selection in the lung. There are three mode of branching during lung branching morphogenesis.**(A)** Domain branching occurs when daughter branches sprout of perpendicular from the elongating parent branch. **(B)** Planar bifurcation is when the tip of the parent branch splits into two daughter branches. **(C)** Orthogonal branching occurs by the same method as planar bifurcation but rotates the plane of bifurcation by 90^{o} between bifurcations. **(D)** The different branching methods are used throughout the entire pseudoglandular stage, however the order in which the different branching modes are used appears to be restricted to four routes. **(E)** A hypothetical example of a branch lineage tree. **(F)** Whole mount images of lungs at e12,13,14 and 15 with the different branching modes overlaid. Domain branching is used to set up the initial scaffolds, planar bifurcation pushes the branching to the edges of the pulmonary lobes while orthogonal bifurcation fills in the gaps. Figure adapted from Affolter et al., 2009

5.1.1.2 Alveolarization

From e16.5-e17.5 (canalicular stage) and e17.5-P0 (saccular stage) the terminal branches narrow and form epithelial sacs or primary septae, tightly associated with the developing vasculature, that will go on to form alveoli postnatally. Epithelial cells lining the primary septae differentiate into thin squamous alveolar epithelial type 1 cells and secretory alveolar epithelial cell type 2 cells. During the final stages alveolisation sacs are subdivided by a second septae derived from migrating myofibroblast progenitors and endothelial cells. The migration of these cells and subsequent depositation of matrix proteins is regulated by a combination of PDGF, TGFβ and ephrin B2 signalling (Boström et al., 1996; Lindahl et al., 1997; Neptune et al., 2003; Wilkinson et al., 2008).

5.1.2 Molecular control of branching morphogenesis

The molecular pathways controlling branching morphogenesis in the lung have been heavily studied and show a complex signalling interaction between the branching lung endoderm and surrounding mesenchyme (fig 5.2). This is a mechanism that is mirrored in the development of other branched structures such as the kidney, mammary gland and pancreas.

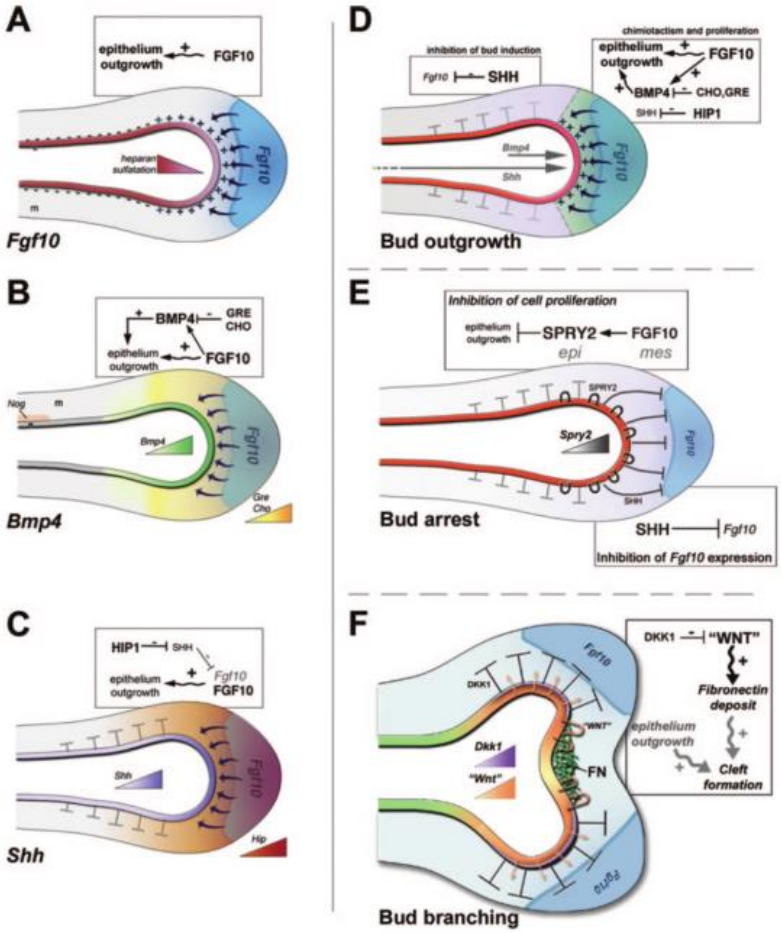

Fig 5.2: Schematic of main molecular pathways involved in lung epithelial growth and branching. (A) *Fgf10* is expressed in the mesenchyme surround the epithelial tip in a decreasing gradient where it binds to FGFR2 in the epithelium to induce bud outgrowth. Heparan sulfaction is required to mediate the inductive influence of FGF10. **(B)** BMP4 expression in the distal lung epithelium has been shown to both simulate and inhibit bud outgrowth by potentially different mechanisms. In this model FGF10 simulates BMP4 expression which stimulates epithelial growth. Gremlin (GRE) and Chordin (CHO) modulate BMP4 protein in the mesenchyme. **(C)** SHH released from the tip inhibits FGF10 expression in the surrounding mesenchyme thereby restricting bud outgrowth. At the branch tip HIP1 inhibits SHH to allow FGF10 induction of bud extension. **(D)** Illustrates the interactions between FGF10, SHH and BMP4 to instruct bud outgrowth. **(E)** FGF10 induces SPRY2 as a method for inducing epithelial bud arrest. High SHH activity proximal to the tip prevents lateral branching by inhibiting FGF10 expression in the mesenchyme. **(F)** Depicts a potential method of bifurcation in which WNT dependent deposition of Fibronection (FN) between the branch tips leads to cleft formation. Recent data has suggested a similar role for smooth muscle accumulation in the same region. Figure adapted from Warburton et al., 2005.

5.1.2.1 FGF10 promotes lung epithelial outgrowth and is attenuated by SHH and SPRY2

FGF10 is dynamically expressed in the mesenchyme surrounding actively elongating and branching regions (Bellusci et al., 1997). Knock-out mice experiments have shown FGF10 to be essential for branching morphogenesis where it binds to FGFR2 in the distal lung epithelium to induce proliferation (De Moerlooze et al., 2000; Min et al., 1998; Sekine et al., 1999). This has been confirmed in *in vitro* experiments showing epithelium in cultured whole lungs and mesenchyme free epithelial cultures are attracted to FGF10 soaked beads (Bellusci et al., 1997; Park et al., 1998). Evidence has shown Heparan sulfates expressed in the distal lung epithelium aids the binding of FGF10 to FGFR2 and is therefore required for bud outgrowth (Izvolsk et al., 2003a; Izvolsky et al., 2003b). FGF10 activity is attenuated by Shh, which is highly expressed in the distal lung epithelium. Genetic overexpression and knock-out studies of Shh both result in a loss of branching (Bellusci et al., 1997; Pepicelli et al.,1998). While addition of Shh to lung culture reduces FGF10 signalling therefore suggesting a dynamic inhibitory role for Shh in regulating epithelial proliferation driven by mesenchymal FGF10 expression (Lebeche et al., 1999). Hip1 (Hedgehog binding protein) is also expressed in Shh responding cells in the mesenchyme where it acts to attenuate Shh activity by a negative feedback loop giving greater control over the localisation of FGF10 expression and bud formation (Chuang et al., 2003). Based on the interactions between FGF10, Shh and its receptor Patched, a reaction diffusion Turin based model has been constructed which robustly predicts bud formation. The model predicted a preference for domain branching over bifurcation in rapidly elongating branches as seen in lung development, and showed concordance when levels of Shh or FGF10 were manipulated to mirror mutant phenotypes, therefore supporting the key role for the Shh-FGF10 signalling network between the distal epithelium and surrounding mesenchyme in bud outgrowth (Menshykau et al., 2012). The Spry genes also negatively regulate FGF10 signalling. Sprouty, the Drosophila homolog, was originally identified to inhibit branching by directly blocking FGF signalling to adjacent tracheal epithelial cells (Hacohen et al.,

1998). In the mouse Spry2 has been shown to be expressed in the distal lung epithelium in response to FGF10 signalling which it then negatively regulates (Mailleux et al., 2001; Tefft et al., 1999). Genetic overexpression of Sprouty4 has also been shown to cause pulmonary hypoplasia suggesting an overlapping role for Sprouty genes in regulating FGF10 signalling and preventing ectopic branch formation (Perl et al., 2003).

5.1.2.2 BMP4 has contradictory roles in branching morphogenesis

BMP signalling has also been implicated in branching morphogenesis with epithelial specific deletion of BMP4 and BMPR1a resulting in severe branching defects, increased apoptosis and cell extrusion and decreased proliferation (Eblaghie et al., 2006). Addition of BMP4 to lung cultures results in an increase in proliferation and branching (Bragg et al., 2001). Paradoxically however it has been shown that FGF10 stimulates BMP4 expression in the distal epithelium and that BMP4 has an inhibitory affect on the budding, chemotaxsis and proliferative influences of FGF10 in mesenchyme free cultures (Lebeche et al., 1999; Weaver et al., 2000). Considering these contradictory reporter it is possible autocine BMP4 signalling within the distal epithelium inhibits proliferation, as shown in the mesenchyme free cultures. But paracrine BMP4 signalling to the mesenchyme enhances epithelial proliferation by an as yet unidentified mechanism.

5.1.2.3 Wnt signalling has multiple roles in branching morphogenesis

The role of Wnt signalling in branching is also not clear. Using the TOPGAL reporter mouse line in which expression of *LacZ* is dependent on the β-catenin-Lef1/Tcf complex. Wnt signalling has been identified throughout the lung epithelium but diminishes in the distal lung epithelium from e14.5-15.5 (De Langhe et al., 2005; Dean et al., 2005; Okubo & Hogan, 2004). Disruption of Wnt signalling either by

addition of Dkk (Wnt inhibitor) to lung cultures or targeted deletion of β-catenin results in disruption of airway development and a proximalisation of the distal epithelium (Mucenski et al., 2003; Shu et al., 2005). Loss of Wnt signalling in these studies directly decreases BMP/FGF and N-myc expression suggesting Wnt signalling is acting up stream of the branching program. There is however a discrepancy in the role of individual Wnt ligands during branching. A genetic knock-down of Wnt5a results in an overexpansion of the distal airway due to increased proliferation of the mesenchymal and epithelial compartments (C. Li et al., 2005; C. Li et al., 2002). An increase in expression of FGF10, BMP4, Shh and Ptch was reported supporting the idea of Wnt signalling acting up stream of the branching program. In contrast, however, conditional Wnt7a knock-out mice have hypoplastic lungs with normal differentiation and branching (Rajagopal et al., 2008; Shu et al., 2002). These discrepancies may be down ligand specific functions or different roles of canonical verses non-canonical Wnt signalling in branching.

5.1.2.4 TGFB signalling mediates interactions between the lung epithelium and mesenchyme

TGFβ signalling has been implicated in mesenchymal organisation during lung branching morphogenesis. TGFβ1 has been shown to co-localise with collagen I and III, fibronectin and glycosaminoglycans around stalk and cleft regions during branching morphogenesis (Heine et al.,1990). Addition of TGFβ1 to lung cultures inhibits branching in a dose dependent manner, suggesting a potential role for TGFβ1 in directing changes to the extracellular matrix. However a tissue specific knock-out mouse showed no branching defects, although it is thought maternal contribution may have masked the phenotype (Letterio et al., 1994; Serra et al., 1994; Zhou et al., 1996). Genetic aberration of TGFβ3 resulted in underdeveloped proximalised lungs and a hyperplastic mesenchyme, suggesting TGFβ signalling functions to mediate the interaction between the mesenchyme and epithelium during branching (Kaartinen et al., 1995).

5.1.2.5 A role for classical axon guidance cues in branching morphogenesis

Recent evidence has implicated a role for classical axon guidance molecules; Slits, Robos, Netrin and Semaphorin in preventing ectopic branching in other branched organs such as the mammary gland. Slit2/Robo1 signalling has been shown to prevent branching in the mammary gland via inhibiting canonical Wnt signalling, while Slit2;Netrin1 knock out mice show disordered branching (Macias et al., 2011; Strickland et al., 2005) In the lung expression of Netrin 1 and 4 is isolated to the non-branching regions of the lung epithelium and addition of Netrin 4 to endodermal cultures has been shown to impair branching (Y. Liu et al., 2004). Addition of Sema3A to lung cultures has also been shown to reduce branch number in a dose dependent manner, suggested a conserved inhibitory role for axon guidance cues in branching morphogenesis (Ito et al., 2000).

5.1.3 Cell shape changes and orientated cell division induce initial bud formation

Although extensive work has begun to shed light on the complex signalling network controlling branching in the lung very little is known about how this translates to morphological changes at a cellular level. Unlike studies in the kidney it has proven difficult to visualise the dynamic processes involved at the cellular level predominantly down to the three dimensional nature of the lung complicating imaging and image analysis. With the recent advances in 3D imaging technologies such as SPIM (Single Plane Illumination Microscopy) and more complex image analysis software this gap should be reduced. Classically it was believed branching was initiated by localised proliferation of the lung epithelium driven by FGF10 signalling. However it has been shown in culture that bud formation occurs before localised proliferation and genes expressed during initial bud formation are associated with cell migration, cell rearrangement, inflammatory response and lipid

metabolism but not proliferation (Lü et al., 2005; Nogawa et al., 1998). Similarity in the branching epithelium of the drosophila trachea cells stop dividing to undergo apical constriction which induces epithelial tube invagination. Orientated cell divisions then drive outgrowth of the new branch (Affolter & Caussinus, 2008). Wnt signalling has been shown to be important in orientating cell division during kidney tubular development (Karner et al., 2009; Yu et al., 2009), and disruption of Wnt signalling in the lung has caused branching defects due to cell shape changes and an increase in the apical domain (Kadzik et al., 2014). This points to a model in which deformations in the epithelial tube are induced by cellular shape changes before orientated cell division drives extension and elongation.

5.1.4 Physical interactions between the lung epithelium and mesenchyme

Increasing evidence shows that in addition to the molecular interaction between the epithelium and surrounding mesenchyme, the physical interactions also need to be considered. Blanc et al showed that spatial and temporal variation in branching is related to modifications in mesenchymal growth, suggesting a mechanism in which the choice to branch or not to branch is solely determined molecularly (Blanc et al., 2012). In addition, a recent paper has shown differentiated smooth muscle forms in cleft regions prior to bifurcation and continues to spread and increase in density around the bifurcating bud. Pharmacological interference of the smooth muscle development resulted in failure to branch normally suggesting a physical role for smooth muscle in the branching process (Kim et al., 2015). Interestingly it has been previously reported that addition of the Wnt inhibitor Dkk to cultured lungs decreased the expression of α-smooth muscle actin and resulted in failed cleft formation (De Langhe et al., 2005).

5.1.5 Fucci2a expression separates branching and non-branching regions by proliferative state

During the early stages of branching morphogenesis (e10.5-14.5) there are two distinct populations of epithial cells. $Sox9^{+}$ epithial progenitors localised in the distal actively branching regions and proximal $Sox2^{+}$ bronchial progenitors (Gontan et al., 2008; Rockich et al., 2013). Prior to e14.5, differentiation of the bronchia epithelia into ciliated, secretory and neuroendocrine cells has not begun which means to two populations of cells can be thought of progenitor niches, one with the ability to branch and one without (Post et al., 2000; Rawlins et al.,2007; Tichelaar et al., 1999). Interestingly, inspection of cultured e11.5 Fucci2a expressing lungs again identified these two distinct regions, proliferative branching distal tips labelled with mVenus-hGem(1/110) and less proliferative non-branching proximal stems labelled with mCherry-hCdt1(30/120) (see fig 2.8 and sup video 3). Based on this differential abundance of the Fucci probes I have conducted a comparative analysis of the lung epithelium separated by proliferative state rather than on gene expression pattern. Using an endoderm specific cre (Sox17-2A-iCre) I have specifically labelled the lung epithelium and a subset of migratory mesenchymal cells (Engert et al., 2009). Using time-lapse and fixed imaging I have identified a transition zone 100-150μm from the tip at which point cells are left behind from the elongating tip and start to drop out of the cell cycle, coinciding with the onset of Sox2 expression. Using FACS I have separated the proliferating and non-proliferating epithelial populations corresponding to the branching and non-branching regions and carried out a comparative gene expression analysis by RNA sequencing. As the separation of the two regions is by proliferative state and not expression of a particular differentiation marker, the Fucci2a system provides an unbiased and finer method for separating these two regions than previous studies where the tracheal regions has been cut from lobe regions (Lin et al., 2002; Lü et al., 2004). In addition, unlike in previous analyses, comparative expression was restricted to the epithelium and will therefore give a better intrinsic molecular understanding of the difference between the branching and non-branching epithelium, with a focus on changes in epithelial cell adhesion and

polarity which is known to be important in regulating branching morphogenesis in other systems (Affolter & Caussinus, 2008; Karner et al., 2009; Yu et al., 2009).

5.2 Results

5.2.1 Lengthening of lung epithelial cell cycle coincides with epithelial cell stagnation and the onset of differentiation during branching morphogenesis

Between e10.5 to e16.5 the mouse embryonic lung epithelium undergoes successive rounds of branching and elongation to form the characteristic branched structure of the bronchial tree (Metzger et al., 2008). High proliferation has been identified at the distal tips of elongating branches and is thought to be the driving force behind branch elongation but not bud initiation (Nogawa et al., 1998). In agreement with this I have shown a high proportion of epithelial cells in the branching tip to be in S/G2/M stages of the cell cycle and a higher proportion of cells in G1 in more proximal regions from live images of *ex vivo* cultures of e11.5 *R26Fucci2aR*$^{+/Tg}$*;CAG::Cre*$^{+/Tg}$ lungs (fig 2.8). In addition the distal and proximal regions of the branching lung epithelium are differentially distinct by gene expression and their lineage potential. Distal epithelial cells are Sox9^{+} and are multipotent up until e13.5, able to produce all lineages found in the adult lung (Rawlins et al., 2009). Proximal epithelial cells are Sox2^{+} and contribute to bronchial but not alveoli lineages (Gontan et al., 2008). To date most research has focused on patterning at the branch level and little is known about the individual cellular movements within the lung epithelium. To quantitatively investigate the changes in proliferation between the distal and proximal regions of the lung epithelium in relation to the onset of differentiation and cell movements, I have conducted time-lapse imaging of cultured e11.5 lungs from *R26Fucci2a*$^{R+/Tg}$*/Sox17-2A-iCr*$^{e+/Tg}$ embryos (fig 5.3). The *Sox17-2A-iCre* line contains a knock-in of 2A-iCre to the 5' end of exon 5 in the Sox17 gene resulting in Cre expression in the developing endoderm, vasculature endothelial cells and cells of the hematopoietic system (Engert et al., 2009). The Cre therefore labels the epithelium of all endoderm derived organs including the lung. A temporary inducible

version of this Cre line (*Sox17-Cre-ERT2*) produces Cre activity specifically in the definitive endoderm when tamoxifen is administered at e7 without activity in the vascular lineages (Engert et al., 2013). This mouse would be more suitable for this study as it would avoid unwanted labelling of vasculature and blood cells. However, initial experiments using this line showed very low efficiency of the Cre to induce Fucci2a expression after tamoxifen administration. This resulted in insufficient cells being labelled for live imaging and poor RNA yields from FACS sorted lungs intended for RNA sequencing.

Live imaging of cultured e11.5 lungs confirmed the segregation of highly-proliferative cells labelled exclusively with mVenus-hGem(1/110) in the actively branching regions and less-proliferative cells labelled predominantly with mCherry-hCdt1(30/120) in the non-branching proximal lung epithelium (fig 5.3B and sup video 16). Considering it has been shown it takes around 120 minutes for mCherry-hCdt1(30/120) to accumulate after mitosis in Fucci2a 3T3 cells (fig 2.2B), the absence of mCherry-hCdt1(30/120) labelled cells within the branching regions suggests cells are progressing through G1 in less than 120 minutes. To investigate the differences in epithelial cell behaviour between these two regions time-lapse imaging was performed on e11.5 lungs cultured in matrigel on a lummox membrane (see 6.4.1 in methods) and cells at different locations along an epithelial branch tracked. In an elongating epithelial branch, there was no relationship in the velocity of epithelial cell movement in relation to distance from the tip (Fig 5.4A). However, the accumulated distance of tracks decreased significantly the greater the distance from the tip, indicating that movement was less directed in these areas (fig 5.4B). In support of this, cells in the more distal regions showed more persistent movement (euclidean/accumulated distance)(fig 5.4C). This suggests cells within the proximal lung epithelium are jostling on the spot while epithelial cells within the tip have directed movement and are travelling forward with the elongating branch. To investigate this further I calculated the Hurst exponent (H value) for each individual track and examined the distribution of these values between proximal and distal regions (Fig. 5.4D). The Hurst exponent is a measure of long term memory in a

system. A high *H* value is indicative of repeated similar movements whereas a low H value is caused by variability in movements over a time series. The *H* value has a range between 0-1 with 0.5 being random movement. The distribution higher *H* values for cells within the distal lung confirms these cells are moving more consistently compared to those in more proximal regions.

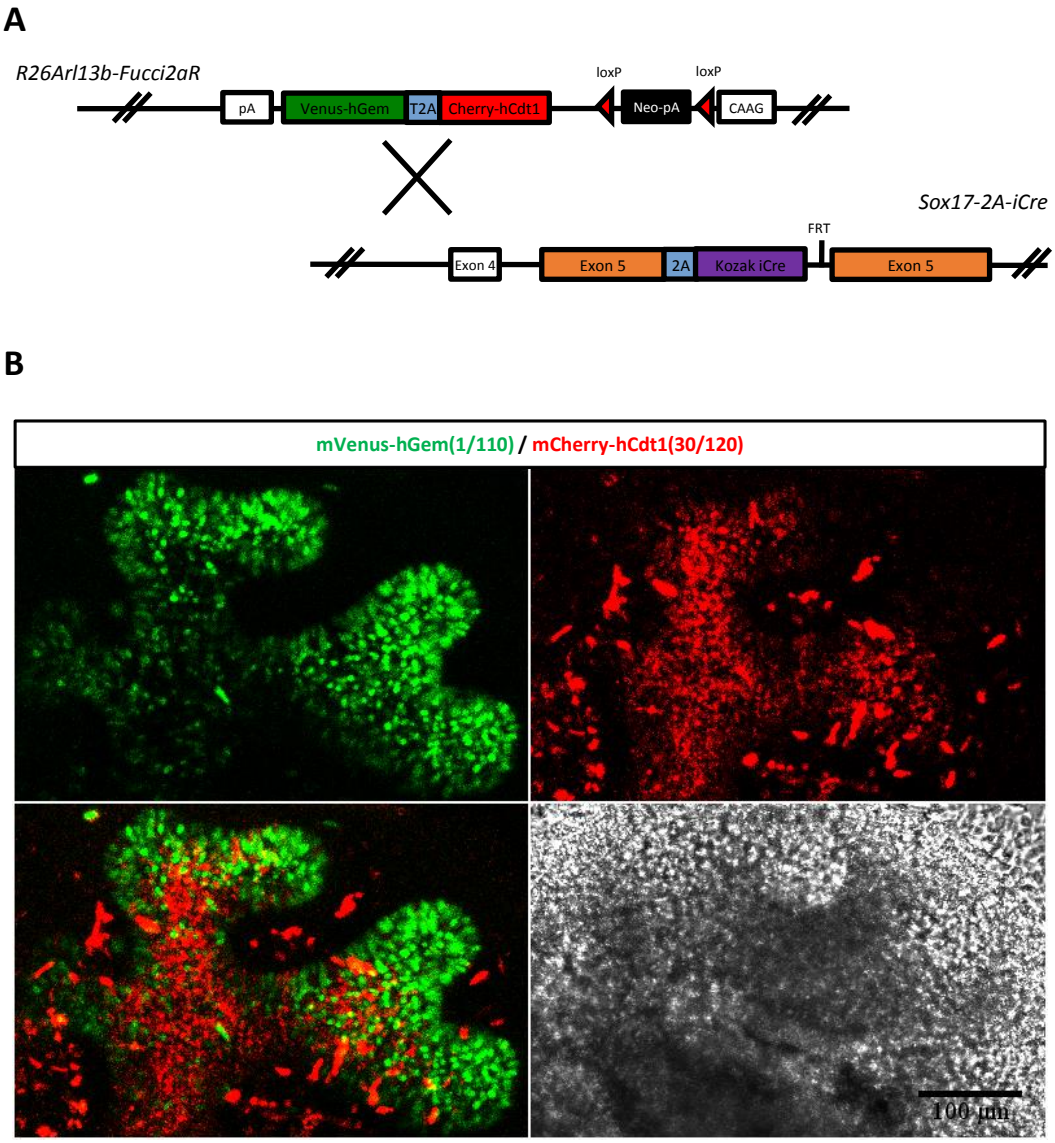

Fig 5.3: Branching and non-branching regions of the developing lung epithelium can be separated by proliferative state. (A) Lung epithelial specific expression of Fucci2a was achieved by crossing with endoderm specific cre *Sox17-2A-iCre* (Engert et al, 2009). A sub population of migratory cells was also labelled in the mesenchyme. (**B)** Z projection taken from a time-lapse of a cultured e11.5 lung dissected from a *R26Fucci2a*$^{+/Tg}$*/Sox17-2A-iCre*$^{+/Tg}$ embryo. Activity branching regions at the distal tip of the lung epithelium are highly proliferative as shown by the high proportion of cells in S/G2/M labelled in green. This is distinct from cells in more proximal non-branching regions of the lung epithelium which are predominantly in G1 labelled in red.

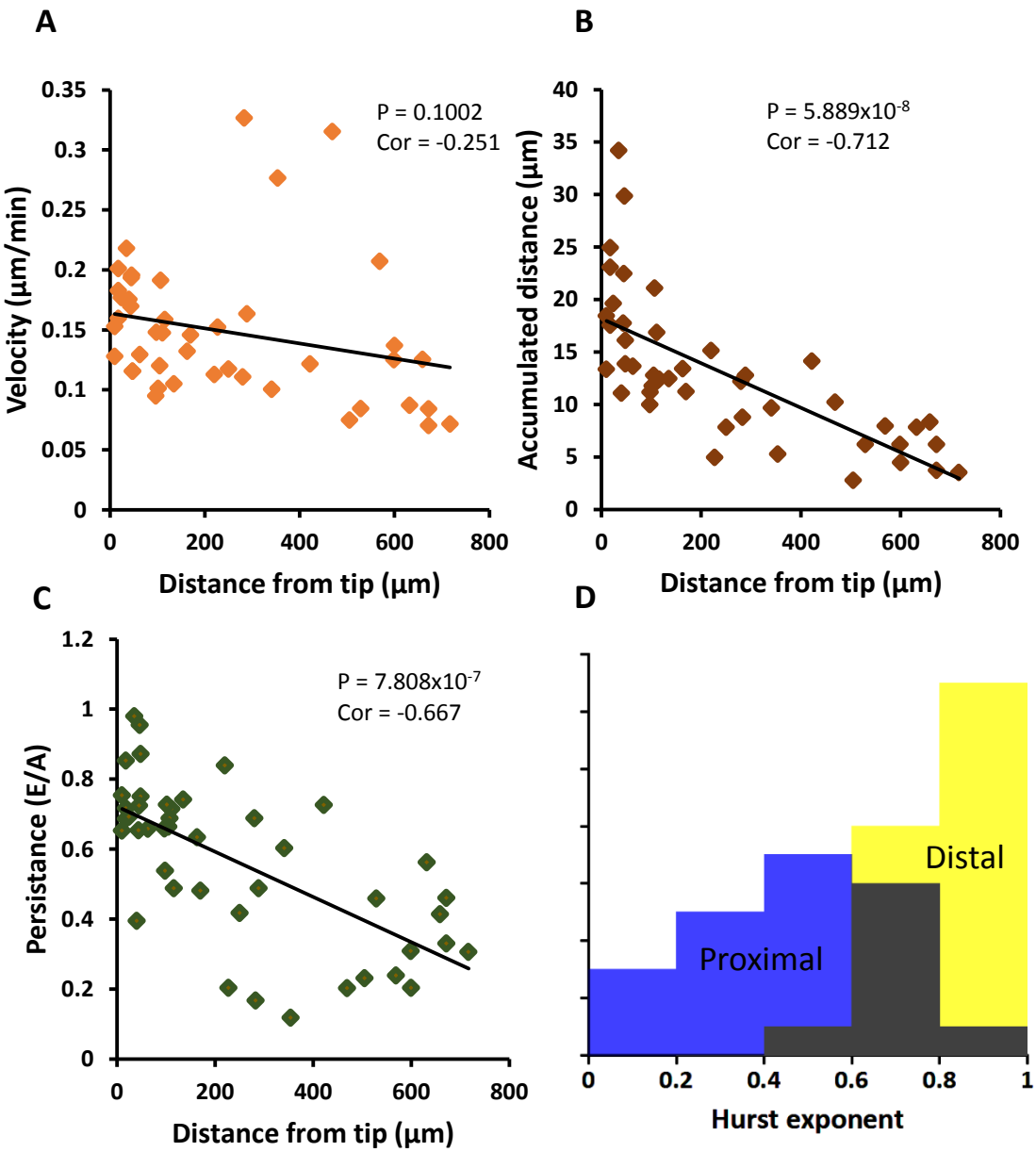

Fig 5.4: Distal lung epithelial cells migrate with the elongating branch. **(A)** Scatter plot showing no significant change in velocity of tracked epithelial cells along the proximal distal axis of the lung epithelium. **(B and C)** Scatter plots showing a significant decease in the accumulated distance and persistence of tracked epithelial cells the more proximal their starting location. **(D)** A histogram of showing the disruption of Hurst exponents of tracked cells in the distal (<150µm from the tip) and proximal regions of the lung epithelium. n = 44 cells. Correlation tested in A-C by Spearman's rank correlation.

Interestingly there is a transition in cell behavior at approximately 100-150μm from the tip after which epithelial cells stop following the extending branch. This corresponds with the position at which epithelial cells start to slow their cell cycle (fig 5.5). The decrease in the proportion of cells in S/G2/M was quantified in cryosections of e13.5 *R26Fucci2a*$^{+/-}$*/Sox17-2A-iCre*$^{+/-}$ embryos stained with anti-GFP and anti-RFP to enhance the Fucci2a signal, which was diminished during fixation, and anti-Sox2 to distinguish proximal from distal regions (fig 5.6A). As seen in time-lapse imaging, the proportion of cells in S/G2/M rapidly starts to decease after 100μm from the tip from 0.5 to 0.39 (fig 5.6B). This coincided with expression of Sox2, a proximal bronchial progenitor marker. The proportion of cells in S/G2/M was also reduced from 0.51 to 0.41 from Sox2^{-} cells to Sox2^{+} cells suggesting a relationship between Sox2 expression and cell cycle length (fig 5.6C).

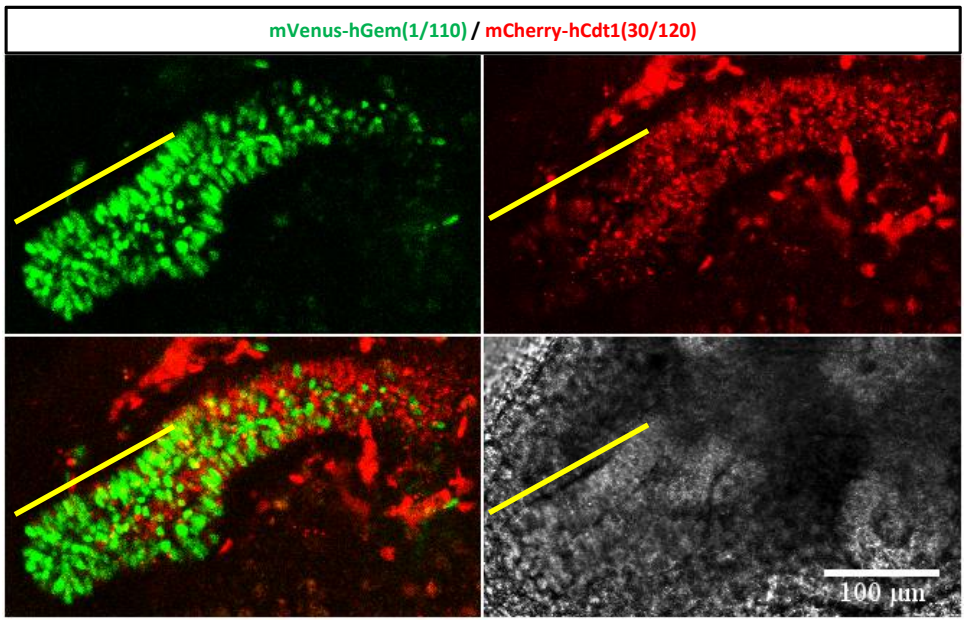

Fig 5.5: Proliferation reduces 100-150µm from the lung epithelial tip. Still taken from a time-lapse of a cultured embryonic lung dissected from an e11.5 *R26Fucci2a*$^{+/-}$*/Sox17-2A-iCre*$^{+/-}$ embryo. The proportion of mCherry-Cdt1(30/120) labelled cells increases after 150µm from the tip highlighted by the yellow bar. Corresponding with the place in which epithelial cells become stationary. n = 44 cells in A and B. Significant correlation in B confirmed by Spearman's rank correlation.

A

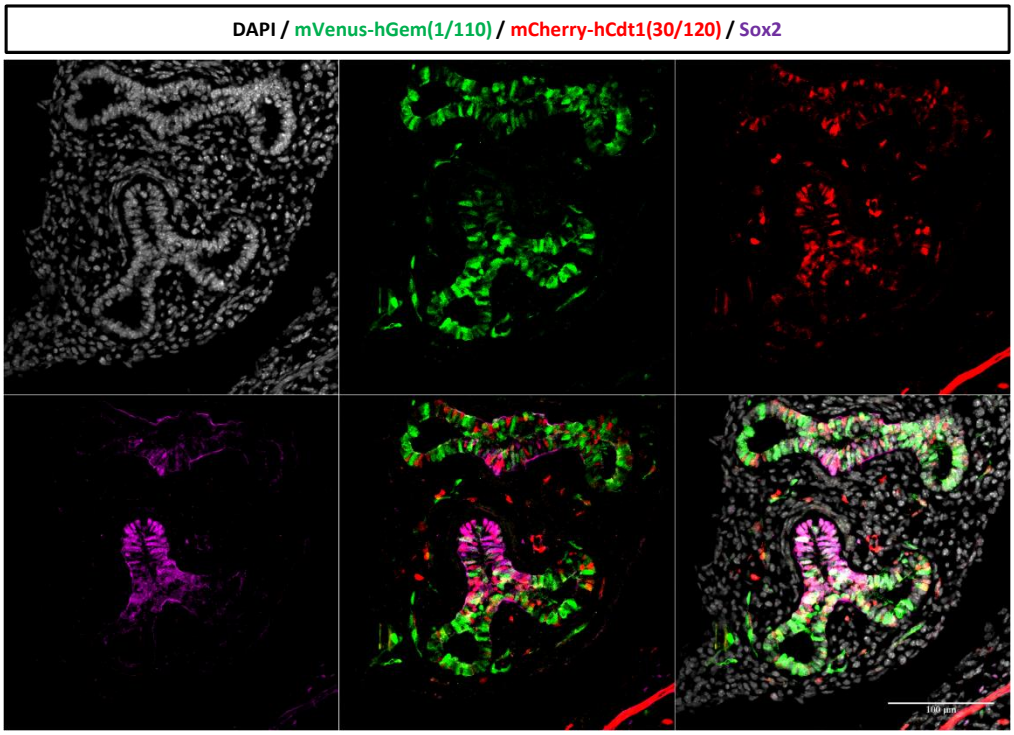

B

Distance from tip (µm)	Proportion of cells in S/G2/M	Proportion of $Sox2^{+}$ cells
1 – 50	0.54	0
51 – 100	0.50	0.29
101 - 150	0.39	0.69

C

	Proportion of cells in S/G2/M
$Sox2^{-}$	0.51
$Sox2^{+}$	0.41

Fig 5.6: Sox2 expression coincides with an increase in the proportion of cells in G1. (A) 10 µm cryosection of an e13.5 embryonic lung dissected from a *R26Fucci2a*$^{+/Tg}$*/Sox17-2A-iCre*$^{+/Tg}$ embryo stained with anti-GFP and anti-RFP to enhance the endogenous Fucci2a signal and anti-Sox2. **(B)** The proportion of cells in S/G2/M decrease after 100µm from the tip which corresponds with an increase in the proportion of Sox2 positive cells. **(C)** Sox2 positive cells have a lower proportion of cells in S/G2/M phases of the cell cycle and suggests they are less proliferative. n = 362 cells

It has been shown that the maintenance of the tip progenitor niche is dependent on Wnt/β-catenin signaling. Conditional knock-out of β-catenin in the lung epithelium or ectopic expression of Wnt inhibitor Dkk1 results in a disruption of branching morphogenesis and proximalisation of the epithelium (Mucenski et al., 2003; Shu et al., 2005; Volckaert et al., 2013). Conversely, ectopic expression of an N-terminally truncated form of β-catenin throughout the lung epithelium using the SFTPC-Cre line resulted in normal alveolar development but significant dilation of the bronchial airways and disorganization of the bronchial epithelium (Hashimoto et al., 2012). Fgf10 expression in the distal mesenchyme has been shown to induce β-catenin signaling in the distal epithelium, leading to the proposal of a model in which tip epithelial cells' identity is determined by their proximity to the source of FGF10 in the distal mesenchyme (Volckaert et al., 2013). Taken together with my findings, this suggest a model in which highly proliferative cells within the tip exposed to FGF10 can either maintain their position within the niche, by migrating in concert with the elongating branch, or are left behind and subsequently slow their cell cycle and become a multipotent $Sox2^{+}$ bronchial progenitor due to a loss of exposure to FGF10 in the distal mesenchyme.

5.2.2 FACS sorting proliferative and non-proliferative populations for RNA sequencing

In order to compare the expression profiles of epithelial cells in branching and non-branching regions by RNA sequencing, I took advantage of the Fucci2a system to separate epithelial cells by cell cycle stage using FACS and, therefore, enrich for proximal and distal cells. I have previously shown by live imaging that the branching lung epithelium is constituted almost exclusively by mVenus-hGem(1/110) positive cells and the non-branching regions contain a majority of mCherry-hCdt1(30/120) positive cells (fig 5.3B). This therefore provides a uniquely unbiased method for separating these two regions by cell cycle status rather than physical separation or by gene expression (Lin et al., 2004; Lü et al., 2004). In addition, unlike previous studies, my analysis is limited to genes expressed in the epithelium and excludes

those in the mesenchyme. This makes the comparison more sensitive to intrinsic differentially expressed genes in the branching versus non-branching regions of the epithelium.

The lung epithelium from e13.5 *R26Fucci2a*$^{+/-}$*/Sox17-2A-iCre*$^{+/-}$ embryos was separated into branching and non-branching regions by FACS based on differential expression of the Fucci probes. Because the Sox17-2A-iCre also labelled a sub-population of migratory cells, identified during time-lapse imaging, anti-EpCAM conjugated to APC was used to enrich for lung epithelial cells before being sorted into mVenus-hGem(1/110) positive and mCherry-hCdt(30/120) positive populations and RNA isolated (fig 5.7A). EpCAM negative Fucci2a positive cells were also collected for characterisation. Enrichment of epithelial tip progenitors in the proliferating mVenus-hGem(1/110) population was confirmed by expression of Sox9 and low expression of Sox2 using RT-PCR. No Sox9 but high Sox2 expression was detected in the mCherry-hCdt1(30/120) positive population confirming this population of cells contained only the more proximal bronchial epithelial progenitors (fig 5.8A and B). No expression of endothelial marker PECAM or smooth muscle marker MHC2 was detected in either population (fig 5.8C and D). However a low level expression of CSFR1 was detected in all samples suggesting a small degree of macrophage contamination (fig 5.8E). Considering this small amount of contamination was present in all samples the decision was made that it should not affect the RNA sequencing differential expression analysis.

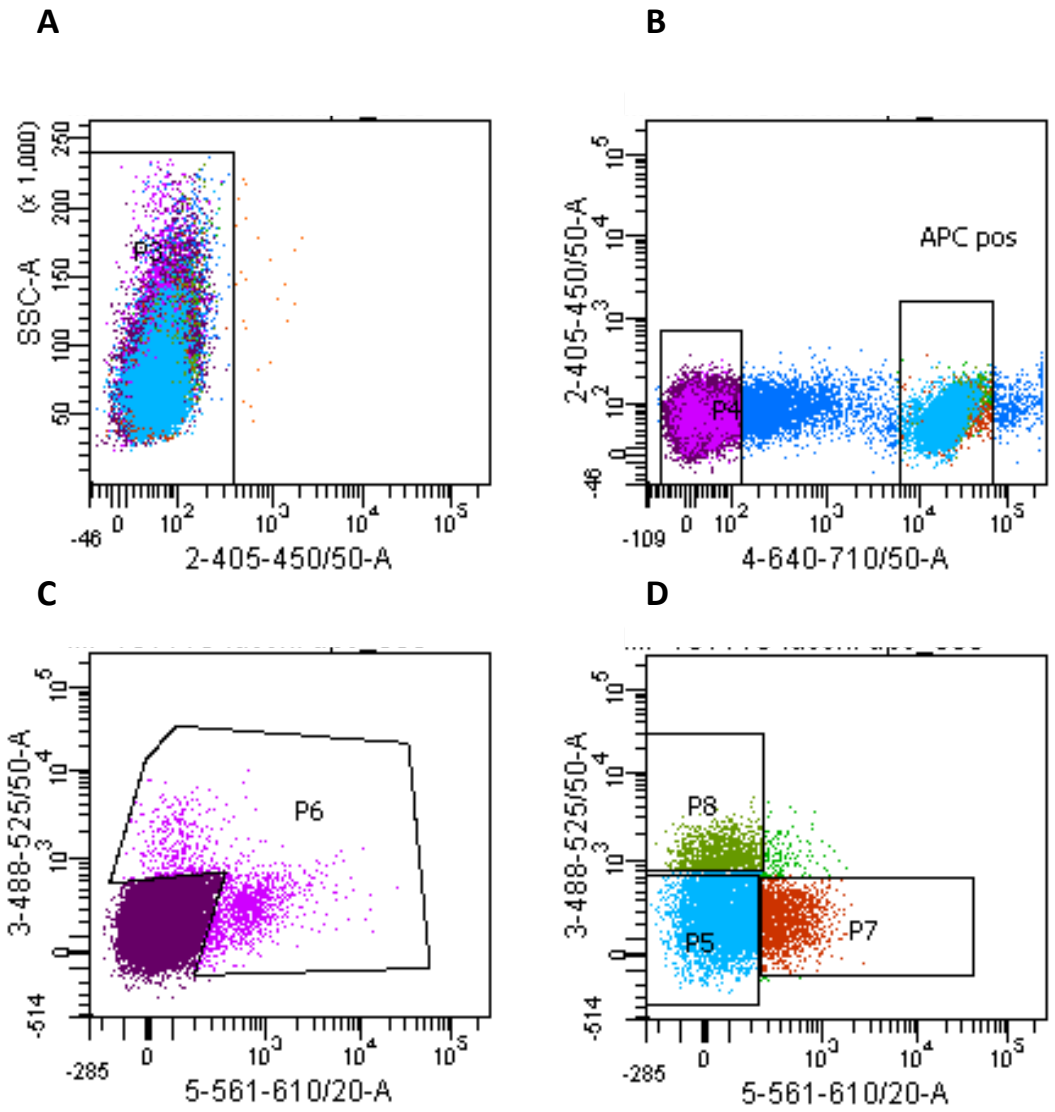

Fig 5.7: FACS sorting proliferative and non-proliferative regions of the lung epithelium. E13.5 lungs dissected from *R26Fucci2a*$^{+/Tg}$*/Sox17-2A-iCre*$^{+/Tg}$ embryos were dissociated into a single cell suspension by serial trypsinisation and stained with epithelial marker EpCAM-APC. **(A)** Live cells were first identified by their side scatter. **(B)** APC positive epithelial cells were separated from APC negative mesenchyme. **(C)** mVenus-hGem and mCherry-hCdt1 positive, APC negative cells were collected and RNA isolated to identify migratory non-epithelial cells labelled with the *Sox17-2A-iCre*. **(D)** APC positive lung epithelial cells were separated into mVenus-hGem and mCherry-hCdt1 populations and RNA isolated.

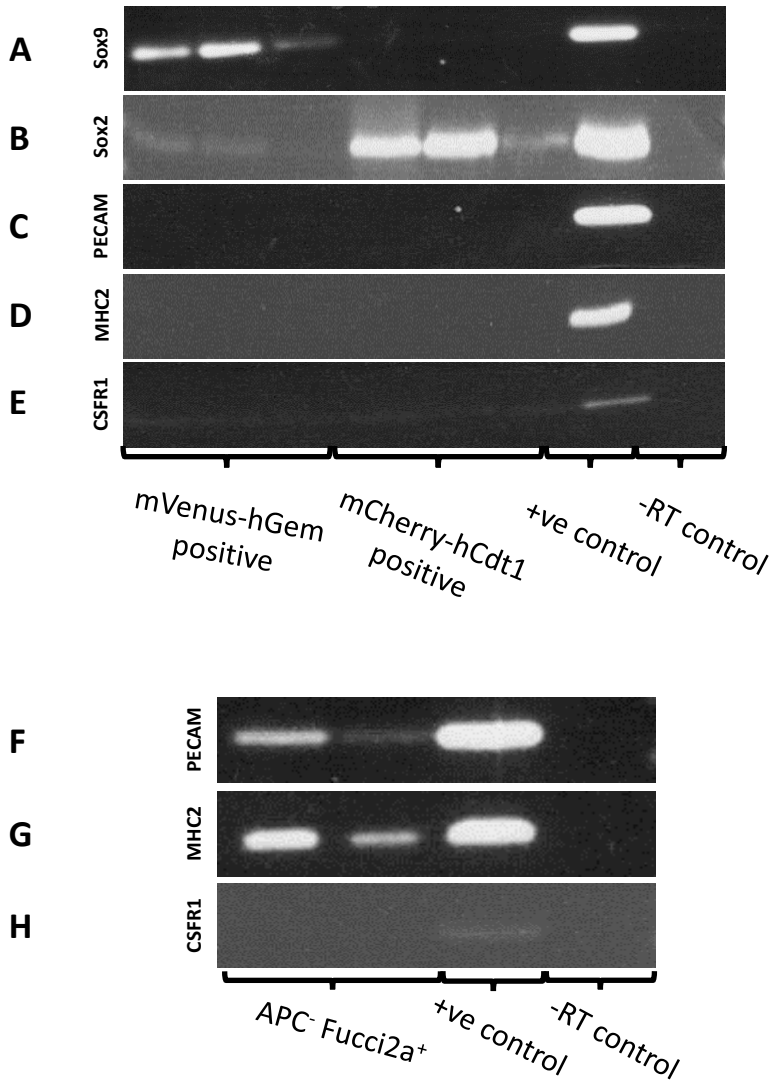

Fig 5.8: FACS sorted proliferative and non-proliferative cells separates epithelial tip progenitors from bronchial progenitors. **(A-H)** RT-PCR of differentiation markers on RNA isolated from FACS sorted lungs. **(A)** Expression of Sox9, a marker of the epithelial tip progenitor pool, is detected in mVenus-hGem(1/110) positive cells but not mCherry-hCdt1(30/120) positive cells. **(B)** Expression of Sox2, a marker of bronchial progenitor cells, was detected predominantly in mCherry-hCdt1(30/120) positive population. **(C and D)** No expression of endothelium marker PECAM or smooth muscle marker MHCII was detected. **(E)** Low levels of macrophage marker CSFR1 was detected in all samples. **(F-H)** Migratory EPCAM-APC negative cells show high expression of smooth muscle cell marker MHC2 and endothelium maker PECAM but no expression of macrophage marker CSFR1. Positive control RNA was isolated from whole e14.5 lungs kindly provided by Girish Mali.

The sub-population of migratory EpCAM negative Fucci positive cells were identified as a mixed population of endothelial and smooth muscle precursors by expression of PECAM, MHC2 and no expression of macrophage specific gene CSFR1 using RT-PCR (fig 5.8F-H). To further characterise the non-epithelial cells labelled with the *Sox17-2A-iCre*. *Sox17-2a-iCre* mice were crossed with an EYFP reporter stain (*R26R-EYFP)* to enable determination of cell morphology (Srinivas et al., 2001). Time-lapse imaging of *ex-vivo* e11.5 lung cultures was then repeated. The lung epithelium was clearly distinguishable from three morphologically distinct populations of mesenchymal cells (fig 5.9A and sup video 17). One population of cells was migratory and have long dynamic dendritic processes that interact with one another to form a meshwork of cells within the mesenchyme and surrounding the branching epithelium (fig 5.9B). A second non-migratory population have formed circular wraps around the more proximal non-branching regions reminiscent of patterns of differentiating smooth muscle cells seen in previous reports (fig 5.9C) (Kim et al., 2015). The third population was rounded in morphology and either lie stationary throughout the mesenchyme or become highly mobile and appear to interact with each other and the lung epithelium (fig 5.9D). These rounded cells are more active when in close proximity to actively branching regions suggesting their activity is stimulated by the distal epithelium and could potentially be macrophages. The vascular system in the lung develops by a combination of angiogenesis (the formation of new vessels from pre-existing vessels) from the pulmonary arteries and vasculogenesis (the development of new vessels from the differentiation of endothelial precurors) to construct the smaller vascular networks (Morrisey & Hogan, 2010). Using the endothelial specific cre flk, endothelial precursors have been identified throughout the lung mesenchyme from e10.5 (Oréal & Santos, 2000). Considering the meshwork structures formed by the migratory dendritic cells it would be tempting to conclude these cells are endothelial progenitors undergoing vasculogenesis. However it is impossible to confirm the identity of the migratory dendritic and rounded cells. Their identity would need to be confirmed by counter staining with endothelial and smooth muscle antibodies using immunohistochemical

techniques. The visualisation of these mesenchymal cells with the branching epithelium using the *Sox17-2a-iCre* would be a useful tool for studying the interaction of these mesenchymal lineages with the branching epithelium in future studies.

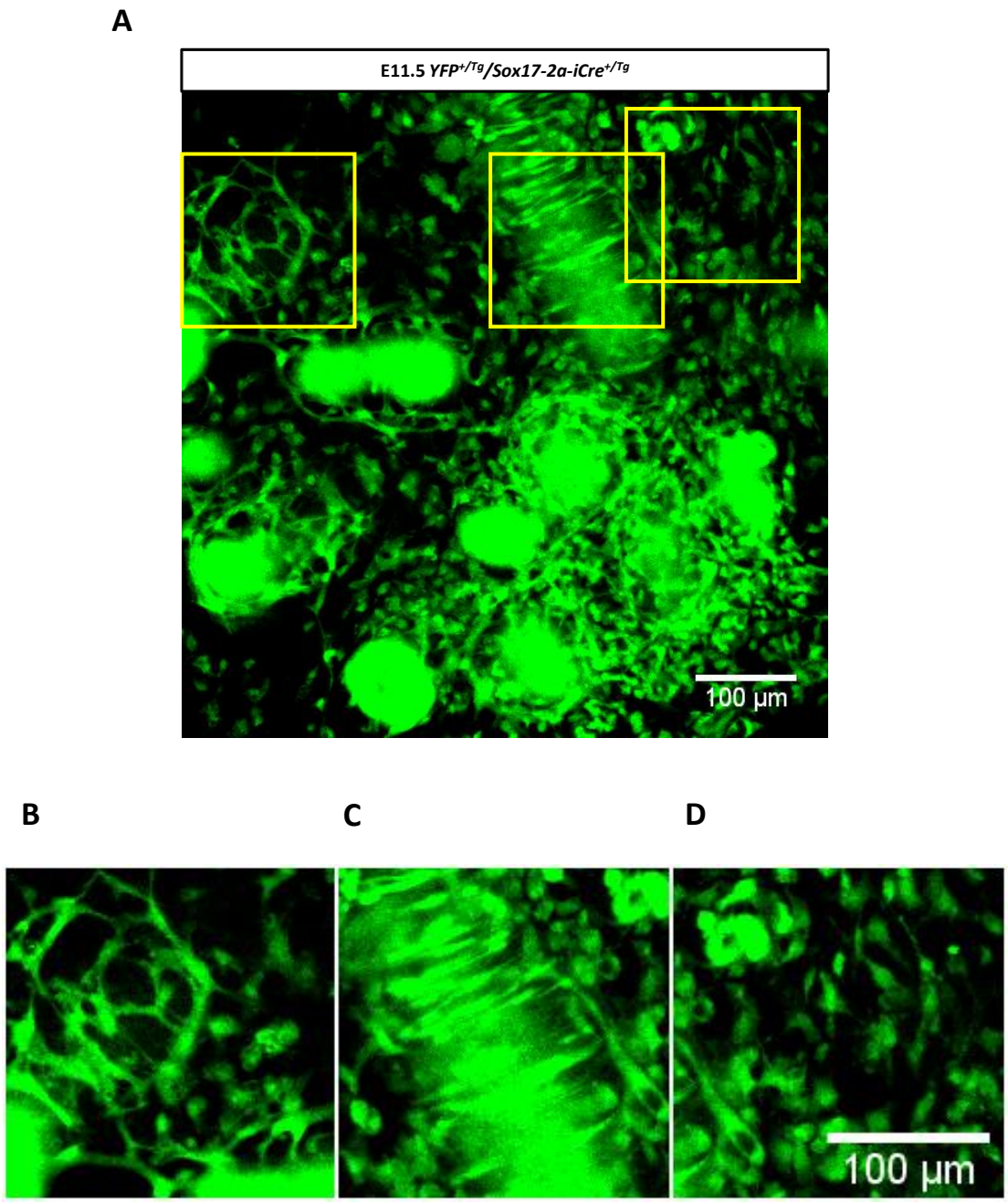

Fig 5.9: Sox17 labelled cells with cytoplasmic YFP identifies three distinct populations of non-epithelial labelled cells. **(A)** A still taken from a time-lapse of an e11.5 cultured *R26R-EYFP$^{+/Tg}$/Sox17-2a-iCre$^{+/Tg}$* lung. Epithelial labelled cells are clearly distinct from 3 non-epithelial populations labelled with the Sox17-2a-iCre. **(B-D)** Magnifications of the three non-epithelial labelled populations. **(B)** Migratory cells with long dendritic process can be seen forming connexions with one another particularly around actively branching regions. **(C)** Long stationary dendritic cells form circular bands around the more proximal non-branching regions. **(D)** Small rounded cells can be seen in the mesenchyme between branches that either remain stationary or become highly mobile and appear to interact with each other and the epithelium.

5.2.3 Global RNA sequencing analysis confirms segregation by cell cycle stage and contamination with non-epithelial cells

RNA sequencing of the FACS-sorted population was used to investigate the gene expression differences between the proliferating and non-proliferating regions of the branching lung epithelium. Three biological replicates from the same litter consisting of two combined lungs were sequenced on two lanes by paired end sequencing using the HiSeq 2500 System from Illumina producing on average 40M reads per biological replicate (Edinburgh Genomics). Clustering of the biological replicates was confirmed by a multidimensional scaling (MDS) plot and dendrogram which showed the greatest amount of variability was between the mVenus-hGem(1/110) and mCherry-hCdt1(30/120) sorted populations (fig 5.10A-B). Some variability was also present in one of the mCherry-hCdt1(30/120) biological replicates along the second axis of variability. Having confirmed that the biological replicates cluster consistently, they were combined for both mCherry-hCdt(30/120) and mVenus-hGem(1/110) positive populations and differential expression calculated using Cuffdiff (Trapnell et al., 2010) summarised in a volcano plot (fig 5.10C). A total of 912 genes were significantly differentially expressed with 731 genes expressed more highly in the mCherry-hCdt1(30/120) population and 181 in the mVenus-hGem(1/110) positive population, using a significance threshold of $p < 0.05$ and a Log2 fold change cut off of 1.5 for gene expression.

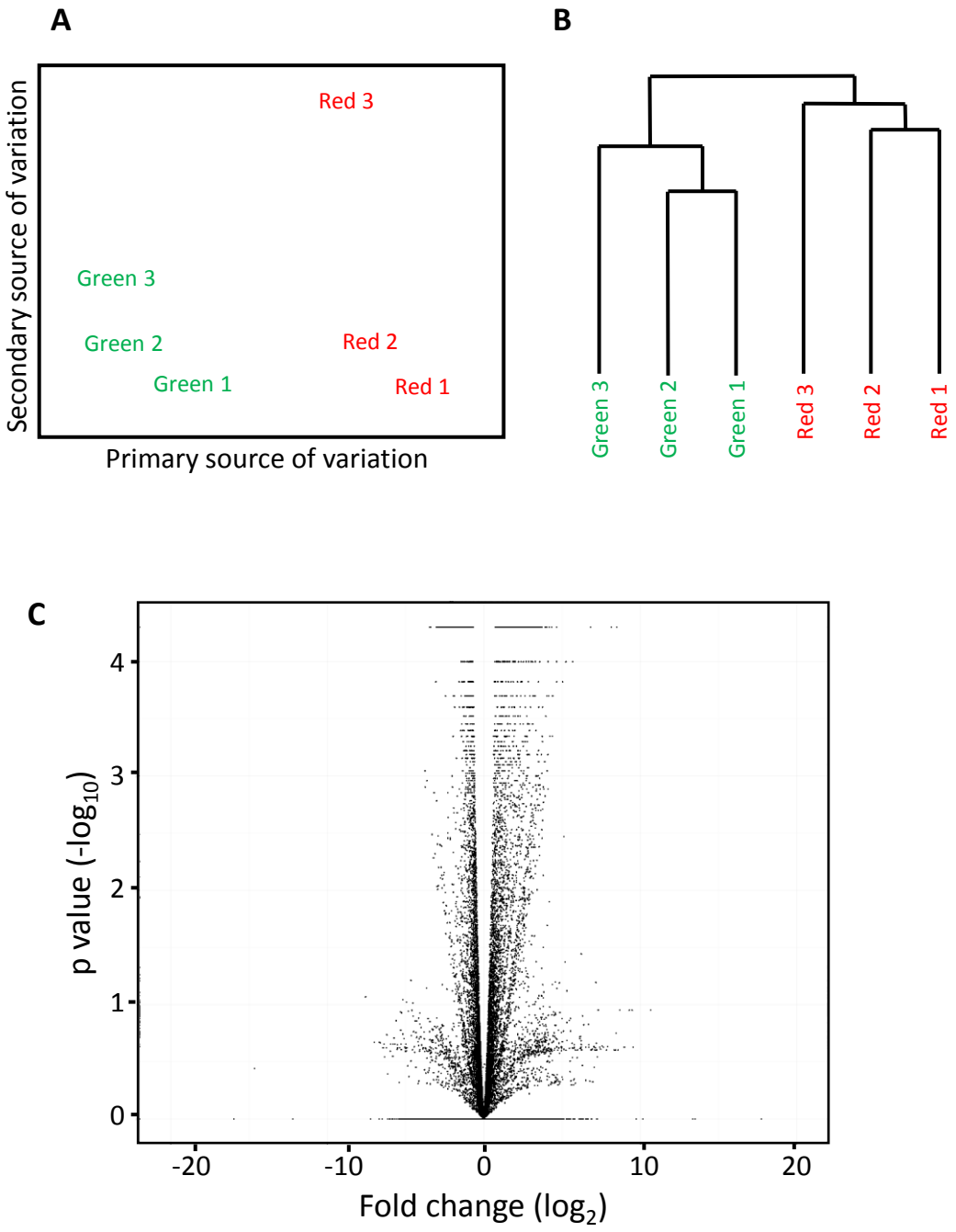

Fig 5.10: RNA sequencing differential expression. (A) Multidimensional scaling plot showing clustering of biological replicates with primary source of variation between FACS sorted populations. **(B)** Dendrogram showing clustering of biological replicates. **(C)** Volcano plot of gene expression comparing mVenus-hGem(1/110) population to mCherry-hCdt1(30/120) positive cells.

A global GO term analysis of genes more highly expressed in the mVenus-hGem(1/110) positive population showed an enrichment for genes involved in mitosis, chromosome segregation and nuclear division (table 5.1). In addition, the majority of the top 20 up regulated genes were involved in mitosis (table 5.4). This therefore confirms the successful separation of cells by cell cycle stage based on the abundance of mVenus-hGem(1/110) in S/G2/M and mCherry-hCdt1(30/120) in G1. An enrichment for cell cycle related genes in the distal lung was also reported in similar studies when the distal regions were physically separated from proximal regions (Lü et al., 2004). A global GO term analysis of genes more highly expressed in the mCherry-hCdt1(30/120) positive population showed an enrichment for genes involved in the immune and inflammatory response (table 5.2). A detailed look at the top 20 differentially expressed genes showed markers of red blood cells (Hba-x and Hbb-y), platelets (Gp1ba), vasculature (Hecw2) and immune cells (TremI2, Runx1t1, Itgb7, Hdc, Ppbp and Siglech) (table 5.5). This suggests a possible contamination of these samples with lung mesenchymal and blood cells. Vascular endothelial cells and cells of the hematopoietic system were identified as being labelled by the *Sox17-2A-iCre* due to the early expression of Sox17 in the visceral endoderm (an embryonic hematopoietic cell source (Medvinsky et al., 2011)) and late (after e9.5) expression vascular endothelial cells (Engert et al., 2009). A potential cause of this contamination could be the promiscuous binding of anti-EpCam-APC to non-epithelial lineages and the RT-PCR checks for contamination were not sensitive enough. The reason for the increased abundance in the mCherry-hCdt1(30/120) FACS sorted population could be explained by the majority of these blood and endothelial cells being in G1/G0. Due to this contamination a global analysis of differential gene expression is impossible and this caveat must be considering when evaluating any differentially expressed genes.

Table 5.1: Top 10 GO terms for mVenus-hGem(1/110) positive cells

GO term	Description	P-value	FDR q-value
GO:0022402	cell cycle process	2.02E-33	1.77E-29
GO:0000280	nuclear division	1.80E-32	7.90E-29
GO:1903047	mitotic cell cycle process	6.05E-32	1.77E-28
GO:0007067	mitotic nuclear division	6.76E-32	1.48E-28
GO:0048285	organelle fission	3.65E-31	6.42E-28
GO:0051301	cell division	7.52E-31	1.10E-27
GO:0007049	cell cycle	1.17E-27	1.47E-24
GO:0007059	chromosome segregation	9.05E-23	9.94E-20
GO:0010564	regulation of cell cycle	3.13E-17	3.05E-14
GO:0006996	organelle organization	5.20E-16	4.57E-13

Table 5.2: Top 10 GO terms for mCherry-hCdt1(30/120) positive cells

GO term	Description	P-value	FDR q-value
GO:0032101	regulation of response to external stimulus	4.30E-07	2.59E-03
GO:0006955	immune response	4.91E-07	1.48E-03
GO:0002376	immune system process	2.08E-06	4.17E-03
GO:0006954	inflammatory response	1.05E-05	1.58E-02
GO:0032103	positive regulation of response to external stimulus	1.45E-05	1.74E-02
GO:0031349	positive regulation of defense response	7.58E-05	7.61E-02
GO:0031347	regulation of defense response	8.36E-05	7.20E-02
GO:0048584	positive regulation of response to stimulus	1.14E-04	8.57E-02
GO:0050727	regulation of inflammatory response	1.84E-04	1.23E-01
GO:0050729	positive regulation of inflammatory response	2.26E-04	1.36E-01

GO germ calculated using GOrilia online software from ranked data filtered by 0.05 significance.

5.2.4 FACS sorting based on cell cycle stage separates distal from proximal lung epithelial populations.

In order to confirm the separation of distal and proximal regions of the lung epithelium in the FACS sorted populations, the expression of 12 genes known to be differentially expressed along the lung epithelium were compared (table 5.3). All tested distally and proximally expressed genes were seen to be upregulated in the mVenus-hGem(1/110) and mCherry-hCdt1(30/120) populations as predicted. However apart from *Sox9* a log2 fold change of less than -1.5 was seen between the mVenus-hGem(1/110) and mCherry-hCdt1(30/120) sorted populations. A significant increase in transcription of proximal *Asc1* and *Foxa3* was seen in the mCherry-hCdt1(30/120) population. However non-significant fold changes below 1.5 were seen for the other two proximal markers tested (*Sox2* and *Foxj1*). This could be because I have chosen differentiation markers (with the exception of *Sox2*) of bronchial cells which have been reported to be expressed in bronchial progenitors around e14.5 and therefore are only just starting to be expressed at e13.5 (Post et al., 2000; Rawlins at al., 2007; Tichelaar et al., 1999). *Foxj1* is a ciliated cell marker, *Ascl1* a neuroendocrine marker and *Foxa3* are mucus producing cell markers. These markers were chosen, as there are no other proximal specific lung epithelial markers at this stage. It is also possible that the low levels of expression of these proximal markers in the mCherry-hCdt1(30/120) population is due to the high contamination of blood and smooth muscle cells which is titrating the number of reads in the RNA sequencing. However if this were to be the case I would expect to see greater differential expression of the distal epithelial markers. Taken together the overall correlation and enrichment of distal epithelial markers within the mVenus-hGem(1/110) population and proximal epithelial markers with the mCherry-hCdt1(30/120) population suggests I have to some extent segregated the distal branching regions from the proximal non-branching regions. However the small fold changes seen in all the tested genes between the two populations, in particular those seen in the highly specific distal marker *Sox9* (fold change of 1.7) and highly specific proximal marker *Sox2* (fold change of 1.2), suggests this enrichment is limited. The low levels of enrichment for proximal versus distal will reduce the sensitivity of this

data set to detect differentially expressed genes between these two regions, therefore limiting detection to those genes that are dramatically differentially expressed. The similarities in the data will also increase the chances of detecting differentially expressed genes caused by the high levels of contaminating blood, endothelial and smooth muscle precursors in the mCherry-hCdt1(30/120) population as this may cause a higher degree of variability than the small enrichment of proximal verses distal epithelium. It will therefore be extremely important to take this into account in interpreting any differentially expressed genes from this data set. In addition, extensive validation of any interesting gene would be required.

Table 5.3: Differential expression of known distal and proximal localised genes

Gene	Expression in mVenus-hGem	Expression in mCherry-hCdt1	log2(fold_change)	p_value	Reference	
Sox9	69.6397	21.379	-1.70372	0.00005	(Rockich et al., 2013)	Distally expressed genes
Id2	138.153	50.2741	-1.45838	0.00005	(Rawlins et al., 2009)	
Mycn	65.2658	30.805	-1.08316	0.00005	(Ma et al.,2014)	
Shh	88.6717	47.4956	-0.90068	0.00005	(Bellusci et al., 1997)	
Bmp4	95.0318	51.0482	-0.89655	0.0003	(Weaver et al., 2000)	
Irx2	230.556	149.034	-0.62947	0.0014	(Becker et al., 2001)	
Irx1	171.078	111.714	-0.61484	0.00055	(Becker et al., 2001)	
Foxp2	73.4504	49.4991	-0.56937	0.00575	(Shu et al., 2007)	
Sox2	5.46036	12.373	1.18012	0.012	(Gontan et al., 2008)	Proximally expressed genes
Foxj1	0.734119	1.69916	1.21073	0.22375	(Rawlins et al., 2007)	
Ascl1	3.63681	13.4066	1.8822	0.00005	(Li & Linnoila, 2012)	
Foxa3	1.13908	19.6176	4.10622	0.0013	(Chen et al., 2009)	

5.2.5 Examination of the top 20 differentially expressed genes in mVenus-hGem(1/110) FACS sorted population

Taking into account all the caveats oulined above I have examined the top 20 differentially expressed genes in both the mVenus-hGem(1/110) and mCherry-hCdt1(30/120) populations to evaluate any potentially interesting differentially expressed genes. Unsurprisingly the majority of genes with higher expression in the mVenus-hGem(1/110) population were associated with cell cycle progression, chromosome segregation and mitotic spindle formation. Increased expression of these genes has also been reported to be associated with cancer development (see table 5.4). This is likely due to the highly proliferative nature of cancer cells and is in line with a previous report showing a clustering of genes periodically expressed during G2/M in HeLa cells with genes highly expressed in tumors (Whitfield et al., 2002).

One notable non-cell cycle related gene differentially expressed higher in the mVenus-hGem(1/110) population is the axon guidance cue Slitrk4. Slitrk4 is a member of the Slitrk family of transmembrane proteins which are thought to modulate neural growth via interactions with Slit ligands via two conserved leucine-rich repeat domains (Aruga & Mikoshiba, 2003a). Expression in the adult mouse is highly restricted to the brain, however expression during development in the lung has not been characterised (Aruga & Mikoshiba, 2003a; Aruga et al., 2003b). Considering the recent evidence implicating a role for classical axon guidance cues Sema3A in the lung and Slit2/Robo1 signalling in the mammary gland, it would be interesting to investigate in the future the role of Slitrk4 in lung development by confirmation of its expression in the distal lung epithelium (Ito et al., 2000; Macias et al., 2011; Strickland et al., 2006). However it is worth noting that, even though there is a significant 3.019 fold change in expression, the relative level of expression in the mVenus-hGem(1/110) population is still very low (0.85). So the fold change could potentially be due to noise in the system, which has extenuated the differential expression due to the low level of expression.

Another potentially interesting gene overexpressed in mVenus-hGem(1/110) population is *Aspm*. ASPM has been shown to be important for symmetric divisions in neuroepithelial cells (Fish et al., 2006). RNAi knock down of *Aspm* was shown to increase the proportion of asymmetric division and alter the plane of division. Considering the proposed importance of orientated cell divisions during trachea branching in the drosophilia (Affolter & Caussinus, 2008), the reported defects in branching morphogenesis in the kidney associated with a change in the plane of mitosis in Wnt mutants (Karner et al., 2009; Yu et al., 2009) and the reported perpendicular orientation of mitosis in the distal lung epithelium (El-Hashash et al., 2011a;El-Hashash et al., 2011b), it would be interesting to see if Aspm has a similar role in controlling the orientation of cell divisions in the lung important for bud formation and outgrowth. It is possible however that the increased level of expression seen in the mVenus-hGem(1/110) population is solely due to these cells being in S/G2/M phases of the cell cycle and upregulating genes involved in spindle formation and therefore unrelated to proximal verses distal differences in plane of division. This could be tested by comparing the orientation of cell divisions in the distal and proximal lung and see how this is influenced by the knock down of Aspm in culture.

Table 5.5: Top 20 differentially expressed genes in mCherry-hCdt1(30/120) population:

Gene	Expression in red population	Expression in green population	log2(fold_change)	p_value	Function	References
Hba-x	1351.31	3.77838	8.48238	0.00005	Part of alpha-like embryonic chain in Hba complex.	https://www.ncbi.nlm.nih.gov/gene/15126
Hbb-y	1906.14	6.79091	8.13283	0.00005	Hemoglobin Y, beta-like embryonic chain.	https://www.ncbi.nlm.nih.gov/gene/15135
Itgb3	6.00974	0.053045	6.82395	0.00005	Integrins are membrane bound proteins involved in relaying signals from the ECM. In-vitro evidence of Itgb3 expression regulating human lung fibroblasts with ECM.	(Merna et al., 2015)
Hecw2	5.85215	0.114268	5.67847	0.0001	E3-ligase shown to strengthen endothelial cell junctions during angiogenesis.	(Choi et al., 2016)
Treml2	3.22545	0.085427	5.23867	0.0001	Triggering receptor, shown to promote T cell responses in myeloid cells.	(Hashiguchi et al., 2008)
Runx1t1	5.28097	0.152518	5.11375	0.0034	Transcriptional repressor. A common translocation with CBFT1 is a common cause of acute myelogenous leukemia.	(Schwieger et al., 2002)
Slit3	3.95663	0.121055	5.03054	0.00015	Reported axon repulsion effects and inhibition of proliferation/migration in lung carcinoma cell line.	(Marsick et al., 2012; Zhang et al., 2015)

Itgb7	10.5492	0.41923	4.65324	0.00015	Integrins are membrane bound proteins involved in relaying signals from the ECM. ITGB7 has been identified in leukocytes in the pregnant mouse uterus.	(Behrends et al., 2008)
Hdc	7.27149	0.290062	4.64782	0.0001	Encodes the enzyme histidine decarboxylase which catalyzes histamine production from histidine. Histamine is known to be important in lung inflammation and immune response.	(Carlos et al., 2009)
Mxra8	12.3025	0.491806	4.64472	0.00005	Matrix remodelling protein	https://www.ncbi.nlm.nih.gov/gene/74761
Gp1ba	4.68093	0.221873	4.39899	0.0002	Platelet surface membrane glycoprotein involved in platelet activation.	(Marco et al., 1991)
Etv1	4.82475	0.232982	4.37216	0.00045	Member of the ETS transcription factors. Chromosomal translocations associated with cancer development.	(Sementchenko & Watson, 2000)
Igf1	60.0826	2.97286	4.33702	0.00005	IGF1 deficient mice have disrupted development and alveologenesis	(Pais et al., 2013)
Tbx4	7.16862	0.38532	4.21757	0.00045	Reported to be expressed in the lung mesenchyme. Shown to induce epithelial branching via FGF10 expression.	(Cebra-Thomas et al., 2003; Chapman et al., 1996)
Ung	102.636	5.6548	4.18191	0.00005	Involved in DNA replication	(Nilsen et al., 2000)
Crybb1	23.6434	1.33048	4.15141	0.0002	Important in lens formation. Expression identified in swine lung.	(An & Liu, 2009; Slingsby & Clout, 1999)

Ascl1	19.6176	1.13908	4.10622	0.0013	Transcription factor which has been shown to label bronchial progenitor niche in the developing lung	(Li & Linnoila, 2012)
Ppbp	19.4573	1.13082	4.10487	0.0001	A chemokine for neutrophils.	https://www.ncbi.nlm.nih.gov/gene/5473
Siglech	2.49231	0.146128	4.09217	0.00065	Plasmacytoid dendritic cell marker	(Bjorck et al., 2011)
Grid2	6.66507	0.404143	4.04368	0.0009	Membrane protein known to be expressed on Purkinje cells and thought to be involved in synapse organisation.	https://www.ncbi.nlm.nih.gov/gene/2895

5.2.6 Examination of the top 20 differenetially expressed genes in the mCherry-hCdt1(30/120) FACS sorted population

Three genes, *Itgb3*, *Itgb7* and *Mxra8*, are significantly upregulated in the mCherry-hCdt1(30/120) population and all have reported or predicted functions in extra cellular matrix (ECM) remodelling (Behrends et al., 2008; Merna et al., 2015, https://www.ncbi.nlm.nih.gov/gene/74761). Recent studies have started to highlight the interactions between the branching epithelium in a lung, kidney, mammary and salivary glands as essential for branching morphogenesis (Kim & Nelson, 2012). In the lung a thin layer of ECM containing a mixture of collagen IV, laminins, glycoproteins and proteoglycans termed the basement membrane (BM) surrounds the epithelium and interacts with epithelium via integrin receptors. Addition of RGD-binding inhibitors to lung cultures, which inhibits integrin ligand binding, has been shown to inhibit branching (Roman et al., 1991). In addition, lung epithelial specific aberration of integrin β1 resulted in impaired branching morphogenesis attributed to impaired migration and adhesion seen in isolated cultured integrin β1 deficient cells (Plosa et al., 2014). Similarly, in the kidney aberration of integrin β1 resulted in branching defects in the uretic bud, characterised by a significant decrease in branch number (Zhang et al., 2009). In addition, isolated renal collecting duct cells exhibited migration and adhesion defects when cultured on an artificial ECM, characterised by a decrease in proliferation and impaired FGF and GDNF signal transduction, suggesting a role of epithelial/ECM communication in signal transduction in addition to mechanical support. Functional blocking of intergins α3, α6 and β1 have also been shown to partially inhibit ureteric bud branching in the rat kidney (Zent et al., 2001). Considering these known interactions of integrins with the ECM during the branching process, it would be interesting to investigate the roles if any of *Itgb3* and *Itgb7* and *Mxra8* in relaying signals between the ECM and proximal lung epithelium. However, it is worth noting that *Itgb3* is highly expressed in the vasculature and is important for the development of the vasculature via angiogenesis (Hayashi et al., 2008). In addition *Itgb7* is known to be expressed in migrating leukocytes where it is involved in mediating interactions between leukocytes and endothelium (Springer, 1994). Therefore it is possible the high level of expression in the mCherry-

hCdt1(30/120) population is caused by the contaminating white blood and endothelial cells.

Four other genes upregulated in the mCherry-hCdt1(30/120) positive population also require consideration; *Slit3, Igf1, AsclI and Tbx4*. *Slit3* expression represents an axon guidance cue which has been shown to repel the protrusion of cultured chick retinal ganglion cells (Marsick et al., 2012). SEMA3A, another classical axon guidance cue, has been shown in lung cultures to inhibit branching (Ito et al., 2000), and there are also reported inhibitory roles of SLIT1 and SLIT2 in mammary branching (Macias et al., 2011; Strickland et al., 2006). This suggests that classical axon guidance cues may have a conserved role in regulating epithelial branching morphogenesis. The higher level of expression of *Slit3* in the proximal regions might suggest that SLIT3 has a role in preventing bud formation. However *Silt3* has been reported to be expressed in endothelial cells during development and has been shown to promote endothelial cell proliferation and migration (Paul et al., 2013; Zhang et al., 2009). It is therefore possible the high levels of expression seen in the mCherry-hCdt1(30/120) population is due to contamination with endothelial cells and not proximal epithelial localised expression so RNA in-situ or immunohistochemsitry is required to verify the expression pattern.

Igf1 encodes the protein insulin-like growth factor 1 and is 4.34 log2 fold more expressed in the mCherry-hCdt1(30/120) population. *Igf1* expression has been shown to play an important role in lung branching morphogenesis (Pais et al., 2013). IGF1 deficient mice exhibit lung hypoplasia, thinning of bronchiolar smooth muscle, a disordered basement membrane and an enlarged microvasculature. It is currently believed that multipotent mesoderm progenitors residing in the lung mesenchyme are induced into different linages by a series of inductive signals from distal lung epithelium and surrounding mesothelium (Morrisey & Hogan, 2010). FGF9 released from the distal epithelium and mesothelium has been shown to be key to inducing proliferation of the surrounding mesenchyme and maintaining the multipotent niche, in part by induction of Shh signalling (A. C. White et al., 2006). FGF9 has also been shown to induce Wnt signalling, which was also found to be essential for the

proliferation and maintenance of the mesenchyme niche (Yin et al., 2008). *Igf1* expression has been detected in bovine isolated aortic endothelial cells and in the lung epithelium, smooth muscle and endothelial cells during human lung development (Dahlfors et al., 2000; Han et al., 2003). The disruption of IGF1 signalling in cultured human embryonic explants and rat lung cultures by immunotargetting with an anti-IGF-IR resulted in a marked loss of endothelial cells, an increase in mesenchymal apoptosis and disrupted lung morphology (R. N. N. Han et al., 2003). These studies, along with work published by Pais et al (2013), suggest a key role of IGF1 in lung mesenchymal development. The differential expression of *Igf1* in non-branching regions suggested by my RNA sequencing data may suggest a role for IGF1 in promoting correct mesenchymal differentiation and ECM organization after cells have left the multipotent niche surrounding the distal lung epithelium. However, differential expression of *Igf1* along the lung epithelium would need to be confirmed by immunohistochemical techniques or RNA in-situ to confirm that the higher level of expression is not due to contamination of mesenchymal derived cells in the mCherry-hCdt1(30/120) population.

Ascl1 also known as HASH1 also showed increased expression in the mCherry-hCdt1(30/120) positive population (log2 fold of 4.12). *Ascl1* is essential for the development of pulmonary neuroendocrine cells and *Ascl1* expressing cells have been shown to contribute to all cell types in the lung epithelium during development and response to injury by lineage tracing experiments (Yan Li & Linnoila, 2012). Interestingly the multipotent potential of *Ascl1* expressing cells is restricted to cells within the airways and not alveoli lineages after e11.5, which would be consistent with my RNA sequencing data showing expression in the more proximal regions which do not contribute to the alveoli.

Finally, *Tbx4* was also shown to have higher expression in mCherry-hCdt1(30/120) positive population (log2 fold change of 4.22). The expression of *Tbx4* has been shown to be important for inducing *Fgf10* expression, necessary for directing epithelial bud outgrowth (Cebra-Thomas et al., 2003). However *Tbx4* has been reported in two separate publications to be solely expressed in the mesenchyme of

the developing lung but not the lung epithelium (Cebra-Thomas et al., 2003; Chapman et al., 1996). If expression is isolated to the mesenchyme, as stated in these reports, it confirms the contamination of my RNA sequencing samples with mesenchyme derived cells and highlights the need to validate any predictions made from this data set.

Considering over representation of mesenchyme derived cells in the mCherry-hCdt1(30/120) population labelled with the *Sox17-2a-iCre,* in combination with the low levels of enrichment of proximal cells compared to the mVenus-hGem(1/110) population, further validation by in-situ hybridisation of any interesting differentially expressed genes would be required.

Table 5.4: Top 20 differentially expressed genes in mVenus-hGem(10/110) population:

Gene	Expression in green populaiton	Expression in red population	log2(fold_change)	p_value	Function	References
Diras2	3.1223	0.231251	3.75508	0.0009	Small Ras GTPase.	(Grünewald et al., 2016)
Depdc1a	4.75589	0.353959	3.74806	0.00125	Reported function in promoting cell cycle progression in malignant plasma cells.	(Kassambara et al., 2013)
Dct	2.59223	0.208289	3.63754	0.0011	Promotes neuroblast proliferation and important in melanin biosynthesis. No published role in the lung.	(Costin et al., 2005; Jiao et al., 2006)
Ccnb1	55.5333	5.05173	3.4585	0.00005	Cyclin B1 with CDK1 promotes cell cycle events during mitosis. Over expression is associated with human lung carcinomas.	(Nam & van Deursen, 2014)
Ube2c	1131.41	104.28	3.43959	0.00005	Ubiquitin enzyme involved in the destruction of mitotic cyclins and for cell cycle progression. Increased expression associated with lung cancer development.	(Perrotta et al., 2012)
Plk1	123.297	11.6411	3.40485	0.00005	Oncogene involved in sister chromatid segregation. Elevated expression reported in non-small-cell lung cancer	(Takai, Hamanaka, Yoshimatsu, & Miyakawa, 2005)
Pif1	7.30667	0.690429	3.40365	0.00005	DNA helicase important for DNA	(Gagou et al., 2014)

					replication and associated with tumour growth.	
Klhl29	1.90966	0.193022	3.30648	0.00325	Part of the family of KLKL genes known to be involved in ubquitination and some have been associated with cancer	(Dhanoa, Cogliati, Satish, Bruford, & Friedman, 2013)
Arhgef39	11.7671	1.26648	3.21585	0.0052	A tumour supressor shown to be down regulated in bladder cancer	(Perez et al., 2014)
Ankle1	3.91167	0.431697	3.1797	0.0014	Predominantly expressed in hematopoietic tissues in humans and is involved in DNA damage response.	(Brachner et al., 2012)
Kifc1	5.47479	0.633234	3.11199	0.0048	Essential for bipolar spindle formation. Increased expression has been associated with brain directed metastasis in lung cancers.	(Grinberg-Rashi et al., 2009; Kim & Song, 2013)
St8sia6	6.67875	0.798221	3.06472	0.00015	Involved in carbohydrate biosynthesis. Identified to be upregulated in lung dysplasia.	(Rohrbeck & Borlak, 2009)
Cenpl	60.8538	7.35481	3.04859	0.00005	Possible oncogene, involved in kinetochore function and mitotic progression.	(Kumar, Rajendran, Sethumadhavan, & Purohit, 2013)
Parpbp	28.4915	3.45874	3.04221	0.00005	Involved in the maintenance of genome stability by repressing homologous recombination. Independently associated with the development of lung adenocarcinoma metastasis.	(Choi et al., 2016)
Slitrk4	0.849967	0.104856	3.019	0.00165	Contains homology to the axonal guidance cue Slit. Thought to be	(Aruga & Mikoshiba, 2003)

					involved in regulating neuronal outgrowth.	
Fam64a	55.0034	6.8224	3.01117	0.00005	Identified as a maker of proliferation in tumour cell lines with increased abundance during the G2/M transition	(Archangelo et al., 2008)
Aspm	59.0924	7.48757	2.9804	0.00005	Involved in mitotic spindle orientiation during proliferation in neuroepithelial cells and highly expressed in proliferating tissues	(Fish, Kosodo, Enard, Pääbo, & Huttner, 2006; Kouprina et al., 2005)
Mis18bp1	49.4875	6.29012	2.97591	0.00005	Centromere associated protein, important for chromosome alignment and segregation	(Fujita et al., 2007)
Ppia	13.0639	1.67409	2.96414	0.00395	Also known as Cyclophilin A, and has a variety of different functions. siRNA knock down has been shown to reduced non-small cells lung cancer growth and metastasis	(Nigro, Pompilio, & Capogrossi, 2013; Qian et al., 2012)
Cep55	29.2344	3.79075	2.94711	0.00005	Essential in orchestrating cytokinesis and overexpressed in many cancers including lung.	(Jeffery, Sinha, Srihari, Kalimutho, & Khanna, 2016)

5.3 Discussion

In mouse lung development the presumptive lung is first identified by expression of *Nkx1-2* in the ventral wall of the foregut, which then extends and forms the primary lung bud around e9-9.5 (Harris-Johnson et al., 2009). The lung epithelial tube then undergoes extensive growth and stereotypical branching to form the bronchial tree until e16.5 (Metzger et al., 2008). Branching morphogenesis in the lung has been extensively studied eluding a complex signalling interaction between the distal lung epithelium and the surrounding mesenchyme involving FGF, BMP, WNT, TGFb and classical axon guidance cues among other molecular pathways (see 5.1.2). Localised proliferation in actively branching regions has been shown to be secondary to cellular shape changes and cell migration in initiating bud outgrowth, therefore suggesting a passive role for proliferation in the morphological changes seen in bud outgrowth (Lü et al., 2005; Nogawa et al., 1998). In agreement with these observations, in my cultures I see extensive proliferation within the whole distal regions but do not see a localised increase in proliferation prior to bud outgrowth. Until recently, most of the research on lung branching morphogenesis has focused on branching at the branch level. Little is known about the behaviour of individual cells within the branching epithelium. My aim was to characterise the behaviour of individual lung epithelial cells during branching using the Fucci system to observe cell cycle progression with cell movement and the onset of differentiation. I have used a combination of time-lapse imaging of *ex vivo* cultured embryonic lungs and immunohistochemial techniques to show lung epithelial cells in the distal, actively branching regions are highly proliferative and migrate with the extending branch. There is then a transition point at around 100-150μm from the tip at which point epithelial cells are left behind from the extending branch, slow down their cell cycle and start to express the proximal bronchial marker *Sox2*. This change in behaviour is likely due to a loss of inductive Wnt and FGF signals being released in the mesenchyme surrounding the tip which have been shown to be essential for maintaining the proliferative and pluripotent tip niche (Hashimoto et al., 2012; Mucenski et al., 2003; Shu et al., 2005; Volckaert et al., 2013).

The Fucci system has previously been used to separate hESC into different cell cycle stages for the determination of differentially expressed genes during different stages of the cell cycle (Singh et al., 2013). Using this method it was shown in addition to known cell cycle regulators, genes associated with pluripotentency and development are also expressed in a cell cycle dependent manner. Building on this techniques I have attempted to develop a method for comparing the expression profile of a highly proliferative domain of a tissue to a less proliferative domain based on the differential abundance of the Fucci probes. In this case the branching and non-branching regions of the lung epithelium using FACS. Previous attempts to conduct a differential expression analysis of the branching and non-branching regions of the lung have involved physical cutting of the lung into the tracheal region containing the most proximal branches from the rest of the lung (S. Lin & Shannon, 2002; Lü et al., 2004). The physical separation of tissues for this kind of analysis however has two limitations. First, there will be a degree of human error and variation in position of separation. Second, due to the highly branched and three-dimensional nature of the lung, it would is impossible to finely separate actively branching regions from non-branching regions and in both studies the comparison was limited to tracheal versus lobe regions (S. Lin & Shannon, 2002; Lü et al., 2004). Based on the highly differential abundance of the mCherry-hCdt1(30/120) labelled cells in the non-branching regions and mVenus-hGem(1/110) in the branching regions, I hypothesised I would be able to finely segregate these two populations with greater accuracy and finer detail than previous reports. Using the endoderm specific *Sox17-2A-iCre* in conjunction with an epithelial specific antibody (Ep-CAM-APC) I hoped to restrict the comparison to the cells within the lung epithelium in order to make the analysis more sensitive to differential expression of intrinsic pathways governing behavioural differences between cells in branching and non-branching regions which has not been heavily studied. However a global GO term analysis and inspection of differentially expressed genes in the FACS sorted populations showed only a minor enrichment for distal verses proximal expressed genes in mVenus-hGem(1/110) and mCherry-hCdt1(30/120) populations respectively. The global GO term analysis and the majority of highly expressed genes in the mVenus-hGem(1/110) population were

associated with proliferation and mitosis as expected. However the mCherry-hCdt1(30/120) population showed high expression for genes known to be upregulated in blood cells and the developing vasculature, suggesting an enrichment of these cell types in this population. An examination of the top 20 differentially expressed genes in the mCherry-hCdt1(30/120) population highlighted several possible genes which could be involved in branching morphogenesis and would warrant further investigation. However the differential expression of each one could equally be explained by the enrichment of non-epithelial cell types within this population. Considering this and the fact that I have not been able to convincingly show separation of the branching and non-branching regions using this method, it is difficult to know if the differentially expressed genes in this data set are due to cells originating in branching verses non-branching regions or due to the enrichment of non-epithial cells within the mCherry-hCdt1(30/120) population. Therefore the differential expression of any interesting gene would need to be validated by RNA in-situ hybridisation. Considering the implication of cell shape change in bud formation, in future work it would be interesting to investigate if any genes involved in cell adhesion, cytoskeletal rearrangement or polarity are differentially expressed in the branching regions on the lung epithelium.

5.3.1 The potential cause of mesenchymal cell enrichment in the mCherry-hCdt1(30/120) population and low distal-proximal enrichment

Based on time-lapse imaging cultured e11.5 *R26Fucci2aR*$^{+/Tg}$*/Sox17-2A-iCre*$^{+/Tg}$ lungs there appeared to be significant enrichment of mVenus-hGem(1/110) positive cells in distal actively branching regions and only mCherry-hCdt(20/130) positive cells in the proximal non-branching regions . RNA sequencing analysis of these two populations, however, showed only a small enrichment for distal and proximal markers within these two populations. It is possible that the regulation of my chosen genes is at the protein level rather than the level of transcription so would not be detected by RNA sequencing. However apart from *Sox9*, *Foxp2* and *Foxa3* all other genes tested were shown to be differentially expressed by in situ hybridisation (see

table 5.3). One possible explanation of this is that mCherry-hCdt1(30/120) labelled cells were present in the distal branching regions but were not detected during live imaging. This could be due to the low sensitivity of the confocal microscope used and the high level of autofluoresence detected between the 695/50 emission range. It is also possible that contaminating mesenchymal cells in both FACS sorted population is masking differential expression from epithelial cell originating of distal verses proximal regions. The expression of *Sox9* and *Sox2* (known makers of the distal and proximal epithelium) was checked by rtPCR in the FACS sorted samples before RNA sequencing and showed significantly higher expression of *Sox2* in the mCherry-hCdt1(30/120) population and *Sox9* in the mVenus-hGem(1/110) population, which was not replicated in my RNA sequencing data. It is possible that this disparity is caused by inaccuracies in pipetting while setting up the rtPCRs. If this method for separating two populations based on the expression of the Fucci probes was to be repeated it would be important to ensure by multiple methods that sufficient separation had been achieved before sequencing.

Sox17 has been reported to be expressed during mouse development in haematopoietic stem cells, vascular endothelial cells, extra embryonic endoderm and the definitive endoderm (Kanai-Azuma et al., 2002; I. Kim et al., 2007; Matsui et al., 2006). In accordance with these observations the *Sox17-2A-iCre* and *Sox17-CreERT*^{2} lines have been shown to label cells derived from all these linages (Engert et al., 2013, 2009). In order to remove these non-epithelial lineages when using the *Sox17-2A-iCre* to FACS sort epithelial cells for RNA sequencing I used the epithial specific antibody Ep-CAM-APC. Ep-CAM (CD326) is a well characterised adhesive molecular found on the surface of all epithelial cells (Schnell et al., 2013). However, upon closer inspection of the literature, its use to isolate epithelial cells from dissociated lungs is insufficient due to Ep-CAM also being present on a proportion of immune and vascular endothelial cells. The additional use of a vascular endothelial marker such as CD32 and immune cell markers CD45 or MHCII markers is required to fully purify the epithelial population (Bantikassegn et al., 2015; Cho et al., 2011; Fujino et al., 2012; Messier et al., 2012; Treutlein et al., 2014). The differential

expression of genes involved in immune response and vascular endothelial cells in the mCherry-hCdt1(30/120) population can therefore be explained by the labelling of these cells by the *Sox17-2A-iCre* and incomplete purification of epithelial cells using anti-EpCAM, with the assumption that the majority of these cells are in G1 and therefore labelled with mCherry-hCdt1(3/120). If this experiment was to be repeated a more specific lung epithelial Cre-line such as the *SftpC-Cre* should be used in combination with additional immune cell and vascular markers to ensure epithelial cell purity in FACS sorted populations (Eblaghie et al., 2006; Okubo & Hogan, 2004).

5.3.2 Epithelial cell movement during branching morphogenesis

By tracking epithelial cells during branching morphogenesis I have characterised the movement of epithelial cells in branching and non-branching regions. I have shown that cells in the distal tip travel with the extending branch but are progressively left behind, become less proliferative and start to differentiate into the bronchial progenitors. The change in cell behaviour is likely due to the loss of extrinsic signals produced in the mesenchyme surrounding the distal tip (Hashimoto et al., 2012; Mucenski et al., 2003; Shu et al., 2005; Volckaert et al., 2013). In light of this behaviour there are two possible models of determining epithelial movement: first, epithelial cells' movement is random and the decision for a cell to remain in the niche or become a bronchial progenitor is determined by the division of cells around it, and, second, there is a population of cells at the distal tip that remain in the tip throughout branching morphogenesis and their progeny are subsequently destined to become more proximal epithelial cells. Considering domain branching occurs laterally from the side an elongating branch (Metzger et al., 2008), which is proximal to the tip niche, these branches will not be constructed by the hypothetical "permanent tip niche" but by a more proximal epithelial cell population, therefore supporting the first model for epithelial movement. It would be interesting to investigate if cells are destined to be bronchial progenitors solely based on extrinsic factors and their distance from the tip or if intrinsic mechanisms such as asymmetric

division followed by epithelial rearrangement directs the progeny of tip cells distally while maintaining tip cells' position in the tip close to the inductive signals released from the surrounding mesenchyme.

In the branching kidney a high proportion of mitosis results in one cell being extruded into the lumen and then reinsertion 1-3 cells away. The two daughter cells then, in the majority of cases, either remain the same distance apart or move further away by a process termed "mitosis-associated cell dispersal" (Packard et al., 2013). Given the large number of cell divisions during branching morphogenesis this process has the potential to promote a high degree of epithelial cell rearrangement. Considering cell division in the distal regions of the lung epithelium has been shown to be perpendicular to the lumen and the documented similarities in the branching programs between the lung and kidney, it is possible this process is occurring in the lung and could be a mechanism for maintaining tip cells within the tip (Davies, 2002; El-Hashash et al., 2011; El-Hashash & Warburton, 2011). One potential method to elude if a permanent tip population exists and the extent of epithelial cell rearrangement, would be to fluorescently label a sub-population of epithelial cells within the tip and then track their movement and the movement of their progeny during branching in *ex-vivo* lung cultures. This would therefore allow you to see if a population of epithelial cells remain in the tip and the extent of epithelial rearrangement in the lung.

6 Summary and Future work

6.1 Summary

The cell cycle is the sequence of stereotyped events a cell goes through in order to replicate its DNA and produce two daughter cells (Nurse, 2000). Precise temporal and spatial control of the cell cycle is essential for tissue morphogenesis during development and homeostasis in adult organisms. Traditional methods for quantifying proliferation either rely on the use of cell cycle phase markers such as

Brd-U and PCNA to calculate the relative proliferative state of a collection of cells (Gratzner et al., 1975; Gratzner, 1982; Kubben et al., 1994), or the calculation of cell cycle times by the use of a dual pulse chase method using two S-phase markers (see introduce 1.4.2) (Bradford & Clarke, 2011; Martynoga et al., 2005; Nowakowski et al., 1989). However both these methods rely on the use of fixed tissues and therefore only give a snap shot of the proliferative state of the tissue.

The Fucci system is a genetic tool which allows for the visualisation of cell cycle progression by the use of two fluorescent probes whose abundance is regulated in relation to the cell cycle resulting in cells being labelled red during G1, yellow during the G1/S transition and green during S/G2/M (Sakaue-Sawano et al., 2008). This systems allows one to visualise cell cycle progression live and therefore fully investigate the dynamics between cell cycle progression with cell movement in tissue development and disease. However the use of the Fucci system in mammalian development has been limited due to the original Fucci mice being generated by random integration of constitutively expressed transgenes. In addition the two Fucci probes were integrated as separate transgenes therefore creating two separate transgenic reporter lines that have to be crossed to generate the Fucci mouse which clearly complicates mouse maintenance and crosses (Sakaue-Sawano et al., 2008). Two attempts were made to overcome these limitations (Abe et al., 2013). However no stably expressed inducible Fucci allele exists in mice, that allows expression of both Fucci probes from a single ORF.

6.1.1 Characterisation of R26R-Fucci2a mouse

In this thesis I have described the generation and characterisation of the *R26Fucci2aR* reporter mouse line which allows for the inducible visualisation of cell cycle progression from expression of a single transgene (Mort et al., 2014). The Fucci2a construct contains both Fucci probes, (mCherry-hCdt1(30-120) and mVenus-hGem(1/110), fused together via the self-cleaving peptide T2A (Kim et al., 2011). This results in equimolar production of both Fucci probes from a single ORF and was characterised by Dr Richard Mort and Mr Adam Douglas (The University of

Edinburgh) 3T3 cells. The *R26Fucci2aR* inducible reporter mouse line was generated by targeted homologous recombination to the *ROSA26* locus in mESC followed by blastocyst injection. The *R26Fucci2aR* transgene was inserted in the reverse orientation into the *ROSA26* locus to avoid transcriptional interference from the endogenous *ROSA26* promoter with expression driven by the synthetic CAG promoter (Miyazaki et al., 1989; Strathdee et al., 2006). The *R26Fucci2aR* transgene also contains a neomycin stop cassette flanked by loxP sites between the CAG promoter and Fucci2a construct to enable Cre dependent expression. Characterisation of the *R26Fucci2aR* mouse was achieved by crossing with the ubiquitous *CAG::Cre* followed by live imaging of a selection of different embryonic tissues including the limb, lung and kidneys (Sakai & Miyazaki, 1997). Strong fluorescence of the Fucci probes was observed in all tissues examined. In addition, a correlation was seen between the lengthening of the cell cycle and the onset of differentiation within each developing tissue. I then went on to confirm the functionality of the Cre-LoxP system by crossing the *R26Fucci2aR* line with the *Tyr::CreB* to label melanoblasts followed by time-lapse imaging of *ex vivo* skin cultures taken from e14.5 embryos (Delmas et al., 2003; Mort et al., 2010).

The *R26Fucci2a* mouse line has clear advantages over all previously published Fucci reporter mice lines especially when complex crosses are required due to stable and inducible expression of the Fucci probes from a single allele (Abe et al., 2013; Mort et al., 2014; Sakaue-Sawano et al., 2008). In addition to advancing the utility of the Fucci system in mammalian research I have also illustrated a novel method of generating quantitative cell cycle data from time-lapses of Fucci expressing cells. This is based on the observation that the proportion of cells within a particular cell cycle phase, in a asynchronised proliferating population, is equal to the proportional length of that phase in relation to the total cell cycle length (Nowakowski et al., 1989). This method enables quantifications of cell cycle times and cell behaviour for a population of cells from a single time-lapse.

6.1.2 Characterisation of tricistronic reporter constructs

In addition to improving the Fucci system in its current form, I have gone on to develop four new tricistronic reporter constructs based on the Fucci2a construct to enable dual visualisation of cell cycle progression with apoptosis, cytokinesis and cilia. For each construct an additional fluorescent probe was inserted to the 5' end of Fucci2a separated by the self-cleaving peptide P2A and characterised in Flp-In 3T3 cells (Invetrogen) before mice were generated by homologous recombination targeted to the *ROSA26* locus in mESC.

In order to visualise cell cycle progression with apoptosis two mCerulean based caspase-activatable fluorescent reporters were tested (Bardet et al., 2008; Nicholls et al., 2011). Both tricistronic constructs (CA-Fucci2a and CC3AI-Fucci2a) functioned as expected in vitro, however a relatively small fold increase in mCerulean fluorescence was observed in cells undergoing apoptosis, which was considered to be too small to be a reliable reporter of apoptosis *in vivo*.

A major limitation of the Fucci system is that fluorescence of both Fucci probes are lost during cell division which makes it difficult to track cells through multiple mitoses. To overcome this limitation I fused the nuclear marker H2B-Cerulean, which labels the nucleus of cells through all stages of mitosis, to the 5' of the Fucci2a construct via a P2A sequence to generate the tricistronic construct H2B-Fucci2a (Hadjantonakis & Papaioannou, 2004). Using this cell line I was able to track cells through multiple mitoses and calculate the lengths of cell cycle phases G1 and S/G2/M from the changes in fluorescence intensities of the Fucci probes. However the subsequent inducible *R26H2B-Fucci2aR* mice line generated using this construct was too dim to be useful as a reporter mouse line. A comparison of the mRNA levels of the H2B-Fucci2a construct compared to Fucci2a in MEFS generated from these two lines by qrt-PCR showed the amount of H2B-Fucci2a mRNA transcript to be around 5% of those seen in Fucci2a MEFS, which suggests the cause for the low levels of fluorescence is either down to a decrease in the level of transcription or impaired RNA stability in the tricistronic construct.

For the final construct I inserted the cilia marker Arl13b-Cerulean to enable the dual visualisation of ciliogenesis with cell cycle progression. Considering the known reciprocal and potential regulatory relationship between the formation of primary cilia and the cell cycle in addition to the myriad of roles for motile cilia in development, homeostasis and disease this construct and conditional reporter mouse line should have a wide range of applications (Afzelius, B, 1976; Greenstone et al., 1984; Seeley & Nachury, 2010; Whitelaw et al., 1981).

In this thesis I characterised the Arl13b-Fucci2a construct in 3T3 cells illustrating how this reporter can be used to track cilia movement live in an adapted wound-healing assay in addition to calculating the timing of primary cilia assembly and disassembly in relation to the cell cycle. The *R26Arl13b-Fucci2aR* mouse line was generated by homologous recombination targeted to the *ROSA26* locus in mESCs using an identical approach as used to generate the *R26Fucci2aR* mice line (Mort et al., 2014). To characterise the inducible tricistronic reporter mice line it was crossed with the ubiquitous *CAG::Cre* and a selection of different tissues including the embryonic brain and node examined. (Sakai & Miyazaki, 1997). Strong fluorescence of each reporter was seen in all tissues examined. In addition the ability to induce tissue specific expression of the reporter using the Cre LoxP system was confirmed by crossing to the endoderm specific Cre *Sox17-2A-iCre* followed by live imaging of embryonic lung explants (Engert et al., 2009). The *R26Arl13-Fucci2aR* mouse line has the additional advantage over other published cilia reporter lines in that it labels cilia with the cell's nucleus live without the need to cross to another reporter line. This is extremely useful for live imaging as it enables cilia dynamics in relation to cell movement to be visualised.

6.1.3 A description of melanoblast behaviour using R26Fucci2aR during migration and investigation into the role of Kit signalling

Using two different developmental systems I went onto illustrate the utility of the *R26Fucci2aR* reporter line in complex genetic crosses and tissue specific expression,

which would be technically challenging or impossible with previously published Fucci systems (Abe et al., 2013; Sakaue-Sawano et al., 2008).

Using an *ex vivo* mouse embryonic skin culture system and time-lapse imaging I characterised the migration of melanoblasts throughout the developing trunk at e14.5 and investigated the role of KIT signalling in melanoblast development (Mort et al., 2010). Previous work using a sporadically activated *Dct-LacZ* reporter to track the progeny of single melanoblast clones showed significant axial mixing conflicting with previous assumptions of directed dorsal-ventral migration (Mintz, 1967; Wilkie et al., 2002). However, to date a detailed analysis of melanoblast migration has not been published. Using the above mentioned embryonic skin culture system and *R26Fucci2a* mice crossed to *Try::CreB* to label melanoblasts, I was able to show that melanoblast migration is random and undirected at e14.5 and e15.5. This is in compliance with a recently published paper that has shown the striped pigmentation patterns, originally supporting the directed migration hypothesis, can be explained in a lattice based model by a combination of random migration, domain expansion and proliferation (Mort et al., 2016). In addition to this I was able to show uniquely using the Fucci system that melanoblast are more persistent in their movement during S/G2/M phases of the cell cycle compared to G1.

KIT signalling has been shown to be essential for melanoblast survival via the RAS signalling pathway and migration via RAS independent signalling (Mackenzie et al., 1997; B Wehrle-Haller et al., 2001). However the exact influence of KIT signalling on cell cycle progression and migrational behaviour is still poorly understood. To investigate this I carried out time-lapse imaging followed by cell cycle and migration analysis of e14.5 *ex vivo* embryonic skin cultures from *R26Fucci2aR*$^{+/Tg}$*/Try::CreB*$^{+/Tg}$ embryos containing either a point mutation in the *Kit* receptor (*Kit*^{Wv}) or a floxed exon in the Ras GAP *Nf1* (Mackenzie et al., 1997; Zhu et al., 2001a). By combining my results with those produced from a similar experiment published by Mort et al 2016 a relationship between melanoblast density and cell cycle length in wild type melanoblasts at e14.5 was seen. Although when taken independently no statistically significant relationship was seen in my data set due to a

small range in melanoblast densities. *Kit*^{Wv} mutants showed a longer cell cycle time while *Nf1* mutants had a shorter cell cycle time than predicted by their respective melanoblast densities therefore suggesting KIT signalling is promoting proliferation in a density dependent manner. An appealing mechanism for the relationship seen between melanoblast density and cell cycle times could be a progressive sequestering of the available membrane bound KIT ligand within the epidermis. This hypothesis is supported by previous reports showing ectopic expression of the KIT receptor in the developing somites and lateral mesenchyme results in a loss or reduction in melanoblast (Duttlinger et al., 1993; Bernhard Wehrle-Haller et al., 1996). In addition binding of KIT ligand has been shown to result in internalisation of the receptor-ligand complex in cultured mast cells (Yee et al., 1994). I found KIT signalling had no significant influence on melanoblast migration in agreement with published reports (Mort et al., 2016).

6.1.4 Comparative analysis of the developing lung epithelium separated by proliferative state

To further illustrate the utility of the *R26Fucci2aR* mouse line I aimed to conduct a comparative gene expression analysis of the branching verses non-branching regions of the developing lung using the differential fluorescence of the Fucci probes to unbiasedly separate these two regions. I have previously observed in other tissues there is often a differential abundance of cells labelled in mCherry-hCdt1(30-120) in G1 and populations of cells predominantly labelled in mVenus-hGem(1-120) in S/G2/M. In the lung, kidney and limb bud these populations of predominantly mCherry-hCdt1(30-120) labelled cells are an indicator of differentiation. I therefore predicted that it may be possible to separate the differentiating population from the less differentiated population by FACS based on the fluorescence of the Fucci probes and compare expression profiles using RNA-sequencing.

As a proof of principle I FACS sorted mCherry-hCdt1(30-120)$^{+}$ and mVenus-hGem(1-110)$^{+}$ populations from dissociated e13.5 *R26Fucci2aR*$^{+/Tg}$*/Sox17-2A-iCre*$^{+/Tg}$ lungs which corresponded with the branching and non-branching regions of

the lung epithelium respectably. Based on the differential abundance of the Fucci probes seen and quantified by live imaging this method for separating the branching and non-branching regions should give a finer separation of these two regions compared to previous reports which relied on the physical separation of the trachea from the branching lobes (S. Lin & Shannon, 2002; Lü et al., 2004). In addition removal of the mesenchyme restricts the analysis to the intrinsic genetic differences between the branching and non-branching regions that has not been heavily studied. Contamination was identified, particularly in the mCherry-hCdt1(30-120)$^{+}$ population, due to incomplete removal of mesenchymal cells also labelled with the *Sox17-2A-iCre*. Separation of the branching and non-branching regions was identified by the differential expression of known distal and proximally expressed genes. As a proof of principle experiment I have therefore shown it is possible to separate developmentally distinct regions by differential fluorescence of the Fucci probes. In addition analysis of the top 20 differentially expressed genes in both populations has identified several potentially interesting genes which should be validated in future work.

6.2 Future work

The use of 2A peptides to create bicistronic reporter transgenes in transgenic mice has proven to be a useful tool to simplify genetic crosses when more than one fluorescent reporter is required (Mort et al., 2014; Shioi et al., 2011; Trichas, Begbie, & Srinivas, 2008). However the use of 2A peptides to generate tri or multicistronic transgenes in mice has not been reported. In this thesis I have generated two tricistronic transgenic mice, both of which exhibited reduced levels of mRNA transcript compared to the bicistronic line from which they are based (*R26Fucci2aR*). For future work it would be interesting to elude the cause of the reduction. First it would be important to ascertain if the reduced mRNA levels seen is a result of reduced transcription or impaired RNA stability. The stability of the transcripts could be measured by calculating the abundance of RNA transcription at set time points by

qrt-PCR after addition of a transcription inhibitor such as actinomycin D to calculate mRNA half-lifes (Harova et al., 2009). Considering very little difference in fluorescence was seen between 3T3 cells expressing the Fucci2a construct and 3T3 cell lines expressing Arl13b-Fucci2a and H2B-Fucci2a. It is possible that the lower abundance of mRNA seen in the MEFS derived from the tricistronic constructs is due to reduced transcription specific to the *ROSA26* locus, which is why little difference in fluorescence is seen between the 3T3 flp-In cell lines where the insertion locus is not known. This hypothesis could be tested by comparing transgene mRNA abundance in 3T3 cell lines generated using the pCAGfloxNEOpA plasmid in which a single copy of the transgene is inserted into the *ROSA26* locus.

6.2.1 *R26Arl13-Fucci2aR*

In addition to this work, further characterisation of the *R26Arl13-Fucci2aR* mice line is required. A broader analysis of different tissues and ages is needed to fully confirm ubiquitous expression of the transgene. Examination of expression patterns of the transgene when crossed to different Cre-lines would also be important to ensure functionality of the Cre-loxP system. In addition to this, the observation of the complete absence of cilia in mESCs cultured in serum conditions would need to be confirmed by immune-fluorescence, as it is possible cilia are not visible due to the dimness of the reporter. If confirmed this would be in contrast to published reports of the presence of cilia in mESCs cultured in 2i media and mESCs differentiated into embryoid bodies (Bangs et al., 2015; Hunkapiller et al., 2011), and would therefore highlight intriguing differences between mESCs cultured under these different conditions which should be investigated further.

6.2.2 Persistence in melanoblast migration

One of the most interesting findings from the *ex vivo* analysis of melanoblast migration was the increased persistence seen in melanoblasts as they progress through S/G2/M phases of the cell cycle. It would be interesting to see if this

increased persistence could have a role in enhancing the expansion of melanoblasts during colonisation of the developing epidermis. This could be tested in a recently published lattice-based model of melanoblast migration (Mort et al., 2016). The model in its current form predicts colonisation of the developing trunk by a combination of random migration, proliferation and colonial expansion. Persistence could be added to the model by giving each melanoblast a "memory" of its last movement. Increased persistence can then be added to the model by increasing the probability of a repeated identical movement. Using this *in silico* system it would be interesting to model if increased persistence has any influence on the speed of colonisation.

6.2.3 Analysis of lung epithelial RNA sequencing data

Further analysis and validation of the comparative RNA sequencing data between the branching and non-branching regions of the developing lung is also required. An analysis of the top 20 differentially expressed genes in each population highlighted several genes that would be interesting to validate by in-situ RNA hybridisation to confirm the differential expression is not caused by contamination. Considering it has been shown that proliferation occurs after the initial budding process in the lung (Lü et al., 2005; Nogawa et al., 1998). In addition to the known role of apical constriction and orientated cell division during the development of other branched organs including the lung (Affolter & Caussinus, 2008; Kadzik et al., 2014; Karner et al., 2009; Yu et al., 2009). A future analysis of genes involved in cell polarity, adhesion, and orientation of cell division would be interesting.

7 Materials and methods

7.1 Protein protocols

7.1.1 Protein extraction from cells

In order to prepare total protein lysate, pelleted cells were resuspended in 1x RIPA buffer (Thermo Sientific) containing 1 x protease inhibitor cocktail (Roche) and 1 x PMSF (Alph Diagnostics) and incubated on ice for 10 minutes. Samples were then sonicated for 3 x 30 second pulses (Bioruptor Diagenode) and centrifuged for 10 minutes at 14,000 RPM at 4^{o}C. The protein lysate was then concentrated using 3K Ultra-0.5 centrifugal filter devices (Amicon) by following manufacturer's instructions, including a 10-minute spin at 14,000 x g. The concentrated supernatant was then stored at -80^{o}C.

7.1.2 Calculating protein concentration

Protein concentrations were calculated using a Pierce BCA protein assay kit (Thermo scientific), following the manufacturer's instructions.

7.1.3 Western blotting

To prepare protein samples for western blotting equal amounts were combined with 1x NuPAGE sample loading buffer (Novex) and 1x reducing agent (Novex) before being heated at 70^{o}C for 10 minutes. Proteins were then separated by molecular weight in a NuPAGE 4-12% Bis-Tris 1mm precast gel using an Xcell Surelock electrophoresis cell (Life Technologies) run at 200V for 50 minutes. 1X NuPAGE MOPS SDS running buffer (Novex) was used with 500ul antioxidant (Novex) added to the inner chamber and 10µl prestained protein standard (Sharp) used as a ladder. The separated proteins were transferred to a PVDF membrane using the iBlot 2 Dry Blotting System (Thermo scientific) following manufacturer's instructions (program P0). The membrane was washed for 10 minutes in PBST (0.1% Tween 20 in 1x Phosphate Buffered Saline), blocked for one hour in 5% Marvel milk PBST at room temperature on shaker before incubation overnight in primary antibody solution at 4^{o}C on shaker. The primary antibody solution was washed off with 3 x 10-minute PBST washes and the membrane incubated in the secondary antibody solution

containing the corresponding ECL secondary antibody conjugated to HRP (Horseradish peroxide) (GE Healthcare) at 1/7500 in blocking buffer for one hour at room temperature on shaker. The secondary antibody solution was washed off with 3 x 10-minute PBST washes and proteins detected with SuperSignal ELISA Femto Substrate (Thermo Fisher). Solutions A and B were mixed at a 1:1 ratio and added to the membrane for 5 minutes at room temperature. Membranes were passed through PBST before being imaged using ImageQuant LAS 4000 (GE Healthcare). Reprobing of the membranes was achieved by incubation of the membrane in NuPAGE stripping buffer (Novex) at room temperature for 10 minutes on a rocker, 3x 3 x 10-minute washes in PBST followed by reprobing with an alternative primary antibody.

7.2 Histology and Immunofluorescence

7.2.1 Paraffin Sectioning

To prepare sections from whole mouse embryos, E14.5 *Tyr::CreB*$^{Tg/+}$*/R26Fucci2aR*$^{Tg/+}$ embryos were dissected from the uterus in ice cold PBS and fixed overnight at 4^{o}C in 4% w/v PFA (PBS) with constant agitation on a roller. Embryos were then dehydrated through an ethanol series of 30-50-70% ethanol before being wax embedded using the VIP Tissue Processor (Sakura). In brief, processing involved: 85% ethanol, 95% ethanol, 2 cycles at 100% ethanol, 2 cycles in xylene and 4 cycles in molten paraffin at 58^{o}C (30 minutes per cycle). Samples were then embedded in paraffin in plastic cassettes and allowed to set on a cooled plate. Embryos were sectioned using a microtome set to generate 10µm sections and mounted on Superfrost glass slides (Thermo Fisher). Slides were then dried at 68^{o}C overnight prior to staining.

7.2.2 Staining paraffin sections

In order to visualise melanoblasts and the expression of the Fucci probes by immunofluorescence, slides were dewaxed through a series of 3 x 5-minute xylene and 3 x 2-minute 100% ethanol washes, followed by 10 seconds in each of 90-70-50-30% ethanol and finally rinsed in H_2O. Antigen retrieval was performed by boiling the slides in preboiled pH 6.4 10mM sodium citrate buffer (H_2O) for 2 x 10-minutes in a microwave. Slides were cooled by rinsing with H_2O and then washed with TBST (TBS containing 0.1% v/v triton-X) for 10 minutes. All wash steps were carried out in a coplin jar. Slides were blocked for 1 hour at room temperature with 10% v/v donkey serum (Sigma) in TBST. Primary antibodies were diluted in 1% v/v donkey serum TBST and 200ul added to each slide and incubated overnight at 4^{o}C in a humidified box. A strip of parafilm was placed on top of the slide to ensure the antibody solution covered the entire slide. Next day the slides were washed 3times in PBS for 5 minutes and 3x in TBST for 10 minutes at room temperature. The corresponding Alexa fluor conjugated secondary antibodies (Thermo Fisher) were diluted 1/400 in 1% donkey serum TBST and 200ul added to each slide and incubated for 1 hour at room temperature in the dark in a humidified box with a strip of parafilm placed on top. Slides were washed 3x 5 minutes in PBS followed by 3x 10 minutes in TBST and then incubated in 2ug/ml DAPI (PBS) for 5 minutes in the dark followed by a 5-minute wash in TBST before being mounted in prolong gold (Thermo Fisher).

7.2.3 Cryosectioning

E13.5 *Sox172a-iCre*$^{Tg/+}$*/R26Fucci2aR*$^{Tg/+}$ embryos were dissected out of the uterus in ice cold PBS and fixed overnight in 4% PFA on a roller at 4^{o}C. The next day the embryos were washed for 3x 10 minutes in PBS at room temperature. The embryos were cryoprotected by incubation in an increasing series of sucrose (PBS) from 5-10-20%, moving the embryos between each step once it had sunk to the bottom. Embryos were then embedded in OCT, snap frozen on dry ice and stored at -80^{o}C

until being sectioned. 10µm sections were cut on the Leica CM3050 S cryostat, left to dry for roughly 1 hour at room temperature and stored at -20^{o}C until staining.

7.2.4 Staining cryosections

In order to visualise the expression of Sox2 and the Fucci probes by immunofluorescence, slides were allowed to return to room temperature for 10 minutes on the bench. All wash steps were performed in a coplin jar at room temperature on a gentile shaker. Slides were washed for 5 minutes in TBST (TBS containing 0.1% triton-X), incubated in 0.5% triton-X TBST to aid penetration of the tissue for 5 minutes and then washed 2 x 5-minutes in TBST. Slides were blocked for 1 hour at room temperature with 10% Donkey serum (Sigma) in TBST. Primary antibodies were diluted in 1% donkey serum TBST and 200ul added to each slide and incubated overnight at 4^{o}C in a humidified box. A strip of parafilm was placed on top of the slide to ensure the antibody solution covered the entire slide. Next day the slides were washed 3x in PBS for 5 minutes and 3x in TBST for 10 minutes at room temperature. The corresponding Alexafluor conjugated secondary antibodies (Invitrogen) were diluted 1/400 in 1% donkey serum TBST and 200ul added to each slide and incubated for 1 hour at room temperature in an opaque humidified box with a strip of parafilm placed on top. Slides were washed 3 x 5-minutes in PBS followed by 3 x 10-minutes in TBST and then incubated in 2ug/ml DAPI (PBS) for 5 minutes in the dark followed by a 5-minute wash in TBST before being mounted in prolong gold (Thermo Fisher).

7.3 RNA protocols

7.3.1 RNA extraction from cells

RNA was isolated from a confluent T75 of MEFS at the same passage number for qRT-PCR. Cells were lysed using RLT buffer (including 2-Mercaptoethanol)

(Qiagen) and lysate added onto QIAshredder spin columns (Qiagen) and spun at 14,000rpm for 1 minute. RNA was then extracted using RNeasy plus micro kit (Qiagen), following manufacturer's instructions, using spin technology protocol and including the on column DNAse digest step. RNA concentration was calculated using Nanodrop 1000 UV-Vis Spectrophotometer (Thermo Scientific) following manufacturer's instructions.

7.3.2 RNA extraction from FACS sorted cells

RNA was isolated for RNA sequencing by dissected lungs from E13.5 *Sox172a-iCre*$^{Tg/+}$*/R26Fucci2aR*$^{Tg/+}$ embryos and dissociated into a single cell suspension by serial trypsinisation. In brief 4x two lungs and one control lung from the same litter were incubated in 1/10, trypsin/versene for 40-minutes at 37^{o}C on a shaker at 1000rpm. Every 10-minutes the supernatant was removed and replaced with fresh 1/10 trypsin/versene. The removed supernatant was added to an equal volume of media (DMEM, 10% v/v FCS, 1% v/v Pen/Strep) to halt digestion. Cells were spun at 1,700g for 5 minutes, resuspended in 100ul 1% w/v BSA/PSB containing 1.25ul anti Ep-CAM-APC and incubated in the dark for 15-minutes at room temperature. Unstained control cells were incubated in 1% w/v BSA/PBS without antibody. Cells were washed once in BSA/PBS and then resuspended in 150ul 1% w/v BSA/PBS for FACS. APC^{+} mVenus^{+}, APC^{+} mCherry^{+} and APC^{-} mVenus^{+} or mCherry^{+} populations were sorted into PBS using the FACS Aria2 SORP cell sorter (Becton Dickinson). 488nm laser with 525/50 bandpass filter was used for mVenus, 560nm laser with 610/20nm bandpass filter for mCherry and 640nm laser with 710/50nm bandpass filter for APC populations. Cells were lysed using RLT buffer (including 2-Mercaptoethanol) (Qiagen) and lysate added onto QIAshredder spin columns (Qiagen) and spun at 14,000 rpm for 1 minute. RNA was then extracted using RNeasy plus micro kit (Qiagen), following manufacturer's instructions, using spin technology protocol. RNA integrity and concentration was calculated using Agilent 2100 Bioanalyzer following manufacturer's instructions using the high sensitivity Pico kit (Agilent).

7.3.3 RNA extraction from whole lung tissue

E13.5 embryonic lungs were disassociated in media (DMEM, 10% v/v FCS, 1% v/v Pen/Strep) by needle series, pelleted by centrifugation and then lysed in RLT buffer containing 2-Mercaptoethanol (Qiagen). The lysate was added onto QIAshredder spin columns (Qiagen) and spun at 14,000 for 1 minute. RNA was then extracted using RNeasy plus micro kit (Qiagen), following manufacturer's instructions, using the spin technology protocol. RNA integrity and concentration was calculated using Agilent 2100 Bioanalyzer or Nanodrop 1000 UV-Vis Spectrophotometer (Thermo Scientific) following manufacturer's instructions.

7.3.4 cDNA synthesis for RT-PCR and qRT-PCR

cDNA was synthesised from total RNA using the First Strand cDNA Synthesis Kit for RT-PCR (AMV) (Roche). Roughly 150ng of RNA was used in each reaction and combined with 1x reaction buffer, 50 units RNase inhibitor, 5mM $MgCl_2$, 1mM deoxynucleotide mix, 1.6µg random primer mix, 20 units AMV reverse transcriptase and up to a total volume of 20ul with RNase free H_2O. Samples were briefly vortexed, centrifuged and then incubated in a PCR machine at 25^{o}C for 10-minutes, 42^{o}C for 60-minutes and 99^{o}C for 5-minutes, held at 4^{o}C and then stored at -20^{o}C. A negative control sample was performed alongside each experiment without AMV reverse transcriptase to examine DNA contamination.

7.3.5 cDNA synthesis for RNA-seq

Owing to the high RNA requirements for RNA sequencing and low amount of RNA isolated by FACS sorted (6.3.2) and whole lungs (6.3.3) the Ovation RNA-Seq System V2 (NuGEN) was used to prepare cDNA. Between 1,500-7,500pg of RNA was used for RNA isolated from FACS sorted lungs and 50ng of RNA for RNA half-life experiments. cDNA synthesis was performed following manufacturer's

instructions using a QIAGEN MiniElute PCR Purification kit for the final purification step and 22µl TE for final elution.

7.3.6 RT-PCR

For RT-PCR experiments, RNA was isolated as outlined in 7.3.2 and cDNA synthesised as in 6.3.4. Intron spanning primers (see table 7.5) were designed by eye. For the PCR, 1µl cDNA was combined with 1X Phusion GC buffer, 0.2mM dNTPs, 1µM forward and reverse primers, 0.5 units of Phusion Hot Start ll DNA Polymerase, made up to 25ul with PCR grade H_2O (Sigma) and the following PCR program:

1) Denaturation – 98^{o}C – 3 minutes
2) Denaturation – 98^{o}C – 10 seconds
3) Annealing – variable – 10 seconds
4) Extension – 72^{o}C – 10 seconds
5) Cycle from step 2-4 34 more times
6) Extension – 72^{o}C – 3 minutes
7) Hold – 4^{o}C – forever

Each sample was combined with 1X loading buffer and run on an agarose gel (pathway to gel). A minus reverse transcriptase control was run in parallel.

7.3.7 Quantitative RT-PCR

Quantitative RT-PCR was performed using the Roche LightCycler-480 with probe-primer combinations designed using the Roche online tool:

(https://lifescience.roche.com/webapp/wcs/stores/servlet/CategoryDisplay?tab=Assay+Design+Center&identifier=Universal+Probe+Library&langId=-1)

For each experiment a 1 in 2 dilution of an amalgamation of the test cDNAs was used to create a standard curve by four sequential 1 in 10 dilutions in PCR grade H_2O. The sample cDNA was diluted 1 in 5 so to fall within the range of the standard curve. 2.5µl of sample or standard curve cDNA was used in a 10µl reaction containing 0.2µM of each primer, 0.1µM probe, 1X Probemaster mix LC-480 (Roche) and 2µl H_2O. Capzb was used as the reference gene in all cases with the following qRT-PCR program:

1) Denaturation – 95^{o}C – 10 minutes
2) Denaturation – 95^{o}C – 10 seconds
3) Annealing – 60^{o}C – 30 seconds
4) Extension – 72^{o}C – 1 second
5) Cycle from step 2-4 44 more times
6) Cooling – 40^{o}C – 30 seconds

Reads were first normalised to the reference gene (Capzb) to compensate for discrepancies in the amount of starting material and then to the control sample to calculate relative expression level for test genes.

7.4 Organ culture

7.4.1 Embryonic skin culture

Embryonic mouse skin was dissected from E14.5 embryos and mounted on a custom made imaging clip filled with 1% w/v agarose (50/50 dH_20/media) to support the tissue (Mort et al, 2010). Tails were taken and DNA extracted for genotyping as in 7.8.6. The skin was then clamped with the epidermal side against a lummox gas-permeable membrane (Greiner Bio-One) in a custom made culture chamber filled with imaging DMEM^{GFP-2} (Envogen) (10% v/v FCS, 1% v/v Pen/Strep, 1X GlutaMax (GIBCO), 1X Rutin (Envogen)). Cultures were allowed to recover for one hour in a 37^{o}C humidified incubator supplied with 5% $CO_{2.}$ Cultures were imaged

using an inverted A1R confocal microscope in an environmental chamber set to 37^{o}C and supplied with 5% CO_2, capturing a 12µm Z-stack every 10 minutes.

7.4.2 Embryonic lung and kidney cultures

Embryonic lung and kidneys were dissected from E11.5 and E12.5 embryos in PBS. Before the dissection 1ml of 2mg/12ml of matrigel/media (BD Bioscience, phenol free, reduced growth factor) (DMEM, 10% FCS, 1% Pen/Strep, 1X GlutaMax (GIBCO)) was incubated on a lummox gas-permeable membrane (Greiner Bio-One) attached to a custom imaging chamber for 1 hour in a 37^{o}C incubator. The matrigel/media solution was aspirated off and organs transferred onto the coated lummox membrane and embedded in 200ul 50/50 matrigel/media. Organs were orientated for imagining and incubated for 1 hour in a 37^{o}C incubator to allow the matrigel to set. The culture chamber was filled with imaging DMEM^{GFP-2} (Envogen) (10% FCS, 1% Pen/Strep, 1X GlutaMax (GIBCO), 1X Rutin (Envogen)) and organs allowed to recover for a few hours to overnight. Organs were imaged using an inverted A1R confocal microscope encased in an environmental chamber set to 37^{o}C and supplied with 5% CO_2. Roughly a 60µm Z-stack was imaged every 20-30 minutes.

7.5 Cell Culture

7.5.1 Generation and maintenance of 3T3 lines

3T3 Flp-In (Thermo Fisher) cell lines were generated and maintained following manufacturer's instructions using the Neon Transfection System (Thermo Fisher). In brief, polyclonal and isogenic cell lines were generated by combining 1x10^{7} cells in 200µl of solution R (Thermo Fisher) with 18ug pOG44 and 2ug pcDNA-FRT (containing insert) and electroporated using 100µl gold plated tips using the following conditions: 1350v, 20ms, 2 pulses. Electroporated cells were seeded in DMEM (10% FCS, without antibiotics) in a T75. The next day cells were imaged on a Nikon Eclipice Ti fluorescent microscope to check for successful transfection and

then put under hygomycin B selection (100µg/ml) 48 hours after transfection for 2 weeks. A selection control was also transfected in parallel in which cells were electroporated without any plasmids. Cell lines were maintained in a humidified 37^{o}C incubator supplied with 5% CO_2 and stored in liquid nitrogen in full media containing 10% DMSO (Sigma). Untransfected 3T3 Flp-In cells were maintained at a low passage in DMEM containing 10% FCS, 1% Pen/Strep, 100µg/ml Zeocin.

7.5.2 Arl13b-Fucci2a 3T3 migration assay

In order to determine the orientation of primary cilia during migration, Ar13b-Fucci2a 3T3 cells were seeded at high density into a custom made silicon ring stuck to the bottom of a 24-well glassed bottomed plate (Greiner Bio-one) by surface tension. The next day the silicon ring was removed and the media replaced with imaging phenol free DMEM (Millipore) (10% FCS, 1% Pen/Strep). Cells were then imaged migrating from the leading edge on an A1R Nikon confocal microscope encased in a 37^{o}C environmental chamber supplied with 5% CO_2. Images were taken every 10 mins at a single Z plane. The angle of cilia in relation to the center of the nucleus was measured in migrating cells after 5 and 10 hours using a custom macro in ImageJ. In brief, a line was drawn from the center of the cell's nucleus to the cilia and the angle calculated by ImageJ. The angle was then corrected for the orientation of the wound edge with respect to the image. A control experiment was also set up in parallel in which Arl13b-fucci2a 3T3 cells were seeded straight into a 24-well glassed bottomed plate so there was no directional movement and their ciliary angles were measured.

7.5.3 Preparation and maintenance of mouse embryonic fibroblast

Mouse embryonic fibroblasts (MEFs) were prepared from individual E12.5 embryos. In PBS the tail, limbs, head and organs were removed and the remainder of the body transferred to a 6-well plate on ice. In a cell culture hood using sterile techniques the PBS was aspirated off and replaced with 50/50 trypsin/versene. The embryos were

then broken up into small pieces using forceps and left for 1 hour. Three ml of MEF media (Opti-mem (GIBOC), 10% v/v FCS, 1% v/v Pen/Strep, 0.1mM 2-Mercaptoethanol (Sigma)) was added and solution pipetted up and down to dissociate the tissue into single cells and seeded into a T75 tissue culture flask. MEFs lines were passaged at least 3 times before being stored in liquid nitrogen in MEF media plus 10% v/v DMSO, 30% v/v FCS. MEF lines were cultured in a humidified 37^{o}C incubator supplied with 5% CO_2, maintained at high confluency and split no harsher than 1/3.

7.5.4 Maintenance of mouse embryonic stem cells

Mouse embryonic stem cells (mESCs) were cultured in a humidified 37^{o}C incubator supplied with 5% CO_2 in GMEM BHK-21 media (10% FBS, 1% Sodium Pyruvate (Sigma), 1% mem non-essential amino acids (Sigma), 2mM Glutamine, 0.1mM 2-Mercaptoethanol (Sigma) and 106 U/L LIF (prepared in house) and frozen in FCS (10% DMSO) for liquid nitrogen storage.

7.5.5 Cre-activation of Fucci2a mouse embryonic stem cell lines

To excise the neomycin stop cassette and activate Fucci2a expression, 1x10^{-7} *R26Fucci2aR* mESCs in 0.5ml of PBS were combined with 100µg pGK-Cre plasmid and incubated on ice for 15 minutes. Cells were transferred to an ice cold 0.4mm electroporation cuvette and electroporated using the Gene Pulser II (Bio-Rad) with the following conditions: low range = high setting, high range = infinity setting, gene pulser = 3uf, volts = 0.8Kv. It was ensured that readings between 0.1-0.2 and the cells were allowed to recover on ice for 15 minutes. Cells were seeded at low density (1000 cells per 10cm pre-gelatinised plate), and grown until clones become visible. Clones were screened for fluorescence and fluorescence clones picked and expanded. In brief, clones were picked using a pipette tip and incubated in a V-bottomed 96 well plate for 10-15 minutes at 37^{o}C in 1X TrypLE Express (GIBCO). An equal volume of media was added and the clones dissociated by pipetting before seeding

into a 96 well flat bottomed plate. Clones were then expanded before being stored in liquid nitrogen. Cre-excision was confirmed by checking clone sensitivity to G418 (250ug/ml).

7.5.6 Generation of rH2B-Fucci2a ES cell line

In order to track mESCs throughout the whole cell cycle the rH2B-Fucci2a ES cell line was generated by transfection of linearised pCerulean-H2B-6 (♯55348 addgene) into cre-activated Fucci2a ES cells. pCerulean-H2B-6 was linearised by restriction digest with ApalI. 5ul of the digest to run on an agarose gel (6.6.3) to confirm linearisation. Linearised DNA was cleaned by ethanol precipitation (6.6.7) and 100µg combined with $2x10^{-7}$ cells in 0.5ml PBS and incubated on ice for 15-minutes. Cells were transferred to an ice cold 0.4mm electroporation cuvette and electroporated using the Gene Pulser II (Bio-Rad) with the following conditions: low range = high setting, high range = infinity setting, gene pulser = 3uf, volts = 0.8Kv. It was ensured that readings fell between 0.1-0.2 and cells were allowed to recover on ice for 15 minutes. Cells were seeded at a density of 2 million cells per 10cm pre gelatinised plate), and grown under G418 section. Clones were picked and screened for H2B-Cerulean and Fucci2a fluorescence.

7.5.7 Differentiation of Fucci2a mouse embryonic stem cell lines

Mouse embryonic stem cells (mESCs) were cultured for four days in standard GMEM BHK-21 media as in 6.5.4 without LIF and with the addition of 1nM retinoic acid. Images were taken using an A1R confocal microscope and the proportion of labelled cells quantified using the FACSAria ll flow cytometer (BD Biosciences). Control cells were grown in parallel under standard conditions as in 6.5.4.

7.6 Cloning and DNA protocols

7.6.1 Subcloning pcDNA5-FRT plasmids

In order to generate 3T3 stable cell lines expressing the tricistronic reporter constructs using the the Flp-In system, CAG-Arl13b-p2a-fucci2a and CAG-H2B-p2a-fucci2a were subcloned from pCAG-Arl13b-fucci2a and pCAG-H2B-fucci2a respectively into pcDNA5-FRT by blunt-sticky restriction cloning. Donor plasmids were digested with SalI and pcDNA5-FRT plasmid (reciprocate) with MluI in their corresponding buffers (New England Biolabs) plus 1X BSA for 1 hour in a 37^{o}C water bath. 2ul dNTP (10mM) and 2ul T4 polymerase (Promega) was added and incubated at room temperature for 10-minutes to blunt the ends, followed by heat inactivation for 15-minutes at 80^{o}C. Samples were cooled on ice followed by a second round of digestion with KpnI at 37^{o}C for 1 hour. 5ul of each digest was run out on a 1% w/v agarose gel to check for correct digestion (7.6.3). Digest mixes were cleaned by phenol chloroform extraction and ethanol precipitation (7.6.7) and 10ul ligase reactions set up using T4 ligase (Promega) with corresponding buffer and a range of insert concentrations. Samples were left to ligate overnight at room temperature. Ligations were transformed (7.6.5) and clones screened for correct insertion by restriction digest.

For pcDNA5-CA-Fucci2a and pcDNA-CC3AI-Fuccia plasmids CA-Cerulean-P2A and CC3AI-P2A were synthesised by Geneart flanked by MluI and BssHII restriction sites. Donor plasmids were digested with MluI and BssHII restriction enzymes while pcDNA5-FRT-Fucci2a was digested for 1 hour with MluI restriction enzyme at 37^{o}C with 1X corresponding buffers. Digest mixes were cleaned by phenol chloroform extraction and ethanol precipitation (7.6.7) and 10ul ligase reactions set up using T4 ligase (Promega) with corresponding buffer and a range of insert concentrations. Samples were left to ligate overnight at room temperature. Ligations were transformed (7.6.5) and clones screened for correct insertion by restriction digest.

7.6.2 PCR cloning H2B and Arl13b constructs into pROSA-CAG-floxNeo-fucci2a

Cloning of Arl13b-Cerulean-p2a was kindly undertaken by Richard Mort following the same protocol as for H2B-Cerulean-p2a outlined below. H2B-Cerulean-p2a was PCR cloned from pcDNA-FRT-H2B-Cerulean in a 50µl Phusion Hot Start II reaction with GC buffer (Thermo Fisher) using the following PCR conditions:

1) Denaturation – 98^{o}C – 1 minutes
2) Denaturation – 98^{o}C – 10 seconds
3) Annealing – 96^{o}C – 10 seconds
4) Extension – 72^{o}C – 20 seconds
5) Cycle from step 2-4 25 more times
6) Extension – 72^{o}C – 3 minutes
7) Hold – 4^{o}C – forever

Primers were designed to add an MluI restriction site and a kozak (GCCACC) sequence to the 5' end of the insert and a BssHII restriction site to the 3' end (BssHII digestion generates a cohesive overhang compatible with MluI). The PCR product was out run on a 1% w/v agarose gel (7.6.3) to ensure only one band of the correct size was present. The band was then extracted as in 6.6.4. The H2B-Cerulean-p2a PCR product was restriction digested with MluI and BssHII and pROSA-CAG-floxNeo-fucci2a with MluI in corresponding buffers (New England Biolabs) for 1 hour in a 37^{o}C water bath. To prevent relegation the recipient plasmid was treated with 3ul Shrimp Alkaline Phosphatase (SAP) for 1 hour at 37^{o}C followed by heat inactivation for 15 minutes at 65^{o}C to prevent religation. Digest mixes were cleaned by phenol chloroform extraction and ethanol precipitation (7.6.7) and 10ul ligase reactions set up using T4 ligase (Promega) with corresponding buffer using a range of insert concentrations. Samples were left to ligate overnight at room temperature. Ligations were transformed (7.6.5) and clones screened for correct insertion by restriction digest. The plasmid was sequenced (7.6.8) to ensure correct insertion and

that no mutations were introduced by PCR errors. 200ug of linearised pROSA-CAG-floxNeo-H2B-fucci2a was sent in TE for ES cell targeting by targeted homologous recombination at The Scottish Centre for Regenerative Medicine Transgenic Service (Joe Mee).

7.6.3 Agarose gel electrophoresis

DNA samples were separated by agarose gel electrophoresis and visualised using a UV transilluminator (BioDoc-It System, UVP). 6 X loading dye (0.4% Orange G, 20% Ficoll Type 400, 100mM EDTA in H_2O) was added to each DNA sample, to produce a final 1X concentration and 20ul run on an agarose gel. Agarose gels were made by boiling 1% agarose (Hi-Pure Low EEO agarose, Biogene) in 1X TBE buffer (89mM Tris base, 89mM boric acid and 20mM EDTA) in a microwave. 5µg/ml ethidium bromide was added once the gel had cooled. Gels were run submerged in 1X TBE for 40-60 minutes at 125V in an Electro-4 Gel System (Thermo Scientific). 1KB plus DNA ladder (Invitrogen) combined with 1X loading buffer was used as a calibrator to determine band size.

7.6.4 Gel extraction

PCR reactions for cloning were run on a 1% w/v agarose gel as in 7.6.3. and DNA fragments of the correct size dissected from the gel on a UV transilluminator. DNA was then extracted using the QIAquick gel extraction kit (Qiagen) following the manufacturer's instructions.

7.6.5 Bacterial transformation

In order to replicate DNA samples 1µl of ligation mixture or 1-100ng of plasmid was added to 100µl DH5α library competent cells (Invitrogen) and incubated on ice for 30 minutes on ice. Cells were heat-shocked for 45 seconds in a 42^{o}C water bath and allowed to recover on ice for 2 minutes. 0.9ml of S.O.C. medium (Invitrogen) was added and the cultured for 1 hour at 37^{o}C with constant shaking at 225rpm in

dual snap-cap conical tubes (Falcon). Cultures were spread onto antibiotic specific agar plates and incubated overnight at 37^{o}C.

7.6.6 Purification of DNA by Mini and Maxiprep

For miniprep purification of DNA, a single bacterial colony was picked and added to 5ml L-broth containing the corresponding antibiotic and incubated overnight in dual snap-cap conical tubes (Falcon) shaking at 225rpm at 37^{o}C. 1ml of the overnight culture was used with Quick plasmid miniprep kit (Invitrogen) following manufacturer's instructions with centrifugation steps.

For maxiprep purification of DNA, a single bacterial colony was picked and grown in 5ml L-broth containing appropriate antibiotics for a few hours at 37^{o}C shaking at 225rpm. The starter culture was added to 200ml L-broth containing appropriate antibiotics and incubated shaking at 225rpm overnight at 37^{o}C. The HiPure plasmid maxiprep kit (Invitrogen) was then used to purify the DNA following manufacturer's instructions.

7.6.7 Phenol Chloroform extraction and ethanol precipitation

Digest mixtures and dirty DNA preps were purified by phenol chloroform extraction followed by ethanol precipitation. In a fume hood an equal volume of PCL (Phenol:Chloroform:Isoamyl Alcohol) was mixed with the dirty DNA prep and spun for 5 minutes at 14,000rpm. The top (clear) layer was removed, combined with 10% v/v 3M NaOAc, 3µl glycogen, 250µl 100% ethanol and incubated on dry ice for 15 minutes while ensuring the solution did not freeze. The precipitated DNA was pelleted by centrifugation at 14,000rpm for 30 minutes at 4^{o}C. The pellet was washed twice with 70% ethanol, air dried for 15 minutes at room temperature and finally dissolved in dH_2O or TE.

7.6.8 Sequencing

All sequencing was carried out on the 3130 Genetic Analyzer (Applied Biosystems) following manufacturer's instructions. Sequence data was analysed using Sequencher (Gene Codes Corporation).

7.7 Fluorescence-activated cell sorting (FACS)

7.7.1 DNA quantification using DAPI

Confirmation of correct cell cycle phase representation by Fucci2 fluorescence was performed by FACS using DAPI intensity as a measure of DNA content. In brief, using a FACS Aria2 SORP cell sorter (Becton Dickinson) cells were sorted into mVenus (488nm laser, 525/50nm bandpass filter), mCherry (560nm laser, 610/20nm band pass filter) double positive and negative populations. Cells were fixed in 70% ethanol overnight at -20^{o}C. The next day cells were stained with DAPI (5µg/ml in PBS) and DNA content analysed using the 405nm laser and 450-50nm bandpass filter. FACSDiVa Version 6.1 (BD) was used to analyse the data.

7.7.2 Ki67 staining confirming all melanoblast are cycling

In order to confirm all melanoblast are actively cycling through the cell cycle the skin from E14.5 *Pmel*$^{tg/+}$ embryos was removed and incubated in 1ml 10mM EDTA (PBS) for 45 minutes at 37^{o}C. Every 10 minutes the tissue was agitated to aid dissociation. The tissue was broken up more by pipetting before being spun down, resuspended in 1ml 0.2U/ml liberase (PBS) and incubated for 45 minutes at 37^{o}C, agitating every 10 minutes. The tissue was then spun, resuspended in media (DMEM, 10% FCS, 1% Pen/Strep, 1X GlutaMax (GIBOC)) and put through a needle syringe series to dissociate into a single cell suspension. Cells were fixed in 100ul Perm/Fix (BD Biosciences) for 10 minutes, washed once in 1X Perm/Wash (BD Biosciences), then incubated for 15 minutes in the dark on ice with 5µg/ml rat anti mouse Ki67-FITC (eBioscience). Unstained control cells were incubated in Perm/Wash without

antibody. Cells were washed with Perm/Wash and then analysed using the FACS Aria2 SORP cell sorter (Becton Dickinson). Melanoblasts were first identified using the 405nm laser with 450-50nm bandpass filter and the proportion of $FITC^+$ cells quantified with the 488nm laser using 525/50nm bandpass filter. FACSDiVa Version 6.1 (BD) was used to analyse the data.

7.8 Generation and maintenance of Fucci2a mice lines

7.8.1 Targeting *ROSA26* in mouse embryonic stem cells

ES cell targeting was undertaken by Joe Mee and the Scottish Centre for Regenerative Medicine Transgenic Service. In brief, E14 ES cells were electroporated with linearised pRosa26-CAG-floxNeo-H2B-Fucci2a/Arl13b-Fucci2a plasmid using standard procedures. Clones were picked after 14 days of G418 selection and DNA isolated.

7.8.2 Screening targeted mouse embryonic stem cells by PCR

Colonies were screened for correct homologous recombination 5' and 3' PCR across the *ROSA26* homology arms using Xu_Wt_For and Rosa5_R1 for the 5' (1.4kb band size) and Rosa3_F1 and Rosa3_R2 for the 3' (4kb band size) (fig 2.3). A control PCR to demonstrate DNA integrity was also conducted using primer Wt_For and Wt_Rev to generate a 450bp wild type band. All PCR reactions were carried out using 50ng genomic DNA with Phusion Hotstart II DNA polymerase (Thermo Fisher) with GC buffer. For PCR primers see table 8.8.

7.8.3 Generation of Fucci2a mice lines

Mice were generated by Margaret Keighren by ES injection into blastocysts and transferred to pseudopregnant foster mothers to generate chimeras. F0 Chimeras were crossed with C57B16/J mice to generate F1 mice which were genotyped and

heterozygotes intercrossed to generate homozygous lines. These mice were back crossed at least three generations to ensure a homogeneous black 6 background.

7.8.4 Breeding and maintenance

Mice were maintained in the animal care facilities at the University of Edinburgh under standard conditions. All animal procedures were performed in accordance with Home Office regulations under the personal license 60/4424.

7.8.5 Genotyping ear clips

For DNA extraction 100ul 25mM NaOH/0.2mM EDTA was added to the ear clip in a PCR tube and run on a thermal cycler at 95^{o}C for 20 minutes. 100ul of 40mM Tris-HCL was added and 1-2µl used for genotyping by PCR (7.8.7).

7.8.6 Genotyping embryonic tail clips

DNA was extracted by overnight incubation in quick lysis buffer (100mM Tris HCL (pH 8.5), 5mM EDTA, 0.2% SDS 200mM NaCl, 200ug/ml proteinase K, H_2O) at 50-55^{o}C. The DNA was then precipitated with equal volumes of isopropanol at room temperature and pelleted by centrifugation. The DNA pellet was washed with 70% ethanol and then air dried for 15-20 minutes before being dissolved in 50µl TE (Tris pH8). DNA concentration and purity was measured using the Nanodrop 1000 UV-Vis Spectrophotometer (Thermo Scientific) following manufacturer's instructions.

7.8.7 Genotyping PCR

In the majority of cases DreamTaq Green (Thermo Fisher) was used. In brief 1X DreamTaq Green PCR Master Mix was combined with roughly 1µg of template DNA and 0.1µM forward and reverse primers to a total volume of 25µl. PCR was performed on a Tetrad2 Peltier Thermal Cycler (BioRad) using standard conditions,

varying the annealing temperature and extension time depending on the Tm of the primer pair and the length of the amplicon.

For genotyping of *R26Fucci2aR*, *R26H2B-Fucci2aR* and *R26Arl13b-Fucci2aR* mice Phusion Hot Start II (Thermo Fisher) was used following manufacturer's instructions. In brief 1X GC buffer was combined with 200uM dNTPs.

7.8.8 Tamoxifen Injections

Tamoxifen (Sigma) was dissolved 20mg/ml in corn oil (Acros Organics) overnight at 37^{o}C in the dark and stored at -20^{o}C. Either 4mg/40g (low dose) or 8mg/40g (high dose) was delivered by gavage or intraperitoneal injection. The mouse was monitored for any potential side effects.

7.9 Microscopy

7.9.1 Confocal imaging

Confocal imaging was carried out using a Nikon A1R confocal set up, composed of a Nikon Eclipse TiE microscope with resonant scanner and spectral detector. The following lasers and band pass filters were used.

Fluorescence source	*Laser*	*Bandpass filter*
Dapi	403.5nm	450/50
Cerulean	457.9nm	482/35
mVenus / YFP	514.5nm	640/30
Alexa 488	488nm	625/50
mCherry / Alexa 594	561.3nm	695/50
Alexa 647	639.8nm	700/75

Bright field images were taken simultaneously with fluorescence imaging by use of a transmitted light detector. For live imaging an environmental chamber that encased the entire microscope was used and set to 37^{o}C with 5% CO_2 supplied. Nikon's

perfect focus system was used to minimalise drift and images captured using NIS elements software (Nikon).

7.10 Statistics

All image analysis was carried out using ImajeJ. For a list of specific macros/plugins see 6.4. Statistics were performed using Microsoft Excel for student T test and R studio for Spearman's rank correlation, one-way ANOVA, Tukey's HSD and Kolmogorov-Smirnov tests.

7.11 RNA sequencing

In order to determine differentially expressed genes in the branching and non-branching regions of the lung epithelium, RNA sequencing was performed of FAC sorted e13.5 *R26Fucci2aR*$^{+/Tg}$*/Sox17-2A-iCre*$^{+/Tg}$ embryos (see 7.3.2 for RNA extraction and 7.3.5 for cDNA synthesis protocols). Sequencing was performed by Edinburgh Genomics using an Illumina HiSeq2500 with each sample being run on two lanes producing on average 40M reads per biological replicate. RNA analysis was performed using the online interface Galaxy (www.usegalaxy.org). Each sample was first run through a sequence quality control using FASTQC (http://www.bioinformatics.babraham.ac.uk/projects/fastqc/). Over represented adaptor sequences were identified and removed before sequences were run again through FASTQC to confirm acceptable sequence quality scores and GC content. Adapter sequences were however left on in subsequent analysis as removing of the adapter sequences misaligned the paired reads. In addition adapter sequences would be discarded during aliment to a reference genome. Paired sequences were then aligned to the mouse reference genome (NCBI37/mm9) using tophat (D. Kim et al., 2013). At this point technical replicates were merged and differential expression calculated using cuffdiff (Trapnell et al., 2010). A clustering analysis confirmed the majority of variation was between the FACs sorted populations rather than biological replicates by MDS plot and dendrogram using the differentiation expression visualisation analysis tool CummeRbund (http://bioconductor.org/packages/release/bioc/html/cummeRbund.html).

8 Appendix

8.1 Antibodies

Table 8.1:

Antibody	*Company (Catalogue number)*	*Species*	*Dilution*	*Application*
RFP	ROCKLAND (600-401-379	Mouse	1:200 IF , 1:1000 WB	IF, WB
GFP	Nacalai tesque (04404-84)	Rat	1:200	IF
Sox2	Abcam (ab79351)	Mouse	1:200	IF
Pmel	Abcam (ab137078)	Rabbit	1:200	IF
Ki67-FITC	eBioscience (11-5698-80)	Rat	1:100	FACS
Epcam-APC	Biolegend (118214)	Mouse	1.25:100	FACS
Cdt1	Santa Cruz (28262)	Rabbit	1:1000	WB
Cdt1	Abcam (ab70829)	Rabbit	1:1000	WB
Cdt1	Millipour (07-1383)	Rabbit	1:1000	WB

8.2 Plasmids

Table 8.2:

Plasmid	*Source*
pGK-Cre	Gift from Joan Slight
pOG44	Flp-In (Thermo Fisher)
pcDNA-FRT	Flp-In (Thermo Fisher)
pCAGiP	Gift from Dr Thomas Pratt
pcDNA5-FRT-Arl13b-fucci2a	Subcloned from pCAG-Arl13b-fucci2a, Richard Mort
pcDNA5-FRT-H2B-fucci2a	Subcloned from pCAG-H2B-fucci2a, Richard Mort
pcDNA5-FRT-CA-fucci2a	Subcloned from P2A-CA-Cerulean, Geneart
pcDNA5-FRT-CC3AI-fucci2a	Subcloned from P2A-CC3AI, Geneart
pRosa26-PA	Addgene
pCAGfloxNEOpA	Gift from Prof. Ian Chambers
pROSA-CAG-floxNeo-Arl13b-fucci2a	PCR cloned from pcDNA-FRT-Arl13b-fucci2a
pROSA-CAG-floxNeo-H2B-fucci2a	PCR cloned from pcDNA-FRT-H2B-fucci2a
pROSA-CAG-floxNeo-fucci2a	Gift from Dr Richard Mort
pCerulean-H2B-6	Addgene

8.2.1 Design of constructs

8.2.1.1 Fucci2a

The Fucci2 probes, mVenus-hGEminin(1/100) and mCherry-hCdt1(30/120), were concatenated in both orientations by Dr Richard Mort. In brief the second gene was amplified by PCR using a generic forward primer incorporating the T2A sequence preceded by restriction sites MluI and MfeI with a reverse primer specific to either mVenus-hGEminin(1/100) or mCherry-hCdt1(30/120) flanked by a KpnI restriction site. The resulting amplicon was resection cloned into pCAGiP via MluI and KpnI restriction sites. The first gene was amplified by a generic forward primer containing MluI restriction site and a reverse primer specific to either mVenus-hGEminin(1/100) or mCherry-hCdt1(30/120) flanked by a MfeI site. Using the restriction sites MfeI and MluI the second amplicon was resection clones to give pCAG-5C3V and pCAG-5V3C.

Flp-targeting and *ROSA26* targeting constructs were constructed by Dr Richard Mort. In brief, pcDNA5-FRT (Thermo Fisher) was modified with a polylinker cloned between NheI and ApaI to introduce EcoRI and AscI restriction sites. Subsequently the two Fucci2a construct, Fucci5V3C or Fucci25C3V were cloned between the EcoRI and AscI restriction sites. To generate pRosa26-CAG-floxNeo-Fucci2a pCAGiP was modified with a polylinker to facilitate the subcloning of Fucci2-pA as a SalI/HindIII fragment. Via the EcoRI restriction site a floxed *Neo* cassette was cloned between CAG and *Fucci2a* from pCAGfloxNEOpA. The pRosa26-PA plasmid was then modified by a polylinker to invert the AscI and PacI sites so that upon insertion of the entire *CAG-floxNeopA-Fucci2-5C3V-pA* construct to generate pRosa26-CAG-floxNeo-Fucci2a plasmid, aliment was in the opposite direction to the endogenous *Rosa26* promoter.

8.3 Primers

8.3.1 Cloning

Table 8.3:

Protocol	*Name*	*Sequence*
H2B-Cerulean-p2a cloning	MluI-Kozak-Fwd	CGGCACACGCGTGCCGCCACCATGCCAGAGCCAGCGAAGTC
H2B-Cerulean-p2a cloning	Rev-BssHII	GGAGGAGAACCCTGGACCTGCGCGCGCCGTC

8.3.2 Sequencing

Table 8.4:

Plasmid	*Name*	*Sequence*
pRosa26-CAG-floxNeo-H2B-Fucci2a	Fwd 1	CACTGCATTCTAGTTGTGGTTTG
pRosa26-CAG-floxNeo-H2B-Fucci2a	Fwd 2	AGGCCATCACCAAGTACACC
pRosa26-CAG-floxNeo-H2B-Fucci2a	Fwd 3	CAAGCTGAAGGTGACCAAGG
pRosa26-CAG-floxNeo-H2B-Fucci2a	Fwd 4	CACCATCGTGGAACAGTACG
pRosa26-CAG-floxNeo-H2B-Fucci2a	Fwd 5	GGCGATGTCGAAGAGAATCC
pRosa26-CAG-floxNeo-H2B-Fucci2a	Fwd 6	GAAGAACTCTGAAGATGATTCA
pRosa26-CAG-floxNeo-H2B-Fucci2a	Rev 1	ATGGCCTTGGACGAAATG
pRosa26-CAG-floxNeo-	Rev 2	AGGGTTCTCCTCCACGTCTC

H2B-Fucci2a		
pRosa26-CAG-floxNeo-H2B-Fucci2a	Rev 3	TCCTTCAGCTTCAGCCTCTG
pRosa26-CAG-floxNeo-H2B-Fucci2a	Rev 4	AATTGGATGGTGTCCTGGTC
pRosa26-CAG-floxNeo-H2B-Fucci2a	Rev 5	CAGGGCTGGAAGTTGTAGATG
pRosa26-CAG-floxNeo-H2B-Fucci2a	Rev 6	TGGGCTGCAGGTTCTTTC

8.3.3 RT-PCR

Table 8.5:

Name	***Sequence***
Sox 2 Fwd	GGAGATCAGCAAGCGCCTG
Sox 2 Rev	CATGCTGTAGCTGCCGTTG
Sox 9 Fwd	CAAGCCACACGTCAAGCGAC
Sox 9 Rev	CTTGTCCGTTCTTCACCGAC
Emr1 Fwd	GTTGATGAGTGTCTGACAATTG
Emr1 Rev	CTCCTCCACTAGATTCAAGTC
CSF1R Fwd	GCTCTCAGTCTCAACGCTGT
CSF1R Rev	AATGGACCTAGGTAGGTCC
Acta2 Fwd	GACATCAAGGAGAAGCTGTG
Acta2 Rev	TGATCTCCTTCTGCATCCTG

Pecam Fwd	CCTTGTGGACATCAGCACCA
Pecam Rev	TGACGTATTCACTCCTGATG
MHC II Fwd	CACATCTTCTACTACCTGCTC
MHC II Rev	GCTGTTCCTCTTCATTGAAGC

8.3.4 qRT-PCR

Table 8.6:

Name	***Sequence***	***Probe***
Capzb Fwd	GTTCCCCACACATAGCCAAC	
Capzb Rev	AGATCTCATTCAGCGTGCTTC	22
mCherry Fwd	GTGACCGTGACCCAGGAC	
mCherry Rev	GCGCAGCTTCACCTTGTAG	152

8.3.5 Genotyping

Table 8.7:

Strain	***Name***	***Sequence***	***Band size bp***
Fucci2a	R26_Wt_fwd	CAAAGTCGCTCTGAGTTGTTATCAG	600 wt
Fucci2a	R26_Wt_Rev	GGAGCGGGAGAAATGGATATGAAG	880 mut

Fucci2a	F2A_Rev	TGGCGGCCGCTCGAGATGAATC	
Sox17-2A-iCre	Wild type Fwd	GTGTATAAGCCCGAGATGG	288 wt
Sox17-2A-iCre	Wild type Rev	CTCAACTGTTCAAGTGGCAG	446 mut
Sox17-2A-iCre	Transgene Fwd	ATTGCATCGCATTGTCTGAGTAG	376 cre excised
Sox17-2A-iCre	Cre excised Fwd	GATCTATGGTGCCAAGGATGAC	
Sox17Cre-ERT2	Wild type Fwd	GTGTATAAGCCCGAGATGG	288 wt
Sox17Cre-ERT2	Wild type Rev	CTCAACTGTTCAAGTGGCAG	470 mut
Sox17Cre-ERT2	Transgene Fwd	CATGCTCCAGACTGCCTTGG	306 cre excised
Sox17Cre-ERT2	Cre excised Fwd	TCCCACATTAGGCACATGAG	
Try::Cre	Fwd	GTCATCCCAGGGGTTGCTGG	473
Try::Cre	Rev	CCGCCGCATAACCAGTGA	
Pmel	Wild type Fwd	GGGTAAAGAAGAGGGGAGAGG	550 wt
Pmel	Wild type Rev	GGGATGTTCCATCACCTTCA	300 transgene
Pmel	Transgene Rev	AGGCAAATTTTGGTGTACGG	
NF1	Wild type Fwd	ACCTCTCTAGCCTCAGGAATG	450 wt
NF1	Wild type Rev	CTTCAGACTGATTGTTGTACC	350 neo

NF1	Neo Rev	TGATTCCCACTTTGTGGT TCT	
Generic cre	Cre Fwd	CCTGGAAAATGCTTCTGTCCG	390
Generic cre	Cre Rev	CAGGGTGTTATAAGCAATCCC	
Generic cre	Internal control Fwd	AACACACACTGGAGGACTGGCTA	290
Generic cre	Internal control Rev	CAATGGTAGGCTCACTCTGGGAG	
KitWv	Fwd	GCCCTAATGTCGGAACTGAA	270 wt *
KitWv	Rev	GTCTGAAGGCTCCCAGCATA	200 mut *

*Following 1 hour digest with NsiI.

All genotyping PCRs performed using DreamTaq Green (Thermo Fisher) apart from Fucci2a which required Phusion II hot start (Thermo Fisher). See …???? for protocol.

8.3.6 ES cell screen

Table 8.8:

Name	***Sequence***
Wt_Fwd	AAAGTCGCTCTGAGTTGTTAT
Wt_Rev	GGAGCGGGAGAAATGGATATG
Xu_Wt_For	GGCGGACTGGCGGGACTA

Rosa5_R1	CCGTAAATAGTCCACCCATTGACG
Rosa3_F1	GGTGGGCTCTATGGCTTCTG
Rosa3_R2	GGAGTAGTTACTCCACTTTCAAG

8.4 ImageJ macros

8.4.1 Melanoblast toolbox

Melanoblast toolbox is a bespoke ImageJ macro package written by Dr Richard Mort. In brief, the macros allow segmentation of fluorescent images followed by automated tracking of particles based on the wrMTrck script (http://www.phage.dk/plugins/wrmtrck.html). Additional macros allow for analysis of the tracking data including the generation of displacement plots and calculation of diffusion coefficients.

8.4.2 Fucci tools

Fucci tools is a novel ImageJ macro package written by Dr Richard Mort to allow quantitative tracking of Fucci expressing cells progressing through the cell cycle. Cells are either tracked manually or semi-automatically and a circle drawn around the nuclei at each time point and the fluorescence measured in each channel. The fluorescence is then self-normalised and plotted against time to generate normalised fluorescence intensity plots from which the lengths of G1 and S/G2/M can be calculated.

9 Bibliography

Aaltomaa, S., Lipponen, P., Eskelinen, M., Kosma, V.-M., Marin, S., Alhava, E., & Syrjänen, K. (1992). Mitotic indexes as prognostic predictors in female breast

cancer. *Journal of Cancer Research and Clinical Oncology*, *118*(1), 75–81. https://doi.org/10.1007/BF01192316

Abe, T., Kiyonari, H., Shioi, G., Inoue, K. I., Nakao, K., Aizawa, S., & Fujimori, T. (2011). Establishment of conditional reporter mouse lines at ROSA26 locus for live cell imaging. *Genesis*, *49*(7), 579–590. https://doi.org/10.1002/dvg.20753

Abe, T., Sakaue-Sawano, A., Kiyonari, H., Shioi, G., Inoue, K., Horiuchi, T., … Fujimori, T. (2013). Visualization of cell cycle in mouse embryos with Fucci2 reporter directed by Rosa26 promoter. *Development (Cambridge, England)*, *140*(1), 237–46. https://doi.org/10.1242/dev.084111

Adameyko, I., Lallemend, F., Aquino, J. B., Pereira, J. A., Topilko, P., Müller, T., … Ernfors, P. (2009). Schwann Cell Precursors from Nerve Innervation Are a Cellular Origin of Melanocytes in Skin. *Cell*, *139*(2), 366–379. https://doi.org/10.1016/j.cell.2009.07.049

Affolter, M., & Caussinus, E. (2008). Tracheal branching morphogenesis in Drosophila: new insights into cell behaviour and organ architecture. *Development (Cambridge, England)*, *135*(12), 2055–64. https://doi.org/10.1242/dev.014498

Afzelius, B, A. (1976). A human syndrome caused by immotile cilia. *Science*, *193*(4250), 317–319.

Akiyama, H., Chaboissier, M. C., Martin, J. F., Schedl, A., & De Crombrugghe, B. (2002). The transcription factor *Sox9* has essential roles in successive steps of the chondrocyte differentiation pathway and is required for expression of *Sox5* and *Sox6*. *Genes & Development*, *16*, 2813–2828. https://doi.org/10.1101/gad.1017802

Aktas, H., Cai, H., & Cooper, G. M. (1997). Ras links growth factor signaling to the cell cycle machinery via regulation of cyclin D1 and the Cdk inhibitor p27KIP1. *Molecular and Cellular Biology*, *17*(7), 3850–7. Retrieved from http://www.pubmedcentral.nih.gov/articlerender.fcgi?artid=232237&tool=pmcentrez&rendertype=abstract

Alberts, B., Johnson, A., Lewis, J., Raff, M., Roberts, K., & Walter, P. (2002). *Molecular Biology of the Cell*.

Almasan, A., Yin, Y., Kelly, R. E., Lee, E. Y., Bradley, A., Li, W., … Wahl, G. M. (1995). Deficiency of retinoblastoma protein leads to inappropriate S-phase entry, activation of E2F-responsive genes, and apoptosis. *Proceedings of the National Academy of Sciences of the United States of America*, *92*(12), 5436–5440. https://doi.org/10.1073/pnas.92.12.5436

Altman, J. (1963). Autoradiographic investigation of cell proliferation in the brains of rats and cats. *The Anatomical Record*, *145*, 573–591. https://doi.org/10.1002/ar.1091450409

Anderson, C. T., & Stearns, T. (2009). Centriole Age Underlies Asynchronous Primary Cilium Growth in Mammalian Cells. *Current Biology*, *19*(17), 1498–1502. https://doi.org/10.1016/j.cub.2009.07.034

Anderson, R. P., Voziyanova, E., & Voziyanov, Y. (2012). Flp and Cre expressed from Flp-2A-Cre and Flp-IRES-Cre transcription units mediate the highest level of dual recombinase-mediated cassette exchange. *Nucleic Acids Research*, *40*(8), 1–9. https://doi.org/10.1093/nar/gks027

Ang, X. L., & Harper, J. W. (2004). Interwoven ubiquitination oscillators and control of cell cycle transitions. *Science's STKE : Signal Transduction Knowledge Environment*, *2004*(242), pe31. https://doi.org/10.1126/stke.2422004pe31

Aoki, H., Yamada, Y., Hara, A., & Kunisada, T. (2009). Two distinct types of mouse melanocyte: differential signaling requirement for the maintenance of non-cutaneous and dermal versus epidermal melanocytes. *Development (Cambridge, England)*, *136*(15), 2511–2521. https://doi.org/10.1242/dev.037168

Aruga, J., & Mikoshiba, K. (2003). Identification and characterization of Slitrk, a novel neuronal transmembrane protein family controlling neurite outgrowth. *Molecular and Cellular Neuroscience*, *24*(1), 117–129. https://doi.org/10.1016/S1044-7431(03)00129-5

Aruga, J., Yokota, N., & Mikoshiba, K. (2003). Human SLITRK family genes: Genomic organization and expression profiling in normal brain and brain tumor tissue. *Gene*, *315*(1–2), 87–94. https://doi.org/10.1016/S0378-1119(03)00715-7

Babu, D., & Roy, S. (2013). Left-right asymmetry: cilia stir up new surprises in the node. *Open Biology*, *3*(5), 130052. https://doi.org/10.1098/rsob.130052

Ballabeni, A., Melixetian, M., Zamponi, R., Masiero, L., Marinoni, F., & Helin, K. (2004). Human Geminin promotes pre-RC formation and DNA replication by stabilizing CDT1 in mitosis. *The EMBO Journal*, *23*(15), 3122–3132. https://doi.org/10.1038/sj.emboj.7600314

Ballabeni, A., Park, I.-H., Zhao, R., Wang, W., Lerou, P. H., Daley, G. Q., & Kirschner, M. W. (2011). Cell cycle adaptations of embryonic stem cells. *Proceedings of the National Academy of Sciences of the United States of America*, *108*(48), 19252–7. https://doi.org/10.1073/pnas.1116794108

Bangs, F. K., Schrode, N., Hadjantonakis, A., & Anderson, K. V. (2015). Lineage specificity of primary cilia in the mouse embryo, *17*(2), 113–122. https://doi.org/10.1038/ncb3091.Lineage

Bannigan, J., & Langman, J. (1979). The cellular effect of 5-bromodeoxyuridine on the mammalian embryo. *Journal of Embryology and Experimental Morphology*, *50*, 123–35. Retrieved from http://www.ncbi.nlm.nih.gov/pubmed/458350

Bantikassegn, A., Song, X., & Politi, K. (2015). Isolation of Epithelial , Endothelial , and Immune Cells from Lungs of Transgenic Mice with Oncogene-Induced Lung Adenocarcinomas, *52*(4), 409–417. https://doi.org/10.1165/rcmb.2014-0312MA

Barber, G. N. (2001). Host defense, viruses and apoptosis. *Cell Death and Differentiation*, *8*(2), 113–126. https://doi.org/10.1038/sj.cdd.4400823

Bardet, P. L., Kolahgar, G., Mynett, A., Miguel-Aliaga, I., Briscoe, J., Meier, P., & Vincent, J. P. (2008). A fluorescent reporter of caspase activity for live imaging. *Proc Natl Acad Sci U S A*, *105*(37), 13901–13905.

https://doi.org/10.1073/pnas.0806983105

Behrends, J., Karsten, C. M., Wilke, S., Röbke, A., & Kruse, A. (2008). Identification of ITGA4/ITGB7 and ITGAE/ITGB7 expressing subsets of decidual dendritic-like cells within distinct microdomains of the pregnant mouse uterus. *Biology of Reproduction*, *79*(June), 624–632. https://doi.org/10.1095/biolreprod.107.067041

Bell, S. P., & Stillman, B. (1992). ATP-dependent recognition of eukaryotic origins of DNA replication by a multiprotein complex. *Nature*, *357*(6374), 128–34. https://doi.org/10.1038/357128a0

Bellusci, S., Furuta, Y., Rush, M. G., Henderson, R., Winnier, G., & Hogan, B. L. M. (1997). Involvement of Sonic hedgehog (Shh) in mouse embryonic lung growth and morphogenesis. *Development*, *124*, 53–63.

Bellusci, S., Grindley, J., Emoto, H., Itoh, N., & Hogan, B. L. (1997). Fibroblast growth factor 10 (FGF10) and branching morphogenesis in the embryonic mouse lung. *Development*, *124*, 4867–4878.

Belmokhtar, C. a, Hillion, J., & Ségal-Bendirdjian, E. (2001). Staurosporine induces apoptosis through both caspase-dependent and caspase-independent mechanisms. *Oncogene*, *20*(26), 3354–3362. https://doi.org/10.1038/sj.onc.1204436

Bicknell, L. S., Bongers, E. M. H. F., Leitch, A., Brown, S., Harley, M. E., Aftimos, S., … Mackenzie, J. (2011). Mutations in the Pre-Replication Complex cause Meier-Gorlin syndrome, *43*(4), 356–359. https://doi.org/10.1038/ng.775.Mutations

Blaheta, R. A., Kronenberger, B., Woitaschek, D., Weber, S., Scholz, M., Schuldes, H., … Markus, B. H. (1998). Development of an ultrasensitive in vitro assay to monitor growth of primary cell cultures with reduced mitotic activity. *Journal of Immunological Methods*, *211*(1–2), 159–169. https://doi.org/10.1016/S0022-1759(97)00202-0

Blanc, P., Coste, K., Pouchin, P., Azaïs, J.-M., Blanchon, L., Gallot, D., & Sapin, V. (2012). A role for mesenchyme dynamics in mouse lung branching morphogenesis. *PloS One*, *7*(7), e41643. https://doi.org/10.1371/journal.pone.0041643

Bochkov, Y. A., & Palmenberg, A. C. (2006). Translational efficiency of EMCV IRES in bicistronic vectors is dependent upon IRES sequence and gene location. *BioTechniques*, *41*(3), 283–292. https://doi.org/10.2144/000112243

Boos, A., Lee, A., Thompson, D. M., & Kroll, K. L. (2006). Subcellular translocation signals regulate Geminin activity during embryonic development. *Biology of the Cell / under the Auspices of the European Cell Biology Organization*, *98*, 363–375. https://doi.org/10.1042/BC20060007

Borman, A. M., Le Mercier, P., Girard, M., & Kean, K. M. (1996). Comparison of Picornaviral IRES-Driven Internal Initiation of Translation in Cultured Cells of Different Origins. *Nucleic Acids Research*, *25*(5), 925–932. https://doi.org/10.1093/nar/25.5.925

Boström, H., Willetts, K., Pekny, M., Levéen, P., Lindahl, P., Hedstrand, H., … Betsholtz, C. (1996). PDGF-A signaling is a critical event in lung alveolar myofibroblast development and alveogenesis. *Cell*, *85*(6), 863–873. https://doi.org/10.1016/S0092-8674(00)81270-2

Bradford, J. A., & Clarke, S. T. (2011). Dual-pulse labeling using 5-ethynyl-2'-deoxyuridine (Edu) and 5-bromo-2'-deoxyuridine (BrdU) in flow cytometry. *Current Protocols in Cytometry*, (SUPPL.55). https://doi.org/10.1002/0471142956.cy0738s55

Bragg, A. D., Moses, H. L., & Serra, R. (2001). Signaling to the epithelium is not sufficient to mediate all of the effects of transforming growth factor ?? and bone morphogenetic protein 4 on murine embryonic lung development. *Mechanisms of Development*, *109*(1), 13–26. https://doi.org/10.1016/S0925-4773(01)00508-1

Brocard, J., Warot, X., Wendling, O., Messaddeq, N., Vonesch, J. L., Chambon, P.,

& Metzger, D. (1997). Spatio-temporally controlled site-specific somatic mutagenesis in the mouse. *Proceedings of the National Academy of Sciences of the United States of America*, *94*(26), 14559–14563. https://doi.org/10.1073/pnas.94.26.14559

Broker, L. E., Kruyt, F. A. E., & Giaccone, G. (2005). Cell death independent of caspases: A review. *Clinical Cancer Research*, *11*(9), 3155–3162. https://doi.org/10.1158/1078-0432.CCR-04-2223

Bronson, S. K., Plaehn, E. G., Kluckman, K. D., & Maeda, N. (1996). Single-copy transgenic mice with chosen-site integration. *Proceedings of the National Academy of Sciences of the United States of America*, *93*(August), 9067–9072. https://doi.org/10.1073/pnas.93.17.9067

Bubendorf, L., Sauter, G., Moch, H., Schmid, H. P., Gasser, T. C., Jordan, P., & Mihatsch, M. J. (1996). Ki67 labelling index: an independent predictor of progression in prostate cancer treated by radical prostatectomy. *The Journal of Pathology*, *178*(4), 437–41. https://doi.org/10.1002/(SICI)1096-9896(199604)178:4<437::AID-PATH484>3.0.CO;2-4

Calegari, F., & Huttner, W. B. (2003). An inhibition of cyclin-dependent kinases that lengthens, but does not arrest, neuroepithelial cell cycle induces premature neurogenesis. *Journal of Cell Science*, *116*(Pt 24), 4947–55. https://doi.org/10.1242/jcs.00825

Campos, E. I., & Reinberg, D. (2009). Histones: annotating chromatin. *Annual Review of Genetics*, *43*(1), 559–99. https://doi.org/10.1146/annurev.genet.032608.103928

Carey, B. W., Markoulaki, S., Hanna, J., Saha, K., Gao, Q., Mitalipova, M., & Jaenisch, R. (2009). Reprogramming of murine and human somatic cells using a single polycistronic vector. *Proceedings of the National Academy of Sciences of the United States of America*, *106*(1), 157–62. https://doi.org/10.1073/pnas.0811426106

Caspary, T., Larkins, C. E., & Anderson, K. V. (2007). The Graded Response to

Sonic Hedgehog Depends on Cilia Architecture. *Developmental Cell*, *12*(5), 767–778. https://doi.org/10.1016/j.devcel.2007.03.004

Casper, A. M., Nghiem, P., Arlt, M. F., & Glover, T. W. (2002). ATR regulates fragile site stability. *Cell*, *111*(6), 779–789. https://doi.org/10.1016/S0092-8674(02)01113-3

Cebra-Thomas, J. A., Bromer, J., Gardner, R., Lam, G. K., Sheipe, H., & Gilbert, S. F. (2003). T-box gene products are required for mesenchymal induction of epithelial branching in the embryonic mouse lung. *Developmental Dynamics*, *226*(1), 82–90. https://doi.org/10.1002/dvdy.10208

Cebrian, C., Borodo, K., Charles, N., & Herzlinger, D. A. (2004). Morphometric index of the developing murine kidney. *Developmental Dynamics*, *231*(3), 601–608. https://doi.org/10.1002/dvdy.20143

Chae, H. J., Kang, J. S., Byun, J. O., Han, K. S., Kim, D. U., Oh, S. M., … Kim, H. R. (2000). Molecular mechanism of staurosporine-induced apoptosis in osteoblasts. *Pharmacological Research*, *42*(4), 373–81. https://doi.org/10.1006/phrs.2000.0700

Chapman, D. L., Garvey, N., Hancock, S., Alexiou, M., Agulnik, S. I., Gibson-Brown, J. J., … Papaioannou, V. E. (1996). Expression of the T-box Family Genes, Tbxl-Tbx5, During Early Mouse Development. *Developmental Dynamics*, *206*, 379–390.

Chen, C., Krohn, J., Bhattacharya, S., & Davies, B. (2011). A comparison of exogenous promoter activity at the ROSA26 locus using a PhiC31 integrase mediated cassette exchange approach in mouse ES cells. *PloS One*, *6*(8), e23376. https://doi.org/10.1371/journal.pone.0023376

Chiang, C., Litingtung, Y., Lee, E., Young, K. E., Corden, J. L., Westphal, H., & Beachy, P. a. (1996). Cyclopia and defective axial patterning in mice lacking Sonic hedgehog gene function. *Nature*. https://doi.org/10.1038/383407a0

Chinnasamy, D., Milsom, M. D., Shaffer, J., Neuenfeldt, J., Shaaban, A. F.,

Margison, G. P., … Chinnasamy, N. (2006). Multicistronic lentiviral vectors containing the FMDV 2A cleavage factor demonstrate robust expression of encoded genes at limiting MOI. *Virology Journal*, *3*, 14. https://doi.org/10.1186/1743-422X-3-14

Cho, H.-C., Lai, C.-Y., Shao, L.-E., & Yu, J. (2011). Identification of Tumorigenic Cells in KrasG12D -Induced Lung Adenocarinoma. *Tumor and Stem Cell Biology*, *71*(23), 7250–7258.

Chuang, P. T., Kawcak, T., & McMahon, A. P. (2003). Feedback control of mammalian Hedgehog signaling by the Hedgehog-binding protein, Hip1, modulates Fgf signaling during branching morphogenesis of the lung. *Genes and Development*. https://doi.org/10.1101/gad.1026303

Ciavatta, D., Kalantry, S., Magnuson, T., & Smithies, O. (2006). A DNA insulator prevents repression of a targeted X-linked transgene but not its random or imprinted X inactivation. *Proceedings of the National Academy of Sciences of the United States of America*, *103*(26), 9958–9963. https://doi.org/10.1073/pnas.0603754103

Coller, H. A., Sang, L., & Roberts, J. M. (2006). A new description of cellular quiescence. *PLoS Biology*, *4*(3), 0329–0349. https://doi.org/10.1371/journal.pbio.0040083

Colombo, S., Champeval, D., Rambow, F., & Larue, L. (2012). Transcriptomic analysis of mouse embryonic skin cells reveals previously unreported genes expressed in melanoblasts. *The Journal of Investigative Dermatology*, *132*(1), 170–8. https://doi.org/10.1038/jid.2011.252

Concha, M. L., & Adams, R. J. (1998). Oriented cell divisions and cellular morphogenesis in the zebrafish gastrula and neurula : a time-lapse analysis. *Development*, *125*, 983–994.

Corbit, K. C., Shyer, A. E., Dowdle, W. E., Gaulden, J., Singla, V., Chen, M.-H., … Reiter, J. F. (2008). Kif3a constrains beta-catenin-dependent Wnt signalling through dual ciliary and non-ciliary mechanisms. *Nature Cell Biology*, *10*(1),

70–76. https://doi.org/10.1038/ncb1670

Cormack, B. P., Bertram, G., Egerton, M., Gow, N. A. R., Falkow, S., & Brown, A. J. P. (1995). Yeast-enhanced green fluorescent protein (yEGFP): a reporter of gene expression in Candida albicans, (1 997), 303–311.

Coronado, D., Godet, M., Bourillot, P. Y., Tapponnier, Y., Bernat, A., Petit, M., … Savatier, P. (2013). A short G1 phase is an intrinsic determinant of naive embryonic stem cell pluripotency. *Stem Cell Research*, *10*(1), 118–131. https://doi.org/10.1016/j.scr.2012.10.004

Cortellino, S., Wang, C., Wang, B., Bassi, M. R., Caretti, E., Champeval, D., … Bellacosa, A. (2009). Defective ciliogenesis, embryonic lethality and severe impairment of the Sonic Hedgehog pathway caused by inactivation of the mouse complex A intraflagellar transport gene Ift122/Wdr10, partially overlapping with the DNA repair gene Med1/Mbd4. *Developmental Biology*, *325*(1), 225–237. https://doi.org/10.1016/j.ydbio.2008.10.020

Cvetkovic, B., Yang, B., Williamson, R. A., & Sigmund, C. D. (2000). Appropriate tissue- and cell-specific expression of a single copy human angiotensinogen transgene specifically targeted upstream of the HPRT locus by homologous recombination. *Journal of Biological Chemistry*, *275*(2), 1073–1078. https://doi.org/10.1074/jbc.275.2.1073

Dahlfors, G., & Arnqvist, H. J. (2000). Vascular Endothelial Growth Factor and Transforming Large Vessel Endothelial Cells *. *Enodcrinology*, *141*(6), 2062–2067.

Das, T., Payer, B., Cayouette, M., & Harris, W. A. (2003). In vivo time-lapse imaging of cell divisions during neurogenesis in the developing zebrafish retina. *Neuron*, *37*(4), 597–609. https://doi.org/10.1016/S0896-6273(03)00066-7

Davidson, A. (2008). Mouse kidney development. *StemBook*, 1–30. https://doi.org/10.3824/stembook.1.34.1

Davies, J. A. (2002). Do different branching epithelia use a conserved developmental

mechanism? *BioEssays*, *24*(10), 937–948. https://doi.org/10.1002/bies.10161

de Felipe, P. (2004). Skipping the co-expression problem: the new 2A "CHYSEL" technology. *Genetic Vaccines and Therapy*, *2*(1), 13. https://doi.org/10.1186/1479-0556-2-13

De Felipe, P., Luke, G. A., Brown, J. D., & Ryan, M. D. (2010). Inhibition of 2A-mediated "cleavage" of certain artificial polyproteins bearing N-terminal signal sequences. *Biotechnology Journal*, *5*(2), 213–223. https://doi.org/10.1002/biot.200900134

De Langhe, S. P., Sala, F. G., Del Moral, P. M., Fairbanks, T. J., Yamada, K. M., Warburton, D., … Bellusci, S. (2005). Dickkopf-1 (DKK1) reveals that fibronectin is a major target of Wnt signaling in branching morphogenesis of the mouse embryonic lung. *Developmental Biology*, *277*(2), 316–331. https://doi.org/10.1016/j.ydbio.2004.09.023

De Moerlooze, L., Spencer-Dene, B., Revest, J. M., Hajihosseini, M., Rosewell, I., & Dickson, C. (2000). An important role for the IIIb isoform of fibroblast growth factor receptor 2 (FGFR2) in mesenchymal-epithelial signalling during mouse organogenesis. *Development (Cambridge, England)*, *127*(3), 483–492. https://doi.org/10.1016/0092-8674(91)90616-7

Dean, C. H., Miller, L.-A. D., Smith, A. N., Dufort, D., Lang, R. a, & Niswander, L. a. (2005). Canonical Wnt signaling negatively regulates branching morphogenesis of the lung and lacrimal gland. *Developmental Biology*, *286*(1), 270–286. https://doi.org/10.1016/j.ydbio.2005.07.034

De Schepper, S., Maertens, O., Callens, T., Naeyaert, J.-M., Lambert, J., & Messiaen, L. (2008). Somatic mutation analysis in NF1 café au lait spots reveals two NF1 hits in the melanocytes. *The Journal of Investigative Dermatology*, *128*(4), 1050–3. https://doi.org/10.1038/sj.jid.5701095

Dehay, C., & Kennedy, H. (2007). Cell-cycle control and cortical development. *Nature Reviews Neuroscience*, *8*(6), 438–450. https://doi.org/10.1038/nrn2097

Delling, M., DeCaen, P. G., Doerner, J. F., Febvay, S., & Clapham, D. E. (2013a). Primary cilia are specialized calcium signalling organelles. *Nature*, *504*(7479), 311–314. https://doi.org/10.1038/nature12833

Delling, M., DeCaen, P. G., Doerner, J. F., Febvay, S., & Clapham, D. E. (2013b). Primary cilia are specialized calcium signalling organelles. *Nature*, *504*(7479), 311–314. https://doi.org/10.1038/nature12833

Delmas, V., Martinozzi, S., Bourgeois, Y., Holzenberger, M., & Larue, L. (2003). Cre-mediated recombination in the skin melanocyte lineage. *Genesis (New York, N.Y. : 2000)*, *36*(2), 73–80. https://doi.org/10.1002/gene.10197

Desai, T. J., Malpel, S., Flentke, G. R., Smith, S. M., & Cardoso, W. V. (2004). Retinoic acid selectively regulates Fgf10 expression and maintains cell identity in the prospective lung field of the developing foregut. *Developmental Biology*, *273*(2), 402–415. https://doi.org/10.1016/j.ydbio.2004.04.039

Desbaillets, I., Ziegler, U., Groscurth, P., & Gassmann, M. (2000). Embryoid bodies: an in vitro model of mouse embryogenesis. *Experimental Physiology*, *85*(6), 645–651.

Devenport, D. (2014). The cell biology of planar cell polarity. *Journal of Cell Biology*, *207*(2), 171–179. https://doi.org/10.1083/jcb.201408039

Diwakar, G., Zhang, D., Jiang, S., & Hornyak, T. J. (2008). Neurofibromin as a regulator of melanocyte development and differentiation. *Journal of Cell Science*, *121*, 167–177. https://doi.org/10.1242/jcs.013912

Donnelly, M. L. L., Hughes, L. E., Luke, G., Mendoza, H., ten Dam, E., Gani, D., & Ryan, M. D. (2001). The “cleavage”activities of foot-and-mouth disease virus 2A site-directed mutants and naturally occurring “2A-like”sequences. *Journal of General Virology*, *82*(5), 1027–1041. https://doi.org/10.1099/0022-1317-82-5-1027

Donnelly, M. L. L., Luke, G., Mehrotra, A., Li, X., Hughes, L. E., Gani, D., & Ryan, M. D. (2001). Analysis of the aphthovirus 2A/2B polyprotein “cleavage”

mechanism indicates not a proteolytic reaction, but a novel translational effect: A putative ribosomal “skip.” *Journal of General Virology*, *82*(5), 1013–1025. https://doi.org/10.1099/0022-1317-82-5-1013

Dou, Q. P., Levin, A. H., Zhao, S., & Pardee, A. B. (1993). Cyclin E and cyclin A as candidates for the restriction point protein. *Cancer Research*, *53*(7), 1493–1497.

Driessens, G., Beck, B., Caauwe, A., Simons, B. D., & Blanpain, C. (2012). Defining the mode of tumour growth by clonal analysis. *Nature*, *488*(7412), 527–530. https://doi.org/10.1038/nature11344

Duque, a., & Rakic, P. (2011). Different Effects of Bromodeoxyuridine and [3H]Thymidine Incorporation into DNA on Cell Proliferation, Position, and Fate. *Journal of Neuroscience*. https://doi.org/10.1523/JNEUROSCI.3092-11.2011

Duttlinger, R., Manova, K., Chu, T. Y., Gyssler, C., Zelenetz, a D., Bachvarova, R. F., & Besmer, P. (1993). W-sash affects positive and negative elements controlling c-kit expression: ectopic c-kit expression at sites of kit-ligand expression affects melanogenesis. *Development (Cambridge, England)*, *118*(3), 705–717.

Eblaghie, M. C., Reedy, M., Oliver, T., Mishina, Y., & Hogan, B. L. M. (2006). Evidence that autocrine signaling through Bmpr1a regulates the proliferation, survival and morphogenetic behavior of distal lung epithelial cells. *Developmental Biology*, *291*(1), 67–82. https://doi.org/10.1016/j.ydbio.2005.12.006

El-Hashash, A. H. K., Turcatel, G., Al Alam, D., Buckley, S., Tokumitsu, H., Bellusci, S., & Warburton, D. (2011). Eya1 controls cell polarity, spindle orientation, cell fate and Notch signaling in distal embryonic lung epithelium. *Development (Cambridge, England)*, *138*(7), 1395–1407. https://doi.org/10.1242/dev.058479

El-Hashash, A., & Warburton, D. (2011). Cell polarity and spindle orientation in the distal epithelium of embryonic lung, *2*(140), 441–445.

https://doi.org/10.1126/scisignal.2001449.Engineering

Engert, S., Burtscher, I., Kalali, B., Gerhard, M., & Lickert, H. (2013). The Sox17CreERT2 knock-in mouse line displays spatiotemporal activation of Cre recombinase in distinct Sox17 lineage progenitors. *Genesis (New York, N.Y. : 2000)*, *51*(11), 793–802. https://doi.org/10.1002/dvg.22714

Engert, S., Liao, W. P., Burtscher, I., & Lickert, H. (2009). Sox17-2A-iCre: a knock-in mouse line expressing Cre recombinase in endoderm and vascular endothelial cells. *Genesis (New York, N.Y. : 2000)*, *47*(9), 603–10. https://doi.org/10.1002/dvg.20540

Erickson, C. A., Duong, T. D., & Tosney, K. W. (1992). Descriptive and experimental analysis of the dispersion of neural crest cells along the dorsolateral path and their entry into ectoderm in the chick embryo. *Developmental Biology*, *151*(1), 251–272. https://doi.org/10.1016/0012-1606(92)90231-5

Evans, T., Rosenthal, E. T., Youngblom, J., Distel, D., & Hunt, T. (1983). Cyclin: A protein specified by maternal mRNA in sea urchin eggs that is destroyed at each cleavage division. *Cell*, *33*(2), 389–396. https://doi.org/10.1016/0092-8674(83)90420-8

Feil, R., Brocard, J., Mascrez, B., LeMeur, M., Metzger, D., & Chambon, P. (1996). Ligand-activated site-specific recombination in mice. *Proceedings of the National Academy of Sciences of the United States of America*, *93*(20), 10887–90. https://doi.org/10.1073/pnas.93.20.10887

Feil, R., Wagner, J., Metzger, D., & Chambon, P. (1997). Regulation of Cre Recombinase Activity by Mutated Estrogen Receptor Ligand-Binding Domains. *Biochemical and Biophysical Research Communications*, *237*(3), 752–757. https://doi.org/10.1006/bbrc.1997.7124

Feng, G., & Kaplowitz, N. (2002). Mechanism of staurosporine-induced apoptosis in murine hepatocytes. *AJ-Gastrointest. Liver Physiol.*, *282*, G825–G834. https://doi.org/10.1152/ajpgi.00467.2001

Fish, J. L., Kosodo, Y., Enard, W., Pääbo, S., & Huttner, W. B. (2006). Aspm specifically maintains symmetric proliferative divisions of neuroepithelial cells. *Proceedings of the National Academy of Sciences of the United States of America*, *103*(27), 10438–43. https://doi.org/10.1073/pnas.0604066103

Friedrich, G., & Soriano, P. (1991). Promoter traps in embryonic stem cells: A genetic screen to identify and mutate developmental genes in mice. *Genes and Development*, *5*(9), 1513–1523. https://doi.org/10.1101/gad.5.9.1513

Fuchs, Y., & Steller, H. (2011). Programmed cell death in animal development and disease. *Cell*, *147*(4), 742–758. https://doi.org/10.1016/j.cell.2011.10.033

Fujii-Yamamoto, H., Jung, M. K., Arai, K. I., & Masai, H. (2005). Cell cycle and developmental regulations of replication factors in mouse embryonic stem cells. *Journal of Biological Chemistry*, *280*(13), 12976–12987. https://doi.org/10.1074/jbc.M412224200

Fujino, N., Kubo, H., Ota, C., Suzuki, T., Suzuki, S., & Yamada, M. (2012). A Novel Method for Isolating Individual Cellular Components from the Adult Human Distal Lung. *Cell Mol Biol*, *46*(4), 422–430. https://doi.org/10.1165/rcmb.2011-0172OC

Gaglia, P., Bernardi, A., Venesio, T., Caldarola, B., Lauro, D., Cappa, A. P. M., … Liscia, D. S. (1993). Cell proliferation of breast cancer evaluated by anti-BrdU and anti-Ki-67 antibodies: Its prognostic value on short-term recurrences. *European Journal of Cancer*, *29*(11), 1509–1513. https://doi.org/10.1016/0959-8049(93)90284-M

Gao, S. Y., Jack, M. M., & O'Neill, C. (2012). Towards optimising the production of and expression from polycistronic vectors in embryonic stem cells. *PLoS ONE*, *7*(11), e48668. https://doi.org/10.1371/journal.pone.0048668

Glover, J. D., Knolle, S., Wells, K. L., Liu, D., Jackson, I. J., Mort, R. L., & Headon, D. J. (2015). Maintenance of Distinct Melanocyte Populations in the Interfollicular Epidermis. *Pigment Cell & Melanoma Research*, n/a-n/a. https://doi.org/10.1111/pcmr.12375

Goh, L. K., & Sorkin, A. (2013). Endocytosis of Receptor Tyrosine Kinases. *CSH Perspectives in Biology*, 1–18.

Gong, Y., Gong, Y., Mo, C., Mo, C., Fraser, S. E., & Fraser, S. E. (2004). Planar cell polarity signalling controls cell division orientation during zebra sh gastrulation. *Nature*, *430*(August), 689–693. https://doi.org/10.1038/nature02789.Published

Gontan, C., de Munck, A., Vermeij, M., Grosveld, F., Tibboel, D., & Rottier, R. (2008). Sox2 is important for two crucial processes in lung development: Branching morphogenesis and epithelial cell differentiation. *Developmental Biology*, *317*(1), 296–309. https://doi.org/10.1016/j.ydbio.2008.02.035

Goss, A. M., Tian, Y., Tsukiyama, T., Cohen, E. D., Zhou, D., Lu, M. M., … Morrisey, E. E. (2009). Wnt2/2b and beta-catenin signaling are necessary and sufficient to specify lung progenitors in the foregut. *Developmental Cell*, *17*(2), 290–8. https://doi.org/10.1016/j.devcel.2009.06.005

Götz, M., & Huttner, W. B. (2005). The cell biology of neurogenesis. *Nat Rev Mol Cell Biol*, *6*(10), 777–788. https://doi.org/10.1038/nrm1739

Gratzner, H. G. (1982). Monoclonal Antibody to 5-Bromo- and 5-Iododeoxyuridine : A New Reagent for Detection of DNA Replication Placental Mononuclear Phagocytes as a Source of Interleukin-1. *Science*, *218*(October), 474–475.

Gratzner, H. G., Leif, R. C., Ingram, D. J., & Castro, A. (1975). The use of antibody specific for bromodeoxyuridine for the immunofluorescent determination of DNA replication in single cells and chromosomes. *Experimental Cell Research*, *95*(1), 88–94. https://doi.org/10.1016/0014-4827(75)90612-6

Greenstone, M. A., Jones, R. W. A., Dewar, A., Neville, B. G. R., & Cole, R. J. (1984). Hydrocephalus and Primary Ciliary Dyskinesia. *Archives of Disease in Childhood*, *59*(5), 481–2. https://doi.org/10.1177/0883073811429856

Guadiana, S. M., Semple-Rowland, S., Daroszewski, D., Madorsky, I., Breunig, J. J., Mykytyn, K., & Sarkisian, M. R. (2013). Arborization of dendrites by developing neocortical neurons is dependent on primary cilia and type 3

adenylyl cyclase. *The Journal of Neuroscience : The Official Journal of the Society for Neuroscience*. https://doi.org/10.1523/JNEUROSCI.2906-12.2013

Guillot, P. V, Liu, L., Kuivenhoven, J. A., Guan, J., Rosenberg, R. D., & Aird, W. C. (2000). Targeting of human eNOS promoter to the Hprt locus of mice leads to tissue-restricted transgene expression. *Physiol Genomics*, *2*(2), 77–83. Retrieved from http://www.ncbi.nlm.nih.gov/cgi-bin/Entrez/referer?http://physiolgenomics.physiology.org/cgi/content/abstract/2/2/77

Gustafsson, C., Govindarajan, S., & Minshull, J. (2004). Codon bias and heterologous protein expression. *Trends in Biotechnology*, *22*(7), 346–353. https://doi.org/10.1016/j.tibtech.2004.04.006

Haanen, C., & Vermes, I. (1995). Apoptosis and inflammation. *Mediators of Inflammation*, *4*(1), 5–15. https://doi.org/10.1155/S0962935195000020

Habets, P. E. M. H., Clout, D. E. W., Lekanne Deprez, R. H., Van Roon, M. A., Moorman, A. F. M., & Christoffels, V. M. (2003). Cardiac expression of Gal4 causes cardiomyopathy in a dose-dependent manner. *Journal of Muscle Research {&} Cell Motility*, *24*(2), 205–209. https://doi.org/10.1023/A:1026055612227

Häcker, G. (2000). The morphology of apoptosis. *Cell and Tissue Research*, *301*(1), 5–17. https://doi.org/10.1007/s004410000193

Hacohen, N., Kramer, S., Sutherland, D., Hiromi, Y., & Krasnow, M. A. (1998). sprouty encodes a novel antagonist of FGF signaling that patterns apical branching of the Drosophila airways. *Cell*, *92*(2), 253–263. https://doi.org/10.1016/S0092-8674(00)80919-8

Hadjantonakis, A.-K., & Papaioannou, V. E. (2004). Dynamic in vivo imaging and cell tracking using a histone fluorescent protein fusion in mice. *BMC Biotechnology*, *4*(1), 33. https://doi.org/10.1186/1472-6750-4-33

Hakem, R., Hakem, A., Duncan, G. S., Henderson, J. T., Woo, M., Soengas, M. S.,

… Mak, T. W. (1998). Differential requirement for Caspase 9 in apoptotic pathways in vivo. *Cell*, *94*(3), 339–352. https://doi.org/10.1016/S0092-8674(00)81477-4

Han, R. N. N., Post, M., Tanswell, A. K., & Lye, S. J. (2003). Insulin-Like Growth Factor-I Receptor–Mediated Vasculogenesis/Angiogenesis in Human Lung Development. *American Journal of Respiratory Cell and Molecular Biology*, *28*(2), 159–169. https://doi.org/10.1165/rcmb.4764

Han, Y., Kim, H. J., Dlugosz, A. A., Ellison, D. W., Richard, J., & Alvarez-buylla, A. (2009). Dual and opposing roles of primary cilia in medulloblastoma development. *Nat Med*, *15*(9), 1062–1065. https://doi.org/10.1038/nm.2020.Dual

Hari, L., Miescher, I., Shakhova, O., Suter, U., Chin, L., Taketo, M., … Sommer, L. (2012). Temporal control of neural crest lineage generation by Wnt/β-catenin signaling. *Development (Cambridge, England)*, *139*(12), 2107–17. https://doi.org/10.1242/dev.073064

Harova, L. V. S., Harov, A. A. S., Edorezov, T. N., Iao, Y. P., Haik, N. S., & Minoru, S. H. K. O. (2009). Database for mRNA Half-Life of 19 977 Genes Obtained by DNA Microarray Analysis of Pluripotent and Differentiating Mouse Embryonic Stem Cells, 45–58.

Harris-Johnson, K. S., Domyan, E. T., Vezina, C. M., & Sun, X. (2009). beta-Catenin promotes respiratory progenitor identity in mouse foregut. *Proceedings of the National Academy of Sciences of the United States of America*, *106*(38), 16287–92. https://doi.org/10.1073/pnas.0902274106

Harris, M. E., Böhni, R., Schneiderman, M. H., Ramamurthy, L., Schümperli, D., & Marzluff, W. F. (1991). Regulation of histone mRNA in the unperturbed cell cycle: evidence suggesting control at two posttranscriptional steps. *Molecular and Cellular Biology*, *11*(5), 2416–24. https://doi.org/10.1128/MCB.11.5.2416.Updated

Harris, S. L., & Levine, A. J. (2005). The p53 pathway: positive and negative

feedback loops. *Oncogene*, *24*(17), 2899–2908. https://doi.org/10.1038/sj.onc.1208615

Hartwell, L. H. (1976). Sequential function of gene products relative to DNA synthesis in the yeast cell cycle. *Journal of Molecular Biology*, *104*(4), 803–817. https://doi.org/10.1016/0022-2836(76)90183-2

Hasegawa, K., Cowan, A. B., Nakatsuji, N., & Suemori, H. (2007). Efficient multicistronic expression of a transgene in human embryonic stem cells. *Stem Cells*, *25*(7), 1707–1712. https://doi.org/10.1634/stemcells.2006-0813

Hashimoto, S., Chen, H., Que, J., Brockway, B. L., Drake, J. a., Snyder, J. C., … Stripp, B. R. (2012). B-Catenin-SOX2 signaling regulates the fate of developing airway epithelium. *Journal of Cell Science*, *125*(4), 932–942. https://doi.org/10.1242/jcs.092734

Hassounah, N. B., Nagle, R., Saboda, K., Roe, D. J., Dalkin, B. L., & McDermott, K. M. (2013). Primary Cilia Are Lost in Preinvasive and Invasive Prostate Cancer. *PLoS ONE*, *8*(7), 1–19. https://doi.org/10.1371/journal.pone.0068521

Hayashi, H., Sano, H., Seo, S., & Kume, T. (2008). The Foxc2 transcription factor regulates angiogenesis via induction of integrin beta3 expression. *The Journal of Biological Chemistry*, *283*(35), 23791–23800. https://doi.org/10.1074/jbc.M800190200

Heine, U. I., Munoz, E. F., Flanders, K. C., Roberts, a B., & Sporn, M. B. (1990). Colocalization of TGF-beta 1 and collagen I and III, fibronectin and glycosaminoglycans during lung branching morphogenesis. *Development (Cambridge, England)*, *109*(1), 29–36.

Hellen, C. U. T., & Sarnow, P. (2001). Internal ribosome entry sites in eukaryotic mRNA molecules Internal ribosome entry sites in eukaryotic mRNA molecules. https://doi.org/10.1101/gad.891101

Hinchcliffe, E. H., & Sluder, G. (2001). "It takes two to tango": Understanding how centrosome duplication is regulated throughout the cell cycle. *Genes and*

Development. https://doi.org/10.1101/gad.894001

Hinds, P. W., Mittnacht, S., Dulic, V., Arnold, A., Reed, S. I., & Weinberg, R. A. (1992). Regulation of retinoblastoma protein functions by ectopic expression of human cyclins. *Cell*, *70*(6), 993–1006. https://doi.org/10.1016/0092-8674(92)90249-C

Hirobe, T. (1984). Histochemical survey of the distribution of the epidermal melanoblasts and melanocytes in the mouse during fetal and postnatal periods. *The Anatomical Record*, *208*(4), 589–594. https://doi.org/10.1002/ar.1092080414

Hirokawa, N. (2000). Stirring up development with the heterotrimeric kinesin KIF3. *Traffic (Copenhagen, Denmark)*, *1*, 29–34. https://doi.org/10.1034/j.1600-0854.2000.010105.x

Hitoshi, N., Ken-ichi, Y., & Jun-ichi, M. (1991). Efficient selection for high-expression transfectants with a novel eukaryotic vector. *Gene*, *108*(2), 193–199. https://doi.org/10.1016/0378-1119(91)90434-D

Hochegger, H., Takeda, S., & Hunt, T. (2008). Cyclin-dependent kinases and cell-cycle transitions: does one fit all? *Nature Reviews. Molecular Cell Biology*, *9*(11), 910–916. https://doi.org/10.1038/nrm2510

Hoess, R. H., & Abremski, K. (1985). Mechanism of strand cleavage and exchange in the Cre-lox site-specific recombination system. *Journal of Molecular Biology*, *181*(3), 351–362. https://doi.org/10.1016/0022-2836(85)90224-4

Houde, C., Dickinson, R. J., Houtzager, V. M., Cullum, R., Montpetit, R., Metzler, M., … Nicholson, D. W. (2006). Hippi is essential for node cilia assembly and Sonic hedgehog signaling. *Developmental Biology*, *300*(2), 523–533. https://doi.org/10.1016/j.ydbio.2006.09.001

Hoy, C. a, Lewis, E. D., & Schimke, R. T. (1990). Perturbation of DNA replication and cell cycle progression by commonly used [3H]thymidine labeling protocols. *Molecular and Cellular Biology*, *10*(4), 1584–92. Retrieved from

http://www.pubmedcentral.nih.gov/articlerender.fcgi?artid=362263&tool=pmcentrez&rendertype=abstract

Huangfu, D., Liu, A., Rakeman, A., Murcia, N., Nilswander, L., & Anderson, K. (2003). Hedgehog signalling in the mouse requires intraflagellar transport proteins. *Nature*, *426*(November), 83–87. https://doi.org/10.1038/nature02080.1.

Hunkapiller, J., Singla, V., Seol, A., & Reiter, J. F. (2011). The ciliogenic protein Oral-Facial-Digital 1 regulates the neuronal differentiation of embryonic stem cells. *Stem Cells and Development*, *20*(5), 831–841. https://doi.org/10.1089/scd.2010.0362

Ibañez-Tallon, I., Heintz, N., & Omran, H. (2003). To beat or not to beat: roles of cilia in development and disease. *Human Molecular Genetics*. https://doi.org/10.1093/hmg/ddg061

Ibrahimi, A., Vande Velde, G., Reumers, V., Toelen, J., Thiry, I., Vandeputte, C., … Gijsbers, R. (2009). Highly efficient multicistronic lentiviral vectors with peptide 2A sequences. *Human Gene Therapy*, *20*(8), 845–860. https://doi.org/10.1089/hum.2008.188

Ikemura, T. (1981). Correlation between the abundance of Escherichia coli transfer RNAs and the occurrence of the respective codons in its protein genes: A proposal for a synonymous codon choice that is optimal for the E. coli translational system. *Journal of Molecular Biology*, *151*(3), 389–409. https://doi.org/10.1016/0022-2836(81)90003-6

Indra, A. K., Warot, X., Brocard, J., Bornert, J. M., Xiao, J. H., Chambon, P., & Metzger, D. (1999). Temporally-controlled site-specific mutagenesis in the basal layer of the epidermis: Comparison of the recombinase activity of the tamoxifen-inducible Cre-ER(T) and Cre-ER(T2) recombinases. *Nucleic Acids Research*, *27*(22), 4324–4327. https://doi.org/10.1093/nar/27.22.4324

Ishimi, Y. (1997). A DNA helicase activity is associated with an MCM4, -6, and -7 protein complex. *J Biol Chem*, *272*(39), 24508–24513.

https://doi.org/10.1074/jbc.272.39.24508

Ito, T., Kagoshima, M., Sasaki, Y., Li, C., Udaka, N., Kitsukawa, T., … Goshima, Y. (2000). Repulsive axon guidance molecule Sema3A inhibits branching morphogenesis of fetal mouse lung. *Mechanisms of Development*, *97*(1–2), 35–45. https://doi.org/10.1016/S0925-4773(00)00401-9

Itskovitz-Eldor, J., Schuldiner, M., Karsenti, D., Eden, a, Yanuka, O., Amit, M., … Benvenisty, N. (2000). Differentiation of human embryonic stem cells into embryoid bodies compromising the three embryonic germ layers. *Molecular Medicine (Cambridge, Mass.)*, *6*(2), 88–95. https://doi.org/10859025

Iwai, H., Züger, S., Jin, J., & Tam, P. H. (2006). Highly efficient protein trans-splicing by a naturally split DnaE intein from Nostoc punctiforme. *FEBS Letters*, *580*(7), 1853–1858. https://doi.org/10.1016/j.febslet.2006.02.045

Izvolsky, K. I., Shoykhet, D., Yang, Y., Yu, Q., Nugent, M. A., & Cardoso, W. V. (2003). Heparan sulfate-FGF10 interactions during lung morphogenesis. *Developmental Biology*, *258*(1), 185–200. https://doi.org/10.1016/S0012-1606(03)00114-3

Izvolsky, K. I., Zhong, L., Wei, L., Yu, Q., Nugent, M. A., & Cardoso, W. V. (2003). Heparan sulfates expressed in the distal lung are required for Fgf10 binding to the epithelium and for airway branching. *American Journal of Physiology. Lung Cellular and Molecular Physiology*, *285*(4), L838-46. https://doi.org/10.1152/ajplung.00081.2003

Jackson, I. J. (1997). Homologous Pigmentation Mutations in Human, Mouse and Other Model Organisms. *Hum Mol Genet.*

Jaegle, M., Ghazvini, M., Mandemakers, W., Piirsoo, M., Driegen, S., Levavasseur, F., … Meijer, D. (2003). The POU proteins Brn-2 and Oct-6 share important functions in Schwann cell development. *Genes and Development*. https://doi.org/10.1101/gad.258203

Jain, R., Pan, J., Driscoll, J. A., Wisner, J. W., Huang, T., Gunsten, S. P., … Brody,

S. L. (2010). Temporal relationship between primary and motile ciliogenesis in airway epithelial cells. *American Journal of Respiratory Cell and Molecular Biology*, *43*(6), 731–739. https://doi.org/10.1165/rcmb.2009-0328OC

Jessell, T. M. (2000). Neuronal specification in the spinal cord: inductive signals and transcriptional codes. *Nature Reviews. Genetics*, *1*(1), 20–9. https://doi.org/10.1038/35049541

Jonassen, J. A., Agustin, J. S., Follit, J. A., & Pazour, G. J. (2008). Deletion of IFT20 in the mouse kidney causes misorientation of the mitotic spindle and cystic kidney disease. *Journal of Cell Biology*. https://doi.org/10.1083/jcb.200808137

Jones, C., Roper, V. C., Foucher, I., Qian, D., Banizs, B., Petit, C., … Chen, P. (2008). Ciliary proteins link basal body polarization to planar cell polarity regulation. *Nature Genetics*, *40*(1), 69–77. https://doi.org/10.1038/ng.2007.54

Jones, L. J., Gray, M., Yue, S. T., Haugland, R. P., & Singer, V. L. (2001). Sensitive determination of cell number using the CyQUANT cell proliferation assay. *Journal of Immunological Methods*, *254*(1–2), 85–98. https://doi.org/10.1016/S0022-1759(01)00404-5

Jordan, S. a, & Jackson, I. J. (2000). MGF (KIT ligand) is a chemokinetic factor for melanoblast migration into hair follicles. *Developmental Biology*, *225*(2), 424–36. https://doi.org/10.1006/dbio.2000.9856

Jovic, D., Sakaue-Sawano, A., Abe, T., Cho, C.-S., Nagaoka, M., Miyawaki, A., & Akaike, T. (2013). Direct observation of cell cycle progression in living mouse embryonic stem cells on an extracellular matrix of E-cadherin. *SpringerPlus*, *2*(1), 585. https://doi.org/10.1186/2193-1801-2-585

Kaartinen, V., Voncken, J. W., Shuler, C., Warburton, D., Bu, D., Heisterkamp, N., & Groffen, J. (1995). Abnormal lung development and cleft palate in mice lacking TGF-beta 3 indicates defects of epithelial-mesenchymal interaction. *Nature Genetics*, *11*, 415–421. https://doi.org/10.1038/ng1295-415

Kadzik, R. S., Cohen, E. D., Morley, M. P., Stewart, K. M., Lu, M. M., & Morrisey,

E. E. (2014). Wnt ligand/Frizzled 2 receptor signaling regulates tube shape and branch-point formation in the lung through control of epithelial cell shape. *Proc. Natl. Acad. Sci. USA*, *111*(34), 12444–12449. https://doi.org/10.1073/pnas.1406639111

Kaminski, A., Belsham, G. J., & Jackson, R. J. (1994). Translation of encephalomyocarditis virus RNA: parameters influencing the selection of the internal initiation site. *The EMBO Journal*, *13*(7), 1673–81. Retrieved from http://www.pubmedcentral.nih.gov/articlerender.fcgi?artid=394998&tool=pmcentrez&rendertype=abstract

Kanai-Azuma, M., Kanai, Y., Gad, J. M., Tajima, Y., Taya, C., Kurohmaru, M., … Hayashi, Y. (2002). Depletion of definitive gut endoderm in Sox17-null mutant mice. *Development*, *129*(10), 2367–79. Retrieved from http://dev.biologists.org/content/129/10/2367.full

Kanda, T., Sullivan, K. F., & Wahl, G. M. (1998). Histone-GFP fusion protein enables sensitive analysis of chromosome dynamics in living mammalian cells. *Current Biology : CB*, *8*(7), 377–85. Retrieved from http://www.ncbi.nlm.nih.gov/pubmed/9545195

Karner, C. M., Chirumamilla, R., Aoki, S., Igarashi, P., Wallingford, J. B., & Carroll, T. J. (2009). Wnt9b signaling regulates planar cell polarity and kidney tubule morphogenesis. *Nature Genetics*, *41*(7), 793–9. https://doi.org/10.1038/ng.400

Kastan, M. B., & Bartek, J. (2004). Cell-cycle checkpoints and cancer. *Nature*, *432*(7015), 316–323. https://doi.org/10.1038/nature03097

Katzenberger, T., Petzoldt, C., Höller, S., Mäder, U., Kalla, J., Adam, P., … Ott, G. (2006). The Ki67 proliferation index is a quantitative indicator of clinical risk in mantle cell lymphoma [1]. *Blood*, *107*(8), 3407. https://doi.org/10.1182/blood-2005-10-4079

Kim, D., Pertea, G., Trapnell, C., Pimentel, H., Kelley, R., & Salzberg, S. L. (2013). TopHat2: accurate alignment of transcriptomes in the presence of insertions, deletions and gene fusions. *Genome Biology*, *14*(4), R36.

https://doi.org/10.1186/gb-2013-14-4-r36

Kim, H. Y., & Nelson, C. M. (2012). Extracellular matrix and cytoskeletal dynamics during branching morphogenesis. *Organogenesis*, *8*(2), 56–64. https://doi.org/10.4161/org.19813

Kim, H. Y., Pang, M. F., Varner, V. D., Kojima, L., Miller, E., Radisky, D. C., & Nelson, C. M. (2015). Localized Smooth Muscle Differentiation Is Essential for Epithelial Bifurcation during Branching Morphogenesis of the Mammalian Lung. *Developmental Cell*, *34*(6), 719–726. https://doi.org/10.1016/j.devcel.2015.08.012

Kim, I., Saunders, T. L., & Morrison, S. J. (2007). Sox17 Dependence Distinguishes the Transcriptional Regulation of Fetal from Adult Hematopoietic Stem Cells. *Cell*, *130*(3), 470–483. https://doi.org/10.1016/j.cell.2007.06.011

Kim, J. H., Lee, S.-R., Li, L.-H., Park, H.-J., Park, J.-H., Lee, K. Y., … Choi, S.-Y. (2011). High cleavage efficiency of a 2A peptide derived from porcine teschovirus-1 in human cell lines, zebrafish and mice. *PloS One*, *6*(4), e18556. https://doi.org/10.1371/journal.pone.0018556

Kim, N., & Song, K. (2013). KIFC1 is essential for bipolar spindle formation and genomic stability in the primary human fibroblast IMR-90 cell. *Cell Sructure and Function*, *38*(1), 21–30. https://doi.org/10.1247/csf.12014

Kos, R., Reedy, M. V, Johnson, R. L., & Erickson, C. a. (2001). The winged-helix transcription factor FoxD3 is important for establishing the neural crest lineage and repressing melanogenesis in avian embryos. *Development (Cambridge, England)*, *128*(8), 1467–1479.

Kubben, F. J., Peeters-Haesevoets, A., Engels, L. G., Baeten, C. G., Schutte, B., Arends, J. W., … Blijham, G. H. (1994). Proliferating cell nuclear antigen (PCNA): a new marker to study human colonic cell proliferation. *Gut*, *35*(4), 530–5. https://doi.org/10.1136/gut.35.4.530

Kuida, K., Haydar, T. F., Kuan, C. Y., Gu, Y., Taya, C., Karasuyama, H., … Flavell,

R. A. (1998). Reduced apoptosis and cytochrome C-mediated caspase activation in mice lacking Caspase 9. *Cell*, *94*(3), 325–337. https://doi.org/10.1016/S0092-8674(00)81476-2

Kulesa, P. M., Bailey, C. M., Kasemeier-kulesa, J. C., & Mclennan, R. (2011). Cranial Neural Crest Migration: New Rules for an Old Road. *Developmental Biology*, *344*(2), 543–554. https://doi.org/10.1016/j.ydbio.2010.04.010.Cranial

Kunisada, T., Lu, S. Z., Yoshida, H., Nishikawa, S., Mizoguchi, M., Hayashi, S., … Longley, B. J. (1998). Murine cutaneous mastocytosis and epidermal melanocytosis induced by keratinocyte expression of transgenic stem cell factor. *The Journal of Experimental Medicine*, *187*(10), 1565–73. https://doi.org/10.1084/jem.187.10.1565

Kunisada, T., Yoshida, H., Ogawa, M., Shultz, L. D., & Nishikawa, S. (1996). Characterization and isolation of melanocyte progenitors from mouse embryos. *Develop. Growth Differ*, *38*, 87–97.

Kunisada, T., Yoshida, H., Yamazaki, H., Miyamoto, A., Hemmi, H., Nishimura, E., … Hayashi, S. (1998). Transgene expression of steel factor in the basal layer of epidermis promotes survival, proliferation, differentiation and migration of melanocyte precursors. *Development (Cambridge, England)*, *125*(15), 2915–23. Retrieved from http://www.ncbi.nlm.nih.gov/pubmed/9655813

Labib, K., Tercero, J. A., & Diffley, J. F. X. (2000). Uninterrupted MCM2-7 Function Required for DNA Replication Fork Progression. *Science*, *288*(5471), 1643–1647.

Lakso, M., Sauer, B., Mosinger, B., Lee, E. J., Manning, R. W., Yu, S. H., … Westphal, H. (1992). Targeted oncogene activation by site-specific recombination in transgenic mice. *Proceedings of the National Academy of Sciences of the United States of America*, *89*(14), 6232–6. https://doi.org/10.1073/pnas.89.14.6232

Lara-Gonzalez, P., Westhorpe, F. G., & Taylor, S. S. (2012). The spindle assembly checkpoint. *Current Biology*, *22*(22), R966–R980.

https://doi.org/10.1016/j.cub.2012.10.006

Larkins, C. E., Aviles, G. D. G., East, M. P., Kahn, R. A., & Caspary, T. (2011). Arl13b regulates ciliogenesis and the dynamic localization of Shh signaling proteins. *Molecular Biology of the Cell*, *22*(23), 4694–703. https://doi.org/10.1091/mbc.E10-12-0994

Larue, L., de Vuyst, F., & Delmas, V. (2013). Modeling melanoblast development. *Cellular and Molecular Life Sciences*, *70*(6), 1067–1079. https://doi.org/10.1007/s00018-012-1112-4

Lebeche, D., Malpel, S., & Cardoso, W. V. (1999). Fibroblast growth factor interactions in the developing lung. *Mechanisms of Development*, *86*(1–2), 125–136. https://doi.org/10.1016/S0925-4773(99)00124-0

Lee, C., Hong, B., Choi, J. M., Kim, Y., Watanabe, S., Ishimi, Y., … Cho, Y. (2004). Structural basis for inhibition of the replication licensing factor Cdt1 by geminin. *Nature*, *430*, 913–917. https://doi.org/10.1038/nature02767.Published

Lee, H. O., Levorse, J. M., & Shin, M. K. (2003). The endothelin receptor-B is required for the migration of neural crest-derived melanocyte and enteric neuron precursors. *Developmental Biology*, *259*(1), 162–175. https://doi.org/10.1016/S0012-1606(03)00160-X

Lee, J.-H., & Paull, T. T. (2005). ATM activation by DNA double-strand breaks through the Mre11-Rad50-Nbs1 complex. *Science (New York, NY)*, *308*(5721), 551–554. https://doi.org/10.1126/science.1108297

Lehtinen, M. K., Zappaterra, M. W., Chen, X., Yang, Y. J., Hill, A. D., Lun, M., … Walsh, C. A. (2011). The Cerebrospinal Fluid Provides a Proliferative Niche for Neural Progenitor Cells. *Neuron*, *69*(5), 893–905. https://doi.org/10.1016/j.neuron.2011.01.023

Leman, A. R., & Noguchi, E. (2013). *The replication fork: Understanding the eukaryotic replication machinery and the challenges to genome duplication*. *Genes* (Vol. 4). https://doi.org/10.3390/genes4010001

Letterio, J. J., Geiser, A. G., Kulkarni, A. B., Roche, N. S., Sporn, M. B., & Roberts, A. B. (1994). Maternal rescue of transforming growth factor-beta 1 null mice. *Science*, *264*(5167), 1936–1938. Retrieved from http://science.sciencemag.org/content/264/5167/1936.abstract

Li, A., Ma, Y., Yu, X., Mort, R. L., Lindsay, C. R., Stevenson, D., … Machesky, L. M. (2011). Rac1 Drives Melanoblast Organization during Mouse Development by Orchestrating Pseudopod- Driven Motility and Cell-Cycle Progression. *Developmental Cell*, *21*(4), 722–734. https://doi.org/10.1016/j.devcel.2011.07.008

Li, C., Hu, L., Xiao, J., Chen, H., Li, J. T., Bellusci, S., … Minoo, P. (2005). Wnt5a regulates Shh and Fgf10 signaling during lung development. *Developmental Biology*, *287*(1), 86–97. https://doi.org/10.1016/j.ydbio.2005.08.035

Li, C., Xiao, J., Hormi, K., Borok, Z., & Minoo, P. (2002). Wnt5a Participates in Distal Lung Morphogenesis. *Developmental Biology*, *248*(1), 68–81. https://doi.org/10.1006/dbio.2002.0729

Li, Y., Gordon, J., Manley, N. R., Litingtung, Y., & Chiang, C. (2008). Bmp4 is required for tracheal formation: A novel mouse model for tracheal agenesis. *Developmental Biology*, *322*(1), 145–155. https://doi.org/10.1016/j.ydbio.2008.07.021

Li, Y., & Linnoila, R. I. (2012). Multidirectional differentiation of achaete-scute homologue-1-defined progenitors in lung development and injury repair. *American Journal of Respiratory Cell and Molecular Biology*, *47*(6), 768–775. https://doi.org/10.1165/rcmb.2012-0027OC

Lin, F., Hiesberger, T., Cordes, K., Sinclair, A. M., Goldstein, L. S. B., Somlo, S., & Igarashi, P. (2003). Kidney-specific inactivation of the KIF3A subunit of kinesin-II inhibits renal ciliogenesis and produces polycystic kidney disease. *Proceedings of the National Academy of Sciences of the United States of America*, *100*(9), 5286–91. https://doi.org/10.1073/pnas.0836980100

Lin, J. Y., & Fisher, D. E. (2007). Melanocyte biology and skin pigmentation.

Nature, *445*(7130), 843–850. https://doi.org/10.1038/nature05660

Lin, S., & Shannon, J. (2002). Microarray Analysis of Gene Expression in the Embryonic Lung. *Ch*, *121*, 80–81.

Lindahl, P., Karlsson, L., Hellström, M., Gebre-Medhin, S., Willetts, K., Heath, J. K., & Betsholtz, C. (1997). Alveogenesis failure in PDGF-A-deficient mice is coupled to lack of distal spreading of alveolar smooth muscle cell progenitors during lung development. *Development (Cambridge, England)*, *124*(20), 3943–3953.

Lindqvist, A., Rodríguez-Bravo, V., & Medema, R. H. (2009). The decision to enter mitosis: feedback and redundancy in the mitotic entry network. *Journal of Cell Biology*. https://doi.org/10.1083/jcb.200812045

Lindqvist, A., Van Zon, W., Rosenthal, C. K., & Wolthuis, R. M. F. (2007). Cyclin B1-Cdk1 activation continues after centrosome separation to control mitotic progression. *PLoS Biology*, *5*(5), 1127–1137. https://doi.org/10.1371/journal.pbio.0050123

Liu, E., Li, X., Yan, F., Zhao, Q., & Wu, X. (2004). Cyclin-dependent Kinases Phosphorylate Human Cdt1 and Induce Its Degradation. *Journal of Biological Chemistry*, *279*(17), 17283–17288. https://doi.org/10.1074/jbc.C300549200

Liu, Y., Stein, E., Oliver, T., Li, Y., Brunken, W. J., Koch, M., … Hogan, B. L. M. (2004). Novel role for netrins in regulating epithelial behavior during lung branching morphogenesis. *Current Biology*, *14*(10), 897–905. https://doi.org/10.1016/j.cub.2004.05.020

Loonstra, A., Vooijs, M., Beverloo, H. B., Allak, B. A., van Drunen, E., Kanaar, R., … Jonkers, J. (2001). Growth inhibition and DNA damage induced by Cre recombinase in mammalian cells. *Proceedings of the National Academy of Sciences of the United States of America*, *98*(16), 9209–14. https://doi.org/10.1073/pnas.161269798

Lu, C. J., Du, H., Wu, J., Jansen, D. A., Jordan, K. L., Xu, N., … Qian, Q. (2008).

Non-random distribution and sensory functions of primary cilia in vascular smooth muscle cells. *Kidney and Blood Pressure Research*, *31*(3), 171–184. https://doi.org/10.1159/000132462

Lü, J., Izvolsky, K. I., Qian, J., & Cardoso, W. V. (2005). Identification of FGF10 targets in the embryonic lung epithelium during bud morphogenesis. *Journal of Biological Chemistry*, *280*(6), 4834–4841. https://doi.org/10.1074/jbc.M410714200

Lü, J., Qian, J., Izvolsky, K. I., & Cardoso, W. V. (2004). Global analysis of genes differentially expressed in branching and non-branching regions of the mouse embryonic lung. *Developmental Biology*, *273*(2), 418–435. https://doi.org/10.1016/j.ydbio.2004.05.035

Luciani, F., Champeval, D., Herbette, A., Denat, L., Aylaj, B., Martinozzi, S., … Delmas, V. (2011). Biological and mathematical modeling of melanocyte development. *Development (Cambridge, England)*, *138*(18), 3943–3954. https://doi.org/10.1242/dev.067447

Luscher, B., Stauber, C., Schindlert, R., & Schumperli, D. (1985). Il, *82*(July), 4389–4393.

Lyons, A. B. (2000). Analysing cell division in vivo and in vitro using flow cytometric measurement of CFSE dye dilution. *Journal of Immunological Methods*, *243*(1–2), 147–154. https://doi.org/10.1016/S0022-1759(00)00231-3

Lyons, A. B., & Parish, C. R. (1994). Determination of lymphocyte division by flow cytometry. *Journal of Immunological Methods*, *171*(1), 131–137. https://doi.org/10.1016/0022-1759(94)90236-4

Ma, M., Tian, X., Igarashi, P., Pazour, G. J., & Somlo, S. (2013). Loss of cilia suppresses cyst growth in genetic models of autosomal dominant polycystic kidney disease. *Nature Genetics*, *45*(9), 1004–12. https://doi.org/10.1038/ng.2715

Macias, H., Moran, A., Samara, Y., Moreno, M., Compton, J. E., Harburg, G., …

Hinck, L. (2011). SLIT/ROBO1 signaling suppresses mammary branching morphogenesis by limiting basal cell number, *20*(6), 827–840. https://doi.org/10.1016/j.devcel.2011.05.012.SLIT/ROBO1

Mackenzie, M. a, Jordan, S. a, Budd, P. S., & Jackson, I. J. (1997). Activation of the receptor tyrosine kinase Kit is required for the proliferation of melanoblasts in the mouse embryo. *Developmental Biology*, *192*(1), 99–107. https://doi.org/10.1006/dbio.1997.8738

Maga, G., & Hubscher, U. (2003). Proliferating cell nuclear antigen (PCNA): a dancer with many partners. *J Cell Sci*, *116*(Pt 15), 3051–3060. https://doi.org/10.1242/jcs.00653

Mailleux, A. A., Tefft, D., Ndiaye, D., Itoh, N., Thiery, J. P., Warburton, D., & Bellusci, S. (2001). Evidence that SPROUTY2 functions as an inhibitor of mouse embryonic lung growth and morphogenesis. *Mechanisms of Development*, *102*(1–2), 81–94. https://doi.org/10.1016/S0925-4773(01)00286-6

Marks, H., Kalkan, T., Menafra, R., Denissov, S., Jones, K., Hofemeister, H., … Stunnenberg, H. G. (2012). The transcriptional and epigenomic foundations of ground state pluripotency. *Cell*, *149*(3), 590–604. https://doi.org/10.1016/j.cell.2012.03.026

Marsick, B. M., Roche, F. K., & Letourneau, P. C. (2012). Repulsive axon guidance cues ephrin-A2 and slit3 stop protrusion of the growth cone leading margin concurrently with inhibition of ADF/cofilin and ERM proteins. *Cytoskeleton*, *69*(7), 496–505. https://doi.org/10.1002/cm.21016

Martynoga, B., Morrison, H., Price, D. J., & Mason, J. O. (2005). Foxg1 is required for specification of ventral telencephalon and region-specific regulation of dorsal telencephalic precursor proliferation and apoptosis. *Developmental Biology*, *283*(1), 113–127. https://doi.org/10.1016/j.ydbio.2005.04.005

Marzluff, W. F., Wagner, E. J., & Duronio, R. J. (2008). Metabolism and regulation of canonical histone mRNAs: life without a poly(A) tail. *Nature Reviews.*

Genetics, *9*(11), 843–54. https://doi.org/10.1038/nrg2438

Matsui, T., Kanai-Azuma, M., Hara, K., Matoba, S., Hiramatsu, R., Kawakami, H., … Kanai, Y. (2006). Redundant roles of Sox17 and Sox18 in postnatal angiogenesis in mice. *Journal of Cell Science*, *119*, 3513–3526. https://doi.org/10.1242/jcs.03081

Matsushime, H., Quelle, D. E., Shurtleff, S. A., Shibuya, M., Sherr, C. J., & Kato, J. Y. (1994). D-type cyclin-dependent kinase activity in mammalian cells. *Mol.Cell Biol.* https://doi.org/10.1128/MCB.14.3.2066.Updated

Maya, R., Balass, M., Kim, S.-T., Shkedy, D., Leal, J.-F. M., SHifman, O., … Oren, M. (2001). ATM-dependent phosphorylation of Mdm2 on serine 394: role in p53 activation by DNA damage. *Genes and Development*, *15*, 1067–1077. https://doi.org/10.1101/gad.886901.Oliner

Mayer, T. C. (1973). The migratory pathway of neural crest cells into the skin of mouse embryos. *Developmental Biology*, *34*(1), 39–46. https://doi.org/10.1016/0012-1606(73)90337-0

McGarry, T. J., & Kirschner, M. W. (1998). Geminin, an inhibitor of DNA replication, is degraded during mitosis. *Cell*, *93*(6), 1043–53. Retrieved from http://www.ncbi.nlm.nih.gov/pubmed/9635433

McGowan, S. E., & McCoy, D. M. (2013). Platelet-derived growth factor-A and sonic hedgehog signaling direct lung fibroblast precursors during alveolar septal formation. *American Journal of Physiology. Lung Cellular and Molecular Physiology*, *305*(3), L229-39. https://doi.org/10.1152/ajplung.00011.2013

Mcilwain, D. R., Berger, T., & Mak, T. W. (2016). Caspase Functions in Cell Death and Disease. https://doi.org/10.1101/cshperspect.a008656

Méchali, M. (2010). Eukaryotic DNA replication origins: many choices for appropriate answers. *Nature Reviews. Molecular Cell Biology*, *11*(10), 728–738. https://doi.org/10.1038/nrm2976

Medvinsky, A., Rybtsov, S., & Taoudi, S. (2011). Embryonic origin of the adult

hematopoietic system: advances and questions. *Development*, *138*(6), 1017–31. https://doi.org/10.1242/dev.040998

Meier, P., Finch, a, & Evan, G. (2000). Apoptosis in development. *Nature*, *407*(6805), 796–801. https://doi.org/10.1038/35037734

Méndez, J., & Stillman, B. (2003). Perpetuating the double helix: Molecular machines at eukaryotic DNA replication origins. *BioEssays*, *25*(12), 1158–1167. https://doi.org/10.1002/bies.10370

Menshykau, D., Kraemer, C., & Iber, D. (2012). Branch mode selection during early lung development. *PLoS Computational Biology*, *8*(2). https://doi.org/10.1371/journal.pcbi.1002377

Menzl, I., Lebeau, L., Pandey, R., Hassounah, N. B., Li, F. W., Nagle, R., … McDermott, K. M. (2014). Loss of primary cilia occurs early in breast cancer development. *Cilia*, *3*(7), 1–16. https://doi.org/10.1186/2046-2530-3-7

Merino, R., Rodriguez-Leon, J., Macias, D., Gañan, Y., Economides, a N., & Hurle, J. M. (1999). The BMP antagonist Gremlin regulates outgrowth, chondrogenesis and programmed cell death in the developing limb. *Development (Cambridge, England)*, *126*(23), 5515–5522.

Merna, N. J., Fung, K. M., Wang, J. J., King, C. R., Hansen, K. C., Christman, K. L., & George, S. (2015). Differential β3 Integrin Expression Regulates the Response of Human Lung and Cardiac Fibroblasts to Extracellular Matrix and Its Components. *Tissue Engineering. Part A*, *21*, 1–11. https://doi.org/10.1089/ten.TEA.2014.0337

Messier, E. M., Mason, R. J., & Kosmider, B. (2012). Efficient and rapid isolation and purification of mouse alveolar type II epithelial cells. *Experimental Lung Research*, *38*(7).

Metzger, R. J., Klein, O. D., Martin, G. R., & Krasnow, M. A. (2008). The Branching Program of Mouse Lung Development, *453*(7196), 745–750. https://doi.org/10.1038/nature07005.The

Meyer, J. S., Cosatto, E., & Graf, H. P. (2009). Mitotic index of invasive breast carcinoma: Achieving clinically meaningful precision and evaluating tertial cutoffs. *Archives of Pathology and Laboratory Medicine*, *133*(11), 1826–1833. https://doi.org/10.1043/1543-2165-133.11.1826

Michael, L., & Davies, J. A. (2004). Pattern and regulation of cell proliferation during murine ureteric bud development. *Journal of Anatomy*, *204*(4), 241–255. https://doi.org/10.1111/j.0021-8782.2004.00285.x

Micheau, O., & Rg Tschopp, J. (2003). Induction of TNF Receptor I-Mediated Apoptosis via Two Sequential Signaling Complexes of these receptors delivers a powerful and rapid proapo- ptotic signal through a DD-mediated recruitment of the adaptor protein FADD and the formation of the so-called. *Cell*, *114*, 181–190. https://doi.org/10.1016/S0092-8674(03)00521-X

Min, H., Danilenko, D. M., Scully, S. a., Bolon, B., Ring, B. D., Tarpley, J. E., … Simonet, W. S. (1998). Fgf-10 is required for both limb and lung development and exhibits striking functional similarity to Drosophila branchless. *Genes & Development*, *12*(20), 3156–3161. https://doi.org/10.1101/gad.12.20.3156

Min, H., Danilenko, D. M., Scully, S. A., Bolon, B., Ring, B. D., Tarpley, J. E., … Simonet, W. S. (1998). Fgf-10 is required for both limb and lung development and exhibits striking functional similarity to Drosophila branchless. *Genes and Development*. https://doi.org/10.1101/gad.12.20.3156

Mintz, B. (1967). Gene Control of Mammalian Pigmentary Differentiation, I. Clonal Origin of Melanocytes. *Proceedings of the National Academy of Sciences of …*, 344–351. Retrieved from http://www.ncbi.nlm.nih.gov/pmc/articles/PMC335639/

Miyawaki, A., Llopis, J., Heim, R., Mccaffery, J. M., Adams, J. a, Ikurak, M., … Ikura, M. (1997). letters to nature Fluorescent indicators for Ca 2 + based on green fluorescent proteins and calmodulin. *Nature*, *388*(August), 882–887. https://doi.org/10.1038/42264

Miyazaki, J., Takaki, S., Araki, K., Tashiro, F., Tominaga, A., Takatsu, K., &

Yamamura, K. (1989). Expression vector system based on the chicken β-actin promoter directs efficient production of interleukin-5. *Gene*, *79*(2), 269–277. https://doi.org/10.1016/0378-1119(89)90209-6

Mizuguchi, H., Xu, Z., Ishii-Watabe, A., Uchida, E., & Hayakawa, T. (2000). IRES-Dependent Second Gene Expression Is Significantly Lower Than Cap-Dependent First Gene Expression in a Bicistronic Vector. *Molecular Therapy*, *1*(4), 376–382. https://doi.org/10.1006/mthe.2000.0050

Morrisey, E. E., & Hogan, B. L. M. (2010). Preparing for the first breath: genetic and cellular mechanisms in lung development. *Developmental Cell*, *18*(1), 8–23. https://doi.org/10.1016/j.devcel.2009.12.010

Mort, R. L., Ford, M. J., Sakaue-Sawano, A., Lindstrom, N. O., Casadio, A., Douglas, A. T., … Jackson, I. J. (2014). Fucci2a: A bicistronic cell cycle reporter that allows Cre mediated tissue specific expression in mice. *Cell Cycle*, *13*(17), 2681–2696. https://doi.org/10.4161/15384101.2015.945381

Mort, R. L., Hay, L., & Jackson, I. J. (2010). Ex vivo live imaging of melanoblast migration in embryonic mouse skin. *Pigment Cell & Melanoma Research*, *23*(2), 299–301. https://doi.org/10.1111/j.1755-148X.2010.00669.x

Mort, R. L., Jackson, I. J., & Patton, E. E. (2015). The melanocyte lineage in development and disease. *Development (Cambridge, England)*, *142*(4), 620–32. https://doi.org/10.1242/dev.106567

Mort, R. L., Ross, R. J. H., Hainey, K. J., Harrison, O. J., Keighren, M. a, Landini, G., … Yates, C. a. (2016). Reconciling diverse mammalian pigmentation patterns with a fundamental mathematical model. *Nature Communications*, *7*, 10288. https://doi.org/10.1038/ncomms10288

Mosmann, T. (1983). Rapid colorimetric assay for cellular growth and survival: Application to proliferation and cytotoxicity assays. *Journal of Immunological Methods*, *65*(1–2), 55–63. https://doi.org/10.1016/0022-1759(83)90303-4

Motoyama, J., Liu, J., Mo, R., Ding, Q., Post, M., & Hui, C. C. (1998). Essential

function of Gli2 and Gli3 in the formation of lung, trachea and oesophagus. *Nature Genetics*, *20*(september), 54–57. https://doi.org/10.1038/1711

Mucenski, M. L., Wert, S. E., Nation, J. M., Loudy, D. E., Huelsken, J., Birchmeier, W., … Whitsett, J. A. (2003). Beta-Catenin Is Required for Specification of Proximal/Distal Cell Fate During Lung Morphogenesis. *Journal of Biological Chemistry*, *278*(41), 40231–40238. https://doi.org/10.1074/jbc.M305892200

Neptune, E. R., Frischmeyer, P. a, Arking, D. E., Myers, L., Bunton, T. E., Gayraud, B., … Dietz, H. C. (2003). Dysregulation of TGF-beta activation contributes to pathogenesis in Marfan syndrome. *Nature Genetics*, *33*(3), 407–11. https://doi.org/10.1038/ng1116

Nevins, J. R. (1998). Toward an understanding of the functional complexity of the E2F and retinoblastoma families. *Cell Growth & Differentiation : The Molecular Biology Journal of the American Association for Cancer Research*. Retrieved from papers2://publication/uuid/FB2E2AEA-8BAF-4409-A9E7-16CB7F8F4346

Nicholls, S. B., Chu, J., Abbruzzese, G., Tremblay, K. D., & Hardy, J. a. (2011). Mechanism of a genetically encoded dark-to-bright reporter for caspase activity. *The Journal of Biological Chemistry*, *286*(28), 24977–86. https://doi.org/10.1074/jbc.M111.221648

Nishimura, E. K., Yoshida, H., Kunisada, T., & Nishikawa, S. I. (1999). Regulation of E- and P-cadherin expression correlated with melanocyte migration and diversification. *Developmental Biology*, *215*(2), 155–66. https://doi.org/10.1006/dbio.1999.9478

Nishitani, H., Lygerou, Z., Nishimoto, T., & Nurse, P. (2000). The Cdt1 protein is required to license DNA for replication in fission yeast. *Nature*, *404*(6778), 625–8. https://doi.org/10.1038/35007110

Nitzan, E., Krispin, S., Pfaltzgraff, E. R., Klar, A., Labosky, P. a, & Kalcheim, C. (2013). A dynamic code of dorsal neural tube genes regulates the segregation between neurogenic and melanogenic neural crest cells. *Development*

(Cambridge, England), *140*(11), 2269–79. https://doi.org/10.1242/dev.093294

Nogawa, H., Morita, K., & Cardoso, W. V. (1998). Bud formation precedes the appearance of differential cell proliferation during branching morphogenesis of mouse lung epithelium in vitro. *Developmental Dynamics : An Official Publication of the American Association of Anatomists*, *213*(2), 228–35. https://doi.org/10.1002/(SICI)1097-0177(199810)213:2<228::AID-AJA8>3.0.CO;2-I

Nonaka, S., Shiratori, H., Saijoh, Y., & Hamada, H. (2002). Determination of left-right patterning of the mouse embryo by artificial nodal flow. *Nature*, *418*(6893), 96–99. https://doi.org/10.1038/nature00849

Nonaka, S., Tanaka, Y., Okada, Y., Takeda, S., Harada, A., Kanai, Y., … Hirokawa, N. (1998). Randomization of left-right asymmetry due to loss of nodal cilia generating leftward flow of extraembryonic fluid in mice lacking KIF3B motor protein. *Cell*, *95*(6), 829–837. https://doi.org/10.1016/S0092-8674(00)81705-5

Nowakowski, R. S., Lewin, S. B., & Miller, M. W. (1989). Bromodeoxyuridine immunohistochemical determination of the lengths of the cell cycle and the DNA-synthetic phase for an anatomically defined population. *Journal of Neurocytology*, *18*(3), 311–8. Retrieved from http://www.ncbi.nlm.nih.gov/pubmed/2746304

Nurse, P. (2000). A long twentieth century of the cell cycle and beyond. *Cell*, *100*(1), 71–78. https://doi.org/10.1016/S0092-8674(00)81684-0

O'Brian,J.,Wilson,I.,Orton,T.,Pognan, F. (2000). Investigation of the Alamar Blue(resazurin) fluorescent dye for the assessment of mammalian cell cytotoxicity. *Europan Journal of Biochemistry*, *267*, 5421–5426.

O 'Connor, A. K., Malarkey, E. B., Berbari, N. F., Croyle, M. J., Haycraft, C. J., Bell, P. D., … Yoder, B. K. (2013). An inducible CiliaGFP mouse model for in vivo visualization and analysis of cilia in live tissue. *Cilia*, *2*(8), 1–14. https://doi.org/10.1186/2046-2530-2-8

Oh, M. K., Scoles, D. R., Haipek, C., Strand, A. D., Gutmann, D. H., Olson, J. M., & Pulst, S. M. (2003). Genetic Heterogeneity of Stably Transfected Cell Lines Revealed by Expression Profiling with Oligonucleotide Microarrays. *Journal of Cellular Biochemistry*, *90*(5), 1068–1078. https://doi.org/10.1002/jcb.10712

Ohtsubo, M., Theodoras, a M., Schumacher, J., Roberts, J. M., & Pagano, M. (1995). Human cyclin E, a nuclear protein essential for the G1-to-S phase transition. *Molecular and Cellular Biology*, *15*(5), 2612–24. https://doi.org/10.1128/MCB.15.5.2612

Okazaki, R., Okazaki, T., Sakabe, K., Sugimoto, K., & Sugino, A. (1968). Mechanism of DNA chain growth. I. Possible discontinuity and unusual secondary structure of newly synthesized chains. *Proceedings of the National Academy of Sciences of the United States of America*, *59*, 598–605. https://doi.org/10.1073/pnas.59.2.598

Oki, T., Nishimura, K., Kitaura, J., Togami, K., Maehara, A., Izawa, K., … Kitamura, T. (2014). A novel cell-cycle-indicator, mVenus-p27K 2 , identifies quiescent cells and visualizes G0–G1 transition. https://doi.org/10.1038/srep04012

Okorokov, A. L., Orlova, E. V, Kingsbury, S. R., Bagneris, C., Gohlke, U., Williams, G. H., & Stoeber, K. (2004). Molecular structure of human geminin. *Nature Structural & Molecular Biology*, *11*(10), 1021–2. https://doi.org/10.1038/nsmb835

Okubo, T., & Hogan, B. L. M. (2004). Hyperactive Wnt signaling changes the developmental potential of embryonic lung endoderm. *Journal of Biology*, *3*, 11. https://doi.org/10.1186/jbiol3

Oppenheim, R. W. (1991). Cell death during development of the nervous system. *Annual Review of Neuroscience*, *14*, 453–501. https://doi.org/10.1146/annurev.ne.14.030191.002321

Oréal, L., & Santos, L. G. (2000). Qualitative and Quantitative Analysis of. *Cell Mol. Biol*, *22*, 157–165.

Osborn, M. J., Panoskaltsis-Mortari, A., McElmurry, R. T., Bell, S. K., Vignali, D. A. A., Ryan, M. D., … Blazar, B. R. (2005). A picornaviral 2A-like sequence-based tricistronic vector allowing for high-level therapeutic gene expression coupled to a dual-reporter system. *Molecular Therapy*, *12*(3), 569–574. https://doi.org/10.1016/j.ymthe.2005.04.013

Packard, A., Georgas, K., Michos, O., Riccio, P., Cebrian, C., Combes, A. N., … Costantini, F. (2013). Luminal Mitosis Drives Epithelial Cell Dispersal within the Branching Ureteric Bud. *Developmental Cell*, *27*(3), 319–330. https://doi.org/10.1016/j.devcel.2013.09.001

Palais, G., Nguyen Dinh Cat, A., Friedman, H., Panek-Huet, N., Millet, A., Tronche, F., … Jaisser, F. (2009). Targeted transgenesis at the HPRT locus: an efficient strategy to achieve tightly controlled in vivo conditional expression with the tet system. *Physiological Genomics*, *37*(2), 140–6. https://doi.org/10.1152/physiolgenomics.90328.2008

Pardee, a B. (1974). A restriction point for control of normal animal cell proliferation. *Proceedings of the National Academy of Sciences of the United States of America*, *71*(4), 1286–90. https://doi.org/10.1073/pnas.71.4.1286

Paridaen, J. T. M. L., Wilsch-Bräuninger, M., & Huttner, W. B. (2013). Asymmetric inheritance of centrosome-associated primary cilium membrane directs ciliogenesis after cell division. *Cell*, *155*(2), 333–344. https://doi.org/10.1016/j.cell.2013.08.060

Parish, C. R. (1999). Fluorescent dyes for lymphocyte migration and proliferation studies. *Immunology and Cell Biology*, *77*(6), 499–508. https://doi.org/10.1046/j.1440-1711.1999.00877.x

Park, W. Y., Miranda, B., Lebeche, D., Hashimoto, G., & Cardoso, W. V. (1998). FGF-10 Is a Chemotactic Factor for Distal Epithelial Buds during Lung Development. *Dev. Biol.*, *134*, 125–134. https://doi.org/10.1006/dbio.1998.8994

Pauklin, S., & Vallier, L. (2013). The cell cycle state of stem cells determines cell fate propensity. *Cell*, *155*(1), 135–147.

https://doi.org/10.1016/j.cell.2013.08.031

Paul, J. D., Coulombe, K. L. K., Toth, P. T., Zhang, Y., Marsboom, G., Bindokas, V. P., … Rehman, J. (2013). SLIT3-ROBO4 activation promotes vascular network formation in human engineered tissue and angiogenesis in vivo. *Journal of Molecular and Cellular Cardiology*, *64*, 124–131. https://doi.org/10.1016/j.yjmcc.2013.09.005

Pepicelli, C. V, Lewis, P. M., & McMahon, a P. (1998). Sonic hedgehog regulates branching morphogenesis in the mammalian lung. *Current Biology : CB*, *8*, 1083–1086. https://doi.org/10.1016/S0960-9822(98)70446-4

Perl, A. K. T., Hokuto, I., Impagnatiello, M. A., Christofori, G., & Whitsett, J. A. (2003). Temporal effects of Sprouty on lung morphogenesis. *Developmental Biology*, *258*(1), 154–168. https://doi.org/10.1016/S0012-1606(03)00106-4

Pestova, T. V, Hellen, C. U., & Shatsky, I. N. (1996). Canonical eukaryotic initiation factors determine initiation of translation by internal ribosomal entry. *Molecular and Cellular Bology*, *16*(12), 6859–6869. Retrieved from http://www.pubmedcentral.nih.gov/articlerender.fcgi?artid=231689&tool=pmcentrez&rendertype=abstract%5Cnhttp://www.ncbi.nlm.nih.gov/pubmed/8943341%5Cnhttp://www.pubmedcentral.nih.gov/articlerender.fcgi?artid=PMC231689

Plosa, E. J., Young, L. R., Gulleman, P. M., Polosukhin, V. V, Zaynagetdinov, R., Benjamin, J. T., … Zent, R. (2014). Epithelial β1 integrin is required for lung branching morphogenesis and alveolarization. *Development (Cambridge, England)*, *5*, 4751–4762. https://doi.org/10.1242/dev.117200

Post, L. C., Ternet, M., & Hogan, B. L. M. (2000). Notch/Delta expression in the developing mouse lung. *Mechanisms of Development*, *98*(1–2), 95–98. https://doi.org/10.1016/S0925-4773(00)00432-9

Potts, W., Tucker, D., Wood, H., & Martin, C. (2000). Chicken beta-globin 5'HS4 insulators function to reduce variability in transgenic founder mice. *Biochemical and Biophysical Research Communications*, *273*(3), 1015–8. https://doi.org/10.1006/bbrc.2000.3013

Pozarowski, P., & Darzynkiewicz, Z. (2004). Analysis of Cell Cycle by Flow Cytometry. In A. H. Schönthal (Ed.), *Checkpoint Controls and Cancer: Volume 2: Activation and Regulation Protocols* (pp. 301–311). Totowa, NJ: Humana Press. https://doi.org/10.1385/1-59259-811-0:301

Quent, V. M. C., Loessner, D., Friis, T., Reichert, J. C., & Hutmacher, D. W. (2010). Discrepancies between metabolic activity and DNA content as tool to assess cell proliferation in cancer research. *Journal of Cellular and Molecular Medicine*, *14*(4), 1003–1013. https://doi.org/10.1111/j.1582-4934.2010.01013.x

Quinn, J. C., Molinek, M., Martynoga, B. S., Zaki, P. A., Faedo, A., Bulfone, A., … Price, D. J. (2007). Pax6 controls cerebral cortical cell number by regulating exit from the cell cycle and specifies cortical cell identity by a cell autonomous mechanism. *Developmental Biology*, *302*(1), 50–65. https://doi.org/10.1016/j.ydbio.2006.08.035

Rajagopal, J., Carroll, T. J., Guseh, J. S., Bores, S. A., Blank, L. J., Anderson, W. J., … Melton, D. A. (2008). Wnt7b stimulates embryonic lung growth by coordinately increasing the replication of epithelium and mesenchyme. *Development (Cambridge, England)*, *135*(9), 1625–34. https://doi.org/10.1242/dev.015495

Ramla Benmaamar, M. P. (2005). Involvement of the SCF Complex in the Control of Cdh1 Degradation in S Phase, (September), 1230–1232.

Rath, P. C., & Aggarwal, B. B. (1999). TNF-induced signaling in apoptosis. *Journal of Clinical Immunology*, *19*(6), 350–364. https://doi.org/10.1023/A:1020546615229

Rawles, M. (1947). Origin of Pigment Cells from the Neural Crest in the Mouse Embryo. *Physiological Zoology*, *20*(3), 248–266.

Rawles, M. E. (1940). The Development of Melanophores from Embryonic Mouse Tissues Grown in the Coelom of Chick Embryos. *Proceedings of the National Academy of Sciences of the United States of America*, *26*(12), 673–80. Retrieved from

http://www.pubmedcentral.nih.gov/articlerender.fcgi?artid=1078252&tool=pmcentrez&rendertype=abstract

Rawlins, E. L., Clark, C. P., Xue, Y., & Hogan, B. L. M. (2009). The Id2+ distal tip lung epithelium contains individual multipotent embryonic progenitor cells. *Development (Cambridge, England)*, *136*(22), 3741–3745. https://doi.org/10.1242/dev.037317

Rawlins, E. L., Ostrowski, L. E., Randell, S. H., & Hogan, B. L. M. (2007). Lung development and repair: contribution of the ciliated lineage. *Proceedings of the National Academy of Sciences of the United States of America*, *104*(2), 410–417. https://doi.org/10.1073/pnas.0610770104

Rees, S., Coote, J., Stables, J., Goodson, S., Harris, S., & Lee, M. G. (1996). Bicistronic vector for the creation of stable mammalian cell lines that predisposes all antibiotic-resistant cells to express recombinant protein. *BioTechniques*, *20*(1), 102–110.

Rehm, M., Dussmann, H., Janicke, R. U., Tavare, J. M., Kogel, D., & Prehn, J. H. M. (2002). Single-cell fluorescence resonance energy transfer analysis demonstrates that caspase activation during apoptosis is a rapid process: Role of caspase-3. *Journal of Biological Chemistry*, *277*(27), 24506–24514. https://doi.org/10.1074/jbc.M110789200

Reimann, J. D. R., Freed, E., Hsu, J. Y., Kramer, E. R., Peters, J. M., & Jackson, P. K. (2001). Emi1 is a mitotic regulator that interacts with Cdc20 and inhibits the anaphase promoting complex. *Cell*, *105*(5), 645–655. https://doi.org/10.1016/S0092-8674(01)00361-0

Rieder, C. L., Jensen, C. G., & Jensen, L. C. W. (1979). The resorption of primary cilia during mitosis in a vertebrate (PtK1) cell line. *Journal of Ultrastructure Research*, *68*(2), 173–185. https://doi.org/10.1016/S0022-5320(79)90152-7

Rizzo, M. a, Springer, G. H., Granada, B., & Piston, D. W. (2004). An improved cyan fluorescent protein variant useful for FRET. *Nature Biotechnology*, *22*(4), 445–449. https://doi.org/10.1038/nbt945

Roccio, M., Schmitter, D., Knobloch, M., Okawa, Y., Sage, D., & Lutolf, M. P. (2013). Predicting stem cell fate changes by differential cell cycle progression patterns. *Development*, *140*(2), 459–470. https://doi.org/10.1242/dev.086215

Rockich, B. E., Hrycaj, S. M., Shih, H. P., Nagy, M. S., Ferguson, M. a H., Kopp, J. L., … Spence, J. R. (2013). Sox9 plays multiple roles in the lung epithelium during branching morphogenesis. *Proceedings of the National Academy of Sciences of the United States of America*, *110*(47), E4456-64. https://doi.org/10.1073/pnas.1311847110

Roman, J., Little, C. W., & McDonald, J. A. (1991). Potential role of RGD-binding integrins in mammalian lung branching morphogenesis. *Development*, *112*(2), 551–558.

Roos, W. P., & Kaina, B. (2016). DNA damage-induced cell death by apoptosis. *Trends in Molecular Medicine*, *12*(9), 440–450. https://doi.org/10.1016/j.molmed.2006.07.007

Ryan, M. D., King, A. M. Q., & Thomas, G. P. (1991). Cleavage of foot-and-mouth disease virus polyprotein is mediated by residues located within a 19 amino acid sequence. *Journal of General Virology*, *72*(11), 2727–2732. https://doi.org/10.1099/0022-1317-72-11-2727

Sakai, K., & Miyazaki, J. (1997). A Transgenic Mouse Line That Retains Cre Recombinase Activity in Mature Oocytes Irrespective of thecreTransgene Transmission. *Biochemical and Biophysical Research Communications*, *237*(2), 318–324. https://doi.org/10.1006/bbrc.1997.7111

Sakaue-Sawano, A., Hoshida, T., Yo, M., Takahashi, R., Ohtawa, K., Arai, T., … Miyawaki, A. (2013). Visualizing developmentally programmed endoreplication in mammals using ubiquitin oscillators. *Development (Cambridge, England)*, *140*(22), 4624–32. https://doi.org/10.1242/dev.099226

Sakaue-Sawano, A., Kobayashi, T., Ohtawa, K., & Miyawaki, A. (2011). Drug-induced cell cycle modulation leading to cell-cycle arrest, nuclear mis-segregation, or endoreplication. *BMC Cell Biology*, *12*(1), 2.

https://doi.org/10.1186/1471-2121-12-2

Sakaue-Sawano, A., Kurokawa, H., Morimura, T., Hanyu, A., Hama, H., Osawa, H., … Miyawaki, A. (2008). Visualizing spatiotemporal dynamics of multicellular cell-cycle progression. *Cell*, *132*(3), 487–98. https://doi.org/10.1016/j.cell.2007.12.033

Salic, A., & Mitchison, T. J. (2008). A chemical method for fast and sensitive detection of DNA synthesis in vivo. *Proceedings of the National Academy of Sciences of the United States of America*, *105*(7), 2415–20. https://doi.org/10.1073/pnas.0712168105

Santamaría, D., Barrière, C., Cerqueira, A., Hunt, S., Tardy, C., Newton, K., … Barbacid, M. (2007). Cdk1 is sufficient to drive the mammalian cell cycle. *Nature*, *448*(7155), 811–815. https://doi.org/10.1038/nature06046

Sastalla, I., Chim, K., Cheung, G. Y. C., Pomerantsev, A. P., & Leppla, S. H. (2009). Codon-optimized fluorescent proteins designed for expression in low-GC gram-positive bacteria. *Applied and Environmental Microbiology*, *75*(7), 2099–2110. https://doi.org/10.1128/AEM.02066-08

Satir, P., Pedersen, L. B., & Christensen, S. T. (2010). The primary cilium at a glance. *Journal of Cell Science*, *123*(Pt 4), 499–503. https://doi.org/10.1242/jcs.050377

Sauer, B. (1987). Functional expression of the cre-lox site-specific recombination system in the yeast Saccharomyces cerevisiae. *Molecular and Cellular Biology*, *7*(6), 2087–2096. https://doi.org/10.1128/MCB.7.6.2087.Updated

Savatier, P., Huang, S., & Szekely, L. (1994). Contrasting patterns of retinoblastoma protein expression in mouse embryonic stem cells and embryonic fibroblasts. *Oncogene*, *9*(September 2016), 809–818. Retrieved from http://130.237.124.100/publications/1994_savatier_es.pdf

Savoian, M. S., & Rieder, C. L. (2002). Mitosis in primary cultures of Drosophila melanogaster larval neuroblasts. *Journal of Cell Science*, *115*(Pt 15), 3061–72.

Retrieved from http://www.ncbi.nlm.nih.gov/pubmed/12118062

Schafer, K. A. (1998). The Cell Cycle: A Review. *Vet Pathol*, *35*, 461–478.

Schmidt, E. E., Taylor, D. S., Prigge, J. R., Barnett, S., & Capecchi, M. R. (2000). Illegitimate Cre-dependent chromosome rearrangements in transgenic mouse spermatids. *Proceedings of the National Academy of Sciences of the United States of America*, *97*(25), 13702–7. https://doi.org/10.1073/pnas.240471297

Schneider, L., Cammer, M., Lehman, J., Sonja, K., Guerra, C. F., Veland, I. R., … Christensen, S. T. (2010). Directional Cell Migration and Chemotaxis in Wound Healing Response to PDGF-AA are Coordinated by the Primary Cilium in Fibroblasts.

Schnell, U., Cirulli, V., & Giepmans, B. N. G. (2013). EpCAM: Structure and function in health and disease. *BBA - Biomembranes*, *1828*(8), 1989–2001. https://doi.org/10.1016/j.bbamem.2013.04.018

Scholzen, T., & Gerdes, J. (2000). The Ki-67 protein: From the known and the unknown. *Journal of Cellular Physiology*, *182*(3), 311–322. https://doi.org/10.1002/(SICI)1097-4652(200003)182:3<311::AID-JCP1>3.0.CO;2-9

Seeley, E. S., & Nachury, M. V. (2010). The perennial organelle: assembly and disassembly of the primary cilium. *Journal of Cell Science*, *123*(Pt 4), 511–8. https://doi.org/10.1242/jcs.061093

Sekar, R. B., & Periasamy, A. (2003). Fluorescence resonance energy transfer (FRET) microscopy imaging of live cell protein localizations. *Journal of Cell Biology*, *160*(5), 629–633. https://doi.org/10.1083/jcb.200210140

Sekine, K., Ohuchi, H., Fujiwara, M., Yamasaki, M., Yoshizawa, T., Sato, T., … Kato, S. (1999). Fgf10 is essential for limb and lung formation. *Nature Genetics*, *21*(1), 138–41. https://doi.org/10.1038/5096

Serra, R., Pelton, R. W., & Moses, H. L. (1994). TGF beta 1 inhibits branching morphogenesis and N-myc expression in lung bud organ cultures. *Development*,

120(8), 2153–2161. Retrieved from http://www.ncbi.nlm.nih.gov/entrez/query.fcgi?cmd=Retrieve&db=PubMed&dopt=Citation&list_uids=7523056

Shaner, N. C., Steinbach, P. A., & Tsien, R. Y. (2005). A guide to choosing fluorescent proteins. *Nature Methods*, *2*(12), 905–909. https://doi.org/10.1038/nmeth819

Sheaff, R., Groudine, M., Gordon, M., Roberts, J., & Clurman, B. (1997). Cyclin E-CDK2 is a regulator of p27Kip1. *Genes Devv*, *11*(11), 1464–78.

Shin, M. K., Levorse, J. M., Ingram, R. S., & Tilghman, S. M. (1999). The temporal requirement for endothelin receptor-B signalling during neural crest development. *Nature*, *402*(December), 496–501. https://doi.org/10.1038/990040

Shinohara, K., Kawasumi, A., Takamatsu, A., Yoshiba, S., Botilde, Y., Motoyama, N., … Hamada, H. (2012). Two rotating cilia in the node cavity are sufficient to break left–right symmetry in the mouse embryo. *Nature Communications*, *3*, 622. https://doi.org/10.1038/ncomms1624

Shioi, G., Kiyonari, H., Abe, T., Nakao, K., Fujimori, T., Jang, C. W., … Aizawa, S. (2011). A mouse reporter line to conditionally mark nuclei and cell membranes for in vivo live-imaging. *Genesis*, *49*(7), 570–578. https://doi.org/10.1002/dvg.20758

Shirakawa, J., Ezura, Y., Moriya, S., Kawasaki, M., Yamada, T., Notomi, T., … Noda, M. (2014). Migration linked to FUCCI-indicated cell cycle is controlled by PTH and mechanical stress. *Journal of Cellular Physiology*, *229*(10), 1353–1358. https://doi.org/10.1002/jcp.24605

Shu, W., Guttentag, S., Wang, Z., Andl, T., Ballard, P., Lu, M. M., … Morrisey, E. E. (2005). Wnt/Beta-catenin signaling acts upstream of N-myc, BMP4, and FGF signaling to regulate proximal-distal patterning in the lung. *Developmental Biology*, *283*(1), 226–239. https://doi.org/10.1016/j.ydbio.2005.04.014

Shu, W., Jiang, Y. Q., Lu, M. M., & Morrisey, E. E. (2002a). Wnt7b regulates

mesenchymal proliferation and vascular development in the lung. *Development (Cambridge, England)*, *129*(20), 4831–4842. https://doi.org/10.1101/gad.13.23.3149

Shu, W., Jiang, Y. Q., Lu, M. M., & Morrisey, E. E. (2002b). Wnt7b regulates mesenchymal proliferation and vascular development in the lung. *Development (Cambridge, England)*, *129*(20), 4831–42. Retrieved from http://www.ncbi.nlm.nih.gov/pubmed/12361974

Shyu, Y. J., & Hu, C. D. (2008). Fluorescence complementation: an emerging tool for biological research. *Trends in Biotechnology*, *26*(11), 622–630. https://doi.org/10.1016/j.tibtech.2008.07.006

Silvestrini, R., Daldone, M. G., Valagussa, P., Fronzo, G. D., G., M., Mariani, L., & Bonadonna, G. (1990). 3H-thymidine-labeling index as a prognostic indicator in node-positive breast cancer. *American Society of Clinical Oncology*, *8*(8), 13212–26.

Simons, M., Gloy, J., Ganner, A., Bullerkotte, A., Bashkurov, M., Krönig, C., … Walz, G. (2005). Inversin, the gene product mutated in nephronophthisis type II, functions as a molecular switch between Wnt signaling pathways. *Nature Genetics*, *37*(5), 537–43. https://doi.org/10.1038/ng1552

Singh, A. M., Chappell, J., Trost, R., Lin, L., Wang, T., Tang, J., … Dalton, S. (2013). Cell-cycle control of developmentally regulated transcription factors accounts for heterogeneity in human pluripotent cells. *Stem Cell Reports*, *1*(6), 532–544. https://doi.org/10.1016/j.stemcr.2013.10.009

Slater, T. F., Sawyer, B., & Sträuli, U. (1963). Studies on succinate-tetrazolium reductase systems. *Biochimica et Biophysica Acta*, *77*, 383–393. https://doi.org/10.1016/0006-3002(63)90513-4

Sofía Pais, R., Moreno-Barriuso, N., Hernández-Porras, I., López, I. P., De Las Rivas, J., & Pichel, J. G. (2013). Transcriptome analysis in prenatal IGF1-deficient mice identifies molecular pathways and target genes involved in distal lung differentiation. *PLoS ONE*, *8*(12).

https://doi.org/10.1371/journal.pone.0083028

Soriano, P. (1999). Generalized lacZ expression with the ROSA26 Cre reporter strain. *Nature Genetics*, *21*(1), 70–71. https://doi.org/10.1038/5007

Spalluto, C., Wilson, D. I., & Hearn, T. (2013). Evidence for reciliation of RPE1 cells in late G1 phase, and ciliary localisation of cyclin B1. *FEBS Open Bio*, *3*, 334–340. https://doi.org/10.1016/j.fob.2013.08.002

Spassky, N. (2005). Adult Ependymal Cells Are Postmitotic and Are Derived from Radial Glial Cells during Embryogenesis. *Journal of Neuroscience*, *25*(1), 10–18. https://doi.org/10.1523/JNEUROSCI.1108-04.2005

Springer, T. A. (1994). Traffic signals for lymphocyte recirculation and leukocyte emigration: The multistep paradigm. *Cell*, *76*(2), 301–314. https://doi.org/10.1016/0092-8674(94)90337-9

Srinivas, S., Watanabe, T., Lin, C. S., William, C. M., Tanabe, Y., Jessell, T. M., & Costantini, F. (2001). Cre reporter strains produced by targeted insertion of EYFP and ECFP into the ROSA26 locus. *BMC Developmental Biology*, *1*, 4. Retrieved from http://www.pubmedcentral.nih.gov/articlerender.fcgi?artid=31338&tool=pmcentrez&rendertype=abstract

Steel, K. P., Davidson, D. R., & Jackson, I. J. (1992). TRP-2/DT, a new early melanoblast marker, shows that steel growth factor (c-kit ligand) is a survival factor. *Development (Cambridge, England)*, *115*(4), 1111–9. Retrieved from http://www.ncbi.nlm.nih.gov/pubmed/1280558

Sternberg, N., & Hamilton, D. (1981). Bacteriophage P1 site-specific recombination. *Journal of Molecular Biology*, *150*(4), 467–486. https://doi.org/10.1016/0022-2836(81)90375-2

Stoller, J. Z., Degenhardt, K. R., Huang, L., Zhou, D. D., Lu, M. M., & Epstein, J. A. (2009). Cre Reporter Mouse Expressing a Nuclear Localized Fusion of GFP and β-Galactosidase Reveals New Derivatives of Pax3-Expressing Precursors,

46(4), 200–204. https://doi.org/10.1002/dvg.20384.Cre

Strathdee, D., Ibbotson, H., & Grant, S. G. N. (2006). Expression of transgenes targeted to the Gt(ROSA)26Sor locus is orientation dependent. *PloS One*, *1*(1), e4. https://doi.org/10.1371/journal.pone.0000004

Strickland, P., Shin, G. C., Plump, A., Tessier-Lavigne, M., & Hinck, L. (2006). Slit2 and netrin 1 act synergistically as adhesive cues to generate tubular bi-layers during ductal morphogenesis. *Development (Cambridge, England)*, *133*, 823–832. https://doi.org/10.1242/dev.02261

Sugimoto, K., Okazaki, T., & Okazaki, R. (1968). Mechanism of DNA chain growth, II. Accumulation of newly synthesized short chains in E. coli infected with ligase-defective T4 phages. *Proceedings of the National Academy of Sciences of the United States of America*, *60*(4), 1356–62. https://doi.org/10.1073/pnas.60.4.1356

Sugimoto, N., Tatsumi, Y., Tsurumi, T., Matsukage, A., Kiyono, T., Nishitani, H., & Fujita, M. (2004). Cdt1 Phosphorylation by Cyclin A-dependent Kinases Negatively Regulates Its Function without Affecting Geminin Binding. *Journal of Biological Chemistry*, *279*(19), 19691–19697. https://doi.org/10.1074/jbc.M313175200

Sutherland, D., Samakovlis, C., & Krasnow, M. A. (1996). branchless encodes a Drosophila FGF homolog that controls tracheal cell migration and the pattern of branching. *Cell*, *87*(6), 1091–1101. https://doi.org/10.1016/S0092-8674(00)81803-6

Svoboda, P., & Di Cara, A. (2006). Hairpin RNA: A secondary structure of primary importance. *Cellular and Molecular Life Sciences*, *63*(7–8), 901–918. https://doi.org/10.1007/s00018-005-5558-5

Szymczak, A. L., Workman, C. J., Wang, Y., Vignali, K. M., Dilioglou, S., Vanin, E. F., & Vignali, D. A. A. (2004). Correction of multi-gene deficiency in vivo using a single “self-cleaving” 2A peptide-based retroviral vector. *Nature Biotechnology*, *22*(5), 589–594. https://doi.org/10.1038/nbt957

Tabone-Eglinger, S., Wehrle-Haller, M., Aebischer, N., Jacquier, M.-C., & Wehrle-Haller, B. (2012). Membrane-bound Kit ligand regulates melanocyte adhesion and survival, providing physical interaction with an intraepithelial niche. *The FASEB Journal*. https://doi.org/10.1096/fj.12-206045

Tefft, J. D., Matt, L., Smith, S., Leinwand, M., Zhao, J., Bringas, P., … Warburton, D. (1999). Conserved function of mSpry-2, a murine homolog of Drosophila sprouty, which negatively modulates respiratory organogenesis. *Current Biology*, *9*(4), 219–222. https://doi.org/10.1016/S0960-9822(99)80094-3

Theveneau, E., & Mayor, R. (2012). Neural crest delamination and migration: From epithelium-to-mesenchyme transition to collective cell migration. *Developmental Biology*, *366*(1), 34–54. https://doi.org/10.1016/j.ydbio.2011.12.041

Thuret, G. (2003). Mechanisms of staurosporine induced apoptosis in a human corneal endothelial cell line. *British Journal of Ophthalmology*, *87*(3), 346–352. https://doi.org/10.1136/bjo.87.3.346

Tichelaar, J. W., Lim, L., Costa, R. H., & Whitsett, J. a. (1999). HNF-3/forkhead homologue-4 influences lung morphogenesis and respiratory epithelial cell differentiation in vivo. *Developmental Biology*, *213*, 405–417. https://doi.org/10.1006/dbio.1999.9380

Tobin, J. L., Di Franco, M., Eichers, E., May-Simera, H., Garcia, M., Yan, J., … Beales, P. L. (2008). Inhibition of neural crest migration underlies craniofacial dysmorphology and Hirschsprung's disease in Bardet-Biedl syndrome. *Proceedings of the National Academy of Sciences of the United States of America*, *105*(18), 6714–9. https://doi.org/10.1073/pnas.0707057105

Tran, P. V, Haycraft, C. J., Besschetnova, T. Y., Turbe-doan, A., Stottmann, R. W., Herron, B. J., … Hospital, W. (2016). THM1 negatively modulates mouse sonic hedgehog signal transfuction and affect retrograte intraflagellar transport in cilia, *40*(4), 403–410. https://doi.org/10.1038/ng.105.THM1

Trapnell, C., Williams, B. a, Pertea, G., Mortazavi, A., Kwan, G., van Baren, M. J.,

… Pachter, L. (2010). Transcript assembly and quantification by RNA-Seq reveals unannotated transcripts and isoform switching during cell differentiation. *Nature Biotechnology*, *28*(5), 511–515. https://doi.org/10.1038/nbt.1621

Treutlein, B., Brownfield, D. G., Wu, A. R., Neff, N. F., Mantalas, G. L., Espinoza, F. H., … Quake, S. R. (2014). Reconstructing lineage hierarchies of the dital lung epithelium using single cell RNA-seq, *509*(7500), 371–375. https://doi.org/10.1038/nature13173.Reconstructing

Trichas, G., Begbie, J., & Srinivas, S. (2008). Use of the viral 2A peptide for bicistronic expression in transgenic mice. *BMC Biology*, *6*(1), 40. https://doi.org/10.1186/1741-7007-6-40

Tucker, R. W., Pardee, A. B., & Fujiwara, K. (1979). Centriole ciliation is related to quiescence and DNA synthesis in 3T3 cells. *Cell*, *17*(3), 527–535. https://doi.org/10.1016/0092-8674(79)90261-7

Tyas, L., Brophy, V. A., Pope, A., Rivett, A. J., & Tavaré, J. M. (2000). Rapid caspase-3 activation during apoptosis revealed using fluorescence-resonance energy transfer. *EMBO Reports*, *1*(3), 266–70. https://doi.org/10.1093/embo-reports/kvd050

Uziel, T., Lerenthal, Y., Moyal, L., Andegeko, Y., Mittelman, L., & Shiloh, Y. (2003). Requirement of the MRN complex for ATM activation by DNA damage. *EMBO Journal*, *22*(20), 5612–5621. https://doi.org/10.1093/emboj/cdg541

van den Heuval, S., & Harlow, E. (1993). Distinct roles for cyclin-dependent kinases in cell cycle control. *Science*, *262*, 2050–2054.

Venezia, T. A., Merchant, A. A., Ramos, C. A., Whitehouse, N. L., Young, A. S., Shaw, C. A., & Goodell, M. A. (2004). Molecular signatures of proliferation and quiescence in hematopoietic stem cells. *PLoS Biology*, *2*(10). https://doi.org/10.1371/journal.pbio.0020301

Vermeulen, K., Van Bockstaele, D. R., & Berneman, Z. N. (2003). The cell cycle: A review of regulation, deregulation and therapeutic targets in cancer. *Cell Proliferation*, *36*(3), 131–149. https://doi.org/10.1046/j.1365-2184.2003.00266.x

Vodermaier, H. C. (2004). APC/C and SCF: controlling each other and the cell cycle. *Current Biology : CB*, *14*(18), R787-96. https://doi.org/10.1016/j.cub.2004.09.020

Volckaert, T., Campbell, A., Dill, E., Li, C., Minoo, P., & De Langhe, S. (2013). Localized Fgf10 expression is not required for lung branching morphogenesis but prevents differentiation of epithelial progenitors. *Development (Cambridge, England)*, *140*(18), 3731–42. https://doi.org/10.1242/dev.096560

Vsevolod V. Rostovtsev, Luke G. Green, Valery V. Fokin, and K. B. S. (2002). A Stepwise Huisgen Cycloaddition Process Catalyzed by Copper (I): Regioselective Ligation of Azides and Terminal Alkynes. *Angew Chem Int Ed Engl*, *41*(14), 2596–2599.

Wajant, H., Pfizenmaier, K., & Scheurich, P. (2003). Tumor necrosis factor signaling. *Cell Death.Differ.*, *10*(1350–9047 (Print)), 45–65. https://doi.org/10.1038/sj.cdd.4401189

Wakamatsu, Y., Endo, Y., Osumi, N., & Weston, J. A. (2004). Multiple Roles of SOX2, an HMG-Box Transcription Factor in Avian Neural Crest Development. *Developmental Dynamics*, *229*(1), 74–86. https://doi.org/10.1002/dvdy.10498

Walmod, P. S., Hartmann-Petersen, R., Prag, S., Lepekhin, E. L., Röpke, C., Berezin, V., & Bock, E. (2004). Cell-cycle-dependent regulation of cell motility and determination of the role of Rac1. *Experimental Cell Research*, *295*(2), 407–420. https://doi.org/10.1016/j.yexcr.2004.01.011

Wang, L., Du, F., & Wang, X. (2008). TNF-α Induces Two Distinct Caspase-8 Activation Pathways. *Cell*, *133*(4), 693–703. https://doi.org/10.1016/j.cell.2008.03.036

Wang, X. Q., Tsai, J.-W. W., Imai, J. H., Lian, W.-N. N., Vallee, R. B., & Shi, S.-H. H. (2009). Asymmetric centrosome inheritance maintains neural progenitors in the neocortex. *Nature*, *461*(7266), 947–955. https://doi.org/10.1038/nature08435

Wang, Z. F., Whitfield, M. L., Ingledue, T. C., Dominski, Z., & Marzluff, W. F. (1996). The protein that binds the 3' end of histone mRNA: A novel RNA-binding protein required for histone pre-mRNA processing. *Genes and Development*, *10*(23), 3028–3040. https://doi.org/10.1101/gad.10.23.3028

Weatherbee, S. D., Behringer, R. R., Rasweiler, J. J., & Niswander, L. a. (2006). Interdigital webbing retention in bat wings illustrates genetic changes underlying amniote limb diversification. *Proceedings of the National Academy of Sciences*, *103*(41), 15103–15107. https://doi.org/10.1073/pnas.0604934103

Weaver, M., Dunn, N. R., & Hogan, B. L. (2000). Bmp4 and Fgf10 play opposing roles during lung bud morphogenesis. *Development (Cambridge, England)*, *127*(12), 2695–704. Retrieved from http://www.ncbi.nlm.nih.gov/pubmed/10821767

Wehrle-Haller, B., Meller, M., & Weston, J. a. (2001). Analysis of melanocyte precursors in Nf1 mutants reveals that MGF/KIT signaling promotes directed cell migration independent of its function in cell survival. *Developmental Biology*, *232*(2), 471–83. https://doi.org/10.1006/dbio.2001.0167

Wehrle-Haller, B., Morrison-Graham, K., & Weston, J. a. (1996). Ectopic c-kit Expression Affects the Fate of Melanocyte Precursors inPatchMutant Embryos. *Developmental Biology*, *177*(2), 463–474. https://doi.org/10.1006/dbio.1996.0178

Wehrle-Haller, B., & Weston, J. a. (1995). Soluble and cell-bound forms of steel factor activity play distinct roles in melanocyte precursor dispersal and survival on the lateral neural crest migration pathway. *Development (Cambridge, England)*, *121*(3), 731–42. Retrieved from http://www.ncbi.nlm.nih.gov/pubmed/7536655

Weinrauch, Y., & Zychlinsky, A. (1999). The Induction of Apoptosis by Bacterial Pathogens. *Microbiol*, *53*, 155–87.

White, A. C., Xu, J., Yin, Y., Smith, C., Schmid, G., & Ornitz, D. M. (2006). FGF9 and SHH signaling coordinate lung growth and development through regulation of distinct mesenchymal domains. *Development (Cambridge, England)*, *133*(8), 1507–1517. https://doi.org/10.1242/dev.02313

White, J., Stead, E., Faast, R., Conn, S., Cartwright, P., & Dalton, S. (2005). Developmental Activation of the Rb–E2F Pathway and Establishment of Cell Cycle-regulated Cyclin-depedent Kinase Activity during Embryonic Stem Cell Differentiation. *Molecular Biology of the Cell*, *16*, 2018–2027.

Whitelaw, A., Evans, A., & Corrin, B. (1981). Immotile cilia syndrome: a new cause of neonatal respiratory distress. *Arch Dis Child*. https://doi.org/10.1136/adc.56.6.432

Whitfield, M. L., Sherlock, G., Saldanha, A. J., Murrary, J. I., Ball, C. A., Alexander, K. E., … Botstein, D. (2002). Identification of Genes Periodically Expressed in the Human Cell Cycle and Their Expression in Tumors. *Molecular Biology of the Cell*, *13*(6), 1977–2000. https://doi.org/10.1091/mbc.02

Widmann, C., Gibson, S., Jarpe, M. B., & Johnson, G. L. (1999). Mitogen-activated protein kinase: conservation of a three-kinase module from yeast to human. *Physiological Reviews*, *79*(1), 143–180.

Wilkie, A. L., Jordan, S. a, & Jackson, I. J. (2002). Neural crest progenitors of the melanocyte lineage: coat colour patterns revisited. *Development (Cambridge, England)*, *129*(14), 3349–57. Retrieved from http://www.ncbi.nlm.nih.gov/pubmed/12091305

Wilkinson, G. A., Schittny, J. C., Reinhardt, D. P., & Klein, R. (2008). Role for ephrinB2 in postnatal lung alveolar development and elastic matrix integrity. *Developmental Dynamics*, *237*(8), 2220–2234. https://doi.org/10.1002/dvdy.21643

Wohlschlegel, J. A., Dwyer, B. T., Dhar, S. K., Cvetic, C., Walter, J. C., & Dutta, A. (2000). Inhibition of Eukaryotic DNA Replication by Geminin Binding to Cdt1. *Science*, *290*(5500), 2309–2312. https://doi.org/10.1126/science.290.5500.2309

Won, K. A., Xiong, Y., Beach, D., & Gilman, M. Z. (1992). Growth-regulated expression of D-type cyclin genes in human diploid fibroblasts. *Proceedings of the National Academy of Sciences of the United States of America*, *89*(20), 9910–4. https://doi.org/10.1073/pnas.89.20.9910

Wong, S. Y., Seol, A. D., So, P., Ermilov, A. N., Christopher, K., Jr, E. H. E., … Reiter, J. F. (2009). Primary cilia can both mediate and suppress Hedgehog pathway-dependent tumorigenesis. *Nat Med*, *15*(9), 1055–1061. https://doi.org/10.1038/nm.2011.Primary

Yang, T. T., Cheng, L., & Kain, S. R. (1996). Optimized codon usage and chromophore mutations provide enhanced sensitivity with the green fluorescent protein. *Nucleic Acids Research*, *24*(22), 4592–4593. https://doi.org/10.1093/nar/24.22.4592

Yates, L. L., Schnatwinkel, C., Murdoch, J. N., Bogani, D., Formstone, C. J., Townsend, S., … Dean, C. H. (2010). The PCP genes Celsr1 and Vangl2 are required for normal lung branching morphogenesis. *Human Molecular Genetics*, *19*(11), 2251–2267. https://doi.org/10.1093/hmg/ddq104

Yee, N. S., Hsiau, C. M., Serve, H., Vosseller, K., & Besmer, P. (1994). Mechanism of Down-regulation of c-kit Receptor, *269*(50), 31991–31998.

Yin, Y., White, A. C., Huh, S.-H., Hilton, M. J., Kanazawa, H., Long, F., & Ornitz, D. M. (2008). A FGF-WNT gene regulatory network controls lung mesenchyme development. *Dev Biol*, *2*(319), 426–436. https://doi.org/10.1126/scisignal.2001449.Engineering

Ying, Q.-L., Ying, Q.-L., Wray, J., Wray, J., Nichols, J., Nichols, J., … Smith, A. (2008). The ground state of embryonic stem cell self-renewal. *Nature*, *453*(May), 519–23. https://doi.org/10.1038/nature06968

Yoshiba, S., Shiratori, H., Kuno, I., Kawasumi, A., Shinohara, K., Nonaka, S., … Hamada, H. (2012). Cilia at the node of mouse embryos sense fluid flow for left-right determination via Pkd2. *Science*, *338*(6104), 226–231. https://doi.org/10.1016/j.cmet.2012.08.002.

Yoshida, H., Hayashi, S. I., Shultz, L. D., Yamamura, K. I., Nishikawa, S., Nishikawa, S. I., & Kunisada, T. (1996). Neural and skin cell-specific expression pattern conferred by steel factor regulatory sequence in transgenic mice. *Developmental Dynamics*, *207*(2), 222–232. https://doi.org/10.1002/(SICI)1097-0177(199610)207:2<222::AID-AJA10>3.0.CO;2-9

Yoshida, H., Kong, Y. Y., Yoshida, R., Elia, A. J., Hakem, A., Hakem, R., … Mak, T. W. (1998). Apaf1 is required for mitochondrial pathways of apoptosis and brain development. *Cell*, *94*(6), 739–750. https://doi.org/10.1016/S0092-8674(00)81733-X

Yoshida, H., Kunisada, T., Grimm, T., Nishimura, E. K., Nishioka, E., & Nishikawa, S. I. (2001). Review: melanocyte migration and survival controlled by SCF/c-kit expression. *The Journal of Investigative Dermatology. Symposium Proceedings / the Society for Investigative Dermatology, Inc. [and] European Society for Dermatological Research*, *6*(1), 1–5. https://doi.org/10.1046/j.0022-202x.2001.00006.x

Yoshida, H., Kunisada, T., Kusakabe, M., Nishikawa, S., & Nishikawa, S. I. (1996). Distinct stages of melanocyte differentiation revealed by anlaysis of nonuniform pigmentation patterns. *Development (Cambridge, England)*, *122*(4), 1207–1214.

Yu, J., Carroll, T. J., Rajagopal, J., Kobayashi, A., Ren, Q., & McMahon, A. P. (2009). A Wnt7b-dependent pathway regulates the orientation of epithelial cell division and establishes the cortico-medullary axis of the mammalian kidney. *Development (Cambridge, England)*, *136*(1), 161–71. https://doi.org/10.1242/dev.022087

Yuan, K., Frolova, N., Xie, Y., Wang, D., Cook, L., Kwon, Y.-J., … Frost, A.

(2010). Primary Cilia Are Decreased in Breast Cancer: Analysis of a Collection of Human Breast Cancer Cell Lines and Tissues. *Journal of Histochemisty & Cytochemisty*, *58*(10), 857–870. https://doi.org/0018726708094863

Zambrowicz, B. P., Imamoto, A., Fiering, S., Herzenberg, L. A., Kerr, W. G., & Soriano, P. (1997). Disruption of overlapping transcripts in the ROSA beta geo 26 gene trap strain leads to widespread expression of beta-galactosidase in mouse embryos and hematopoietic cells. *Proceedings of the National Academy of Sciences of the United States of America*, *94*(8), 3789–94. https://doi.org/10.1073/pnas.94.8.3789

Zanier, K., Luyten, I., Crombie, C., Linge, J. P., Nilges, M., & Sattler, M. (2002). Structure of the histone mRNA hairpin required for cell cycle regulation of histone gene expression.

Zent, R., Bush, K. T., Pohl, M. L., Quaranta, V., Koshikawa, N., Wang, Z., … Nigám, S. K. (2001). Involvement of laminin binding integrins and laminin-5 in branching morphogenesis of the ureteric bud during kidney development. *Developmental Biology*, *238*, 289–302. https://doi.org/10.1006/dbio.2001.0391

Zetterberg, a, & Larsson, O. (1985). Kinetic analysis of regulatory events in G1 leading to proliferation or quiescence of Swiss 3T3 cells. *Proceedings of the National Academy of Sciences of the United States of America*, *82*(16), 5365–5369. https://doi.org/10.1073/pnas.82.16.5365

Zettler, J., Schütz, V., & Mootz, H. D. (2009). The naturally split Npu DnaE intein exhibits an extraordinarily high rate in the protein trans-splicing reaction. *FEBS Letters*, *583*(5), 909–914. https://doi.org/10.1016/j.febslet.2009.02.003

Zhang, B., Dietrich, U. M., Geng, J. G., Bicknell, R., Esko, J. D., & Wang, L. (2009). Repulsive axon guidance molecule Slit3 is a novel angiogenic factor. *Blood*, *114*(19), 4300–4309. https://doi.org/10.1182/blood-2008-12-193326

Zhang, J., Wang, X., Cui, W., Wang, W., Zhang, H., Liu, L., … Li, B. (2013). Visualization of caspase-3-like activity in cells using a genetically encoded fluorescent biosensor activated by protein cleavage. *Nature Communications*, *4*,

2157. https://doi.org/10.1038/ncomms3157

Zhang, X. D., Gillespie, S. K., & Hersey, P. (2003). Staurosporine induces apoptosis of melanoma by both caspase-dependent and -indepenent apoptotic pathways. *Molecular Cancer Therapeutics*, *3*(2), 187–197.

Zhang, X., Mernaugh, G., Yang, D.-H., Gewin, L., Srichai, M. B., Harris, R. C., … Zent, R. (2009). b1 Integrin Is Necessary for Ureteric Bud Branching Morphogenesis and Maintenance of Collecting Duct Structural Integrity. *Development*, *136*(19), 3357–3366. https://doi.org/10.1242/dev.036269

Zhang G, Gurtu V, K. S. (1996). An enhanced green fluorescent protein allows sensitive detection of gene transfer in mammalian cells. *Biochem Biophys Res Commun.*, *227*(3), 707–11.

Zhou, L., Dey, C. R., Wert, S. E., & Whitsett, J. a. (1996). Arrested lung morphogenesis in transgenic mice bearing an SP-C-TGF-beta 1 chimeric gene. *Developmental Biology*, *175*(2), 227–238. https://doi.org/10.1006/dbio.1996.0110

Zhu, Y., Romero, M. I., Ghosh, P., Ye, Z., Charnay, P., Rushing, E. J., … Parada, L. F. (2001a). Ablation of NF1 function in neurons induces abnormal development of cerebral cortex and reactive gliosis in the brain. *Genes and Development*. https://doi.org/10.1101/gad.862101

Zhu, Y., Romero, M. I., Ghosh, P., Ye, Z., Charnay, P., Rushing, E. J., … Parada, L. F. (2001b). Ablation of NF1 function in neurons induces abnormal development of cerebral cortex and reactive gliosis in the brain. *Genes and Development*, *15*(7), 859–876. https://doi.org/10.1101/gad.862101

Zindy, F., Lamas, E., Chenivesse, X., Sobczak, J., Wang, J., Fesquet, D., … Bréchot, C. (1992). Cyclin A is required in S phase in normal epithelial cells. *Biochemical and Biophysical Research Communications*, *182*(3), 1144–1154. https://doi.org/10.1016/0006-291X(92)91851-G

Zou, H., & Niswander, L. (1996). Requirement for BMP signaling in interdigital

apoptosis and scale formation. *Science (New York, N.Y.)*, *272*(5262), 738–41. https://doi.org/10.1126/science.272.5262.738

Zou, L., & Elledge, S. J. (2003). Sensing DNA damage through ATRIP recognition of RPA-ssDNA complexes. *Science (New York, N.Y.)*, *300*(June), 1542–1548. https://doi.org/10.1126/science.1083430